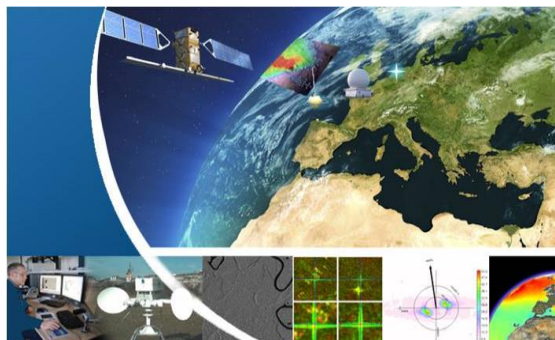




S-1 Annual Performance Report for 2023



Reference: SAR-MPC-0634

Nomenclature: DI-MPC-APR

Issue 1.3 - 19/04/2024



The SAR Mission Performance Cluster (MPC) Service is financed by the European Union, through the Copernicus Programme implemented by ESA.

Views and opinion expressed are however those of the author(s) only and the European Commission and/or ESA cannot be held responsible for any use which may be made of the information contained therein.

This report provides results generated and compiled by the S-1 Mission Performance Centre. The main contributions were provided by:

| | | | |
|------------------------------------------------------------------------------------|-------------------------------------------------------------------------------------------------------------------------------------------------------------------------------------------------------------|-------------------------------------------------------------------------------------|---------------------------------------------------------|
|  | <p><i>Guillaume Hajduch,</i> <i>Marie Berniere</i> <i>Karen Cordier</i> <i>Mélanie Grignoux</i> <i>Romain Husson</i> <i>Charles Peureux</i> <i>Amine</i> <i>Benchaabane</i></p> |  | <p><i>Harald Johnsen</i></p> |
|  | <p><i>Riccardo Piantanida</i> <i>Andrea Recchia</i> <i>Alessandro Cotrufo</i></p> |  | <p><i>Alexis Mouche</i> <i>Antoine Grouazel</i></p> |
|  | <p><i>Kersten Schmidt</i> <i>Christoph Gisinger</i> <i>Helko Breit</i></p> |  | <p><i>Fabrice Collard</i> <i>Gilles Guitton</i></p> |

CHRONOLOGY ISSUES/HISTORIQUE DES VERSIONS

| Issue/ Version | Date | Object/Objet | Written by/ Rédigé par |
|-------------------|------------|------------------------------------------------------------------------------------------------------------------------------------------------------------------------------------------------------------------------------------------------------------------------------|---------------------------------|
| 1.0 | 31.01.2024 | First version | SAR-MPC |
| 1.1 | 01.02.2024 | Correction of figure numbering | SAR-MPC |
| 1.2 | 18.04.2024 | Correction of broken links. Correction of spelling and typos Add missing references inter alia to geodetic sites, to weather forecast, to the S-1 product definition, etc Add example of RFI originated from satellite tracking stations, and example of mitigation | SAR-MPC |
| 1.3 | 19.04.2024 | Fix remaining style issues Add reference to CSA Transponders | SAR-MPC |

DISTRIBUTION/LISTE DE DIFFUSION

| Company/Organisme | Means of distribution/ Format de diffusion | Names/Destinataires |
|-------------------|-----------------------------------------------|---------------------|
| CLS | Notification | G. Hajduch |
| ESA | Notification | M. Pinheiro |

LIST OF CONTENTS/SOMMAIRE

| | | |
|-----------|-------------------------------------------------|-----------|
| 1. | Introduction..... | 15 |
| 1.1 | Purpose of this document..... | 15 |
| 1.2 | Document organisation | 15 |
| 1.3 | Applicable and Reference Documents..... | 15 |
| 1.3.1 | Applicable Documents | 15 |
| 1.3.2 | Reference Documents..... | 16 |
| 1.4 | Acronyms and Definition | 19 |
| 2. | Executive Summary | 21 |
| 2.0 | S1 IPF and Auxiliary Files | 21 |
| 2.1 | SETAP and Auxiliary Files | 21 |
| 2.2 | Instrument Status..... | 22 |
| 2.3 | Level 1 Product Status..... | 23 |
| 2.4 | ETAD Product Status | 24 |
| 2.5 | Level 2 Product Status..... | 25 |
| 2.5.1 | Wind (OWI) | 25 |
| 2.5.2 | Swell (OSW) | 25 |
| 2.5.3 | Radial Velocity (RVL) | 27 |
| 3. | Processing Updates | 28 |
| 3.0 | SAR Processor | 28 |
| 3.0.1 | IPF 3.7.1 (from 19/10/2023)..... | 28 |
| 3.0.2 | IPF 3.6.1 (from 30/03/2023 to 19/10/2023)..... | 28 |
| 3.1 | SETAP Processor | 29 |
| 3.1.1 | SETAP 2.20 (from 30/11/2023)..... | 29 |
| 3.1.2 | SETAP 2.10 (from 21/07/2023 to 30/11/2023)..... | 29 |
| 3.2 | Auxiliary Data Files..... | 29 |
| 3.2.1 | AUX_INS..... | 29 |
| 3.2.2 | AUX_CAL..... | 29 |
| 3.2.3 | AUX_PP1 | 30 |
| 3.2.4 | AUX_PP2..... | 30 |
| 3.2.5 | AUX_SCS | 30 |
| 3.2.6 | AUX_ITC | 30 |
| 3.2.7 | AUX_SCF | 30 |
| 4. | Instrument Status | 31 |
| 4.0 | RFC Monitoring..... | 31 |
| 4.0.1 | Antenna Status | 31 |

| | | |
|-------|--------------------------------------------------------|-----|
| 4.0.2 | TRM Trends | 32 |
| 4.1 | Instrument temperature | 37 |
| 4.2 | Internal Calibration | 40 |
| 4.3 | Noise Power | 55 |
| 4.4 | Instrument Unavailability | 58 |
| 4.5 | Radar Data Base Updates..... | 58 |
| 5. | L1 Products Status | 59 |
| 5.0 | Level 1 Basic Image Quality Parameters | 59 |
| 5.0.1 | Spatial Resolution..... | 59 |
| 5.0.2 | Sidelobe Ratios | 60 |
| 5.1 | Radiometric Calibration | 61 |
| 5.1.1 | Absolute Radiometric Calibration..... | 61 |
| 5.1.2 | Geophysical Calibration..... | 65 |
| 5.2 | Geometric Validation | 66 |
| 5.2.1 | Nominal Geometric Validation..... | 66 |
| 5.2.2 | Geometric Validation with ETAD Products | 75 |
| 5.3 | Polarimetric Calibration | 78 |
| 5.3.1 | Gain Imbalance | 78 |
| 5.3.2 | Phase Imbalance | 78 |
| 5.3.3 | Coregistration | 79 |
| 5.3.4 | Crosstalk..... | 79 |
| 5.4 | Elevation Antenna Patterns | 80 |
| 5.5 | Azimuth Antenna Patterns..... | 80 |
| 5.6 | Noise Equivalent Radar Cross-section | 80 |
| 5.7 | Interferometric Performances | 82 |
| 5.7.1 | S-1 Orbit Baseline..... | 83 |
| 5.7.2 | S-1 Burst Synchronization | 87 |
| 5.7.3 | Instrument Pointing | 91 |
| 5.8 | Radio Frequency Interferences | 94 |
| 5.8.1 | RFI annotations and RFI mitigation | 94 |
| 5.8.2 | Effectiveness of RFI mitigation | 94 |
| 5.8.3 | Regular reporting on RFI | 96 |
| 5.8.4 | Geographic distribution of RFI sources | 97 |
| 5.8.5 | Mutual Interferences with Radarsat-2 | 99 |
| 5.8.6 | Mutual Interferences with Gaofen-3 constellation | 102 |
| 5.8.7 | Mutual Interferences with the RCM constellation | 106 |
| 5.8.8 | Mutual interferences with RISAT-1A (EOS4) | 111 |



| | | |
|---------------------------------------------------------|----------------------------------------------|-----|
| 5.8.9 | Mutual Interferences with other sources..... | 114 |
| 5.9 | L1 Quality Disclaimers | 116 |
| 6. | Level 2 Products | 117 |
| 6.0 | Wind Measurement..... | 117 |
| 6.0.1 | Image Mode (IW -EW)/ OWI..... | 117 |
| 6.0.2 | Wave Mode / OWI | 123 |
| 6.0.3 | Wave Mode / OSW..... | 124 |
| 6.1 | Swell Measurement..... | 128 |
| 6.1.1 | Wave Mode | 128 |
| 6.1.2 | Other modes | 138 |
| 6.2 | Radial Velocity Measurement | 139 |
| 6.2.1 | Wave Mode | 139 |
| 6.2.2 | TOPS Mode | 142 |
| 6.3 | L2 Quality Disclaimers | 143 |
| Appendix A - S-1A & S-1B Technical Reports | | 144 |
| Appendix B - S-1A Instrument Unavailability | | 148 |
| Appendix C - S-1A & S-1B Quality Disclaimers | | 149 |
| Appendix D - S-1A Orbit Cycles | | 156 |
| Appendix E - S-1A Transmit Receive Module Failures..... | | 158 |
| Appendix F - S-1A & S-1B Auxiliary Data Files..... | | 159 |



LIST OF FIGURES

| | |
|----------------------------------------------------------------------------------------------------------------------------------------------------------------------|----|
| Figure 4-1: S-1A antenna status: gain (left) and phase (right) deviation of the TRMs from the nominal status. The white “F” marks the failed antenna elements. | 31 |
| Figure 4-2: Gain (<i>top</i>) and phase (<i>bottom</i>) stability of the S-1A SAR antenna tiles: average of the RFC coefficients in TX H over rows. | 32 |
| Figure 4-3: Gain (<i>top</i>) and phase (<i>bottom</i>) stability of the S-1A SAR antenna tiles: average of the RFC coefficients in TX V over rows. | 33 |
| Figure 4-4: Gain (<i>top</i>) and phase (<i>bottom</i>) stability of the S-1A SAR antenna tiles: average of the RFC coefficients in RX H over rows. | 33 |
| Figure 4-5: Gain (<i>top</i>) and phase (<i>bottom</i>) stability of the S-1A SAR antenna tiles: average of the RFC coefficients in RX V over rows. | 34 |
| Figure 4-6 S-1A tiles average gain (<i>top</i>) and phase (<i>bottom</i>) in TX mode and H polarization, plotted from the mission start to the end of 2023. | 35 |
| Figure 4-7 S-1A tiles average gain (<i>top</i>) and phase (<i>bottom</i>) in TX mode and V polarization, plotted from the mission start to the end of 2023. | 35 |
| Figure 4-8 S-1A tiles average gain (<i>top</i>) and phase (<i>bottom</i>) in RX mode and H polarization, plotted from the mission start to the end of 2023. | 36 |
| Figure 4-9 S-1A tiles average gain (<i>top</i>) and phase (<i>bottom</i>) in RX mode and V polarization, plotted from the mission start to the end of 2023. | 36 |
| Figure 4-10: S-1A temperature evolution during 2023 for Electronic Front Elements (EFEs) and Tile Amplifiers (TAs). | 37 |
| Figure 4-11: Antenna elements temperature evolution as function of acquisition duration, in 2023. | 38 |
| Figure 4-12 S-1A temperature evolution from mission start to 2023 for Electronic Front Elements (EFEs) and Tile Amplifiers (TAs). | 39 |
| Figure 4-13 Antenna elements temperature evolution as function of acquisition duration, from mission start to 2023. | 40 |
| Figure 4-14 PG trend in time for IW VV in 2023 | 41 |
| Figure 4-15 PG trend in time for IW VH in 2023 | 42 |
| Figure 4-16 PG trend in time for EW HH in 2023 | 43 |
| Figure 4-17 PG trend in time for EW HV in 2023 | 44 |
| Figure 4-18 PG distribution for EW HV in 2023. | 45 |
| Figure 4-19 Comparison of measured and model PG values for IW in 2023 | 46 |
| Figure 4-20 Comparison of measured and model PG values for EW in 2023 | 47 |
| Figure 4-21 PG trend in time for EW HH from mission start to 2023 | 48 |
| Figure 4-22 PG trend in time for EW HV from mission start to 2023 | 49 |
| Figure 4-23 PG trend in time for EW VV from mission start to 2023. | 50 |
| Figure 4-24 PG trend in time for EW VH from mission start to 2023 | 51 |
| Figure 4-25 PG trend in time for IW VV from mission start to 2023 | 52 |
| Figure 4-26 PG trend in time for IW VH from mission start to 2023 | 53 |
| Figure 4-27 PG trend in time for IW HH from mission start to 2023 | 54 |
| Figure 4-28 PG trend in time for IW HV from mission start to 2023 | 55 |

| | |
|----------------------------------------------------------------------------------------------------------------------------------------------------------------------------------------------------------------------------------------------------------------------------------------------------------------------------------------------------------------------------------------------------------------------------------------|----|
| Figure 4-29: Noise power versus time for beams IW1 (top), EW1 (middle), and WV1 (bottom) of S-1A in 2023 | 56 |
| Figure 4-30: Histograms of noise measurements registered during December 2023, separated by swath (vertically) and by polarization (horizontally). | 57 |
| Figure 4-31 Noise power versus time for beams IW1 (top), EW1 (middle), and WV1 (bottom) of S-1A from mission start until 2023 | 58 |
| Figure 5-1: S-1A IW azimuth and slant-range spatial resolution (lines correspond to targeted performance from the product definition) | 59 |
| Figure 5-2: ISLR (left) and PSLR (right) for azimuth (y-axis) and range direction (x-axis) derived from DLR transponder measurements using S-1A IW acquisitions (lines correspond to targeted performance from the product definition)..... | 60 |
| Figure 5-3: S-1A calibration factor for IW acquisitions in 2023 derived from DLR reference targets; the polarization is depicted by colour: VV in red, VH in blue. | 61 |
| Figure 5-4: S-1A calibration factor derived from each DLR target under constant acquisition geometry (i.e. same elevation or look angle) acquired in 2023. The symbols depict the mean value, error bars the standard deviation; each target type can be identified by its symbol: corner reflectors as open triangles, transponders as filled squares or circles. The polarization is depicted by colour, VV in red, VH in blue. | 63 |
| Figure 5-5: S-1A calibration factor for IW acquisitions from Mar 2017 to Dec 2023 derived from DLR reference targets; the polarization is depicted by colour: VV in red, VH in blue. | 64 |
| Figure 5-6: assessment of the WV SLC calibration (denoised Sigma0) using geophysical approach i.e. comparison with Cmod-5n with ECMWF0.125° (3h)..... | 66 |
| Figure 5-7: S-1A IW SLC ALE time series for products over the <i>Surat Basin</i> site acquired in 2023, with post-processing corrections. | 70 |
| Figure 5-8: S-1A IW SLC ALE performance estimates for products over the <i>Surat Basin</i> site acquired in 2023, with post-processing corrections. | 71 |
| Figure 5-9: S-1A IW SLC ALE time series for products over the <i>Geodetic Observatory</i> sites (Wetzell, Metsähovi, Yarragadee, Côte d’Azur) acquired in 2023, with post-processing corrections..... | 72 |
| Figure 5-10: S-1A IW SLC ALE performance estimates for products over <i>Geodetic Observatory</i> sites (Wetzell, Metsähovi, Yarragadee, Côte d’Azur) acquired in 2023, with post-processing corrections..... | 72 |
| Figure 5-11: S-1A and S1-B IW SLC ALE time series for products over the <i>Surat Basin</i> site acquired between Oct 2016 and Dec 2023, with post-processing corrections. | 73 |
| Figure 5-12: S-1A and S1-B IW SLC ALE time series for products over the <i>Geodetic Observatory</i> sites (Wetzell, Metsähovi, Yarragadee, Côte d’Azur) acquired between Oct 2016 and Dec 2023, with post-processing corrections. | 73 |
| Figure 5-13: S-1A IW SLC ALE time series for products over the <i>Surat Basin</i> site acquired in 2023, without post-processing corrections. | 74 |
| Figure 5-14: IW SLC product ALE estimates for S-1A for all 2023 acquisitions over the <i>Surat Basin</i> calibration site without the post-processing corrections. | 75 |
| Figure 5-15: S-1A IW SLC ALE time series for products over the <i>Surat Basin</i> site acquired between July to December 2023, applying <i>ETAD</i> post-processing corrections. | 77 |
| Figure 5-16: S-1A IW SLC ALE performance estimates for products over the <i>Surat Basin</i> site acquired between July to December 2023, applying <i>ETAD</i> post-processing corrections. | 77 |
| Figure 5-17: IW Gain Imbalance of S-1A using the DLR transponders. | 78 |
| Figure 5-18: Phase Imbalance using the DLR transponders. | 79 |



| | |
|----------------------------------------------------------------------------------------------------------------------------------------------------------------------------------------------------------------------------------------------------------------------------------------------------------------------------------------------|----|
| Figure 5-19: Crosstalk derived from DLR corner reflectors for S-1A..... | 80 |
| Figure 5-20: Annotated denoising vectors compare to measured NESZ. Green: low-backscatter image profile Orange: annotated noise vector with IPF 3.5.2. Blue: annotated noise vector with IPF 3.6.0 | 81 |
| Figure 5-21: Range profile (blue) and corresponding noise vector (yellow) of a burst with very low backscatter level. | 81 |
| Figure 5-22: (Left) Distribution of the difference between data and noise vectors as a function of the incidence angle for EW2 HV beam. (Right) Same distribution after applying the estimated noise calibration correction factor..... | 82 |
| Figure 5-23: S-1A parallel (top), normal (mid) and along-track (bottom) interferometric baseline components during 2023, computed for the given cycle with respect to a fixed reference cycle. Warm colours are used for the maximum value and cold colours for the minimum value of each orbit. The colours represent the track number..... | 83 |
| Figure 5-24 S-1A parallel (top), normal (mid) and along-track (bottom) interferometric baseline components during 2023, computed for the given cycle with respect to its previous one. Warm colours are used for the maximum value and cold colours for the minimum value of each orbit. The colours represent the track number. | 84 |
| Figure 5-25 S-1A interferometric baseline components from 2015 to 2023, computed for the current cycle with respect to a reference cycle in 2015 | 85 |
| Figure 5-26 S-1A interferometric baseline components from 2015 to 2023, computed for the current cycle with respect to its previous cycle | 86 |
| Figure 5-27: S-1A IW (top) and EW (bottom) burst synchronization error distribution during 2023, computed for each cycle with respect to a fixed reference cycle..... | 88 |
| Figure 5-28 S-1A IW (top) and EW (bottom) burst synchronization error distribution during 2023, computed for each cycle with respect to its previous cycle. | 89 |
| Figure 5-29 S-1A IW burst synchronization error distribution from 2015 to 2023, computed for each cycle with respect to a reference cycle..... | 90 |
| Figure 5-30 S-1A EW burst synchronization error distribution from 2015 to 2023, computed for each cycle with respect to a reference cycle..... | 90 |
| Figure 5-31 S-1A IW burst synchronization error distribution from 2015 to 2023, computed for each cycle with respect to its previous cycle | 91 |
| Figure 5-32 S-1A EW burst synchronization error distribution from 2015 to 2023, computed for each cycle with respect to its previous cycle | 91 |
| Figure 5-33: S-1A Doppler Centroid measured in 2023. Histogram bins are set to white if empty. | 92 |
| Figure 5-34 S-1A Doppler Centroid measured from mission start to 2023. Histogram bins are set to white if empty. | 92 |
| Figure 5-35 Doppler Centroid evolution in 2023, with legend labelling current Star Trackers configuration. | 93 |
| Figure 5-36: Residual RFI for S1A and the month of May 2023. | 95 |
| Figure 5-37: Examples of residual Radio Frequency Interference observed in 2023 | 96 |
| Figure 5-38: result of RFI pre-screening for EW products of cycle 309 (ascending and descending tracks) | 97 |
| Figure 5-39: result of RFI pre-screening for IW products of cycle 309 (ascending and descending tracks) | 98 |
| Figure 5-40: result of RFI characterisation through the Max Fisher Z coefficient for EW and IW products of cycle 309 (ascending and descending tracks)..... | 99 |



| | |
|--------------------------------------------------------------------------------------------------------------------------------------------------------------------------------------------------------------------------------------------------------------------------------------------------------------------|-----|
| Figure 5-41: Potential locations of S-1A IW images at the time of close S1A vs RS-2 fly-bys in 2023..... | 100 |
| Figure 5-42: Location of S-1A products acquired close to S1A vs RS-2 fly-bys, and status of RFI mitigation in 2023. | 101 |
| Figure 5-43: Potential locations of S-1A IW images at the time of close S1A vs GF-3-01 fly-bys in 2023..... | 103 |
| Figure 5-44: Potential locations of S-1A IW images at the time of close S1A vs GF-3-03 fly-bys in 2023..... | 103 |
| Figure 5-45: Location of S-1A products acquired close to S1A vs GF-3-01 fly-bys, and status of RFI mitigation in 2023. | 104 |
| Figure 5-46: Location of S-1A products acquired close to S1A vs GF-3-03 fly-bys, and status of RFI mitigation in 2023. | 104 |
| Figure 5-47: Residual RFI observed at time of fly-bys between S-1A and Gaofen-3-03 (most probably not due to Gaofen-3-03) | 105 |
| Figure 5-48: Locations of potential S1A vs RCM-1 RFI based on geometry (not associated to systematic acquisitions) | 107 |
| Figure 5-49: Locations of potential S1A vs RCM-2 RFI based on geometry (not associated to systematic acquisitions) | 107 |
| Figure 5-50: Locations of potential S1A vs RCM-3 RFI based on geometry (not associated to systematic acquisitions) | 108 |
| Figure 5-51: Location of S-1A products acquired close to S1A vs RCM-1 fly-bys, and status of RFI mitigation in 2023. | 108 |
| Figure 5-52: Location of S-1A products acquired close to S1A vs RCM-2 fly-bys, and status of RFI mitigation in 2023. | 109 |
| Figure 5-53: Location of S-1A products acquired close to S1A vs RCM-3 fly-bys, and status of RFI mitigation in 2023. | 109 |
| Figure 5-54: Examples of residual RFI observed close to S1A vs RCM-1 fly-bys in 2023 | 110 |
| Figure 5-55: Examples of residual RFI observed close to S1A vs RCM-3 fly-bys in 2023 | 110 |
| Figure 5-56: Locations of potential S1A vs EOS-4 RFI based on geometry (not associated to systematic acquisitions) | 112 |
| Figure 5-57: Location of S-1A products acquired close to S1A vs EOS-4 fly-bys, and status of RFI mitigation in 2023. | 112 |
| Figure 5-58: Examples of residual RFI observed close to S1A vs EOS-4 fly-bys in 2023 | 113 |
| Figure 5-59: Example of RFI believed to be from a satellite tracking station. Left nominal processing, Right with RFI mitigation process activated (as for nominal production of Sentinel-1 data since 22 nd March 2022). Sentinel-1A product acquired on 09/09/2021, orbit 39609, datatake 04AEA5..... | 115 |
| Figure 5-60: Example of long RFI patterns stopping close to the limit of intervisibility between Sentinel-1A and a tracking station in Houston, USA with an elevation of 5 degrees. All products being from Sentinel-1A unit acquired in 2016 and 2017..... | 116 |
| Figure 6-1: Effects of IPF update from 3.5.2 to 3.6.1 on the incidence and elevation angle dependent SAR wind speed bias with respect to ECMWF for the data sets concerned. ... | 118 |
| Figure 6-2: Effects of IPF update from 3.6.1 to 3.6.2 on SAR wind speed bias with respect to ECMWF as functions of the incidence and elevation angle. | 119 |
| Figure 6-3: Mean SAR wind speed bias with respect to ECMWF model detailed by sub-swath along time for the DV polarization acquisitions. (Top: general trend, bottom: zoom on the trend curves)..... | 120 |



| | |
|-----------------------------------------------------------------------------------------------------------------------------------------------------------------------------------------------------------------------------------------------------------------------------------------------------------------------------------------------------------------------------------------------------------------------------------------------------------------------------------------------------------------------|-----|
| Figure 6-4: Mean SAR wind speed bias with respect to NCEP model detailed by sub-swath along time for the DV polarization acquisitions. (top: general trend, bottom: zoom on the trend curves)..... | 121 |
| Figure 6-5: SAR wind speed standard deviation with respect to ECMWF model detailed by sub-swath along time for the DV polarization acquisitions. (Top: general trend, bottom: zoom on the trend curves)..... | 121 |
| Figure 6-6: SAR wind speed standard deviation with respect to NCEP model detailed by sub-swath along time for the DV polarization acquisitions. (Top: general trend, bottom: zoom on the trend curves)..... | 122 |
| Figure 6-7: Ebuchi diagrams for S-1A SAR retrieved and ECMWF wind directions detailed by wind speed domain in December 2023..... | 122 |
| Figure 6-8: Scatter plots of SAR vs ECMWF wind speeds for Wave Modes in Dec. 2023, for S-1A. | 123 |
| Figure 6-9: Ebuchi diagrams for S-1A SAR retrieved and ECMWF wind directions detailed by wind speed domain in December 2023..... | 123 |
| Figure 6-10: Coverage map of S-1 WV acquisition..... | 124 |
| Figure 6-11: Scatter plot of <i>oswWindSpeed</i> as respect to ECMWF 0.125 (3h) left: S-1A WV1, right: S-1A WV2..... | 125 |
| Figure 6-12: Difference in ocean surface wind speed between <i>oswWindSpeed</i> (S-1 WV OCN variable) and ECMWF numerical model (0.125° spatial resolution grid and 3-hours for time resolution). Bold line is the daily mean of the individual measurement differences and the background colour is the daily standard deviation..... | 125 |
| Figure 6-13: Distribution of the ocean surface wind direction, respectively <i>oswWindDirection</i> S-1 WV OCN variable and ECMWF numerical model (0.125° spatial resolution grid and 3-hours for time resolution). | 126 |
| Figure 6-14 : ocean surface wind direction bias: <i>oswWindDirection</i> S-1 WV OCN variable compared to ECMWF numerical model (0.125° spatial resolution grid and 3-hours for time resolution) as function of Time. | 126 |
| Figure 6-15 Top left: scatter plot of the <i>oswTotalHs</i> from L2 OCN WV1 products compared (and collocated) to CFOSAT nadir beam (product CMEMS WAV TAC L3). Top right: Same but with WV2. Bottom: SWH bias between S-1 WV1/2 versus different altimetric missions (j3: Jason-3, cfo: CFOSAT SWIM, al: SARAL-AltiKa, c2: Cryosat-2) from CMEMS WAV product. | 128 |
| Figure 6-16: scatter plot of effective significant wave height computed on the whole spectra S-1 WV OCN and associated WW3 spectra. Top left: S-1A WV1, top right: S-1A WV2. | 129 |
| Figure 6-17: Daily difference of SAR effective azimuth + range 2D cut-off Hs and WW3 numerical model Hs (using same spectral cut-off domain). For each sensor, on the upper panel the bold line is the daily mean of the individual measurement differences, and the background colour is the daily standard deviation. On the lower panel the colour indicates the number of available matchups between WV (20 km by 20 km) S-1 acquisitions and WW3 spectra computed at the nearest 0.5° resolution grid point..... | 130 |
| Figure 6-18 : Partition quality flag occurrence for both S1A-WV1 and S1A-WV2 for the year 2023. | 131 |
| Figure 6-19: Partition effective Hs performance on partitions flagged with “very good” and “poor” class for both WV1 and WV2. | 132 |
| Figure 6-20 : Partitions wavelength performance on partitions flagged with “very good” and “poor” class for both WV1 and WV2. | 133 |
| Figure 6-21 : Partitions wave directions performance on partitions flagged with “very good” and “poor” class for both WV1 and WV2..... | 134 |



Figure 6-22: Figures of OSW wave partitions performances with respect to WW3 numerical model. The lines represent the mean bias for each wave partition quality flag. Minimum distance to coast is 100km. To avoid ice contamination: $-55^\circ < \text{latitude} < 55^\circ$. Left column is WV1 (24° incidence angle), right is WV2 (37° incidence angle). A): Significant wave height B): Peak wavelength, C): Peak wave direction..... 136

Figure 6-23: Daily mean S-1A WV OCN Doppler frequency (rvlDcObs) for January 2023 (upper) and December 2023 (lower). 140

Figure 6-24: Scatterplot of of S-1A WV1 OCN RVL Doppler frequency (rvlDcObs) versus ECMWF range wind speed acquired over global ocean areas. Upper: January 2023, Lower: December 2023, Left: Swath WV1, Right: Swath WV2 141

Figure 6-25: Example of S-1B IW DC showing jumps in both Level 2 OCN Dc (left) and Level 0 IPF Dc (right). 142

Figure 6-26: Another example of IW DC jumps
(S1A_IW_OCN__2SDV_20191023T171202_20191023T171227_029589_035E66_FF1F.SAFE)
..... 143



LIST OF TABLES

| | |
|--------------------------------------------------------------------------------------------------------------------------------------------------------------------------------------------------------------------------------------------------------------------|-----|
| Table 1: Average noise power measured during December 2023. The value in parenthesis is the average noise power measured during December 2022. | 56 |
| Table 2: Azimuth and slant-range spatial resolution for S-1A derived for IW mode | 59 |
| Table 3: S-1A IW Sidelobe Ratios..... | 60 |
| Table 4 : Mean value, standard deviation and absolute radiometric accuracy derived from DLR targets (transponders and corner reflectors) for IW mode DV polarization (VV+VH) acquired over DLR’s calibration site in 2023 for S-1A. | 62 |
| Table 5 : Mean value and standard deviation of the absolute calibration factor for IW mode with V-polarization on transmit derived from acquisitions over the DLR calibration site in 2023. | 63 |
| Table 6: Mean value and standard deviation of derived RCS from the Australian Corner Reflectors | 65 |
| Table 7 : Summary of IW SLC product ALE estimates for S-1A for all 2023 acquisitions over the <i>Surat Basin</i> calibration site with the post-processing corrections. | 68 |
| Table 8 : Summary of IW SLC product ALE estimates for S-1A for all 2023 acquisitions over the <i>Geodetic Observatory</i> calibration sites (Wettzell, Metsähovi, Yarragadee, Côte d’Azur) with the post-processing corrections. | 68 |
| Table 9 : Summary of IW SLC product ALE estimates for S-1A and S-1B for all acquisitions since October 2016 over the <i>Surat Basin</i> calibration site with the post-processing corrections. | 69 |
| Table 10 : Summary of IW SLC product ALE estimates for S-1A and S-1B for all acquisitions since October 2016 over the <i>Geodetic Observatory</i> calibration sites (Wettzell, Metsähovi, Yarragadee, Côte d’Azur) with the post-processing corrections. | 70 |
| Table 11: Summary of IW SLC product ALE estimates for S-1A for all 2023 acquisitions over the <i>Surat Basin</i> calibration site without the post-processing corrections. | 75 |
| Table 12: Summary of IW SLC product ALE estimates for S-1A for July to December 2023 acquisitions over the <i>Surat Basin</i> calibration site with <i>ETAD</i> post-processing corrections. | 76 |
| Table 13: Gain Imbalance using the DLR transponders. | 78 |
| Table 14: Phase Imbalance using the DLR transponders. | 79 |
| Table 15: Polarimetric Calibration Measurements..... | 79 |
| Table 16: Cross-talk Measurements | 80 |
| Table 17: Percentage of products for which the RFI mitigation was activated for cycles 280 to 307 per mode and polarisation..... | 95 |
| Table 18: Sentinel-1 and Radarsat-2 Orbit characteristics..... | 100 |
| Table 19: Summary of Sentinel-1A vs Radarsat-2 RFI mitigation in 2023 | 101 |
| Table 20: Sentinel-1 and GAOFEN 3 Orbit Characteristics. | 102 |
| Table 21: Summary of Sentinel-1A vs Gaofen-03 mitigation in 2023 | 105 |
| Table 22: Sentinel-1 and RCM 1/2/3 Orbit Characteristics..... | 106 |
| Table 23: Locations of potential S1A vs RCM 1/2/3 mutual RFI due based on geometry. The observation of RFI is not systematic (requiring that both spacecraft are operating at the same time and that the RFI mitigation in the processing is not sufficient). | 106 |
| Table 24: Summary of Sentinel-1A vs RCM RFI mitigation in 2023 | 111 |
| Table 25: Sentinel-1 and RISAT-1A (EOS4) Orbit Characteristics | 111 |
| Table 26: Summary of Sentinel-1A vs EOS-4 mitigation in 2023 | 113 |

Table 27: Effective significant wave height performances (w.r.t.) WW3 model in meter for S-1 WV swell partitions depending on the swell partition quality flag..... 137

Table 28: Peak wavelength performances (w.r.t.) WW3 model in meter for S-1 WV swell partitions depending on the swell partition quality flag 138

Table 29: Dominant wave direction performances (w.r.t.) WW3 model in degree for S-1 WV swell partitions depending on the swell partition quality flag 138



1. Introduction

1.1 Purpose of this document

The purpose of this document is to provide the status on the S-1 constellation instruments and products performance during year 2023.

1.2 Document organisation

The outline of this report is given below:

- Chapter 1: This introduction
- Chapter 2: Executive Summary
- Chapter 3: Processing Updates
- Chapter 0: Instrument Status
- Chapter 5: Level 1 Product Status
- Chapter 6: Level 2 Product Status

The following appendices are also provided:

- Appendix A - S-1A & S-1B Technical Reports
- Appendix B - S-1A Instrument Unavailability
- Appendix C - S-1A & S-1B Quality Disclaimers
- Appendix D - S-1A Orbit Cycles
- Appendix E - S-1A Transmit Receive Module Failures
- Appendix F - S-1A & S-1B Auxiliary Data Files

1.3 Applicable and Reference Documents

1.3.1 Applicable Documents

- [AD-01] Sentinel-1 Product Specification, S1 RS-MDA-52-7441, SAR-MPC-0240, Issue 3/14.1, October 2023
- [AD-02] Sentinel-1 Level 1 Detailed Algorithm Definition, SEN-TN-52-7445, SAR-MPC-0307, Issue 2/5 November 2022
- [AD-03] Sentinel-1 IPF Auxiliary Product Specification, S1-RS-MDA-52-7443, SAR-MPC-0241, Issue 3/11/1, Octobre 2023
- [AD-04] Sentinel-1 Doppler and Ocean Radial Velocity (RVL) ATBD, ISSN 1890-5226, MPC-0534, Issue 01.6, October 2022
- [AD-05] Sentinel-1 Ocean Wind Fields (OWI) ATBD, MPC-0469 DI-MPC-IPF-OWI, Issue 02.2, October 2022
- [AD-06] Sentinel-1 Ocean Swell Wave Spectra (OSW) ATBD, S1-TN-NRT-52-7450, MPC-0469, DI-MPC-IPF-OSW, Issue 01.6, 12 October 2022
- [AD-07] Annual Performance Report 2022, DI-MPC-APR-0588, Issue 1.1, March 2023
- [AD-08] Sentinel-1 Level-2 Ocean Processor, Main ATBD, DI-MPC-LOP-MPC-0583, Issue 1.1, October 2022

- [AD-09] S1-ETAD Product Format Specification Document, ETAD-DLR-PS-0014, Issue 1.9, November 2023
- [AD-10] S1-ETAD Algorithm Technical Baseline Document, ETAD-DLR-DD-0008, Issue 2.3, November 2023
- [AD-11] S1 Extended Timing Annotation (ETAD) - Auxiliary Product Specification Document, ESA-EOPG-CSCOP-TN-80, Issue 1.18, November 2023
- [AD-12] S1-ETAD Product Definition Document, ETAD-DLR-PS-0002, Issue 2.4, March 2023
- [AD-13] S-1 Product Definition Document, S1-RS-MDA-52-7440, DI-MPC-PB, MPC-0239, issue 2.7, March 2016 <https://sentiwiki.copernicus.eu/attachments/1673968/S1-RS-MDA-52-7440%20-%20Sentinel-1%20Product%20Definition%202016%20-%20202.7.pdf>

1.3.2 Reference Documents

The following documents provide useful reference information associated with this document. These documents are to be used for information only. Changes to the date/revision number (if provided) do not make this document out of date.

- [S1-RD-01] Nuno Miranda, Peter Meadows, Riccardo Piantanida, Andrea Recchia, David Small, Adrian Schubert and Pauline Vincent, ‘The Sentinel-1 Constellation Performance Status: 2019 Update’, Proceedings of the CEOS SAR Workshop, November 18-22, 2019, ESA/ESRIN, Frascati, Italy.
- [S1-RD-02] Peter Meadows, David Small, Adrian Schubert and Nuno Miranda, ‘Sentinel-1 Radiometric and Geometric Calibration’, Proceedings of the CEOS SAR Workshop, November 18-22, 2019, ESA/ESRIN, Frascati, Italy.
- [S1-RD-03] Guillaume Hajduch, ‘Mutual Interferences between C-Band SAR: Prediction of occurrences identification of sources’, Proceedings of the CEOS SAR Workshop, November 18-22, 2019, ESA/ESRIN, Frascati, Italy
- [S1-RD-04] Medhavy Thankappan, Matthew Garthwaite, Christoph Gisinger, Adrian Schubert, Peter Meadows, Nuno Miranda, ‘Improvements to the position coordinates for the Australian corner reflector array and new infrastructure to support SAR calibration and multi-technique validation at the Yarragadee fundamental geodetic station’, Proceedings of the CEOS SAR Workshop, December 5-7, 2018, Buenos Aires, Argentina.
- [S1-RD-05] Schubert A., D. Small, N. Miranda, D. Geudtner, E. Meier. Sentinel-1A Product Geolocation Accuracy: Commissioning Phase Results. Remote Sens. 2015, 7, 9431-9449. doi: 10.3390/rs70709431.
- [S1-RD-06] Schubert A., D. Small, N. Miranda, D. Geudtner, E. Meier. Sentinel-1A Product Geolocation Accuracy: Beyond the Calibration Phase. Presented at CEOS SAR Calibration & Validation Workshop; Noordwijk, The Netherlands, 2015.
- [S1-RD-07] GMES Sentinel-1 Team. GMES Sentinel-1 System Requirements Document, Ref. S1-RS-ESA-SY-0001, Iss. 3, Rev. 3, 2010.
- [S1-RD-08] Rodriguez-Cassola M. et al., Doppler-related distortions in TOPS SAR images, IEEE Trans. Geosci. Remote Sens. 2015, 53, 25-35.
- [S1-RD-09] Piantanida R., A. Recchia, N. Franceschi., A. Valentino, N. Miranda, A. Schubert, D. Small, Accurate Geometric Calibration of Sentinel-1 Data, Proc. EUSAR 2018, 63-68.
- [S1-RD-10] Schubert A., N. Miranda, D. Geudtner, D. Small, Sentinel-1A/B Combined Product Geolocation Accuracy. Remote Sensing 2017, 9, 1-16. doi: 10.3390/rs9060607

- [S1-RD-11] Small, D., A. Schubert. Guide to Sentinel-1 Geocoding, UZH technical note for ESA-ESRIN, UZH-S1-GC-AD, Issue 1.10, 26.03.2019; University of Zurich: Zurich, Switzerland, 42p.
- [S1-RD-12] Niccolo Franceschi, 'Cross Sensor Calibration of Sentinel-1 Noise Level', Proceedings of the CEOS SAR Workshop, November 18-22, 2019, ESA/ESRIN, Frascati, Italy
- [S1-RD-13] Moiseev, A., Johnsen, H., Johannessen, J. A., Collard, F., & Guitton, G. (2020). On removal of sea state contribution to Sentinel-1 Doppler shift for retrieving Reliable Ocean surface current. *Journal of Geophysical Research: Oceans*, 125, e2020JC016288. <https://doi.org/10.1029/2020JC016288>
- [S1-RD-14] Schwerdt M., K. Schmidt, N. Tous Ramon, G. Castellanos Alfonso, B. Döring, M. Zink, P. Prats. Independent Verification of the Sentinel-1A System Calibration. *IEEE J. Sel. Top. Appl. Earth Observ. Remote Sens.* 2016, 9, 994-1007. doi:10.1109/JSTARS.2015.2449239.
- [S1-RD-15] Schwerdt M., K. Schmidt, N. Tous Ramon, N., P. Klenk, N. Yague-Martinez, P. Prats-Iraola, M. Zink, and D. Geudtner. Independent System Calibration of Sentinel-1B, *Remote Sensing*, 9(6), 511, doi:10.3390/rs9060511, 2017.
- [S1-RD-16] Reimann, J., M. Schwerdt, K. Schmidt, N. Ramon, B. Döring. The DLR Spaceborne SAR Calibration Center. *Frequenz* 71, 619-627. doi:10.1515/freq-2016-0274, 2017.
- [S1-RD-17] Schmidt, K., N. Tous Ramon, M. Schwerdt. Radiometric Accuracy and Stability of Sentinel-1A Determined using Point Targets. *Int. J. Microw. Wirel. Technol.* 10, 538-546. doi:10.1017/S1759078718000016, 2018.
- [S1-RD-18] Schmidt K, M. Schwerdt, N. Miranda N, J. Reimann. Radiometric Comparison within the Sentinel-1 SAR Constellation over a Wide Backscatter Range. *Remote Sensing*. 2020; 12(5):854
- [S1-RD-19] A. M. Guarnieri, C. Albinet, A. Cotrufo, N. Franceschi, M. Manzoni, N. Miranda, R. Piantanida, A. Recchia. Passive sensing by Sentinel-1 SAR: Methods and applications, *Remote Sensing of Environment*, Volume 270, 2022.
- [S1-RD-20] A. Recchia, D. Giudici, R. Piantanida, N. Franceschi, A. Monti-Guarnieri and N. Miranda, "On the Effective Usage of Sentinel-1 Noise Pulses for Denoising and RFI Identification," *EUSAR 2018; 12th European Conference on Synthetic Aperture Radar*, 2018
- [S1-RD-21] C. Gisinger, L. Libert, P. Marinkovic, L. Krieger, L. Y. Larsen, A. Valentino A., H. Breit, U. Bals, S. Suchandt, T. Nagler, M. Eineder, N. Miranda, "The Extended Timing Annotation Dataset for Sentinel-1—Product Description and First Evaluation Results," in *IEEE Transactions on Geoscience and Remote Sensing*, vol. 60, pp. 1-22, 2022, doi: 10.1109/TGRS.2022.3194216.
- [S1-RD-22] T. Fuhrmann, J. Batchelor., T. McCall., M.C. Garthwaite. Positions and orientations for the Queensland corner reflector array, Australia: Report on geodetic surveys conducted in May and June 2018. RECORD 2020/034. Geoscience Australia, Canberra. doi 10.11636/Record.2020.034
- [S1-RD-23] B. Rommen, I. Barat, M. Chabot, C. Lambert and D. Williams, Joint Investigation on Radarsat-2 / Sentinel-1A Mutual RFI, Noordwijk, October 27 2015, https://calvalportal.ceos.org/html/portal/sarc/documents/documents/05_CEOS_S1A_RS_AT2_final.pdf
- [S1-RD-24] C. Gisinger, A. Schubert, H. Breit, M. Garthwaite, U; Bals, M. Willberg, D. Small. In-Depth Verification of Sentinel-1 and TerraSAR-X Geolocation Accuracy Using the Australian Corner Reflector Array," in *IEEE TGRS*, vol. 59, no. 2, pp. 1154-1181, Feb. 2021, doi: 10.1109/TGRS.2019.2961248
- [S1-RD-25] U. Bals, C. Gisinger, M. Eineder, H. Breit, A. Schubert, D. Small, Survey Protocol for Geometric SAR Sensor Analysis, April 28, 2018, https://calvalportal.ceos.org/documents/10136/11045/FRM4SAR_TN200_Site_Survey_Protocol_Definition_V1_4.pdf

- [S1-RD-26] H. Peter and M. Fernández, Sentinel-1 Full Mission Reprocessing 2021, GMV-CPOD-MEM-0052 v1.1, 2021, <https://sentinel.esa.int/documents/247904/3455957/Sentinel-1-C-POD-Full-Mission-Reprocessing-2021-v1.1.pdf>
- [S1-RD-27] K. Schmidt, M. Schwerdt, G. Hajduch, P. Vincent, A. Recchia, M. Pinheiro. "Radiometric Re-Compensation of Sentinel-1 SAR Data Products for Artificial Biases due to Antenna Pattern Changes" in Remote Sensing, 15, 1377, 2023, doi: 10.3390/rs15051377.
- [S1-RD-28] C. Gisinger, G. Hajduch, M. Pinheiro, A. Valentino. "Update of S-1 Instrument Timing Calibration for ETAD ". SAR-MPC technical note, issue 1.2, 27.10.2023.
- [S1-RD-29] Balss, U., Gisinger, C., and Eineder, M. "Measurements on the Absolute 2-D and 3-D Localization Accuracy of TerraSAR-X", Remote Sensing, 10, pp. 1-21, 2018, doi: 10.3390/rs10040656
- [S1-RD-30] X. Collilieux, C. Courde, B. Fruneau, M. Aimar, G. Schmidt, I. Delprat, M. Defresne, D. Pesce, F. Bergerault, G. Wöppelmann, Validation of a corner reflector installation at Côte d'Azur multi-technique geodetic observatory, Advances in Space Research, Vol. 70, Iss. 2, pp. 360-370, 2022, doi: <https://doi.org/10.1016/j.asr.2022.04.050>
- [S1-RD-31] Kallio, U. et al. (2022). Datum Problem Handling in Local Tie Surveys at Wettzell and Metsähovi. In: Freymueller, J.T., Sánchez, L. (eds) Geodesy for a Sustainable Earth. International Association of Geodesy Symposia, vol 154. Springer, https://doi.org/10.1007/1345_2022_155
- [S1-RD-32] National Oceanic and Atmospheric Administration (NOAA), Solar Cycle Progression, Online Service of NOAA, accessed 2023/01/23: <https://www.swpc.noaa.gov/products/solar-cycle-progression>
- [S1-RD-33] European Centre for Medium-Range Weather Forecasts (ECMWF) Deterministic Atmospheric Model Products in GRIB format. Meteorological Bulletin M3.1. <http://www.ecmwf.int/sites/default/files/3.1.pdf>, section 4.2 Products in GRIB code
- [S1-RD-34] CMOD5.N: A C-band geophysical model function for equivalent neutral wind <https://www.ecmwf.int/en/elibrary/74795-cmod5n-c-band-geophysical-model-function-equivalent-neutral-wind>
- [S1-RD-35] Pinheiro, M., Valentino, A., Albinet, C., Hajduch, G., Vincent, P., Recchia, A., ... & Gisinger, C. (2023). Sentinel-1 instruments status, product performance and evolutions, CEOS SAR WG on Calibration and Validation
- [S1-RD-36] Sentinel-1 Interferometric Parameters Monitoring By SAR-MPC And Burst IDs In TOPS Products, Cotrufo Alessandro; Recchia, Andrea; Franceschi, Niccolo; Hajduch, Guillaume ; Vincent, Pauline ; Schmidt, Kersten ; et al, Fringe 2023, 11-15 September 2023 | University of Leeds <https://fringe2023.esa.int/iframe-agenda/files/presentation-251.pdf>
- [S1-RD-37] Meteo France, AROME model https://donneespubliques.meteofrance.fr/?fond=produit&id_produit=131&id_rubrique=51
- [S1-RD-38] Meteo France, ARPEGE model https://donneespubliques.meteofrance.fr/client/document/doc_arpege_pour-portail_20190827-249.pdf
- [S1-RD-39] NOAA National Centers for Environmental Prediction (NCEP). 2011, updated 2023. NOAA/NCEP Global Forecast System (GFS) Atmospheric Model. [2023]
- [S1-RD-40] "Status of the RADARSAT Constellation Mission in the Third Year of Operation," S. Cote, M. Lapointe, P. -P. Vezina, E. Arsenault, C. Casgrain and A. Boyer, EUSAR 2022; 14th European Conference on Synthetic Aperture Radar, Leipzig, Germany, 2022, pp. 1-6.

A set of technical documents, issued by S-1 Mission Performance Centre or more generally relevant with respect to this report, giving more information on the S-1A and S-1B products quality could also be cited as reference in this document and is available on the [Sentinel-1 Online Library](#). The full list is provided on Appendix A -

1.4 Acronyms and Definition

| | |
|-----------|----------------------------------------------------|
| AD | Applicable Document |
| ADF | Auxiliary Data File |
| ALE | Absolute Localisation Error |
| AOCS | Attitude and Orbit Control Systems |
| AUX ITC | Auxiliary Product Instrument Timing Calibration |
| AUX SCF | Auxiliary Product SETAP Configuration File |
| CFI | Customer Furnished Item |
| CP | Commissioning Phase |
| CSA / ASC | Canadian Space Agency / Agence Spatiale Canadienne |
| DC | Doppler Centroid |
| EAP | Elevation antenna Pattern |
| ECMWF | European Centre for Medium-Range Weather Forecasts |
| EFE | Electronic Front End |
| ENL | Equivalent Number of Look |
| ETAD | Extended Timing Annotation Dataset |
| FDBAQ | Flexible Dynamic Block Adaptive Quantisation |
| GMF | Geophysical Model Function |
| IRF | Impulse Response Function |
| IPF | Instrument Processing Facility |
| MTF | Model Transfer Function |
| NESZ | Noise Equivalent Sigma Zero |
| OWI | Wind component of OCN products |
| OSW | Swell component of OCN products |
| OCN | Sentinel-1 Level 2 product |
| PDGS | Payload Data Ground Segment |
| PG | Power x Gain |
| PSC | Permanent Scatterers Calibration |
| QD | Quality Disclaimer |
| QCSS | Quality Control SubSystem |
| (N)RCS | (Normalised) Radar Cross Section |
| Nv | Normalised Variance (of SAR image) |

| | |
|-------|-------------------------------------------------|
| RD | Reference Document |
| RDB | Radar DataBase |
| RFC | Radio Frequency Characterization mode |
| RFI | Radio Frequency Interference |
| RVL | Radial Velocity (component of OCN products) |
| S-1A | Sentinel-1A |
| S-1B | Sentinel-1B |
| SAR | Synthetic Aperture Radar |
| SETAP | Sentinel-1 Extended Timing Annotation Processor |
| SNR | Signal to Noise Ratio |
| STT | STar Tracker |
| TA | Tile Amplifier |
| TBC | To be confirmed |
| TBD | To be defined |
| TRM | Transmit Receive Module |

2.Executive Summary

This report gives the status of the Sentinel-1 instruments and product performance during year 2023.

During this period, Sentinel-1A was the only operated instrument due to end of end of the S-1B mission officially declared on the 3rd August 2022.

As will be seen in Chapter 3 (Processor Updates), Chapters 4 (Instrument Status), Chapters 5 (Level 1 Product Status) and Chapter 6 (Level 2 Product Status) many aspects of the Instrument Processing Facility (IPF), instrument and products are considered with the aim of ensuring users receive high quality products.

2.0 S1 IPF and Auxiliary Files

The S1 IPF is generating the Level 1 (SLC and GRD) products and the Level 2 (OCN) products.

On 30rd March 2023, the IPF was updated to IPF v3.6.1, with the following most relevant changes:

- Level 1 content:
 - Introduction of annotation in the manifest of L0 A / C / N products used during the processing.
 - Fix issue with products containing xsd files with execution permission.
 - Fix issue on quicklook from data overlapping the antemeridian
 - Avoid missing data in range denoising vectors annotations for TOPS GRD products on long data takes.
 - Enhance resilience of the SAR burst processing to data reception contingencies
- Level 2 content:
 - Introduction of L2 Quicklook for TOPS and SM products
 - Improvement of preview.html
 - Correction on land mask for products crossing the antemeridian.
 - Improvement of land mask using OpenStreetMap as source
 - Introduction of new osw global attribute and variables helping the data handling
 - Annotation as global NetCDF attribute of the status of the subprocess (osw/owi/rvl)
 - Change of RVL processing in the case without ERRMAT: usage of 1-exitiation coefficient instead of internal default Errmat
 - Usage of validity mask for rvlSnr variable
 - Implementation of a new algorithm for TotalHs computation

On 19th Octobre 2023, the IPF was upgraded to IPF v3.7.1, with the following most relevant changes:

- Level 1 content:
 - Ensure support of Sentinel-1C and Sentinel-1D data
 - Correction of annotation of ANX date in the manifest, aiming at solving issue of invalid burst ID annotations. Refer to quality disclaimer 115 and following ones.
 - Correction of impact of RFI on denoising vectors
 - Correction of annotation of line number of range denoising vectors for TOPS/SLC products (the azimuth time was correct). Refer to quality disclaimers 117 and 118.
- Level 2 content:
 - No change compared to IPF v3.6.1

2.1 SETAP and Auxiliary Files

The SETAP processor is generating the Extended Timing Annotation Dataset Products (ETAD).

In July 2022, the SETAP IPF v2.0.0 was introduced to S-1 ground segment production service and a test phase based on systematic generation of ETAD products started. At this stage, the ETAD products were

not disseminated but utilized for SAR-MPC internal purposes and pilot studies. Based on integration, operations, interface, and product evaluation experiences in the test phase, change requests for the next SETAP version were collected and implemented in the next SETAP version.

On 10th March 2023, the SETAP IPF was upgraded to version v2.1.0. This version was evaluated in full-scale operations and greenlighted on 21st of July for final operational production and product dissemination. The production started with a set of first version of AUX_SCF and AUX_ITC auxiliary files. The most relevant changes are:

- Implementation of burst ID annotation in the ETAD product
- Update of the AUX TEC product naming convention
- Evolution of SETAP to support datatake level sampling grid consistency even in case of independent single-slice-based ETAD product generation.
- Correction of ETAD product manifest file content
- Accommodate revision of the AUX ITC product internal parameter structures

On 30th November 2023, the SETAP processor was upgraded to version 2.20, with the following most relevant changes:

- Fix for a rare footprint error in KML for bursts over equator.
- Add reference to AUX_SCF in the manifest.
- Initial support of S-1C and S-1D input products
- Fix quality flags for TEC maps exceeding limits.
- Improve handling of SLC products generated in NRT Slicing Mode
- Improve management of GRIB2 data of ECMWF (use newer version of ecCode library and support unsorted grib files)

The ETAD products can be accessed from the Copernicus Data Space Ecosystem. It must be noticed that only the SM and IW ETAD products are validated. The EW ETAD products are experimental and not validated.

Since the start of operational production of ETAD products, there was no changes in the configuration of the SETAP processor. Early versions of the auxiliary files (AUX_SCF and AUX_ITC) were prepared for validation and are available on the SAR-MPC website [HERE](#) for ITC and [HERE](#) for SCF. The changes are as follows:

- On 30th March, the new auxiliary files AUX_ITC and AUX_SCF of SETAP were introduced and circulated, see specification [AD-11].
- On 12th of April, updated versions of S-1A AUX ITC and S-1B AUX ITC were circulated which contain the latest instrument timing calibration data as determined in the S-1 instrument re-calibration activity performed in March 2023 [S1-RD-28].
- On 25th July 2023, ETAD auxiliary product specification document [AD-11] was updated and made publicly accessible. The latest version accommodates the specification of AUX ITC and AUX SCF.

2.2 Instrument Status

The analysis of RFC and Internal Calibration products shows that S-1A instrument is stable. No major instrument events have been recorded during 2023. No quality degradation associated to issues which happened in previous years is observed in S-1 products.

The analysis of Noise products shows that the instrument noise level is stable.

The monitoring of burst synchronization error and baseline has been extended to consider a check w.r.t the previous cycle. This is in addition to the checks performed so far which consider a reference cycle in the beginning of the mission. The baseline remained below 10% of the critical value (5 km for the normal baseline), and the values of the burst synchronization error are within +/- 15 ms.

S-1A Doppler-Centroid (DC) is showing jumps on the order of 30 Hz, with peaks of 50 Hz, when the STT configuration changes. The issue is continuously monitored and, in case the DC jumps get worse, this could lead to the execution of a new STT alignment campaign during 2024.

RFI mitigation was activated with IPF 3.5.1 on 23rd March 2022. However, some strong RFI contamination events have been observed during 2023. RFI contamination has no permanent effect on the instrument but reduces the quality of affected data takes introducing radiometric artefacts. For these strong events, the IPF mitigation strategy remains not effective.

Sentinel-1B instrument is unavailable since the 23rd December 2021.

For each instrument parameter under scrutiny, long term plots have been added to describe the evolution of the system from the mission start until the end of 2023.

2.3 Level 1 Product Status

The various image quality parameters such as spatial resolution, sidelobe parameters, equivalent number of looks and ambiguity ratios derived from distributed target or using DLR transponders & corner reflectors (CRs), and the Australian corner reflector array all give nominal results.

The radiometric performance of S-1A has been monitored and the radiometric accuracy has been determined for IW mode DV polarization using point targets of the DLR calibration site. During 2023, the overall mean and standard deviation for the absolute calibration factor has been derived to be $-0.04 \text{ dB} \pm 0.2 \text{ dB}$ which includes the observation of both polarizations (VV and VH) and all three sub-swathes (IW1, IW2, and IW3). Including all error contributions, an absolute radiometric accuracy for the IW mode of 0.331 dB (1σ) could be verified. Furthermore, the radiometric performance has been monitored using CRs over Australia [S1-RD-22] evaluating IW mode acquisitions with HH and VV polarization. For each target and each polarization channel. The low variation ($\leq 0.20 \text{ dB}$) found for both polarization channels and all targets confirm the high radiometric stability. Furthermore, a small offset between HH and VV of 0.15 dB has been found for IW2.

The channel imbalance in amplitude and phase for dual-pol channels has been derived from DLR transponder measurements. In average, the VV polarization channel shows slightly higher values than the VH polarization channel with remaining biases of 0.15 dB . The phases are also well balanced with remaining biases below 2 degrees. The co-registration of the IRF peaks for both polarizations show deviations below 0.1 m in average. The crosstalk of S-1A derived from DLR corner reflector measurements are in average -39.4 dB which confirms the very good quality concerning the separation of the co- and cross polarization channels of both SAR instruments.

- Geolocation accuracy was assessed considering well-surveyed corner reflectors at Surat Basin site (Australia), and at several geodetic observatories located in Finland [S1-RD-29], France [S1-RD-30], Germany [S1-RD-29], and Australia [S1-RD-22]. Both out-of-the box accuracy (i.e., using the L1 SLCs as is without performing any post-processing correction) and best achievable accuracy (i.e., performing a set of corrections to remove instrument and geophysical biases and using the S-1 precise orbit products) have been tested. Complementary long-term results are also provided for S-1 mission as of October 2016, i.e., the operational introduction of the S-1B unit.

The out-of-the box geolocation accuracy for S-1A measured at Surat Basin site during 2023 is:

| | |
|--------------|------------------------------|
| S-1A: Range: | $-3.565 \pm 0.369 \text{ m}$ |
| Azimuth: | $2.124 \pm 0.857 \text{ m}$ |

The best achievable geolocation accuracy for S-1A measured at Surat Basin site during 2023 is (long-term results for comparison):

S-1A: Range: 0.059 ± 0.058 m (-0.006 ± 0.059 m)
Azimuth: -0.140 ± 0.292 m (-0.138 ± 0.291 m)

The best achievable geolocation accuracy for S-1A measured at Geodetic Observatories during 2023 is (long-term results for comparison):

S-1A: Range: 0.057 ± 0.052 m (0.025 ± 0.054 m)
Azimuth: -0.130 ± 0.335 m (-0.057 ± 0.354 m)

The ALE estimates at the different sites for IW mode confirm a consistent localisation performance well within the requirements. All ALE results are within the specified 1σ of 3.33m, i.e. 10m at 3σ (section 5.5.2.2 of [S1-RD-07]). An average residual range bias of 0.06m has been observed in the best achievable geolocation results of 2023, which is attributed to limitations of the applied ionospheric path delay correction due to currently increased solar activity.
S1-RD-07

A few examples of radio frequency interference occurred during 2023 from (i) sources on the ground (ii) unknown source(s) causing long-duration interference, (iii) the Chinese GAOFEN 3 C-Band SAR satellite and the Canadian RCM Constellation C-Band SAR also causing long-duration interferences.

2.4 ETAD Product Status

Operational production and dissemination of the new Extended Timing Annotation Dataset (ETAD, [AD-09, AD-12]) for S-1 have started in 2023. ETAD products as of July 21st are now available in the Copernicus Data Space Ecosystem. The generation is nominally performed by S-1 ground segment for level 1 SM and IW products and at an experimental level for the EW products as well.

Product quality have been validated by comparing nominal geolocation results with the results applying only ETAD data. Comparable results are expected since ETAD contains all post-processing corrections in a comprehensive package. The best achievable geolocation accuracy with ETAD products for S-1A measured at *Surat Basin* site [S1-RD-21] during 2023 is:

S-1A: Range: 0.075 ± 0.059 m
Azimuth: -0.144 ± 0.289 m

Overall range and azimuth geolocation results with ETAD are in very close agreement with the nominal 2023 geolocation results obtained at *Surat Basin* site [AD-07]. A nearly identical range bias has been measured in the ETAD geolocation results because it applies same methods to calculate the ionospheric delay corrections. The spread in azimuth is due to the coarse azimuth resolution of IW products and the sub-swath variation of IW data that is an inherent characteristic of S-1A, which limits attainable geolocation accuracy in azimuth. Therefore, product performance as measured at *Surat Basin* calibration site [S1-RD-21] is considered in agreement with the ETAD correction specification of 0.2 m range and 0.1 m azimuth (1σ , [AD-12]). Improvements to ETAD products will be studied in 2024 to address the limitations of current ionospheric delay correction and to possibly mitigate the sub-swath characteristics of S-1A.

2.5 Level 2 Product Status

2.5.1 Wind (OWI)

No major changes occurred in 2023 on performance for OWI products on TOPS, WV and SM modes. 2023 represents a remarkably stable year in terms of wind speed performances, apparently unaffected by neither IPF nor auxiliary file changes, which could make it a reference year for further investigation. SAR wind retrieval performances remain within ± 0.25 m/s bias and between 1.5 and 1.75 m/s Root Mean Square Error for IW products in DV polarization with respect to ECMWF atmospheric reanalysis [S1-RD-33].

2.5.2 Swell (OSW)

The OSW product is produced from WV and SM modes. However, for SM the number of acquisitions is too small to perform any geophysical validation. The S-1 WV OSW wave spectra are systematically validated against global collocated WW3 spectra.

Current performances of wave parameters provided in the OSW component allow to address scientific applications related to physics of oceans. It is particularly true because of the large number of WV acquisitions since 2014, also because the acquisition plan covering all open oceans and despite the lack of a full mission reprocessed dataset, ocean users have now a 2-years long period without quality change.

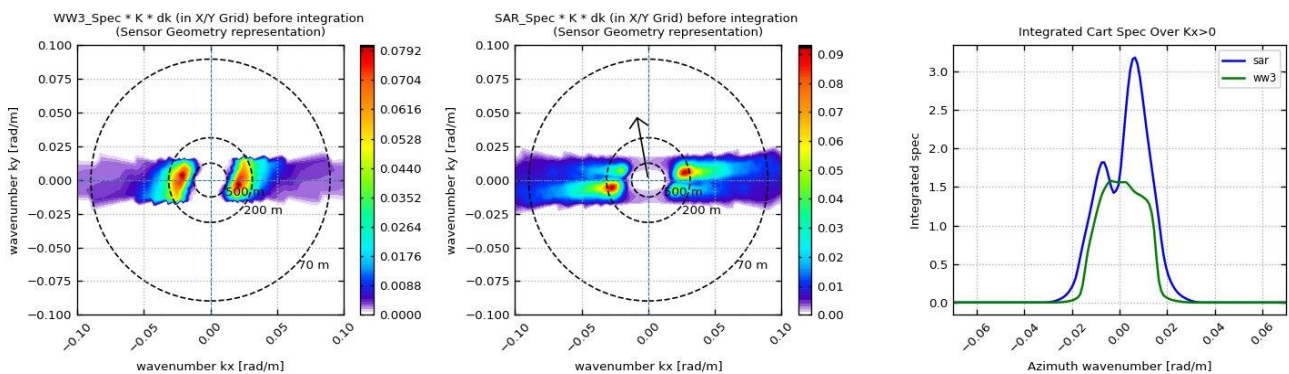
Some issues are identified on OSW component, but all of them are now addressed by MPC group

[08/08]:

MTF and range splitting:

The problem identified is clearly illustrated in the following two figures. Depending on the satellite heading, we observe a splitting of the SAR spectral energy in the range dimension with respect to the model. This is mainly due to poor MTF compensation. All our efforts are focused on finding this fault and correcting it in the MTF.

OCN : s1a-wv2-ocn-vv-20230101t034014-20230101t034017-046584-05952f-126.nc
S1 Wind Speed : 15.56 m/s, Heading: 349.72977°



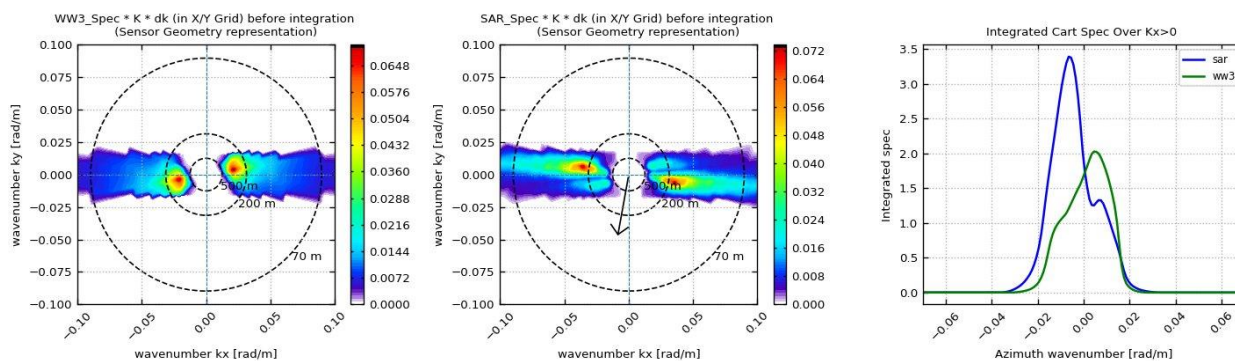


Figure ... : SAR energy is splitted along the range axis. On the Top, a case of ascending heading and on the bottom, a case of descending heading. For each figure, from right to left: the pre-integrated WW3 swell spectrum, the pre-integrated SAR swell spectrum and the integrated spectrums along the range dimension for both WW3 and SAR.

swell directions inverted in some cases, wavenumber grid error, The OSW partitions Quality Flag (QF) is used to qualify the 2D ocean wave spectrum partitioning performances into five categories: "very good", "good", "medium", "low", and "poor". New diagnostics carried out over a longer period of WV acquisition show no particular anomalies in the spatial distribution of the different categories.

On the 7th June 2022, the *oswTotalHs* variable started to be populated in L2 OCN products, based on Deep-Learning model approach [AD-06]. This variable is an "altimetric like" significant wave height. The Inputs of the model are SAR polar image cross spectrum (real and imaginary) plus high-level features: incidence angle, longitude, latitude, NRCS, Normalized variance, etc. The performances are assessed with collocated data from altimeters, and show good agreement aligned with specification of RMSE<0.5 m and bias<0.1 m (considering the same target performances as the one for SAR Significant Waveheight per partition as defined in [AD-13]). However, a little overestimated bias (~5 cm) could be observed on WV2 compared to altimeter while WV1 is underestimated (~10 cm). The accuracy and precision of *oswTotalHs* and its standard deviation should continue to be improved in the future (especially for acquisitions in strong sea states).

As for the wind sea Hs (*oswWindHs*), the current algorithm of the Sentinel-1 OSW processor attempts to estimate the geophysical feature from the SAR measurements, even if it is not well imaged by the instrument, based on inherited empirical relationship between SAR-derived wind speed, azimuth cut-off and WW3 wind sea Hs. The current retrieval suffers from the limitation of the azimuth cut-off. A new algorithm is currently being developed to better manage these limitations and improve Hs wind sea estimation.

Investigations over 2D SAR ocean wave spectra have identified an issue in the distribution of spectral energy along the range axis. The behaviour is more pronounced at higher wind speeds for WV2 than for WV1. Initial results show that improvements to the existing MTF are needed to correct this behaviour and improve the inversion scheme.

2.5.3 Radial Velocity (RVL)

The Sentinel-1 Level 2 Doppler centroid anomaly (DCA) and radial velocity (RVL) measurements are currently coloured by the AOCs derived Doppler frequency. The predicted Doppler centroid (DC) frequency computed from the downlinked quaternions does not reflect the actual DC frequency as measured by the SAR. This prevents the current version of the Level 2 processor to provide calibrated DCA and RVL estimates. However, promising results are achieved off-line using an estimated attitude from calibrated Gyro data and WV DC data. A post-processing approach has been implemented as part of the "Copernicus Sentinel-1 RVL Assessment" project. The results have been shown during 2022 Living Planet Symposium (talk entitled "Towards Calibrated Sentinel-1 OCN RVL Products").

For some IW and EW products, a sudden jump in DC ($>10\text{Hz}$) is still observed from one burst to another over all swaths. The investigations suggest that these jumps come from temperature compensation which subsequently alters the antenna characteristics. It is now assumed that temperature compensation may also create DC jumps between WV imageries. Moreover, another kind of jumps was observed for TOPS products, coming from the L0 to L1 (internal SL2) IPF processing whose modification is under consideration. There is at present no simple means to predict when and where these two types of jumps occur.

It is planned for 2024 to release a separated RVL calibrated dataset. The calibration strategy will be based on the post-processing approach derived in the past and a local DC bias computed from DC values over land in order to reduce the impact of jumps as much as possible. At the same time, longer-term investigations are continuing to properly detect and quantify the DC jumps due to temperature compensation.

3. Processing Updates

The main improvements introduced in the Level-1 and Level-2 Processor and impacting data quality are described below, classified according to the release in which they have been included.

The full details of IPF upgrades including date of usage and content description of the different IPF versions are available on <https://sar-mpc.eu/ipf/>

3.0 SAR Processor

3.0.1 IPF 3.7.1 (from 19/10/2023)

Level 1 content:

- Ensure support of Sentinel-1C and Sentinel-1D data
- Correction of annotation of ANX date in the manifest, aiming at solving issue of invalid burst ID annotations. Refer to quality disclaimer 115 and following ones.
- Correction of impact of RFI on denoising vectors
- Correction of annotation of line number of range denoising vectors for TOPS/SLC products (the azimuth time was correct). Refer to quality disclaimers 117 and 118.

Level 2 content:

- No change compared to IPF v3.6.1

3.0.2 IPF 3.6.1 (from 30/03/2023 to 19/10/2023)

Level 1 content:

- Introduction of annotation in the manifest of L0 A / C / N products used during the processing.
- Fix issue with products containing xsd files with execution permission.
- Fix issue on quicklook overlapping the antemeridian
- Avoid missing data in range denoising vectors annotations for TOPS GRD products on long data takes.
- Enhance resilience of the SAR burst processing to data reception contingencies

Level 2 content:

- Introduction of L2 Quicklook for TOPS and SM products
- Improvement of preview.html
- Correction on land mask for products crossing antemeridian.
- Improvement of land mask using OpenStreetMap as source
- Introduction of new osw global attribute and variables helping the data handling
- Annotation as global NetCDF attribute of the status of the subprocess (osw/owi/rvl)
- Change of RVL processing in the case without ERRMAT: usage of 1-excitation coefficient instead of internal default Errmat
- Usage of validity mask for rvlSnr variable
- Implementation of a new algorithm for TotalHs computation

3.1 SETAP Processor

3.1.1 SETAP 2.20 (from 30/11/2023)

On 30th November 2023, the SETAP processor was upgraded to version 2.20, with the following most relevant changes:

- Fix footprint error in KML for bursts over equator
- Add reference to AUX_SCF in the manifest.
- Initial support of S-1C and S-1D
- Fix quality flags for TEC maps exceeding limits.
- Improve handling of SLC products generated in NRT Slicing Mode
- Improve management of grib data (use newer version of ecCode library and support unsorted grib files)

3.1.2 SETAP 2.10 (from 21/07/2023 to 30/11/2023)

On 21st July 2023, the SETAP processor was deployed in version 2.10 as first operational version. The production started with a set of first version of AUX_SCF and AUX_ITC auxiliary files. The changes are:

- Implementation of burst ID annotation in the ETAD product
- Update of the AUX TEC product naming convention
- Evolution of SETAP to support datatake level sampling grid consistency even in case of independent single-slice-based ETAD product generation
- Correction of ETAD product manifest file content
- Accommodate revision of the AUX ITC product internal parameter structures

The ETAD products can be accessed from the Copernicus Data Space Ecosystem.

Since the start of operational production of ETAD products, there was no changes in the configuration of the SETAP processor. Early versions of the auxiliary files (AUX_SCF and AUX_ITC) were prepared for validation and are available on the SAR-MPC website [\[HERE\]](#) for ITC and [\[HERE\]](#) for SCF.

3.2 Auxiliary Data Files

In addition to the described L1 and L2 Processor upgrades, and the SETAP processor upgrade, a summary of Auxiliary Data Files (ADFs) updates during the reporting period is provided, together with an explanation of the updates, in Appendix F - .

The main ones are summarised below:

3.2.1 AUX_INS

AUX_INS provides information on Instrument configuration required by the Sentinel-1 L1 processor. This configuration is provided separately for S-1A and S-1B.

No update of AUX_INS was performed during 2023.

3.2.2 AUX_CAL

AUX_CAL provides configuration required by the Sentinel-1 L1 processor for radiometric calibration. This configuration is provided separately for S-1A and S-1B.

No update of AUX_CAL was performed during 2023.

3.2.3 AUX_PP1

AUX_PP1 provides configuration required by the Sentinel-1 L1 processor to activate specific processing parameters. This configuration is provided separately for S-1A and S-1B.

No update of AUX_PP1 was performed during 2023.

3.2.4 AUX_PP2

AUX_PP2 provides configuration required by the Sentinel-1 L2 processor to activate specific processing parameters. This configuration is provided separately for S-1A and S-1B.

No update of AUX_PP2 was performed during 2023.

3.2.5 AUX_SCS

AUX_SCS provides Simulated Cross Spectra required by the Sentinel-1 L2 processor. This configuration is the same for both S-1A and S-1B.

No AUX-SCS update was performed in 2023.

3.2.6 AUX_ITC

AUX_ITC provides the Instrument Timing Correction required by the SETAP processor.

During 2023, two updates of AUX_ITC were performed for both S-1A and S-1B.

The first update was performed on 30th March 2023 corresponding to the first operational version of the configuration and with a timing offset set to zero, matching the calibration status as of August 2022.

The second update was performed on 06th April 2023 and aiming to update the S-1A specific range and azimuth reference timing correction. The reference values were determined during the re-calibration activity summarized in [S1-RD-28].

3.2.7 AUX_SCF

AUX_SCF provides configuration required by the SETAP processor for its execution. This configuration is the same for both S-1A and S-1B.

During 2023, there was only one publication of AUX_SCF corresponding to the first operational version of the processor. No further update was required.

4. Instrument Status

Hereafter, the status of the S-1A instruments during 2023 is described:

4.0 RFC Monitoring

The S-1A Antenna status is routinely monitored using products acquired in the dedicated RFC calibration mode. The RFC products are processed to generate the Antenna Error Matrix, from which it is possible to retrieve the failure and drift of each TRM.

4.0.1 Antenna Status

Figure 4-1 shows the S-1A antenna Transmit/Receive Module (TRM) average status during December 2023. The images represent the gain (4 images on the left) and phase (4 images on the right) deviation with respect to the nominal antenna status, measured from the first in-orbit acquisitions in April 2014. One image for each TX/RX mode and polarization combination is shown. No relevant changes in the S-1A antenna status occurred during 2023. Ten (10) failures (happened before 2023) are counted in total among TX-RX and H-V corresponding to the antenna elements marked with a “F” in the images. The figure also shows that half of tile 11 (TRMs from 1 to 10 in both polarizations) is transmitting with reduced power (about -13 dB) and with a phase offset (about -30 degrees) since an antenna issue occurred in June 2016. In October 2017 the tile 11 was electronically reconfigured to improve the status of its TRMs still transmitting at full power (TRMs from 11 to 20 in both polarizations). The most recent S-1A antenna significant event occurred on 04/01/21, when the TRM on tile 7 and row 7, both in TxH and RxH, suffered a small gain reduction and phase jump with no noticeable impact on data quality. The loss is about 1 dB in TX and 3 dB in Rx for H-pol channel. No major events have been observed in 2023.

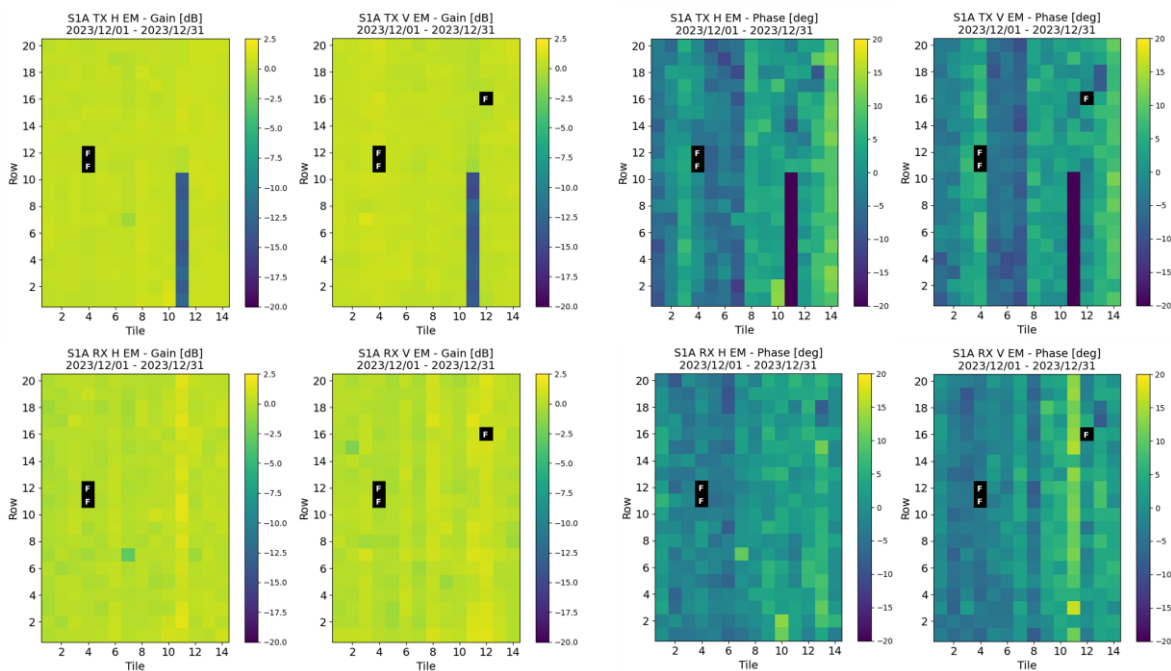


Figure 4-1: S-1A antenna status: gain (left) and phase (right) deviation of the TRMs from the nominal status. The white “F” marks the failed antenna elements.

4.0.2 TRM Trends

The plots from Figure 4-2 to Figure 4-5 show the evolution in time of the TX and RX excitation coefficients, averaged per tile, obtained processing the RFC products of 2023.

The overall TRMs behaviour is quite stable. Seasonal fluctuations, related to the instrument temperature, can be observed for the TX phase. The RX gain and phase coefficients are more affected by the thermal compensation performed on board, but their trend is stable for all the tiles. S-1A tile 11 TX gain shows a reduced power (close to -4 dB) due to the antenna issue occurred in June 2016.

Plots like the ones discussed are shown in Figure 4-6 to Figure 4-9 over a period ranging from the mission start until the end of 2023. The reduced number of measurements in the centre of the plots is due to the eclipse season.

Those long terms plots highlight

- Successive failures of tile 5 between 2014-10-18 and 2015-07-21 and documented in the quality disclaimers number 2, 5 to 9, 12, 13 and 15.
- The failure of part of Tile 11 in 2016, partially recovered by activation of redundancy.

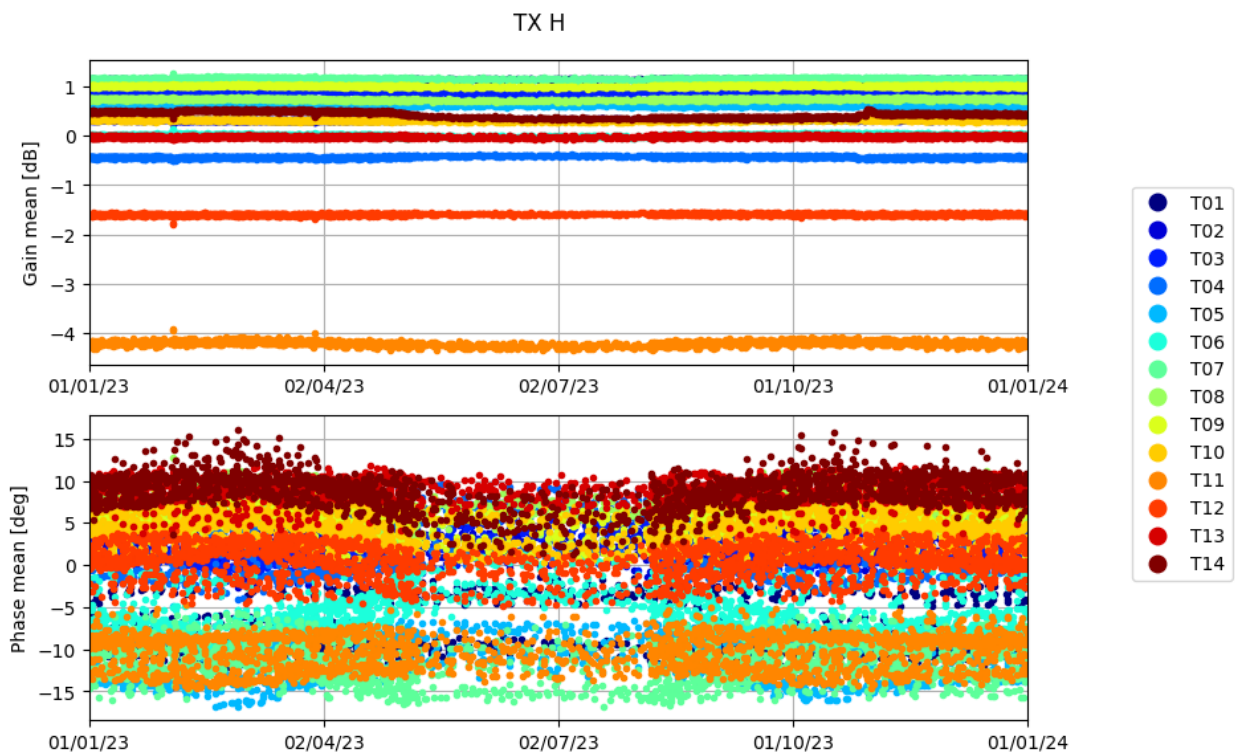


Figure 4-2: Gain (*top*) and phase (*bottom*) stability of the S-1A SAR antenna tiles: average of the RFC coefficients in TX H over rows.

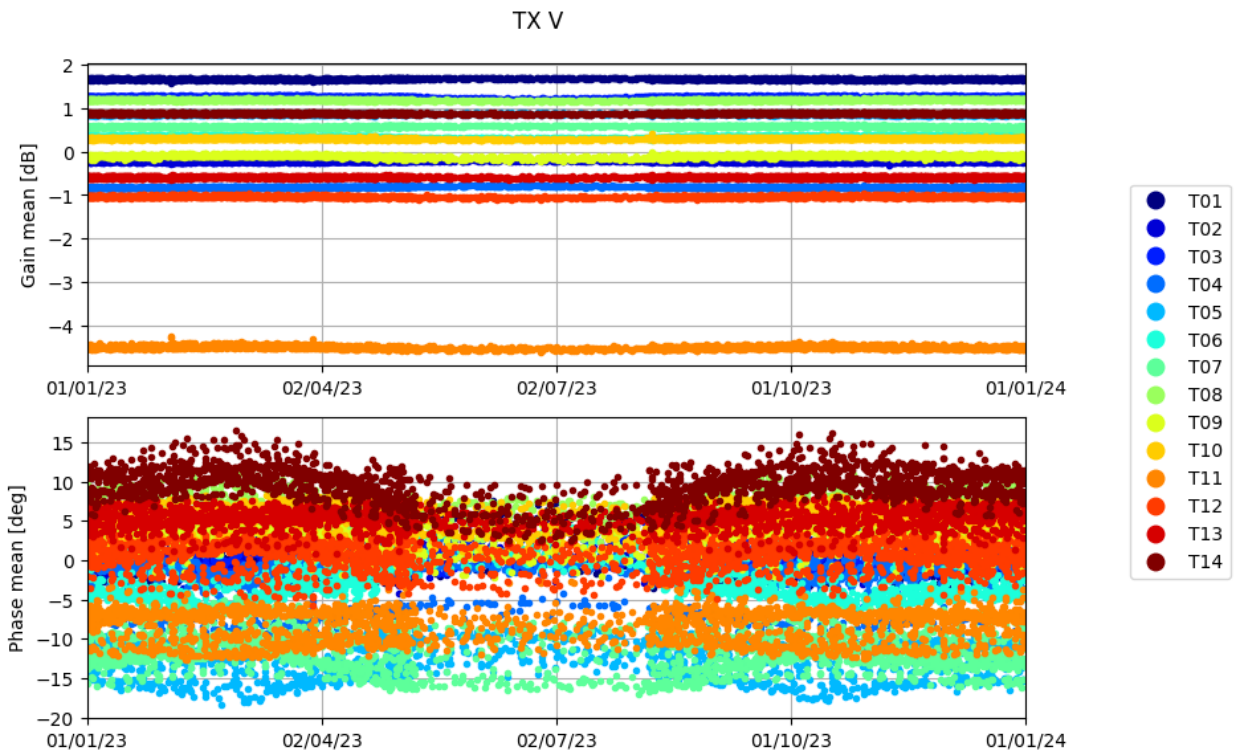


Figure 4-3: Gain (top) and phase (bottom) stability of the S-1A SAR antenna tiles: average of the RFC coefficients in TX V over rows.

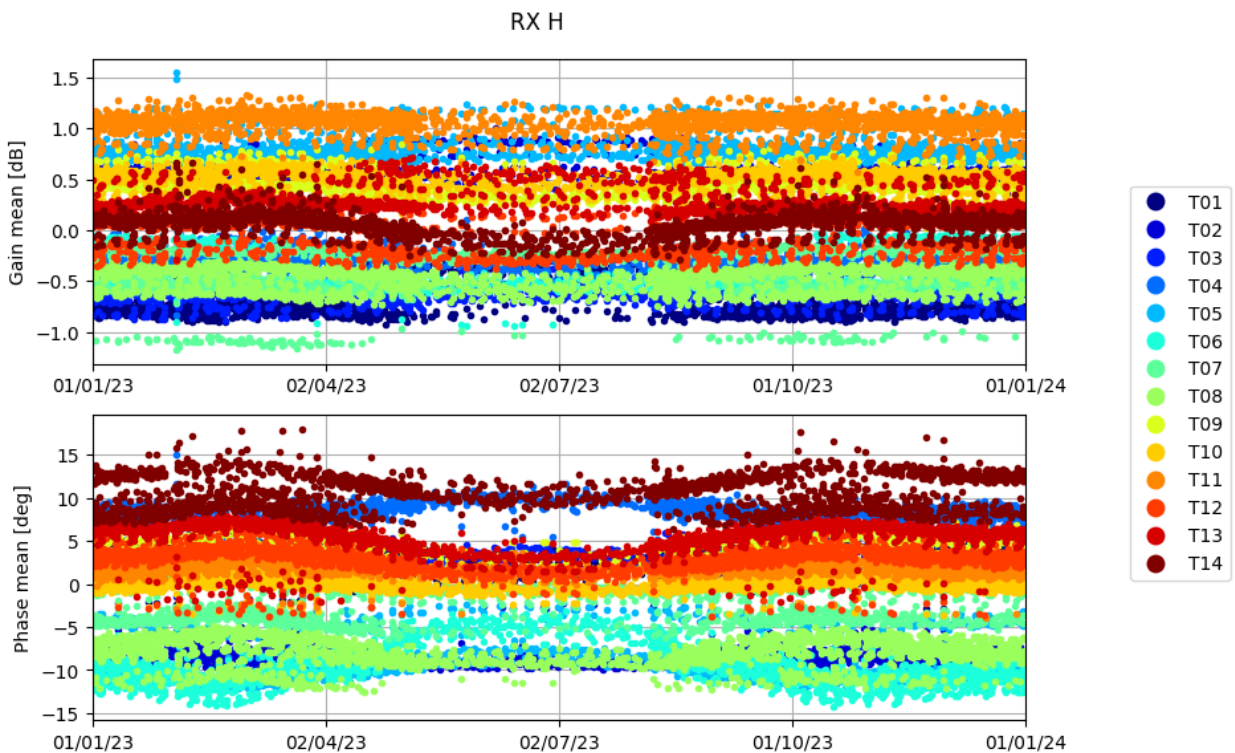


Figure 4-4: Gain (top) and phase (bottom) stability of the S-1A SAR antenna tiles: average of the RFC coefficients in RX H over rows.

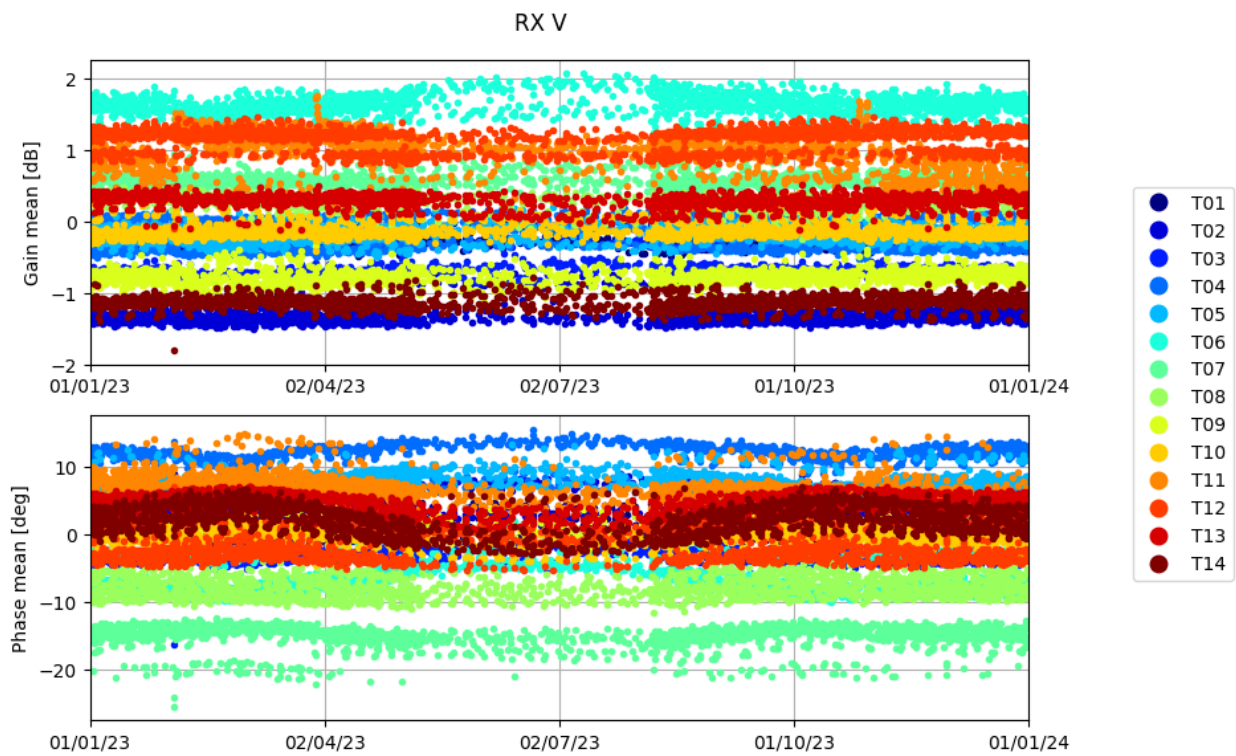


Figure 4-5: Gain (top) and phase (bottom) stability of the S-1A SAR antenna tiles: average of the RFC coefficients in RX V over rows.

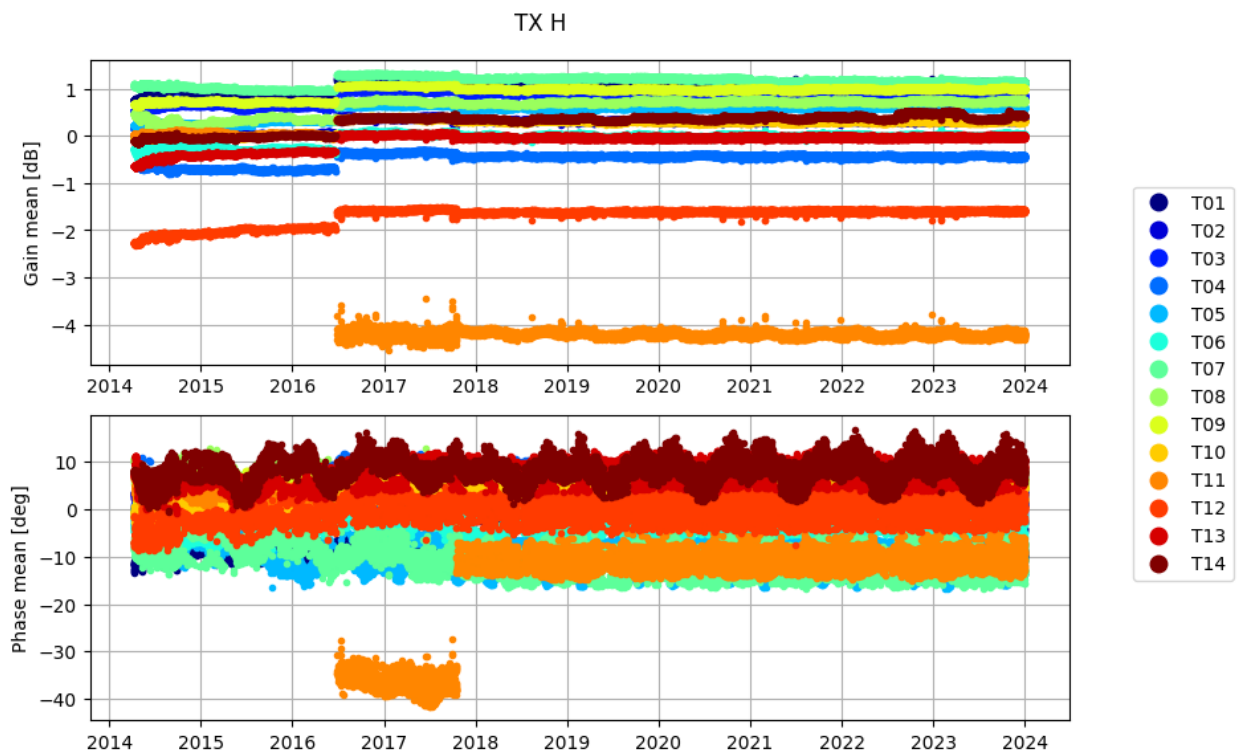


Figure 4-6 S-1A tiles average gain (top) and phase (bottom) in TX mode and H polarization, plotted from the mission start to the end of 2023.

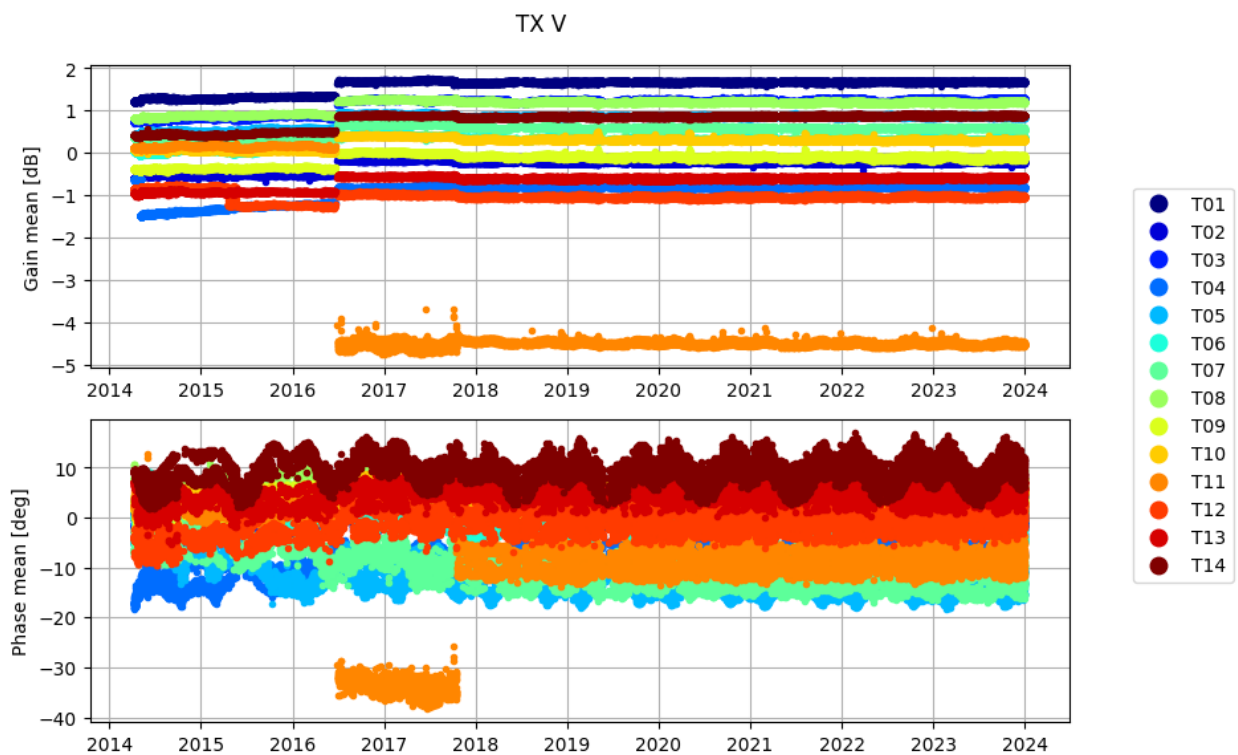


Figure 4-7 S-1A tiles average gain (top) and phase (bottom) in TX mode and V polarization, plotted from the mission start to the end of 2023.

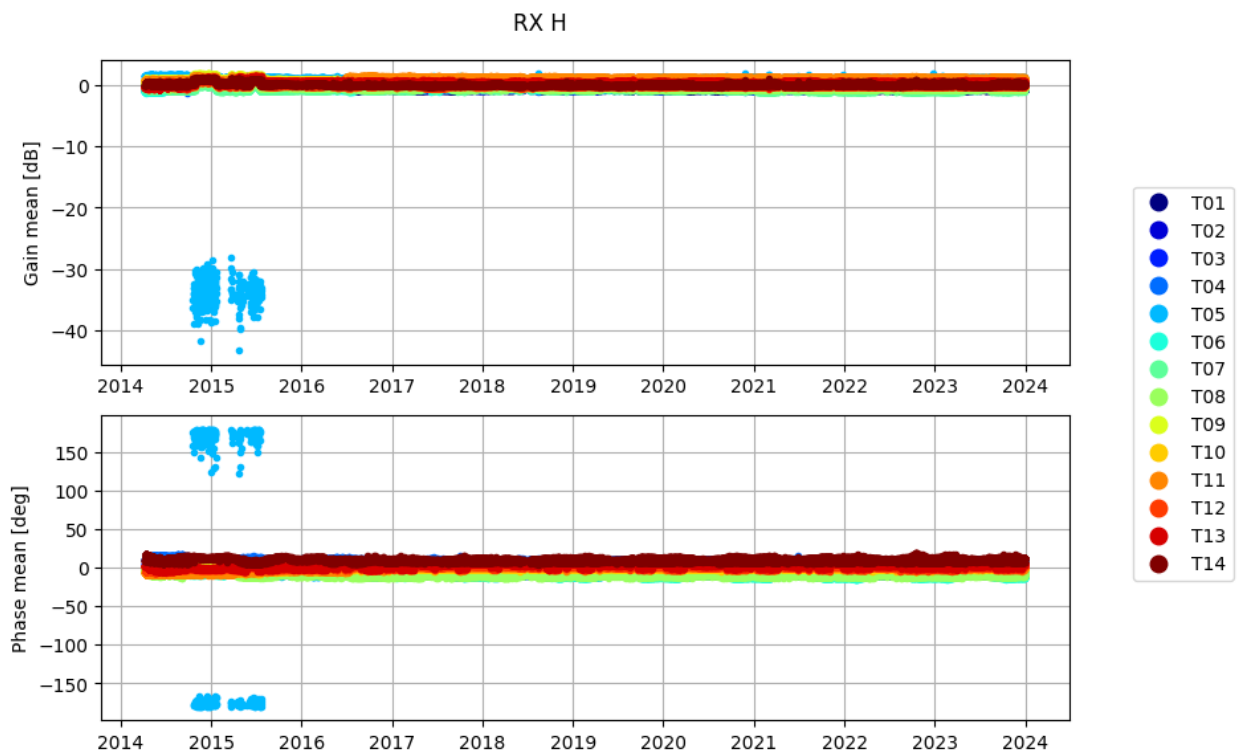


Figure 4-8 S-1A tiles average gain (top) and phase (bottom) in RX mode and H polarization, plotted from the mission start to the end of 2023.

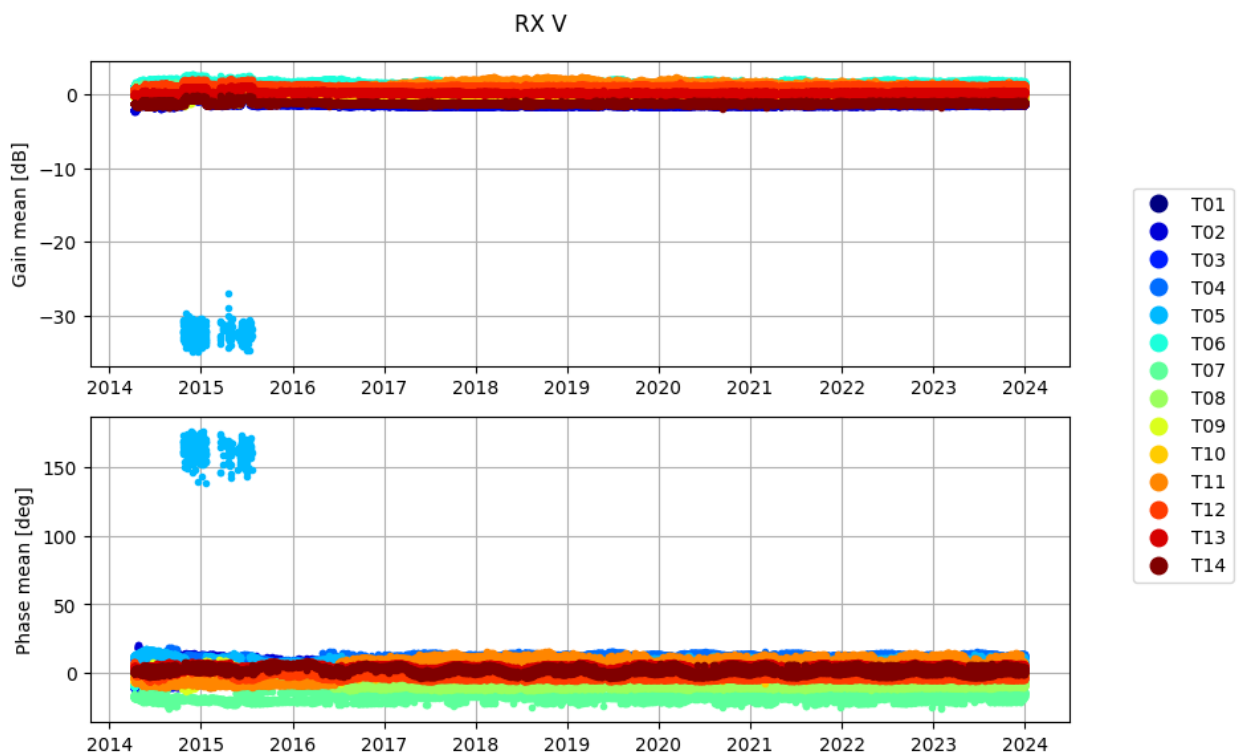


Figure 4-9 S-1A tiles average gain (top) and phase (bottom) in RX mode and V polarization, plotted from the mission start to the end of 2023.

4.1 Instrument temperature

The S-1 instrument temperature is monitored through the information annotated in the header of the SAR Space Packets. Figure 4-10 shows the evolution of the temperature of the different antenna elements (Electronic Front End modules and Tile Amplifiers) during 2023 for S-1A. The low temperature spikes observed in the plots correspond to the instrument switch-off events or reduction of number of acquisitions at a given date.

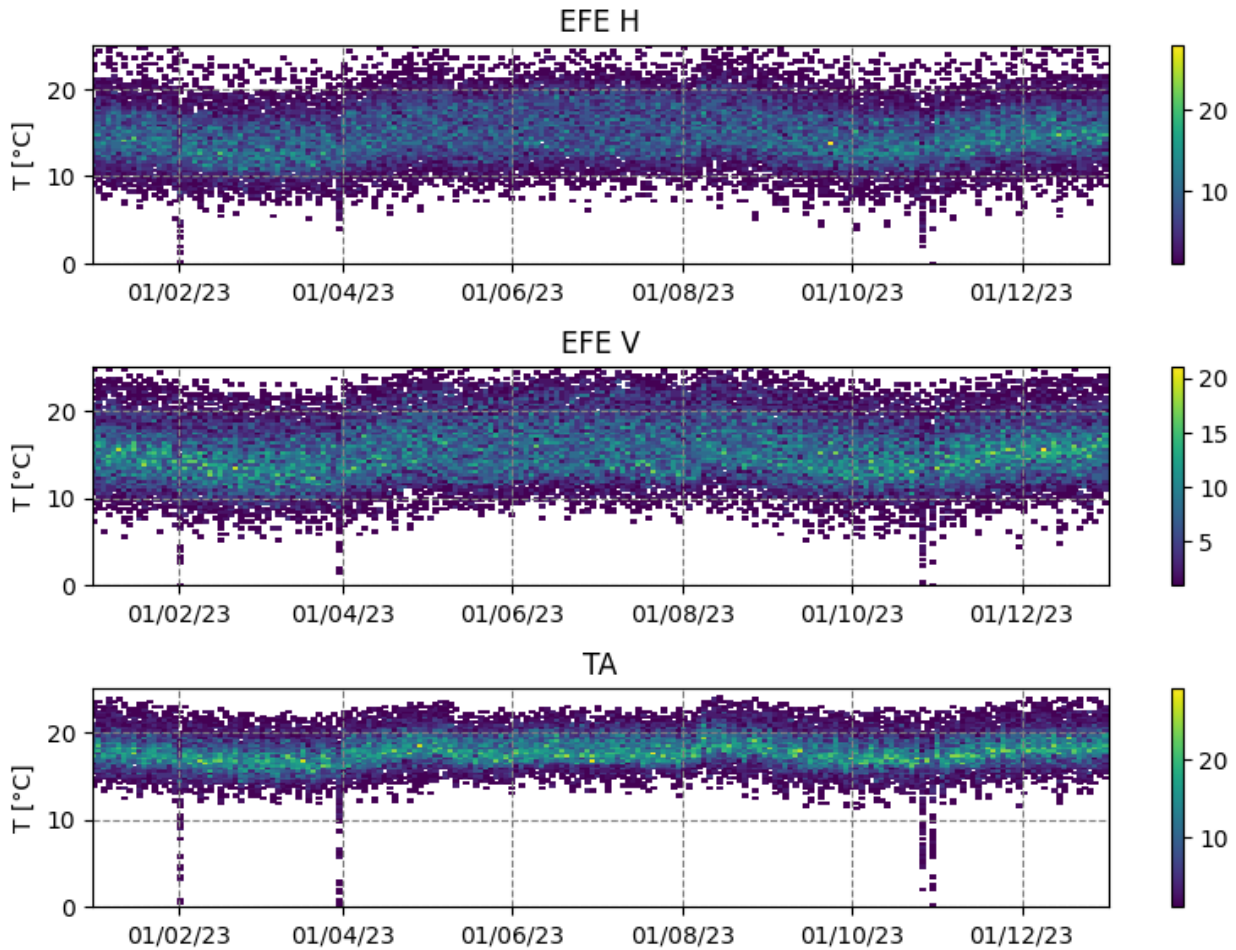


Figure 4-10: S-1A temperature evolution during 2023 for Electronic Front Elements (EFEs) and Tile Amplifiers (TAs).

Figure 4-11 shows the variation of the temperature of the different antenna elements as a function of the data takes duration for S-1A. The colours represent the different acquisition modes and polarizations. For long data takes (up to 15 minutes) the EFE temperature can increase up to 10 degrees and the TA temperature up to 6 degrees. This behaviour is expected, and the effects are compensated automatically on board.

2023/01/01 - 2023/12/31

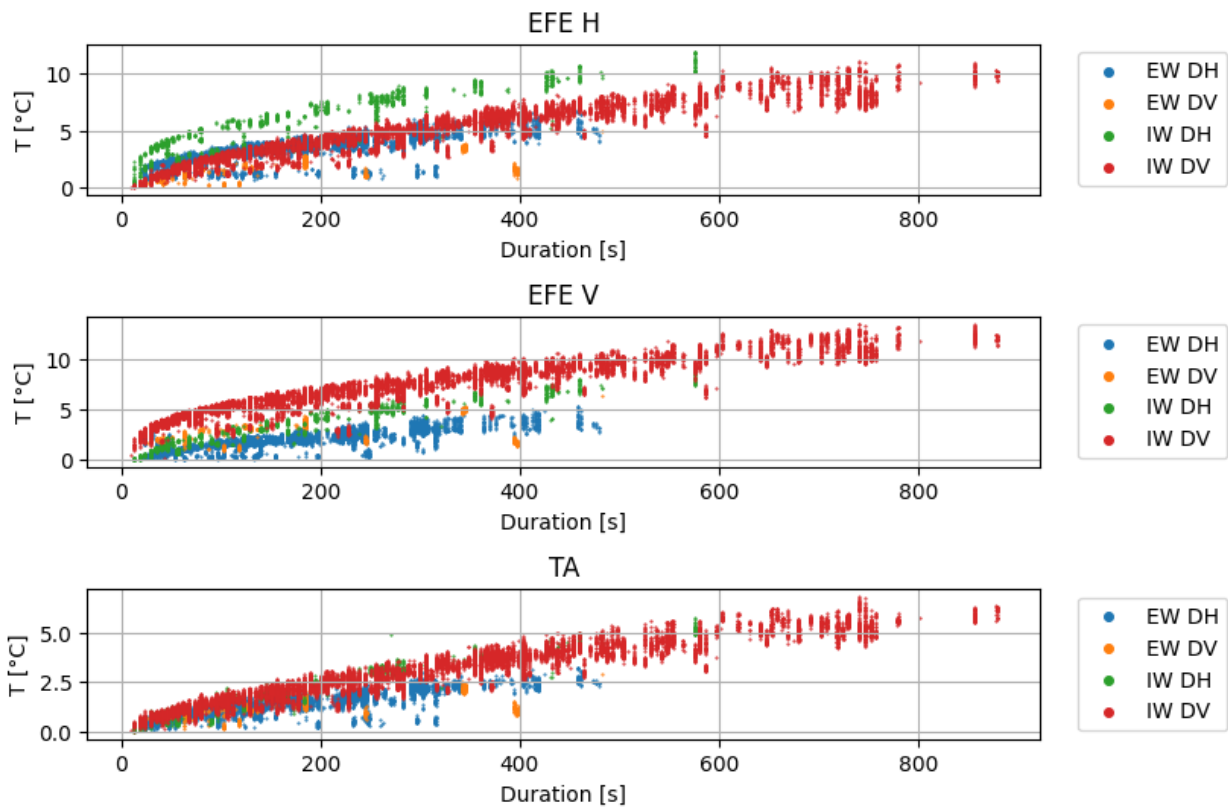


Figure 4-11: Antenna elements temperature evolution as function of acquisition duration, in 2023.

Figure 4-12 and Figure 4-13 show temperature monitoring plots similar to the ones discussed, showing the system behaviour from the mission start until the end of 2023. Figure 4-12 shows that the temperature trend of the antenna elements is quite stable from about 2017 until today. The progressive increase of temperature since mission start up to end of 2017 is due to the progressive increase of instrument duty cycle.

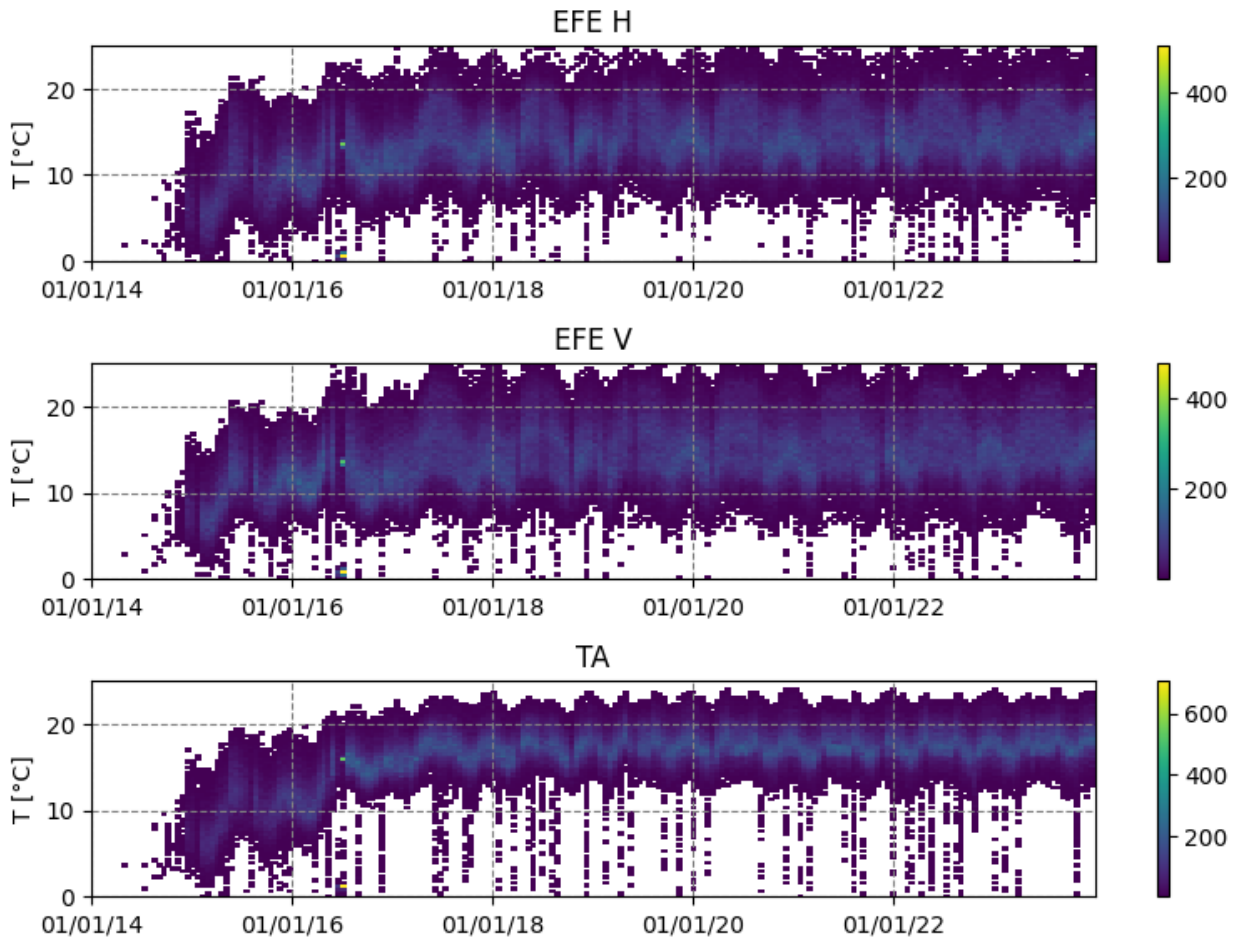


Figure 4-12 S-1A temperature evolution from mission start to 2023 for Electronic Front Elements (EFEs) and Tile Amplifiers (TAs).

2014/04/25 - 2023/12/31

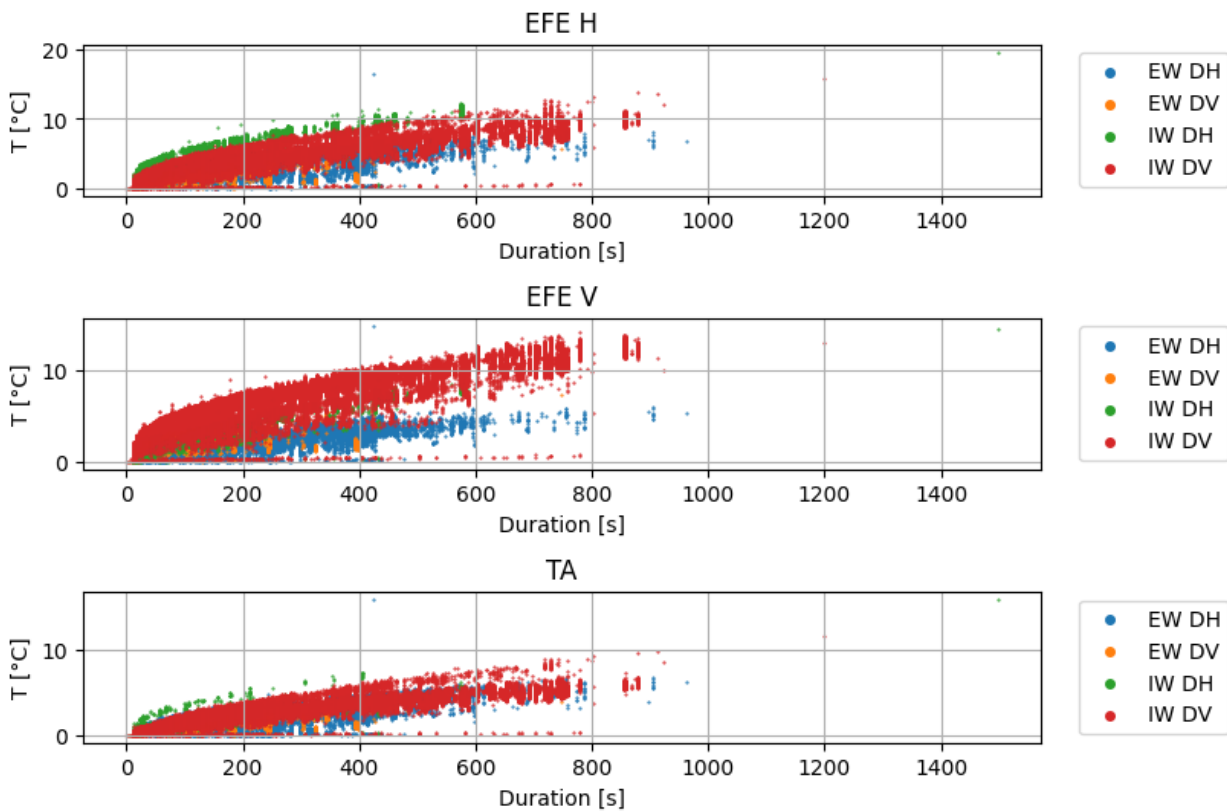


Figure 4-13 Antenna elements temperature evolution as function of acquisition duration, from mission start to 2023.

4.2 Internal Calibration

The S-1A instrument stability over time is monitored through the acquisition of internal calibration signals, which are used to obtain measurements of PG products (Transmit Power - Receive Gain products). The PG products are exploited to compensate for the instrument gain fluctuations to maintain the requested radiometric stability of the data. The PG values are measured using chirp parameters of the first sub-swath for each acquisition mode. The dependency on different sub-swaths is added a posteriori by means of a proper multiplication factor, which, in dB, becomes an additive constant in between plots of different sub-swaths.

The IPF performs an evaluation of the PG values to establish whether they are suited for drift compensation. Namely, measured PG values are compared to a fixed “PG model” value (extracted from a LUT, changing with sub-swath and polarization), and they are discarded if their difference exceeds a given threshold. If the percentage of discarded PG measurements is too high, the IPF discards all PG values altogether and used the PG model value instead for drift compensation. Therefore, in this monitoring we compare the current PG model values with the measured PG distribution.

The PG is monitored separately for each sub-swath and polarization, as shown from Figure 4-14 to Figure 4-17. For a given sub swath and polarization, the PG ideally follows a gaussian distribution at a given point in time and is affected by a seasonal trend along the year. For a given polarization and acquisition mode (IW or EW), the PG trends in time from different sub-swaths are expected to follow the same trend up to a constant offset.

Only plots for IW DV and EW DH are shown, as other polarizations for IW and EW have a lower number of calibration products, hence the visual inspection of their plots is less significant.

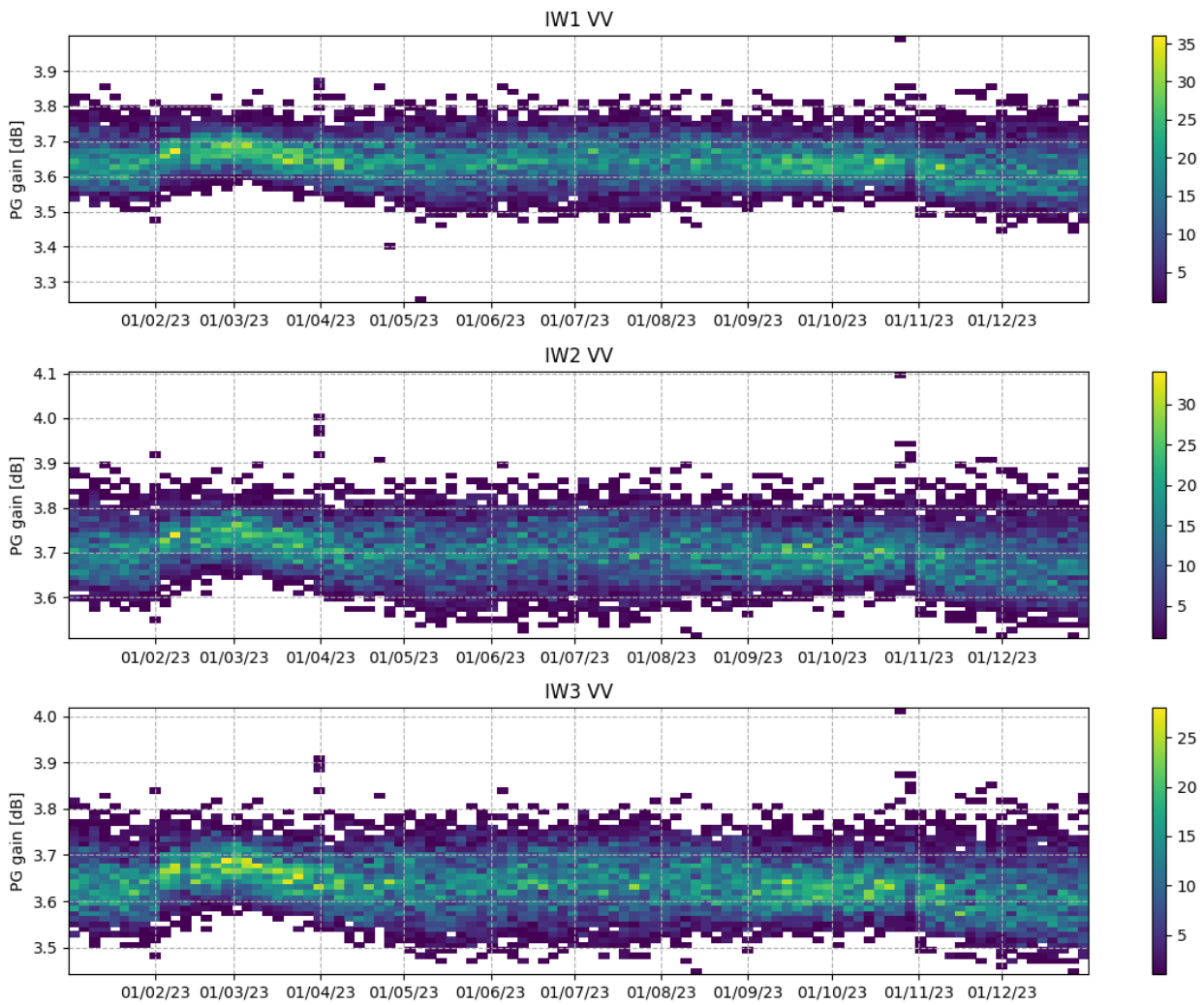


Figure 4-14 PG trend in time for IW VV in 2023

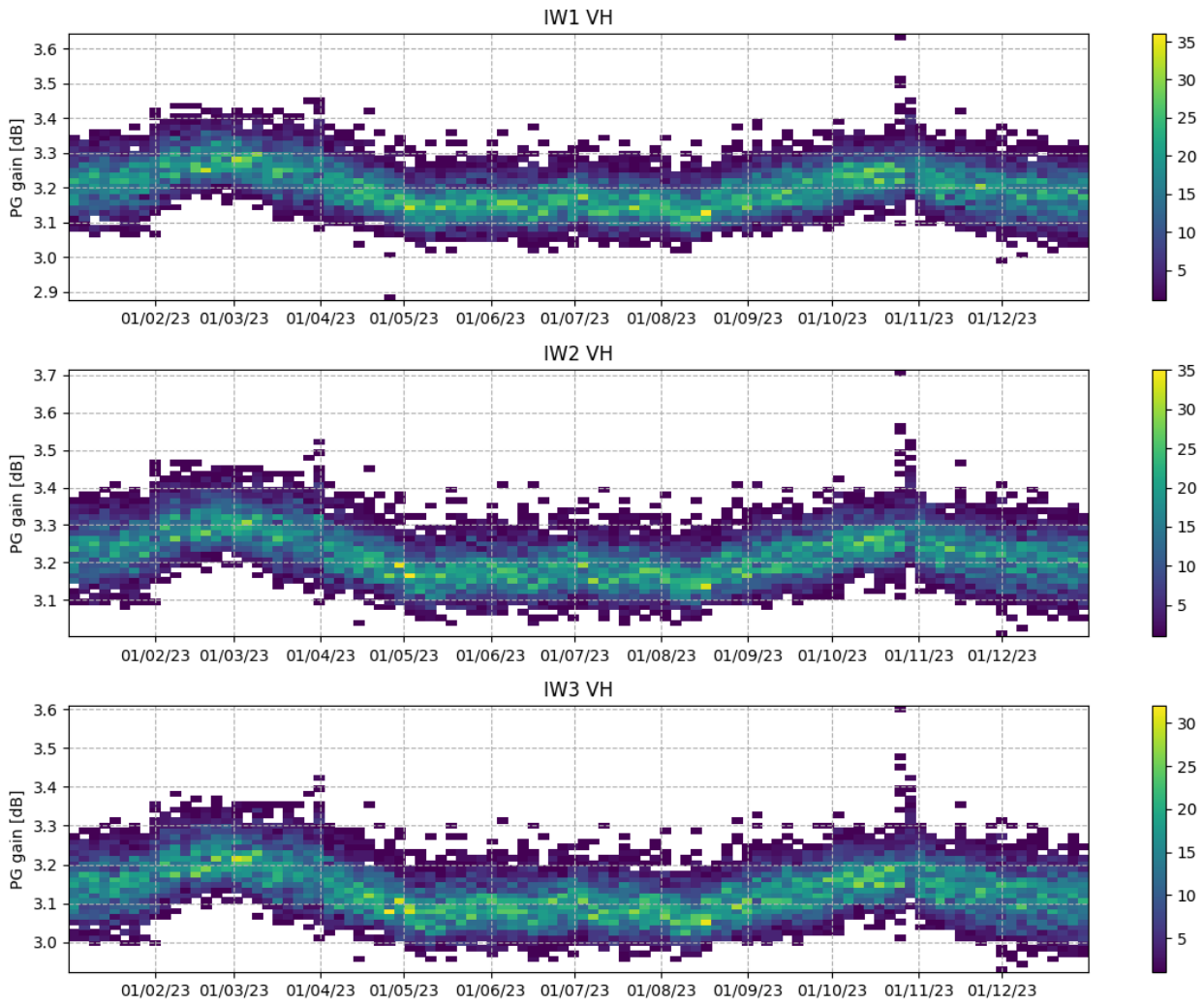


Figure 4-15 PG trend in time for IW VH in 2023

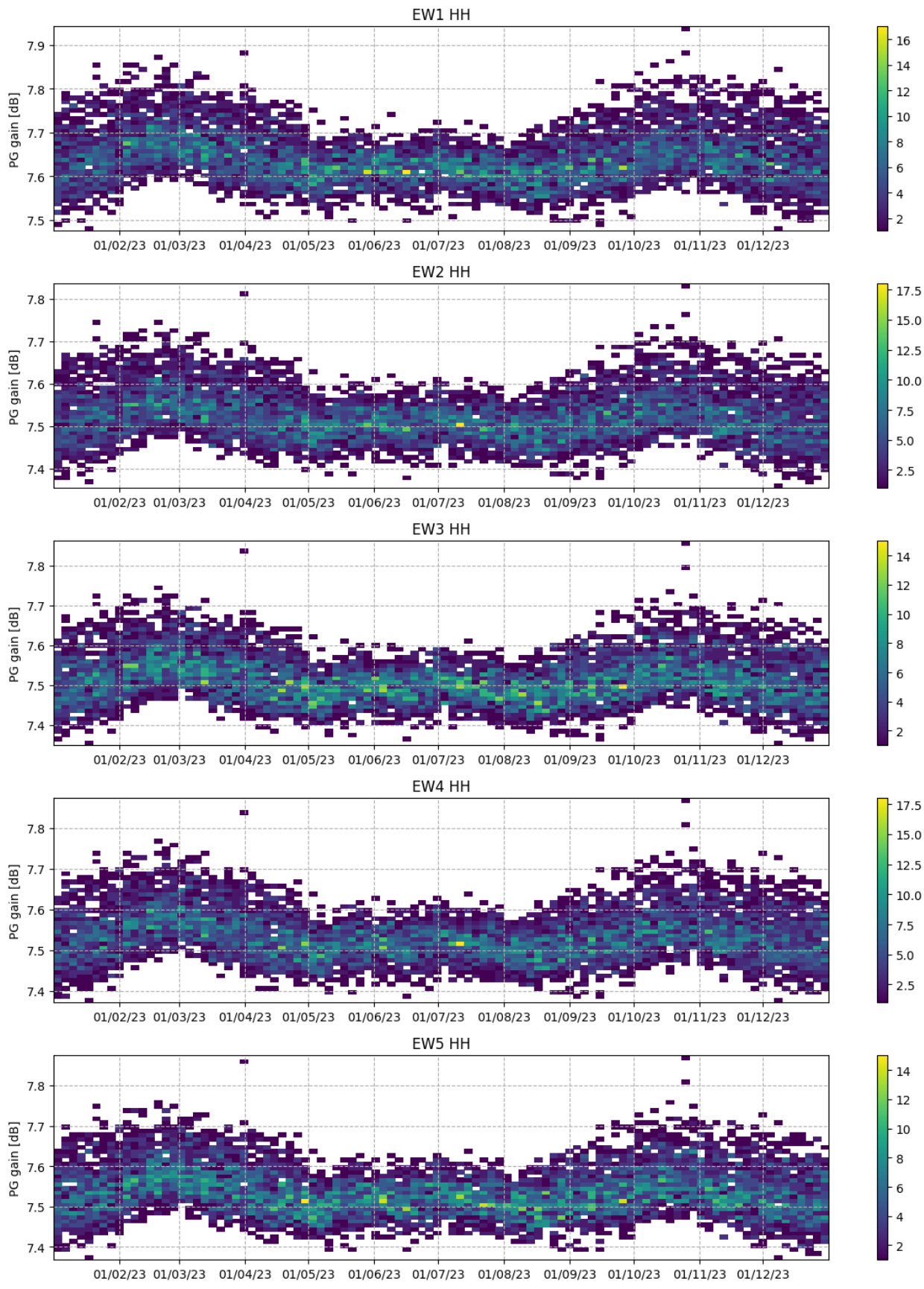


Figure 4-16 PG trend in time for EW HH in 2023

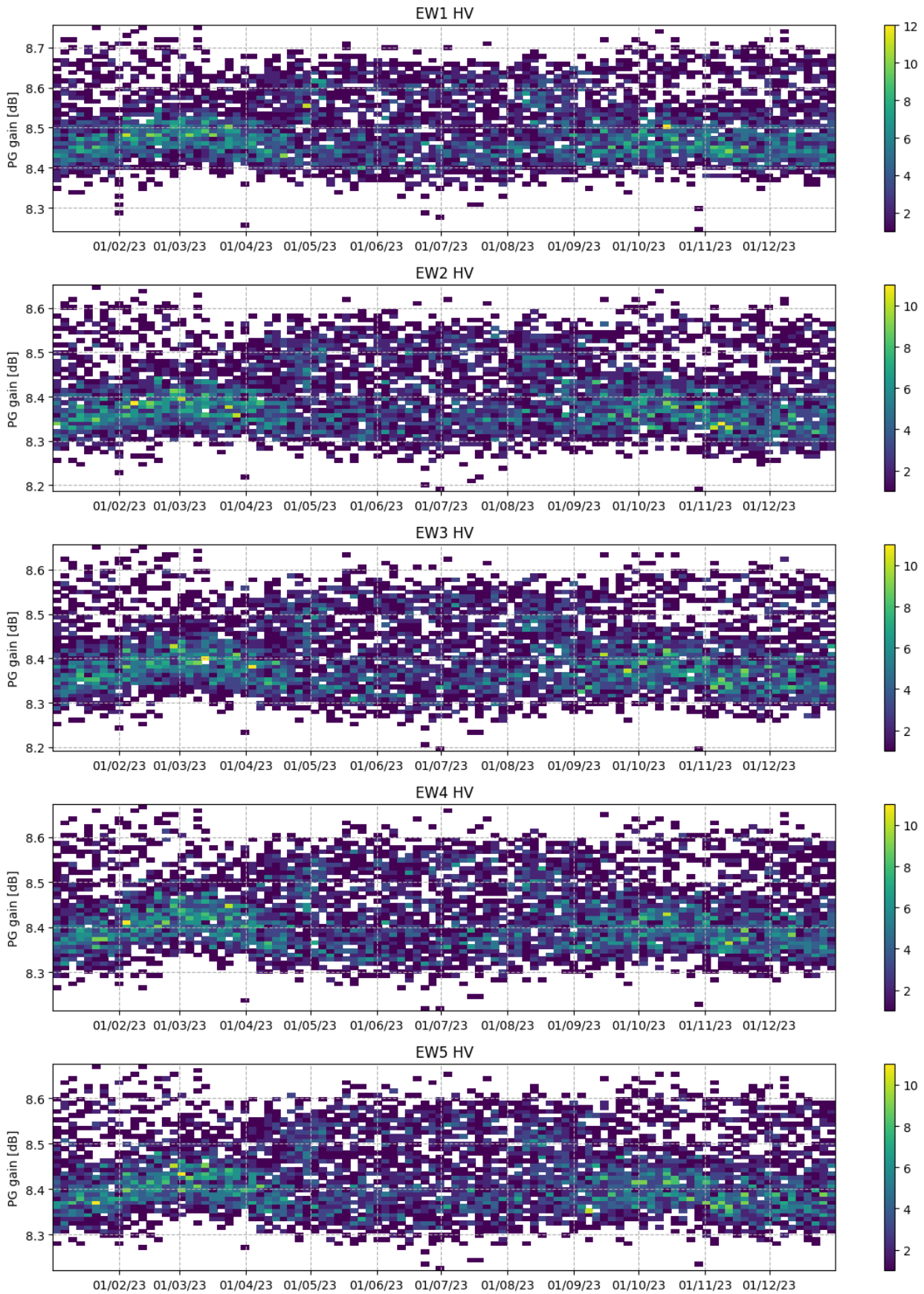


Figure 4-17 PG trend in time for EW HV in 2023

The inspection of Figure 4-17 shows that for EW HV the PG distribution at a given time largely deviates from a simple gaussian, having a longer tail at upper values. This is confirmed by inspecting the histogram integrated over the whole of 2023, see Figure 4-18. An examination of longer time series of PG values shows that the PG distribution for EW HV has this characteristic from about May 2016. This matter will be further addressed in future reports.

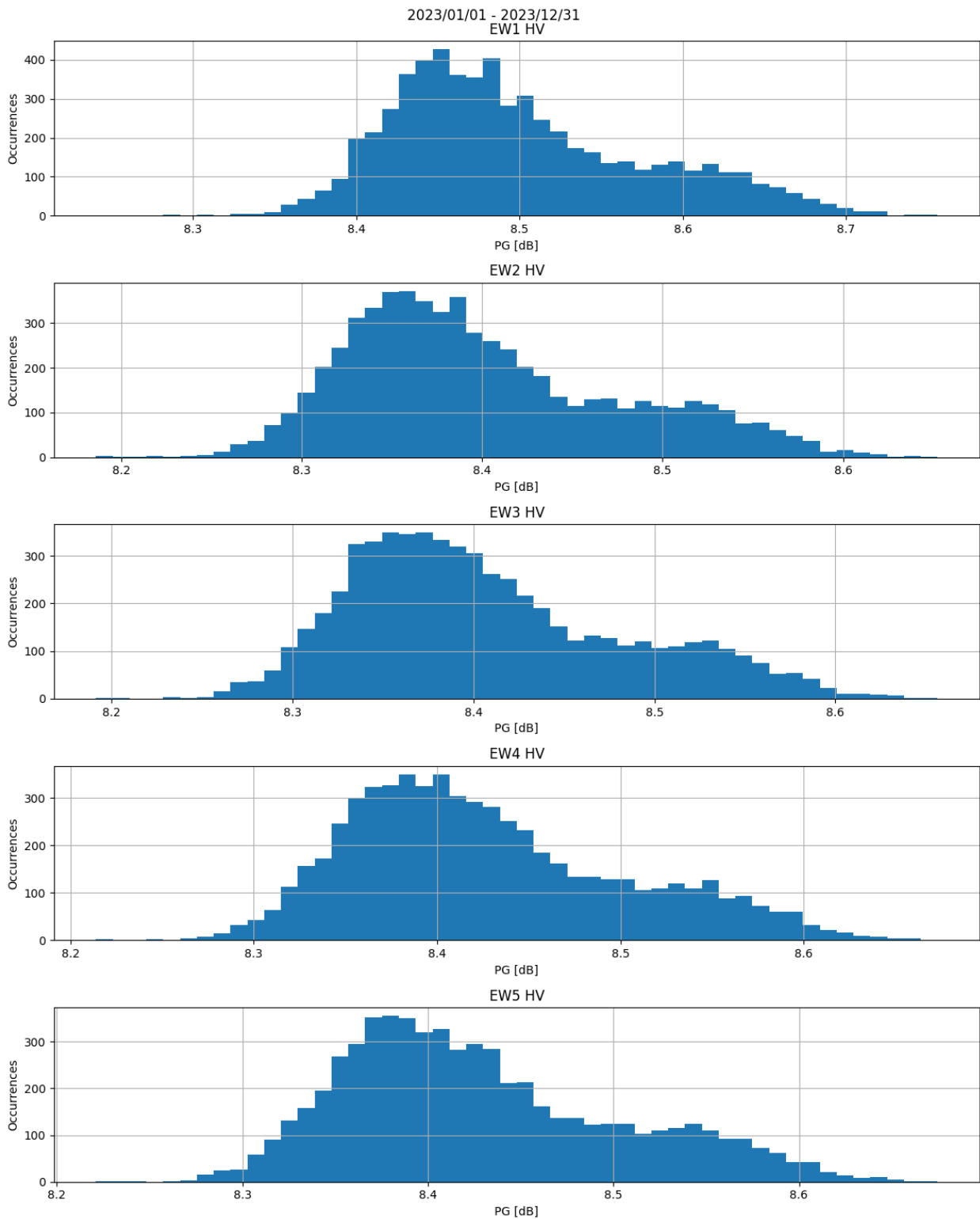


Figure 4-18 PG distribution for EW HV in 2023.

Figure 4-19 and Figure 4-20 show the average PG values, measured over the whole of 2023, compared with the PG model values as extracted from last version of the AUX_INS file, for IW and EW respectively. The measured PG values are accompanied by vertical windows corresponding to an interval of $\pm 2\sigma$. The PG model values fall in the expected interval for almost all cases. A borderline case happens to be the one of EW DV, which is also the case in which the statistics is less significant due to the lower number of products to analyse.

The PG model in the AUX_INS is provided to the S-1 IPF in case it is not able to extract the PG gain and phase from the data. The occurrences of such situations are monitored and in fact did not happen in recent years.

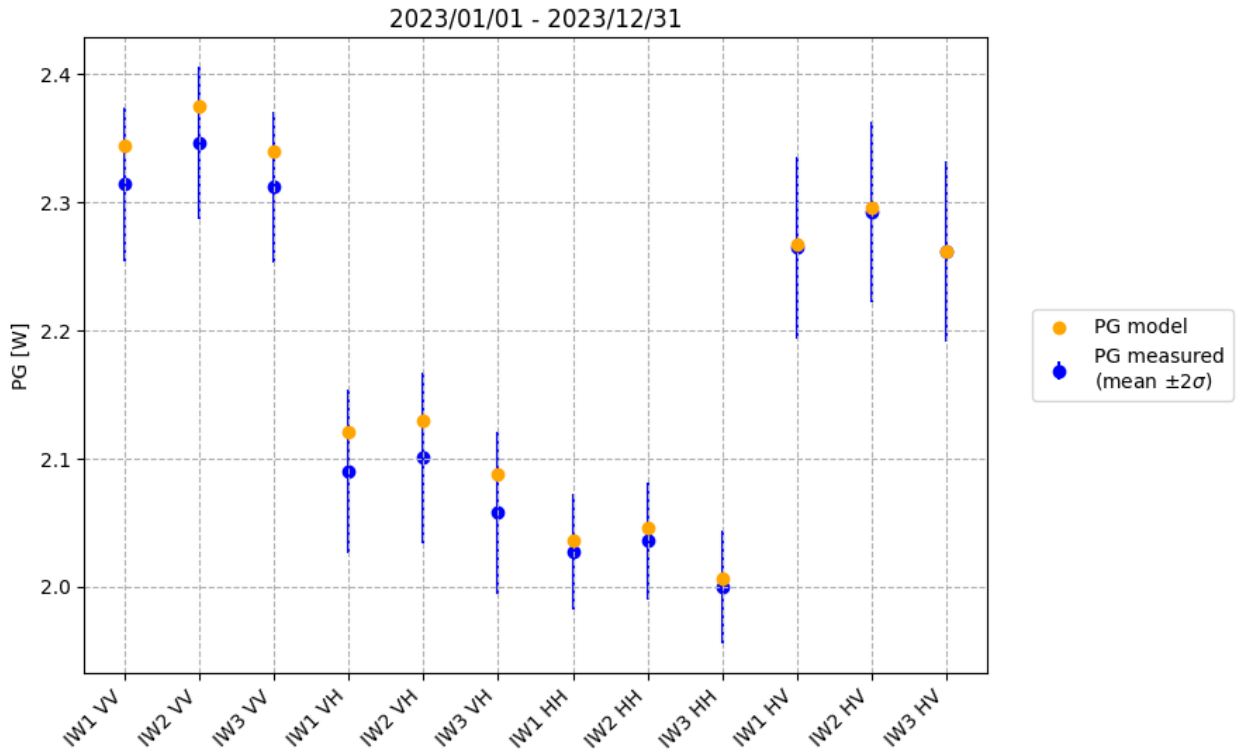


Figure 4-19 Comparison of measured and model PG values for IW in 2023

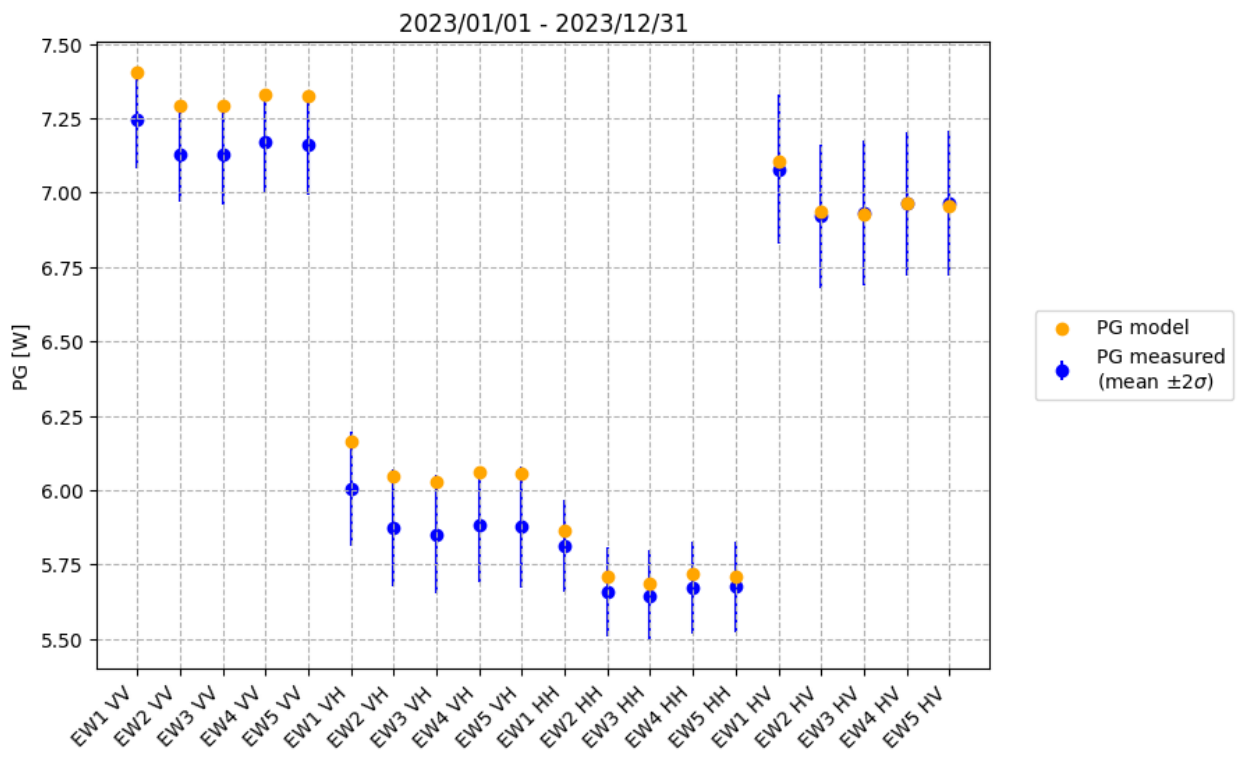


Figure 4-20 Comparison of measured and model PG values for EW in 2023

Long term trends of PG in time for all acquisition modes and polarizations, from mission start to 2023, are shown in Figure 4-21 to Figure 4-28.

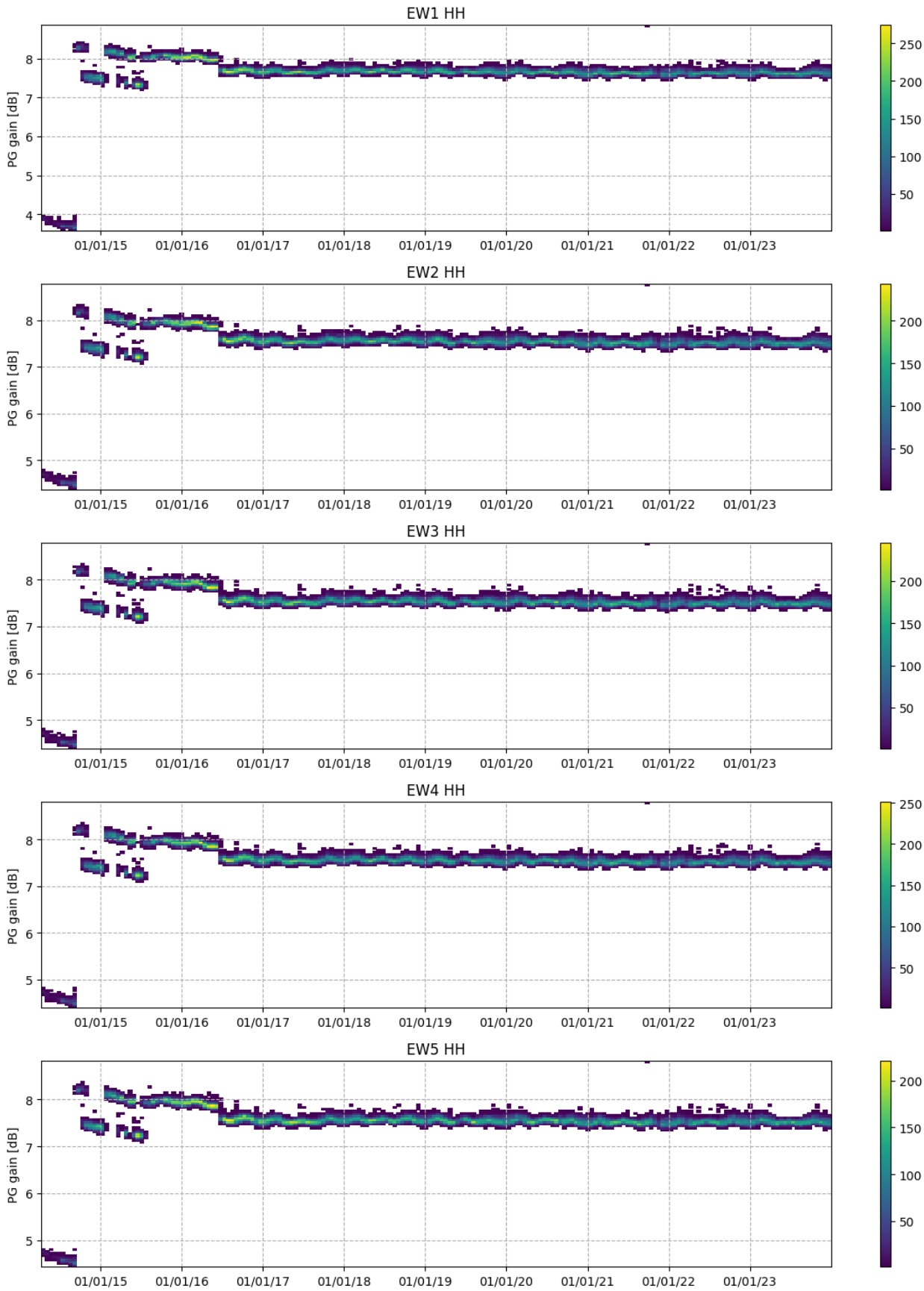


Figure 4-21 PG trend in time for EW HH from mission start to 2023



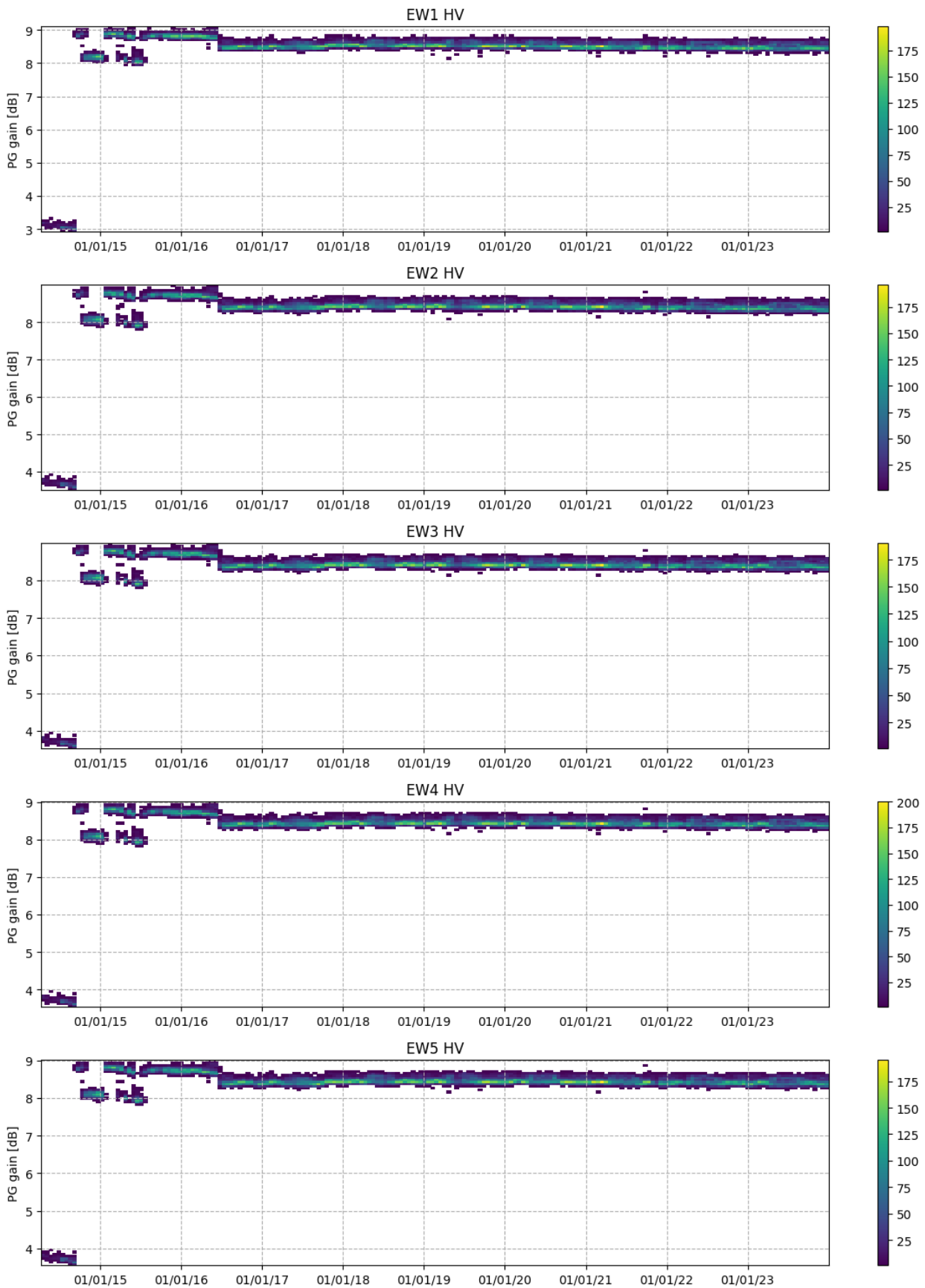


Figure 4-22 PG trend in time for EW HV from mission start to 2023



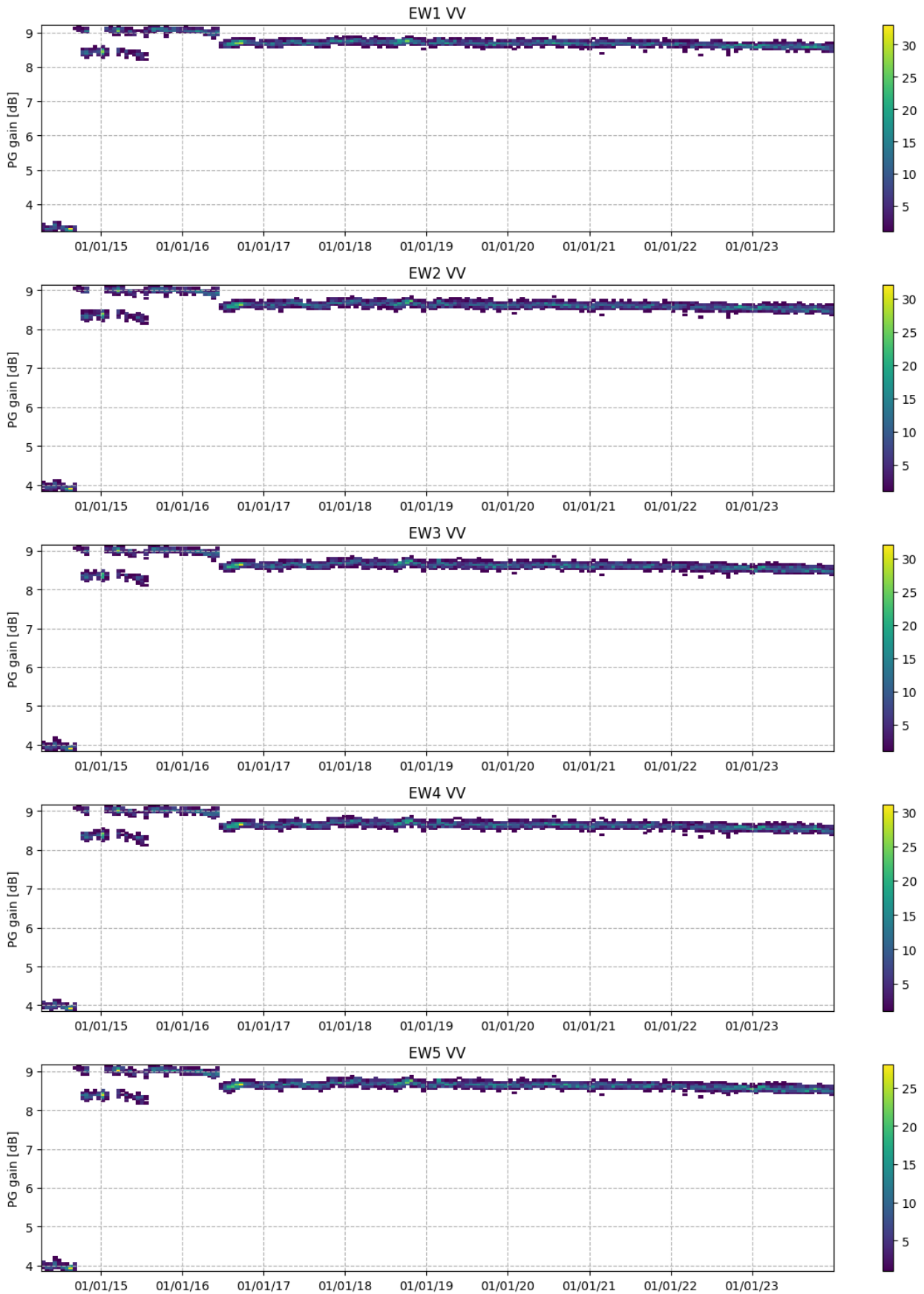


Figure 4-23 PG trend in time for EW VV from mission start to 2023



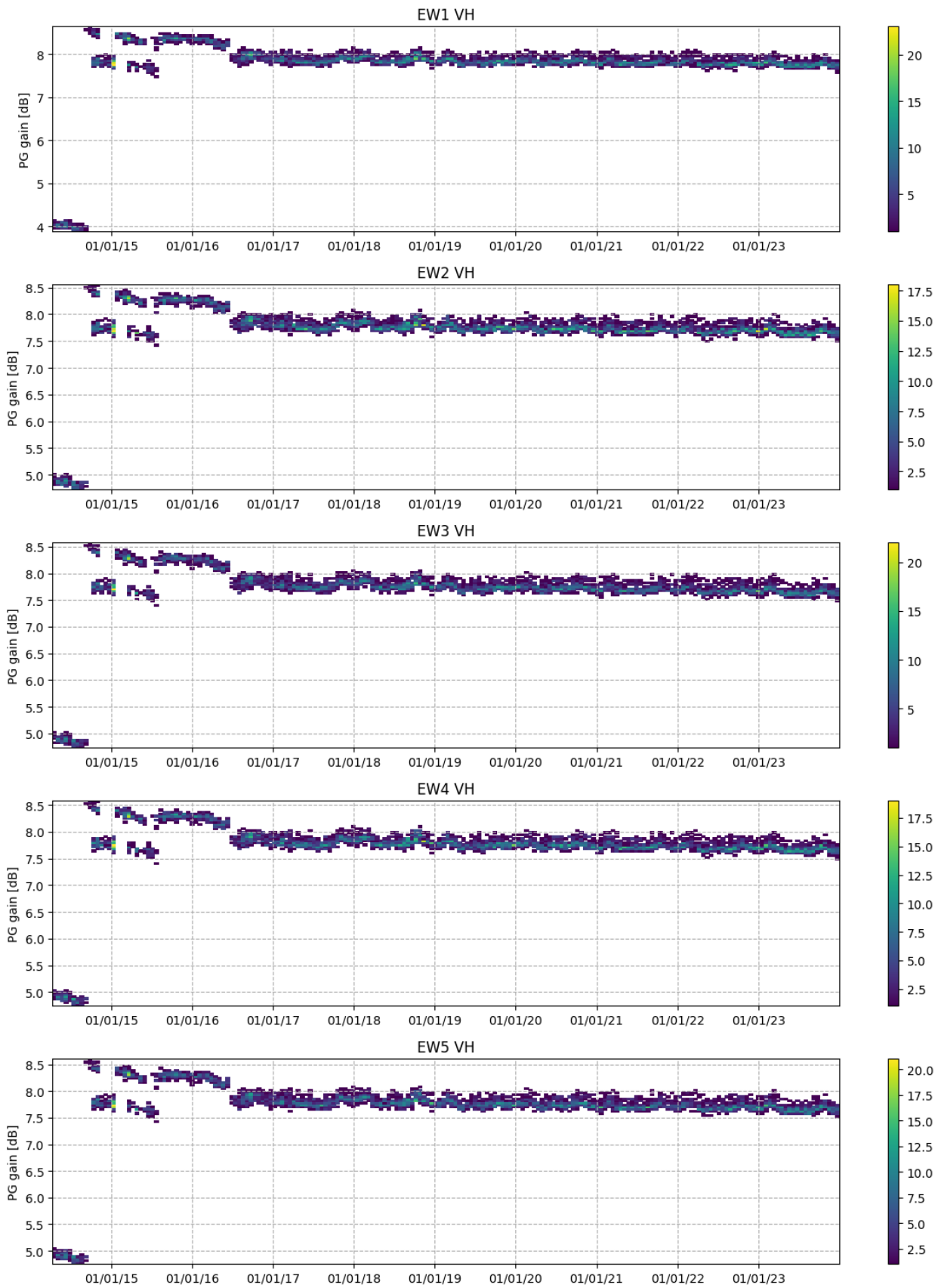


Figure 4-24 PG trend in time for EW VH from mission start to 2023

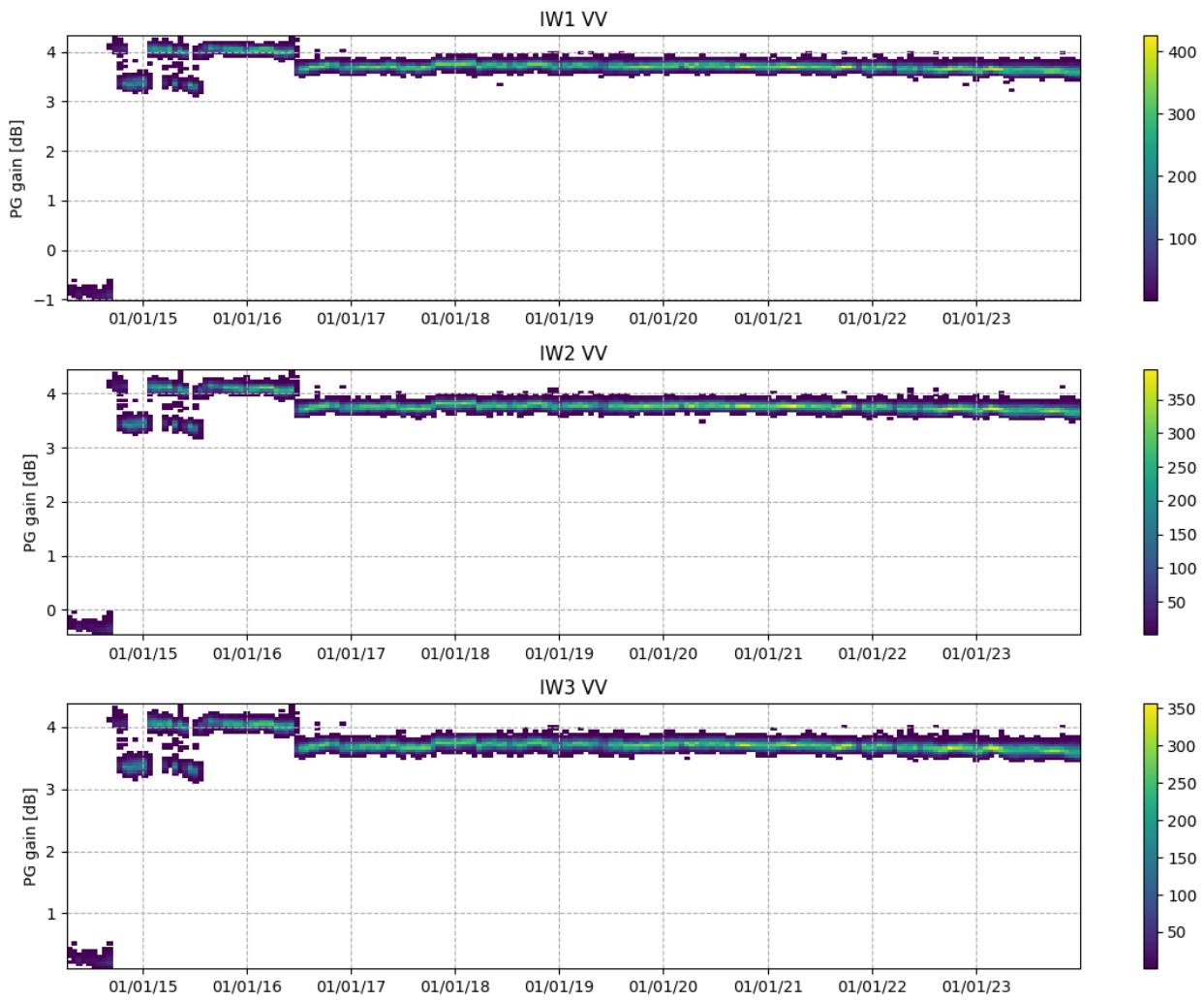


Figure 4-25 PG trend in time for IW VV from mission start to 2023

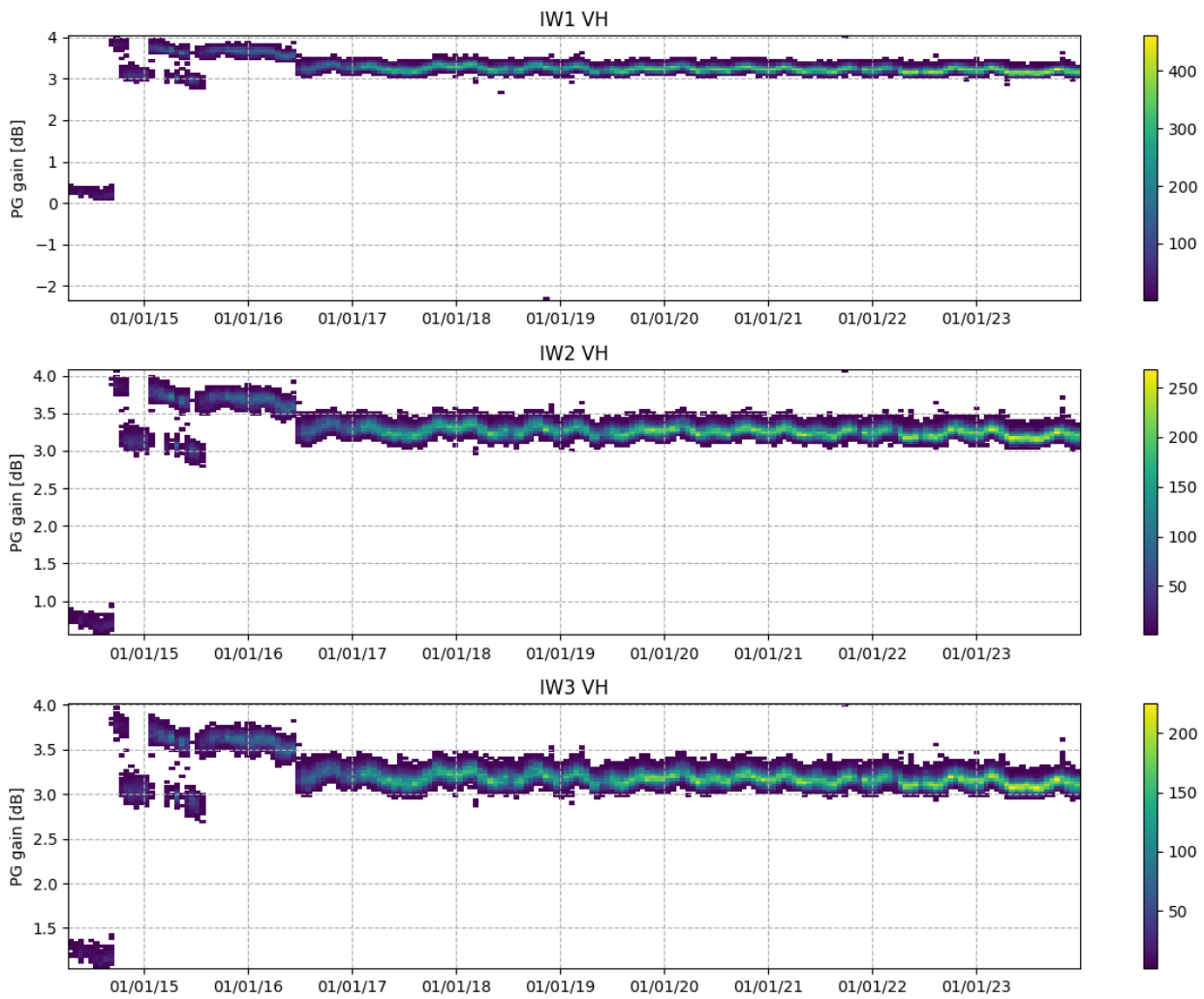


Figure 4-26 PG trend in time for IW VH from mission start to 2023

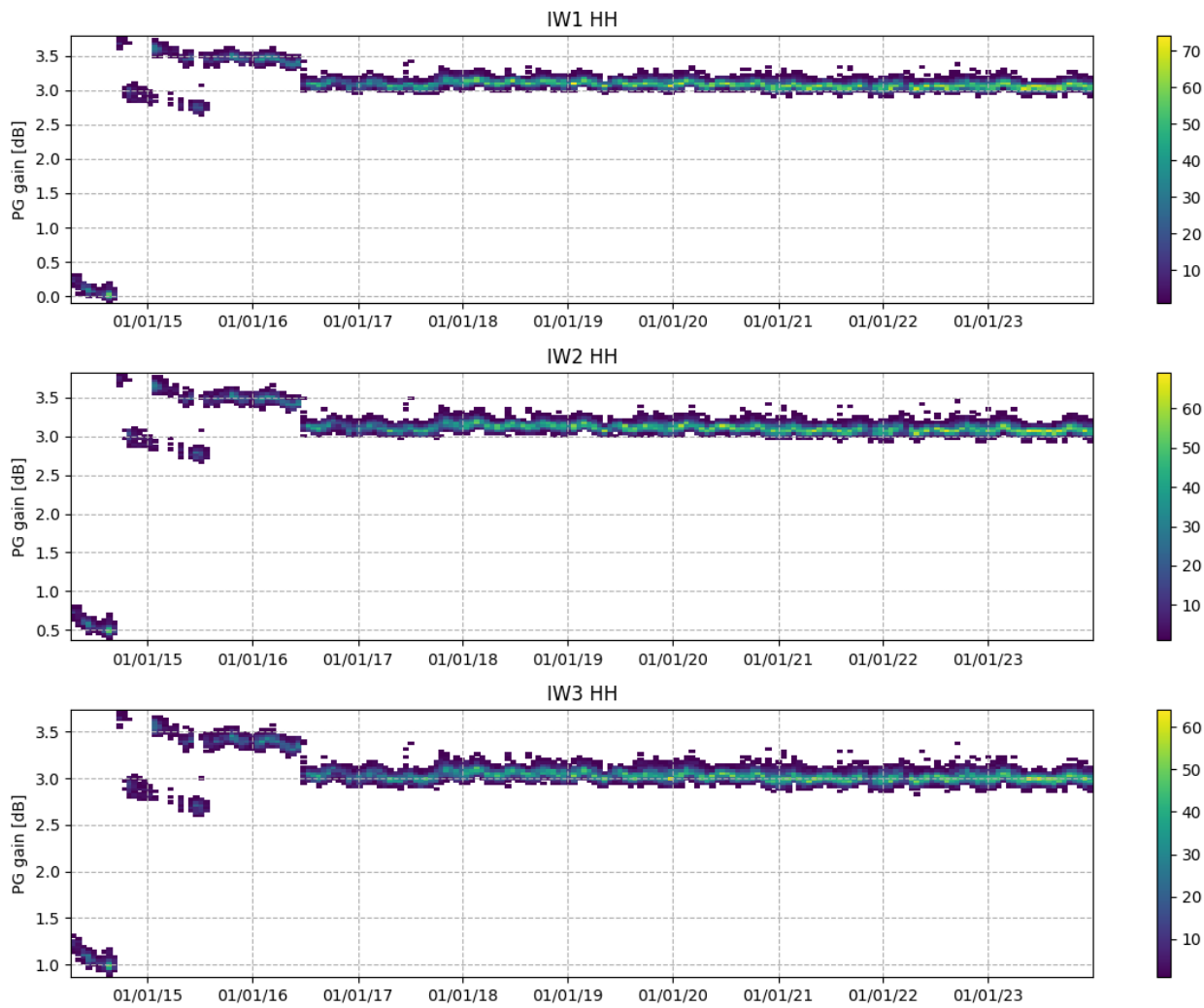


Figure 4-27 PG trend in time for IW HH from mission start to 2023

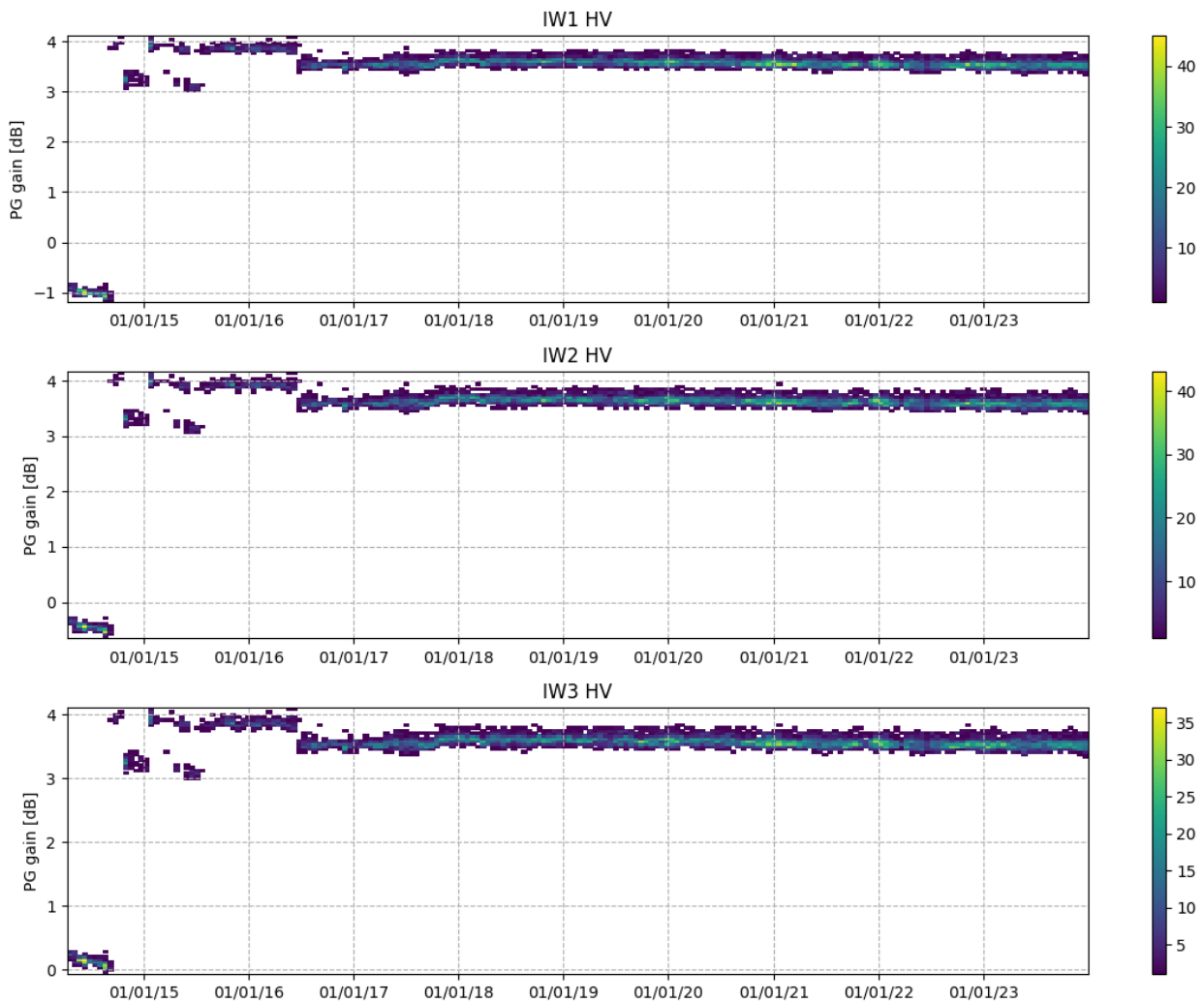


Figure 4-28 PG trend in time for IW HV from mission start to 2023

4.3 Noise Power

The noise power is monitored through the dedicated RX-only pulses embedded at the start/stop of each data-take (preamble and postamble). Furthermore, since the 26th June 2018 (deployment of IPF 2.9.1) the noise evolution in TopSAR data is also monitored exploiting the first echoes of each burst, the so-called “rank echoes”, which are signal free echoes and hence can be considered as noise pulses [S1-RD-20].

The new noise tracking strategy was introduced to cope with the fact that the energy radiated from the Earth surface is recorded by the instrument, thus biasing the noise power measure. This results in an almost 1 dB offset between noise power measures over land (high noise power) and over sea (low noise power) [S1-RD-19].

Table 1 provides the average noise power computed during December 2023 for sea and land echoes. The values in parenthesis are the average noise powers during December 2022 for comparison. The noise power is stable since last year, with variations of at most 0.1 dB.

Figure 4-29 shows the distribution of noise power measurements as a function of time in 2023 for S-1A IW1, EW1, and WV1 products. The noise power is stable over the year.

Figure 4-30 shows the histograms of the noise measurements registered during December 2023, separated vertically by swath and horizontally by polarization. Separating plots by swath and polarization allows to



clearly distinguish the distribution with two peaks, corresponding to noise measurements over sea and land.

| Acquisition mode | S-1A Noise power [dB] |
|------------------|---------------------------------------|
| IW1 V/V | Sea: 7.01 (7.02) Land: 7.79 (7.79) |
| IW1 V/H | Sea: 6.42 (6.35) Land: 7.23 (7.18) |
| EW1 H/H | Sea: 5.55 (5.52) Land: 6.17 (6.13) |
| EW1 H/V | Sea: 6.56 (6.56) Land: 7.19 (7.18) |

Table 1: Average noise power measured during December 2023. The value in parenthesis is the average noise power measured during December 2022.

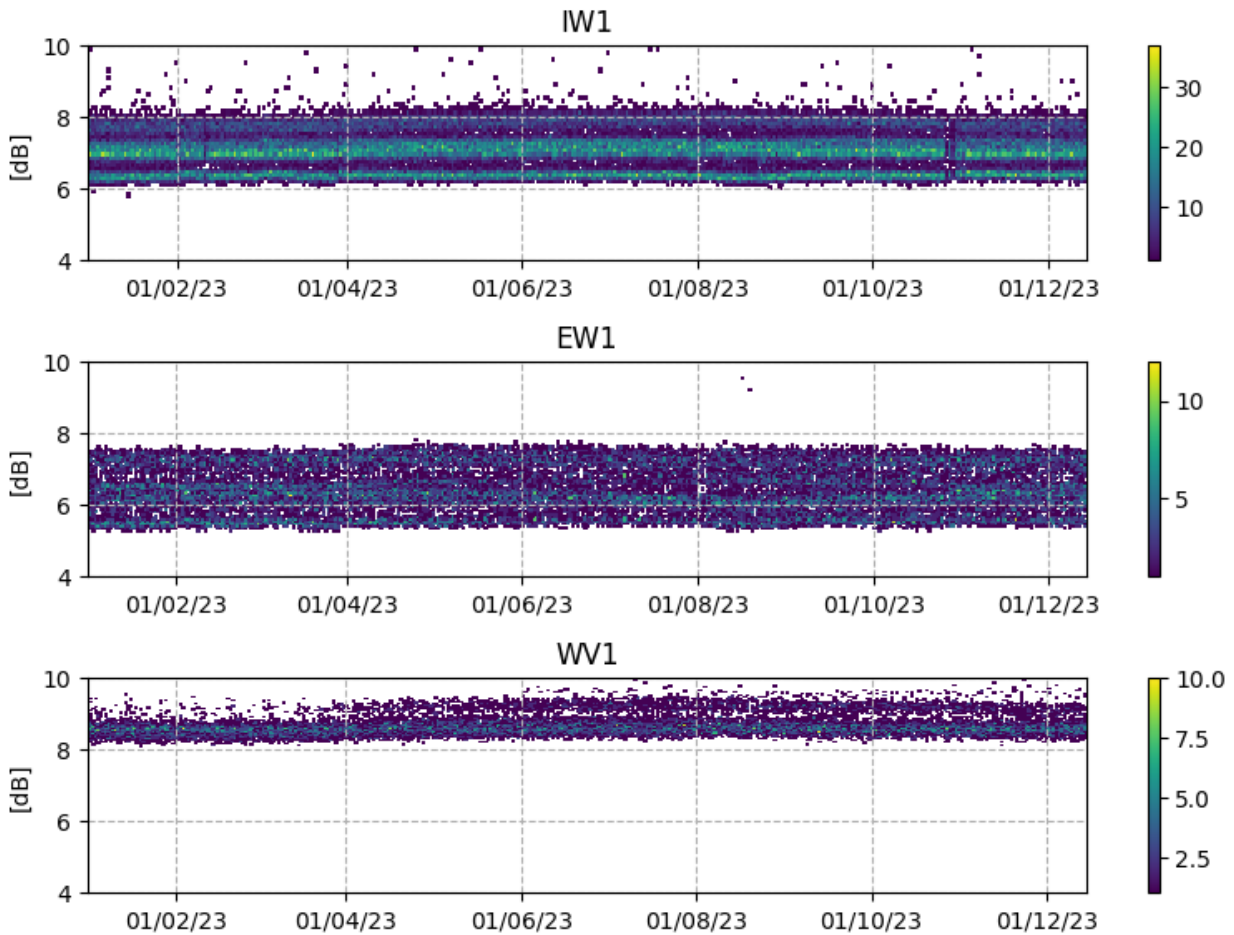


Figure 4-29: Noise power versus time for beams IW1 (top), EW1 (middle), and WV1 (bottom) of S-1A in 2023

2023/12/02 - 2023/12/14

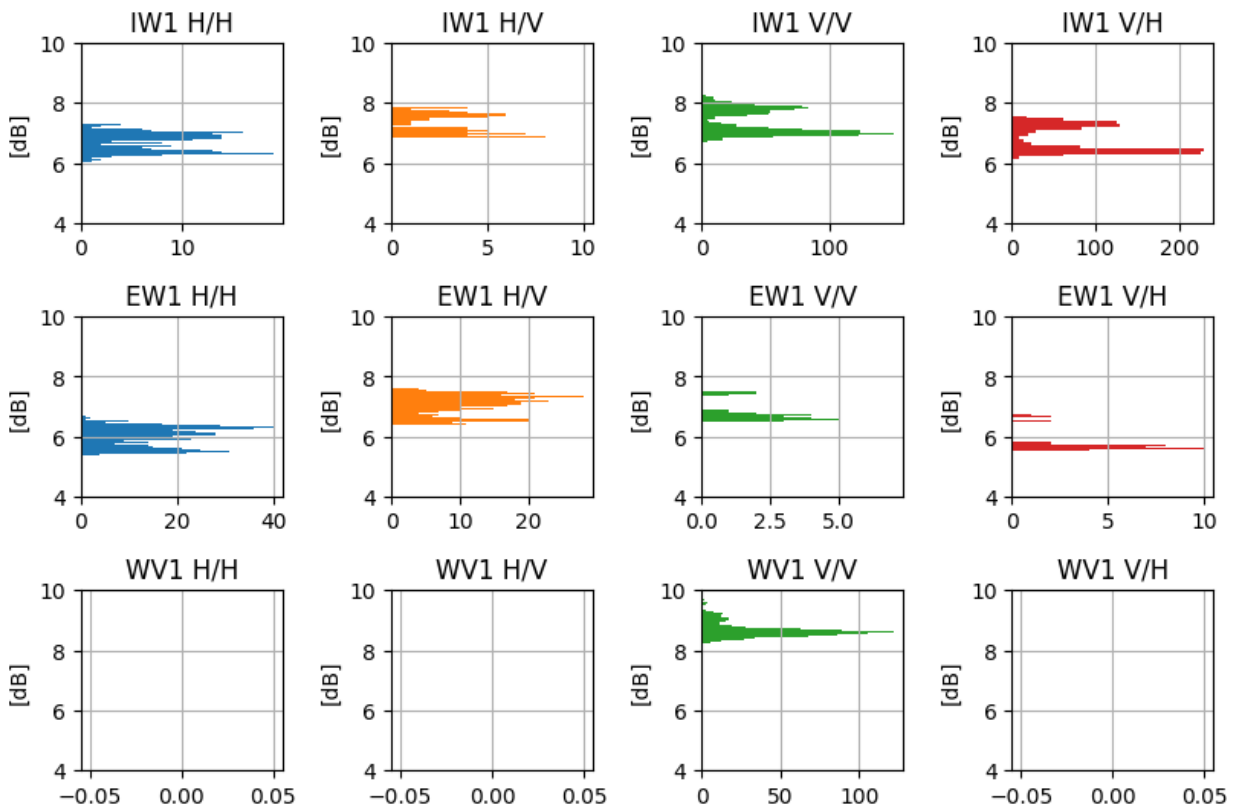


Figure 4-30: Histograms of noise measurements registered during December 2023, separated by swath (vertically) and by polarization (horizontally).

Figure 4-31 shows the noise power evolution for IW1, EW1, and WV1, from the mission start to 2023.

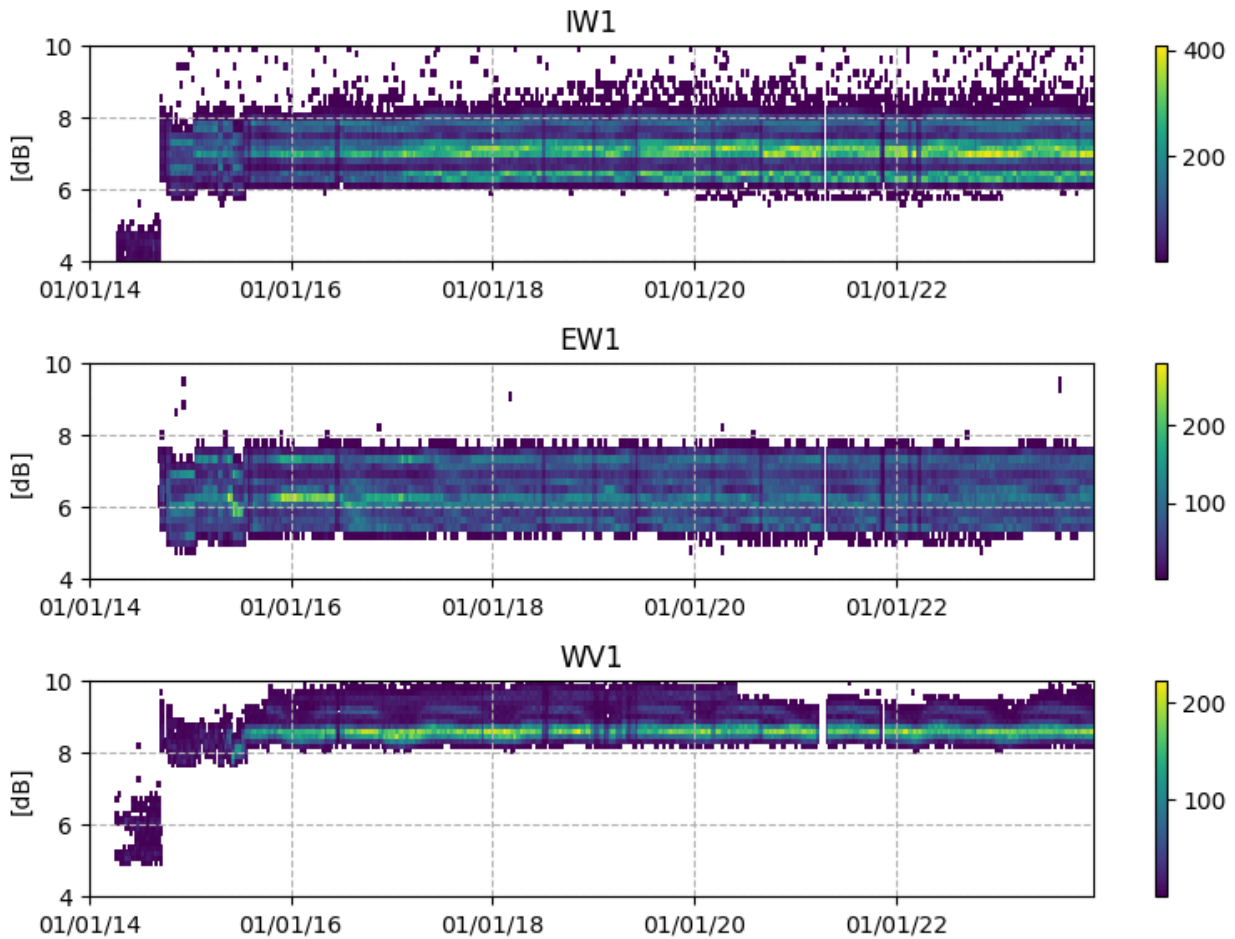


Figure 4-31 Noise power versus time for beams IW1 (top), EW1 (middle), and WV1 (bottom) of S-1A from mission start until 2023

4.4 Instrument Unavailability

A list of S-1A instrument unavailability during 2023 is given in Appendix B -.

4.5 Radar Data Base Updates

There was no update of S-1A Radar Data Base in 2023.

5.L1 Products Status

Hereafter, the status of the S-1A products during 2023 is described. A general summary of status of S-1A & S-1B Level 1 products was presented at several conferences and workshops during 2023 (see [S1-RD-01], [S1-RD-02], [S1-RD-03], [S1-RD-04] and [S1-RD-12]).

5.0 Level 1 Basic Image Quality Parameters

The DLR transponders and corner reflectors [S1-RD-29] and the Australian Corner Reflector array [S1-RD-04] have been used to assess various impulse response function parameters as described below. The products analysed were acquired in 2023 and processed with the current Sentinel-1 IPF version.

5.0.1 Spatial Resolution

Figure 5-1 and Table 2 below give the azimuth and range spatial resolutions derived from S-1A IW mode SLC data (there were no measurements for SM and EW modes during 2023). The numbers in brackets indicate the number of measurements.

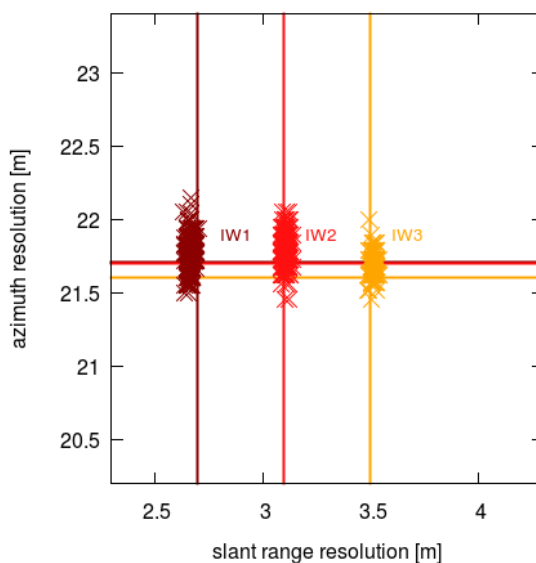


Figure 5-1: S-1A IW azimuth and slant-range spatial resolution (lines correspond to targeted performance from the product definition)

| Mode/Swath | Azimuth Spatial Resolution (m) | Slant Range Spatial Resolution (m) |
|------------|--------------------------------|------------------------------------|
| IW1 | 21.75 ± 0.11 (347) | 2.67 ± 0.01 (347) |
| IW2 | 21.79 ± 0.10 (264) | 3.11 ± 0.01 (264) |
| IW3 | 21.69 ± 0.09 (130) | 3.51 ± 0.01 (130) |

Table 2: Azimuth and slant-range spatial resolution for S-1A derived for IW mode

5.0.2 Sidelobe Ratios

Table 3 presents the integrated sidelobe ratio (ISLR) and peak-to-sidelobe ratio (PSLR) separated for azimuth and range direction. These sidelobe ratios are derived from S-1A IW SLC acquisitions using impulse response functions from transponders of DLR calibration field.

| Satellite/Mode | Azimuth ISLR (dB) | Range ISLR (dB) | Azimuth PSLR (dB) | Range PSLR (dB) |
|----------------|-------------------|-----------------|-------------------|-----------------|
| IW1 | -17.42 ± 0.16 | -15.78 ± 0.20 | -23.51 ± 0.41 | -20.60 ± 0.50 |
| IW2 | -16.08 ± 0.15 | -15.51 ± 0.16 | -20.83 ± 0.35 | -19.97 ± 0.39 |
| IW3 | -16.04 ± 0.11 | -15.72 ± 0.14 | -20.86 ± 0.23 | -20.66 ± 0.34 |

Table 3: S-1A IW Sidelobe Ratios

Figure 33 show the performed ISLR (left) and PSLR (right) for all transponder IRFs acquired in 2023; the three coloured data clouds correspond to the related sub-swath IW1 (brown), IW2 (red) and IW3 (yellow). The results indicate a nominal performance in terms of SAR data image quality for S-1A in 2023.

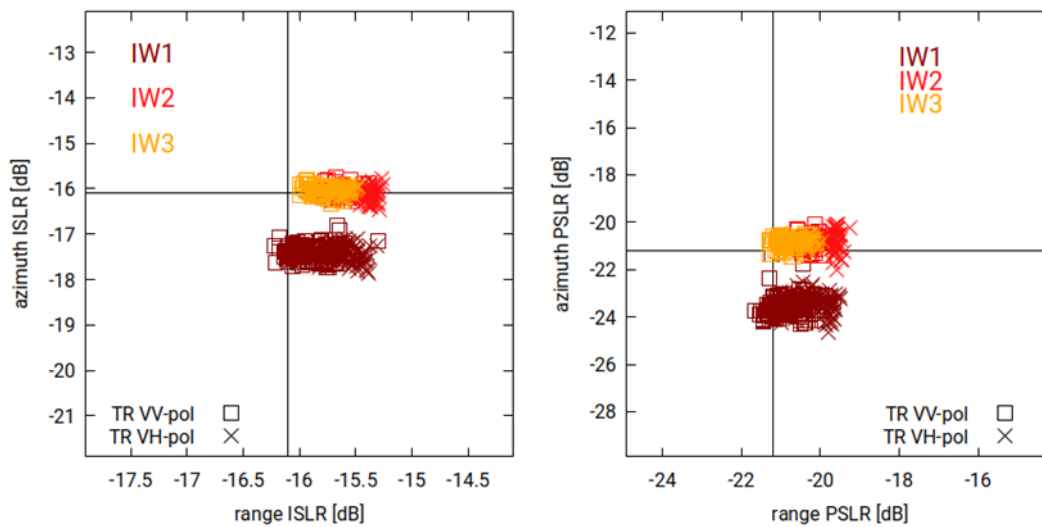


Figure 5-2: ISLR (left) and PSLR (right) for azimuth (y-axis) and range direction (x-axis) derived from DLR transponder measurements using S-1A IW acquisitions (lines correspond to targeted performance from the product definition)

5.1 Radiometric Calibration

The DLR transponders and corner reflectors [S1-RD-24] and the Australian Corner Reflector [S1-RD-04] array have been used to measure their radar cross-section as described below. The products analysed were acquired in 2023 and processed with Sentinel-1 IPF in operation at the time of acquisition.

5.1.1 Absolute Radiometric Calibration

The absolute radiometric calibration of each SAR instrument was initially performed during the respective commissioning phases in 2014 (S-1A) [S1-RD-14] and 2016 (S-1B) [S1-RD-15]. For this calibration purpose, reference targets like corner reflectors (CR) and transponders (TR) with well-known RCS were used [S1-RD-16]. In particular, DLR's remote controlled transponders and remote-controlled corner reflectors with 2.8 m leg length have been used operated continuously since the beginning of S-1A operation in 2014 (inter alia [S1-RD-17], [S1-RD-18]).

During the observation period in 2023 SAR acquisitions with IW mode and DV polarization (VV+VH) have been acquired regularly over the DLR calibration site located in Southern Germany for S-1A [S1-RD-16]. Long-term monitoring of the radiometric performance has been systematically evaluated for this period.

To determine the radiometric accuracy, the absolute calibration factor derived from DLR's point targets has been analysed from the acquired datatakes by investigating each target's impulse response function and considering the nominal target RCS. The deviation of the absolute calibration factor as a function of time is depicted in Figure 5-3 for S-1A for the observation period in 2023. The trihedral corner reflectors produce impulse responses only for co-polarized products. Thus, results from the VV-polarization channel (red) appear more often compared to VH-polarization channel (blue) which represents the cross-polarization results derived from corresponding transponder measurements only.

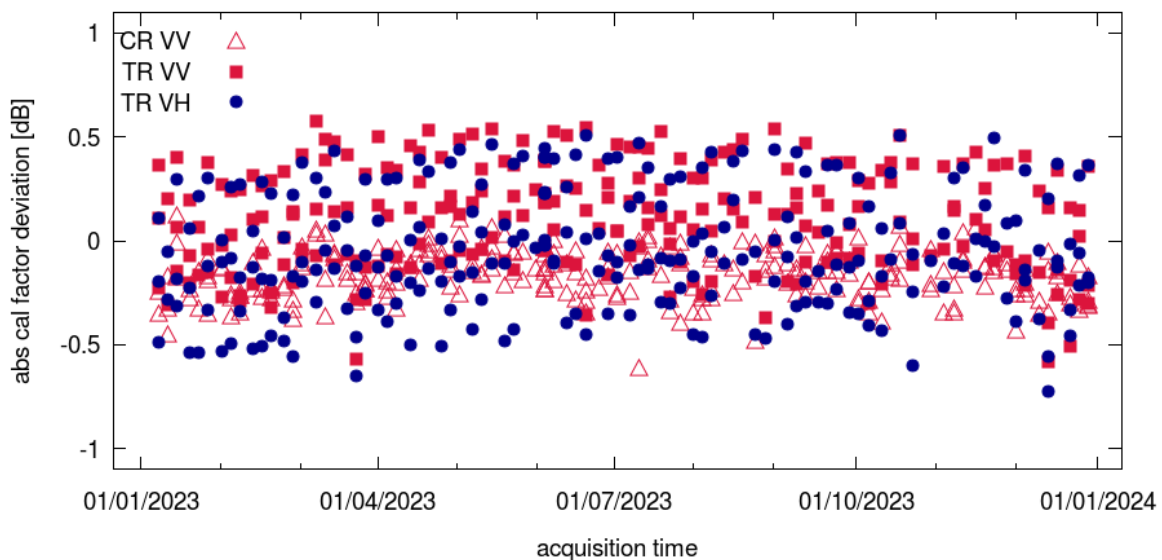


Figure 5-3: S-1A calibration factor for IW acquisitions in 2023 derived from DLR reference targets; the polarization is depicted by colour: VV in red, VH in blue.

The calibration factor deviations have a low remaining bias of -0.04 dB for S-1A (see Table 4). This indicates that the SAR instrument is well balanced in terms of absolute radiometric calibration. A higher spread visible for certain acquisitions (in Figure 5-3) may arise from rainy weather conditions during the respective measurement; small RCS drifts over time (up and down) may occur due to remaining SAR instrument drifts.

Furthermore, a standard deviation of the absolute calibration factor of 0.25 dB for S-1A has been derived for the observation period in 2023 (see Table 4) which includes the measurement of both polarizations (VV and VH) and all three sub-swathes (IW1, IW2, and IW3).

In order to derive the overall absolute radiometric accuracy of a spaceborne SAR system during the mission time, the following additional error contributions are further considered:

- Long term stability of the instrument 0.05 dB (1σ)
- Dynamic range error 0.067 dB (1σ)
- Reference target accuracy 0.20 dB (1σ)

Considering these error contributions an absolute radiometric accuracy of 0.331 dB for S-1A (1σ) is derived.

| | S-1A IW (VV and VH) |
|---------------------------------------------|------------------------|
| Mean value \pm standard deviation | -0.04 dB \pm 0.25 dB |
| Absolute radiometric accuracy (1σ) | 0.331 dB |

Table 4 : Mean value, standard deviation and absolute radiometric accuracy derived from DLR targets (transponders and corner reflectors) for IW mode DV polarization (VV+VH) acquired over DLR’s calibration site in 2023 for S-1A.

In order to focus on dependencies within the swath, statistics of the calibration factor for a given configuration (track, elevation angle, polarization) were derived. For a given track, each target has a specific geometric alignment w.r.t. the satellite, i.e., the target is “seen” by the SAR instrument under the same elevation or look angle. The mean values and standard deviations of the calibration factor are determined for each configuration with similar acquisition geometry and depicted in Figure 5-4 for S-1A. The mean values are marked by symbols, the standard deviations by error bars, VV polarization results are shown in red, VH polarization in blue. This plot shows the elevation dependency of the calibration factor for the IW mode for all three sub-swathes with no evident trend.

The mean values (symbols in Figure 5-4) show a low variation over elevation angle: between -0.22 dB and 0.42 dB for the VV polarization channel (red) and between -0.44 dB and 0.37 dB for the VH polarization channel (blue). The standard deviation found for each configuration is an indicator for the radiometric stability. These deviations (error bars in Figure 5-4) are remarkable small; the average value is 0.12 dB with variations between 0.03 dB (min) and 0.21 dB (max).



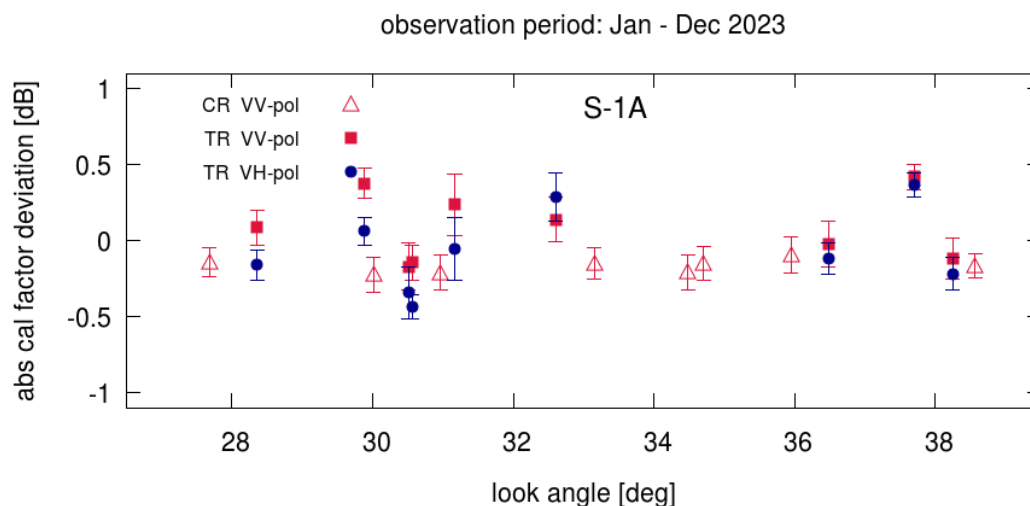


Figure 5-4: S-1A calibration factor derived from each DLR target under constant acquisition geometry (i.e. same elevation or look angle) acquired in 2023. The symbols depict the mean value, error bars the standard deviation; each target type can be identified by its symbol: corner reflectors as open triangles, transponders as filled squares or circles. The polarization is depicted by colour, VV in red, VH in blue.

The absolute calibration factor is further analysed for each sub-swath (IW1, IW2, IW3) for all S-1A acquisitions over DLR point targets in 2023. The mean value and standard deviation are summarized for each sub-swath and also each polarization channel (VV and VH) in Table 5.

The table documents that the S-1A SAR instrument is well balanced indicated by low mean values (biases) found for each sub-swath. Furthermore, the standard deviation is very similar for all sub-swathes and both satellites. Slightly higher standard deviations are found for IW3 compared to IW1 and IW2.

| Sub-swath | polarization | S-1A μ [dB] \pm σ [dB] |
|-----------|--------------|----------------------------------------|
| IW1 | VV | -0.02 \pm 0.25 |
| | VH | -0.17 \pm 0.23 |
| | VV and VH | -0.07 \pm 0.25 |
| IW2 | VV | -0.09 \pm 0.16 |
| | VH | -0.09 \pm 0.24 |
| | VV and VH | -0.05 \pm 0.20 |
| IW3 | VV | 0.07 \pm 0.29 |
| | VH | 0.11 \pm 0.31 |
| | VV and VH | 0.08 \pm 0.30 |

Table 5 : Mean value and standard deviation of the absolute calibration factor for IW mode with V-polarization on transmit derived from acquisitions over the DLR calibration site in 2023.

Furthermore, the radiometric performance for S1A is derived for the long-term monitoring period from Mar 2017 until Dec 2013 using DV polarization acquisitions acquired using reference targets at the DLR calibration site. Figure 5-5 shows the absolute calibration factor derived from corner reflectors for VV

polarization (red triangles), and transponders for both: VV polarization (red squares) and VH polarization (blue circles). This evaluation considers artificial radiometric biases due to antenna elevation pattern updates and processing gains applied at the time of their processing time. This re-compensation method is applied by using related auxiliary files but without explicit reprocessing of the SAR data products from the past [S1-RD-27]. The absolute calibration factor for this observation period is derived to be $-0.085 \text{ dB} \pm 0.213 \text{ dB}$; the absolute radiometric accuracy is 0.304 dB .

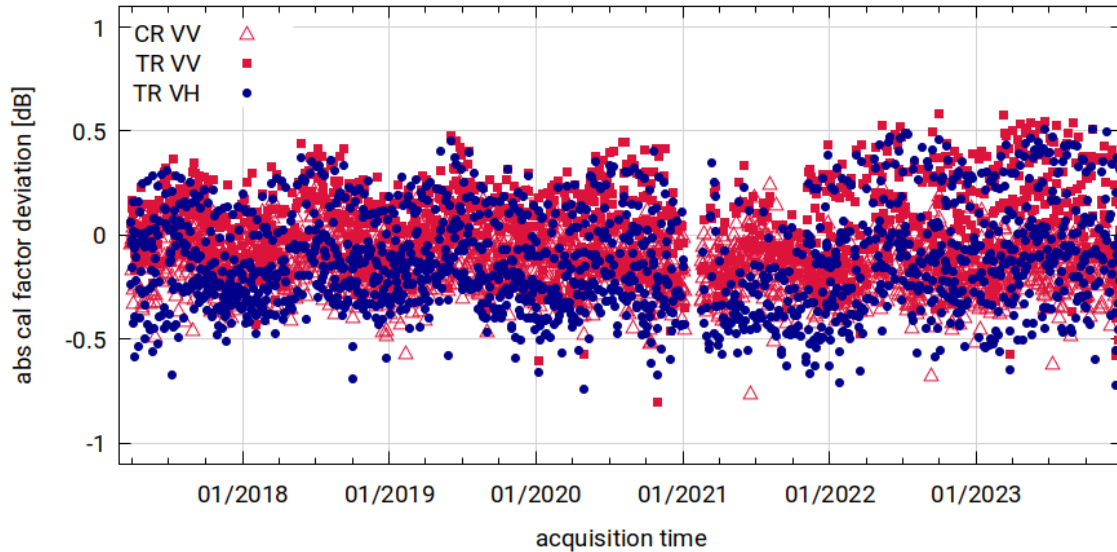


Figure 5-5: S-1A calibration factor for IW acquisitions from Mar 2017 to Dec 2023 derived from DLR reference targets; the polarization is depicted by colour: VV in red, VH in blue.

In 2023, a change of observation scenario was implemented over the Surat Basin calibration site [S1-RD-04] and the transponders operated by the Canadian Space Agency (CSA) to try to characterise HH calibration [S1-RD-40]. The results are not reported in this document and are still under analysis.

An array of 40 corner reflectors has been deployed near Brisbane, Australia as a component of the Australian Geophysical Observing System (AGOS) (*Surat Basin* calibration site) [S1-RD-04]. The CRs are size 1.5m (34), 2.0m (3) and 2.5m (3) with fixed orientations. Given that these corner reflectors have a fixed elevation and azimuth orientation they will not be pointing directly at S-1A. For evaluating the radiometric stability only large CRs ($\geq 2 \text{ m}$) have been selected for sufficient results. The six remaining CRs are all located in sub-swath IW2 only. The evaluated RCS with mean value and standard deviation for each of the six CRs acquired in 2023 is depicted in Table 6. The numbers in brackets refer to the number of measurements.

The low standard variations ($\leq 0.20 \text{ dB}$) found for both polarization channels and all six CRs confirm the high radiometric stability already found using the reference point targets from the DLR calibration site [S1-RD-18]. Furthermore, for these targets all RCS values are slightly higher for HH polarization compared to VV polarization indicating a slightly offset between HH and VV of 0.15 dB in average for IW2.

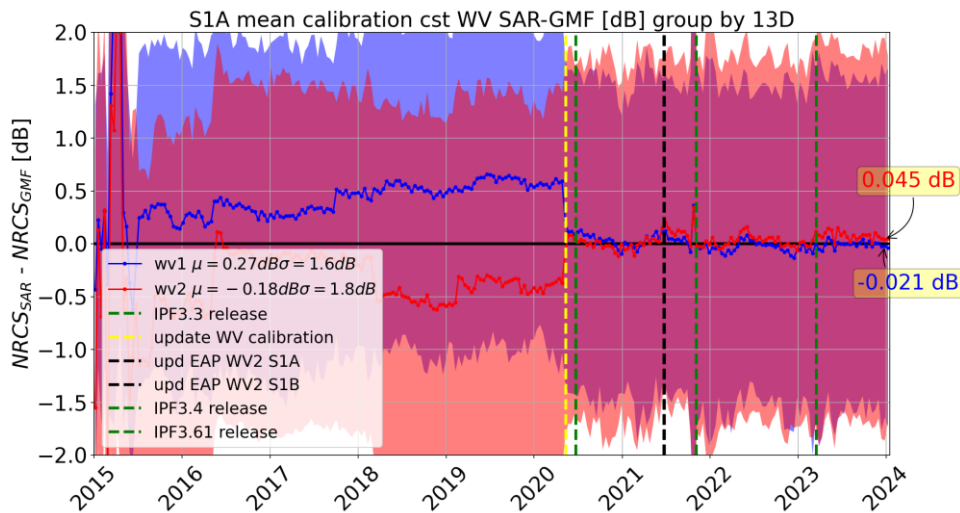
| Satellite | HH RCS [dB] | VV RCS [dB] |
|-----------|-------------------|-------------------|
| AUCR#03 | 46.74 ± 0.16 (14) | 46.54 ± 0.08 (15) |
| AUCR#04 | 43.18 ± 0.13 (14) | 43.01 ± 0.20 (15) |
| AUCR#05 | 47.04 ± 0.09 (14) | 46.93 ± 0.11 (15) |
| AUCR#08 | 43.10 ± 0.13 (14) | 42.94 ± 0.17 (16) |
| AUCR#09 | 42.96 ± 0.19 (13) | 42.89 ± 0.19 (15) |
| AUCR#14 | 46.80 ± 0.12 (14) | 46.62 ± 0.09 (16) |

Table 6: Mean value and standard deviation of derived RCS from the Australian Corner Reflectors

5.1.2 Geophysical Calibration

Due to the absence of WV mode acquisitions over the DLR calibration site located in Germany, the WV mode calibration relies only on the geophysical calibration methodology. Geophysical calibration is performed comparing statistically the values of the SAR normalized radar cross section over oceans with a prediction given by a Geophysical Model Function (GMF) [S1-RD-34] combined with Wind Model Information (ECMWF 0.125° 3h and 1h depending on the period) [S1-RD-33]. The results are presented in Figure 5-6.

Since May 2020, the monitoring is performed using de-noised NRCS compared to Cmod5n GMF.



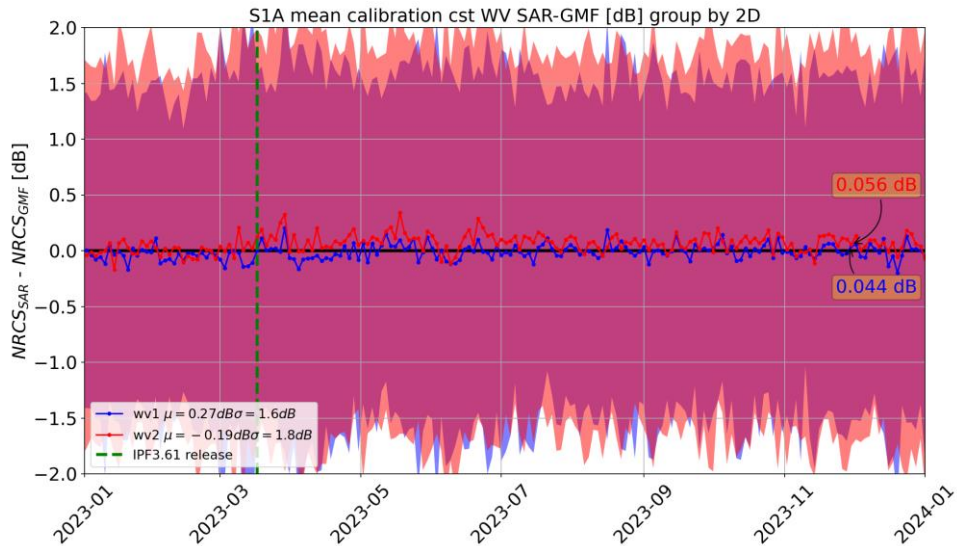


Figure 5-6: assessment of the WV SLC calibration (denoised Sigma0) using geophysical approach i.e. comparison with Cmod-5n with ECMWF0.125° (3h)

Time evolution: The WV SLC NRCS bias is stable in time on year 2023. There was no instrument nor processor evolution impacting the backscatter during the year.

Performances with respect to specifications: The absolute mean NRCS difference between SAR observations and empirical C-band model since May 2020 is below 0.3 dB. The standard deviation of this NRCS bias is computed through two consecutive averaging of the sigma0, i.e., one at imagette level and a second one at SAFE level. The computed standard deviation for 2023 is about 1.6 dB for WV1 and 1.8 dB for WV2.

Discussion about the performances: WV geophysical calibration is already satisfying the calibration accuracy needed for wind inversion.

5.2 Geometric Validation

S-1 nominal geolocation quality was regularly monitored during 2023 using SLC products from the IW mode. EW and SM acquisitions, while not acquired in 2023 over considered calibration sites, were obtained during the earlier S-1A and -B calibration and validation campaigns and are thus not considered for the report at hand. Moreover, geolocation quality was assessed with Extended Timing Annotation Dataset (ETAD) products which have become available in 2023 via the S-1 ground segment production service. They allow for accurate geolocation of level 1 SLC products without the need of further external data or model calculations [S1-RD-21].

5.2.1 Nominal Geometric Validation

Nominal geometric performance monitoring was performed over the *Surat Basin* (Australia) calibration site [S1-RD-04] as well as over the permanently installed corner reflectors of the geodetic stations *Wettzell* (Germany), *Metsähovi*, (Finland), *Yarragadee* (Australia) and *Côte d’Azur Observatory* (France) [S1-RD-30]. The methodology underlying Sentinel-1 geolocation was published in a technical note [S1-RD-25]. The stability and reliability of the wide-area test site in Australia (*Surat Basin*) makes it ideal to perform geometric calibration and validation of SAR sensors. The site includes 40 trihedral CRs covering an area of nearly 13000 km², most of them with 1.5m side lengths and three targets with 2.0m and 2.5m side lengths, respectively. Their positions were confirmed by several research groups to be both accurate

and stable enough for precise geolocation monitoring over long periods and were accurately re-surveyed in 2018 by its maintainer Geoscience Australia [S1-RD-22]. The site has only one significant disadvantage, i.e., all reflectors are oriented towards an ascending orbit, not allowing to easily detect azimuth timing errors via ascending/descending comparisons. For this reason (among others), observations from other sites remain important, especially as a cross-reference complementing larger, longer-term sites such as *Surat Basin*.

The calibration sites at geodetic observatories provide a small number of highly reliable corner reflectors with very accurately determined reference positions at the millimeter level [S1-RD-04][S1-RD-30]. Some of these targets have been installed more than 10 years ago and are used for geometrical calibration and validation of SAR missions such as TerraSAR-X [...]. The sites of *Wettzell* and *Yarragadee* each host two CRs with 1.5m side length, one for ascending and one for descending passes, whereas *Metsähovi* provides one CR with 1.5m edge length facing East (= descending passes, right-looking SAR sensors), and *Côte d'Azur Observatory* hosts one CR with 1.44m edge length facing West (= ascending passes, right-looking SAR sensors). All of these sites are regularly covered in IW-mode with S-1 as ensured by the mission's nominal acquisition plan. In addition, SM-mode data is acquired at the Yarragadee site as permitted by mission capacity.

In this report, we show measurements from products acquired over the *Surat Basin* site, established for many cycles as the reference site for the S-1A/B N-cyclic reports. The results are complemented with the measurements at the geodetic stations *Wettzell*, *Metsähovi*, *Yarragadee*, and *Côte d'Azur Observatory*, allowing for cross-comparison and global assessment of S-1 level 1 data geometric performance.

Overall, the post-processing corrections applied during geolocation estimation may be grouped into the broad categories: (1) geophysical effects, and (2) timing offsets due to inherent S-1 processor design.

For a given CR visible in an S-1 image product, its predicted azimuth and slant range image pixel position was calculated as follows:

- The surveyed CR position was adjusted for acquisition-time (“epoch”) plate **tectonic drift and solid Earth deformation signals**, as described in [S1-RD-24].
- The relevant timing annotations were extracted from the level 1 product annotations; these included the azimuth zero-Doppler time stamps, the orbital state vectors, the near-range fast time, and the range and azimuth sample spacings. Please note that in case of post-processing corrections, the orbital state vectors are extracted from external orbit files (AUX_POEORB) provided at Copernicus Data Space Ecosystem (<https://dataspace.copernicus.eu>) in order to ensure the maximum accuracy in the derived geolocation information.
- Range-Doppler geolocation was performed for the CR coordinate as described e.g., in [S1-RD-11], giving predicted range and azimuth reference times as the output.
- The slant range prediction was corrected by adding the modelled **tropospheric and ionospheric path delays**, and the azimuth time was corrected by subtracting the **bistatic** residual. These effects and their associated corrections are described in detail in [S1-RD-09].
- For TOPS products (IW and EW), a **range shift caused by the Doppler shift dependent on the target azimuth position** within the TOPS burst was shown to be affecting the corresponding ALE estimates [S1-RD-24]. Correcting for these biases on a target-by-target basis yielded a lower range ALE spread, and slightly shifted the mean bias.
- The beam-dependent azimuth biases previously observed in IW and EW analyses were shown to be caused by an error in the way the S-1 IPF was interpreting the azimuth timing annotations (during the so-called **bulk bistatic correction**). While this was mostly visible in TOPS-mode product analyses, the error was also shown to affect SM mode products [S1-RD-09].
- A sub-swath dependent error in the S-1 processor's interpretation of the line time tags was discovered and shown to be causing beam-dependent azimuth shifts corresponding to a given sub-swath's sampling window start time. The ensuing correction was called the **Instrument Timing Correction**. Correcting for this brought the ALE scatter from different IW sub-swaths closer together and moved them toward a zero mean [S1-RD-09].
- Differences between the true height of a reference target and height approximations used by the S-1 processor were shown to be causing a **mismatch between the target azimuth FM rate** and the value annotated in each product [S1-RD-09]. The effect was additionally dependent on the target

azimuth position within a burst (offset from the burst centre). Correction for this effect decreased the ALE standard deviation in azimuth. Because the effect is connected to the target burst position, the magnitude of the correction varies by site. It is generally a much smaller shift than the Instrument Timing Correction described above but in areas significant topographic variation it can amount to more than 1m [S1-RD-08].

- Empirically determined instrument range and azimuth timing calibration constants are applied to compensate for the overall systematic timing biases of the sensors. New reference calibration numbers were derived in 2023 (cf. Appendix F, AUX_ITC), combining multiple corner reflector targets across four sites (Surat Basin, Wettzell, Metsähovi, Côte d’Azur Observatory) and 5.5 years of S-1A and S-1B data [S1-RD-28]. Compared to the previous instrument timing calibration, the values of S-1A changed from 0.1691m to 0.1111m and from 0.0875m to 0.0432m in range and azimuth, respectively. For S-1B, the values changed from 0.0097m to -0.0193m and from -0.3380m to -0.2416m in range and azimuth, respectively.

Adding the above steps resulted in a range-azimuth *predicted* position for each target that could be compared to the position of the peak intensity in the image raster itself, i.e., the *measured* CR position. The differences between predicted and measured positions were then plotted. The S-1A SLC ALE time series for products over the *Surat Basin* site and for products over the geodetic stations acquired in 2023 are shown figures below. Please refer to [S1-RD-05], [S1-RD-06] and [S1-RD-24] for details on the evolution of the standard IPF processing and the geolocation methodology. Figure and Figure show extended time series over joint S-1A/B mission timeline to complement interpretation of the 2023 results.

Since the loss of S-1B satellite in December 2021, only the S-1A satellite is actively monitored by SAR-MPC. The ALE measurements for S-1A are shown separately in figures below (time series) and Figure (2-D plot) for the *Surat Basin* site. The overall statistics are also detailed on a swath basis in Table 8. Complementary results for the geodetic observatory sites are shown in Figure and Figure , and are listed in Table 8. As S-1A suffered the loss of tile #11 in June 2016, a swath dependency is clearly visible from the separated azimuth ALE statistics. With the exception of IW3 sub-swath, which displays a larger offset in the geodetic observatory results, the swath-separation of -0.27m to 0.01m is consistently observed across the azimuth results of 2023 for the different sites.

| | Range ALE [m] | Azimuth ALE [m] |
|----------------------------|----------------------|-----------------------|
| Sentinel-1A (108 products) | 0.059 ± 0.058 | -0.140 ± 0.292 |
| IW-1 | 0.059 ± 0.050 | -0.274 ± 0.283 |
| IW-2 | 0.053 ± 0.052 | 0.018 ± 0.217 |
| IW-3 | 0.068 ± 0.062 | -0.102 ± 0.279 |

Table 7 : Summary of IW SLC product ALE estimates for S-1A for all 2023 acquisitions over the *Surat Basin* calibration site with the post-processing corrections.

| | Range ALE [m] | Azimuth ALE [m] |
|----------------------------|----------------------|-----------------------|
| Sentinel-1A (194 products) | 0.057 ± 0.052 | -0.130 ± 0.335 |
| IW-1 | 0.044 ± 0.046 | -0.241 ± 0.353 |
| IW-2 | 0.054 ± 0.052 | -0.020 ± 0.299 |
| IW-3 | 0.086 ± 0.047 | -0.250 ± 0.305 |

Table 8 : Summary of IW SLC product ALE estimates for S-1A for all 2023 acquisitions over the *Geodetic Observatory* calibration sites (Wettzell, Metsähovi, Yarragadee, Côte d’Azur) with the post-processing corrections.



Despite our careful recalibration of S-1A instrument timings [S1-RD-28], there remains a bias of approximately 0.06 m in the range results of 2023, which is similar for all the sites and sub-swaths. The reason for this bias is not attributed to S-1A SAR instrument degradation but to the increase in solar activity, approaching the maximum of its 11-years cycle that is expected in 2025 [S1-RD-32]. Solar activity significantly affects the ionospheric delay which may become as large as 1 meter for S-1 C-band. The effect is probably not fully captured by our applied ionospheric delay correction, because the factor accounting for top-side ionosphere, i.e., the ionospheric portion not contributing to the delay due to S-1 orbit height [S1-RD-24], was determined with 0.90 during the ionospheric quiet years. Therefore, this factor may not apply to the present situation, leading to an overcompensation of ionospheric delay. First tests with a lower factor of 0.80 show more balanced results between ionospheric quiet and ionospheric active periods. Investigation will continue in 2024 and a possible adjustment of the scaling factor will be considered. The same factor is assumed for implementation in ETAD products.

Interpretation of 2023 results are supported by the long-term mission results shown in Figure 5-11 and Figure 5-12, again comprising the *Surat Basin* calibration site and the geodetic observatory sites. Corresponding statistics are listed in Table 9 and Table 10. The azimuth results of the S-1B satellite, having fully functional antenna tiles, are more consistent than the azimuth results of S-1A. Moreover, the impact of the ionosphere on the range measurements only becomes visible by the end of 2021 which is in line with the onset of increased solar activity [S1-RD-32].

At the science level, there are parts of S-1 geolocation quality that can be further improved in the future (inter-beam consistency, ionospheric delay). However, at the mission requirements level the geolocation performs very well within the specification of the IW mode. The observed ALE lies within the specified 1σ of 3.33m, i.e. 10m at 3σ (section 5.5.2.2 of [S1-RD-07]).

| | Range ALE [m] | Azimuth ALE [m] |
|-----------------------------------|-----------------------|-----------------------|
| Sentinel-1A (481 products) | -0.006 ± 0.059 | -0.138 ± 0.291 |
| IW-1 | -0.011 ± 0.056 | -0.273 ± 0.272 |
| IW-2 | -0.020 ± 0.056 | 0.011 ± 0.233 |
| IW-3 | 0.034 ± 0.055 | -0.067 ± 0.276 |
| Sentinel-1B (156 products) | -0.019 ± 0.044 | -0.005 ± 0.253 |
| IW-1 | -0.017 ± 0.043 | 0.014 ± 0.265 |
| IW-2 | -0.020 ± 0.044 | -0.031 ± 0.234 |
| IW-3 | N/A | NA/ |

Table 9 : Summary of IW SLC product ALE estimates for S-1A and S-1B for all acquisitions since October 2016 over the *Surat Basin* calibration site with the post-processing corrections.

| | Range ALE [m] | Azimuth ALE [m] |
|------------------------------------|----------------------|-----------------------|
| Sentinel-1A (1230 products) | 0.025 ± 0.054 | -0.057 ± 0.354 |
| IW-1 | 0.023 ± 0.052 | -0.088 ± 0.372 |
| IW-2 | 0.020 ± 0.053 | -0.008 ± 0.319 |
| IW-3 | 0.053 ± 0.054 | -0.209 ± 0.404 |
| Sentinel-1B (737 products) | 0.017 ± 0.048 | 0.034 ± 0.333 |
| IW-1 | 0.018 ± 0.043 | 0.039 ± 0.265 |



| | | |
|------|-------------------|-------------------|
| IW-2 | 0.015 ± 0.044 | 0.036 ± 0.234 |
| IW-3 | 0.026 ± 0.053 | 0.018 ± 0.434 |

Table 10 : Summary of IW SLC product ALE estimates for S-1A and S-1B for all acquisitions since October 2016 over the *Geodetic Observatory* calibration sites (Wetzell, Metsähovi, Yarragadee, Côte d’Azur) with the post-processing corrections.

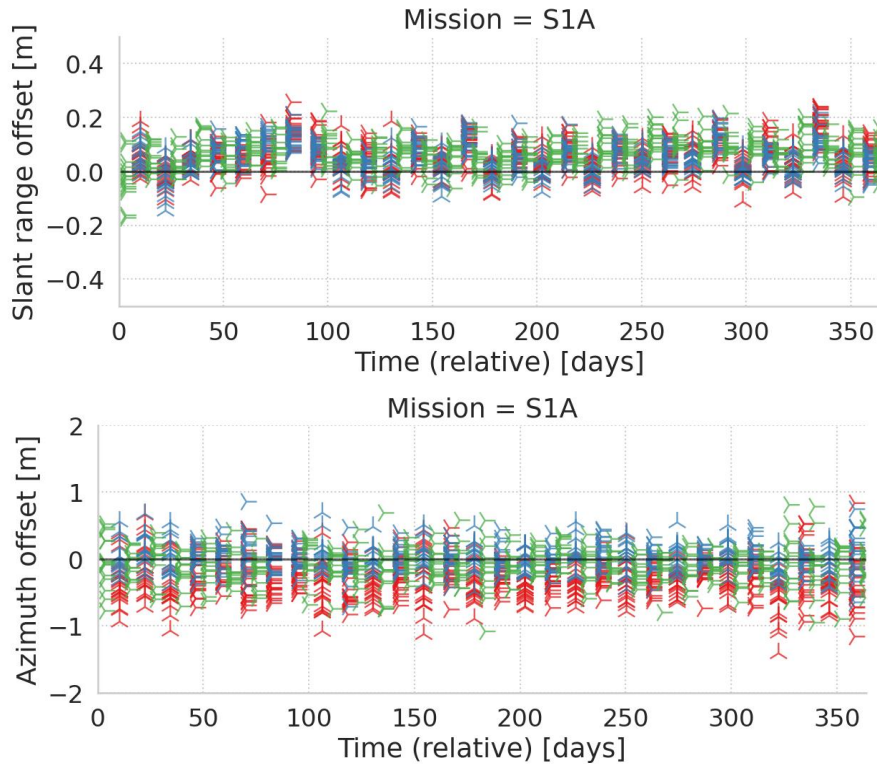


Figure 5-7: S-1A IW SLC ALE time series for products over the *Surat Basin* site acquired in 2023, with post-processing corrections.

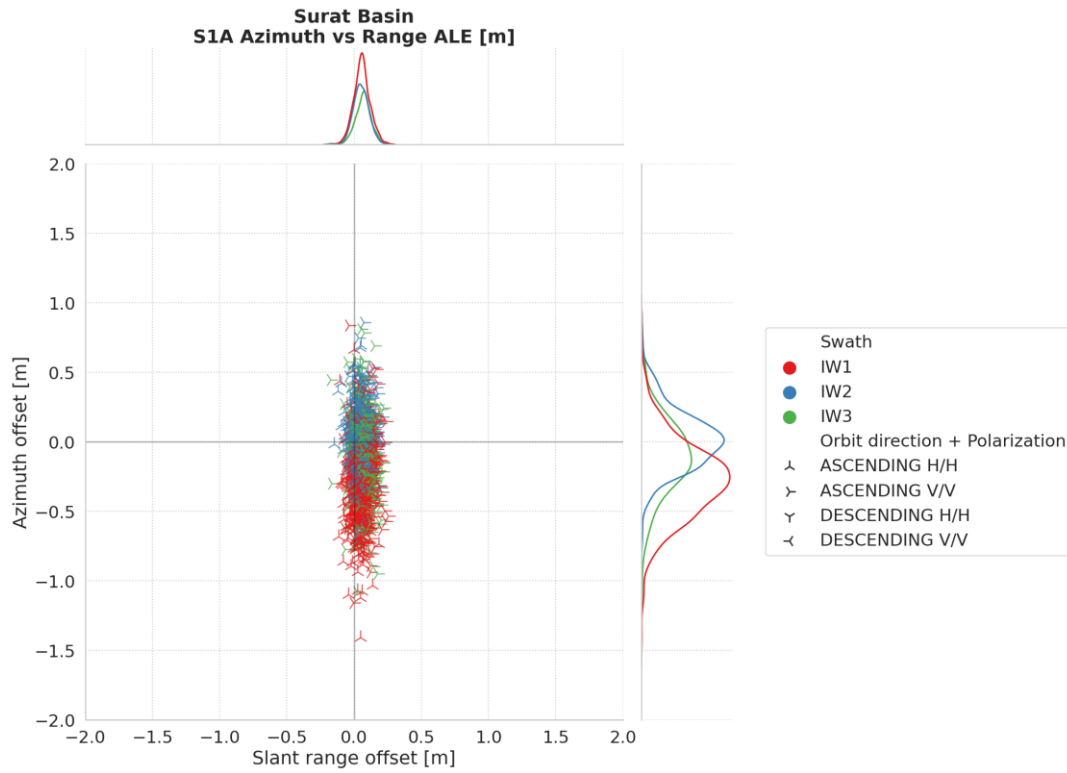


Figure 5-8: S-1A IW SLC ALE performance estimates for products over the *Surat Basin* site acquired in 2023, with post-processing corrections.

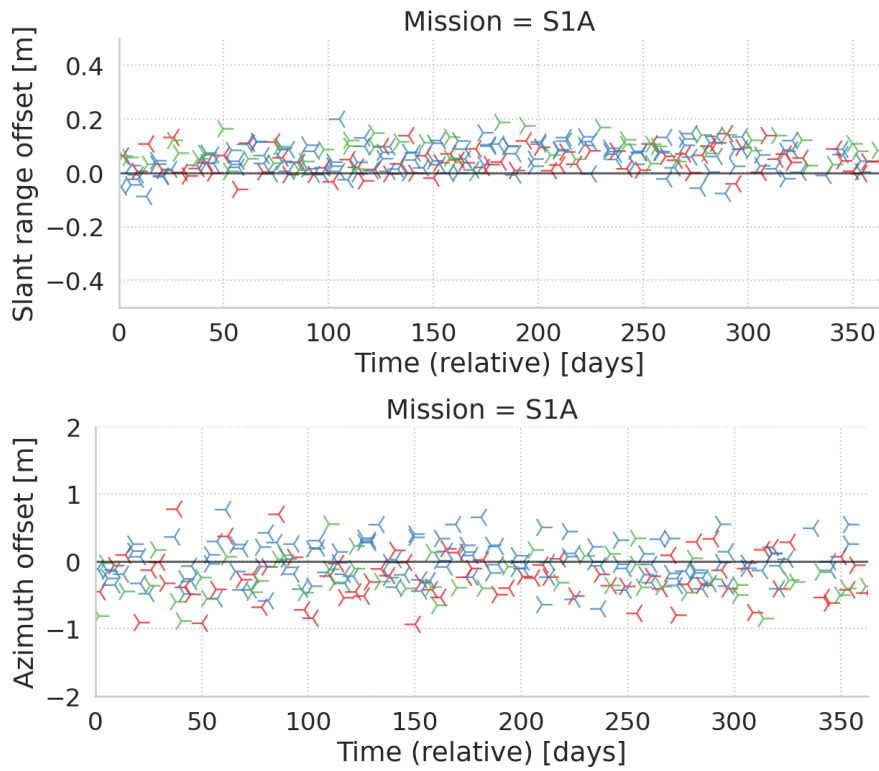


Figure 5-9: S-1A IW SLC ALE time series for products over the *Geodetic Observatory* sites (Wettzell, Metsähovi, Yarragadee, Côte d’Azur) acquired in 2023, with post-processing corrections.

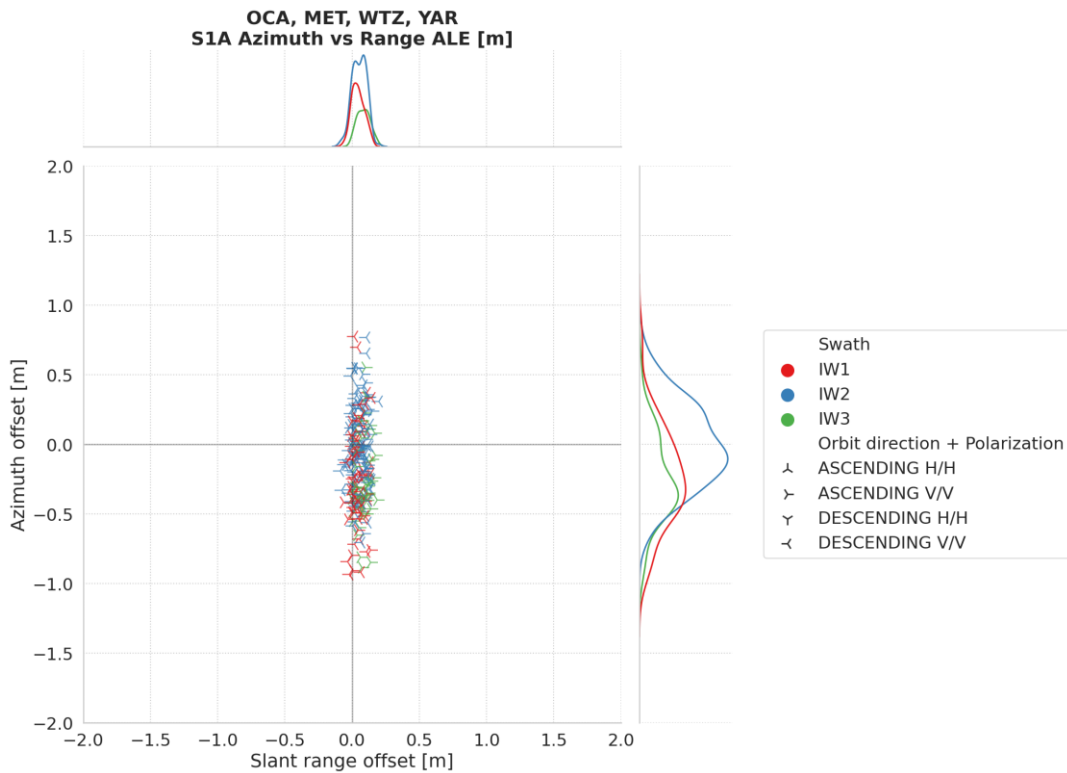


Figure 5-10: S-1A IW SLC ALE performance estimates for products over *Geodetic Observatory* sites (Wettzell, Metsähovi, Yarragadee, Côte d’Azur) acquired in 2023, with post-processing corrections.

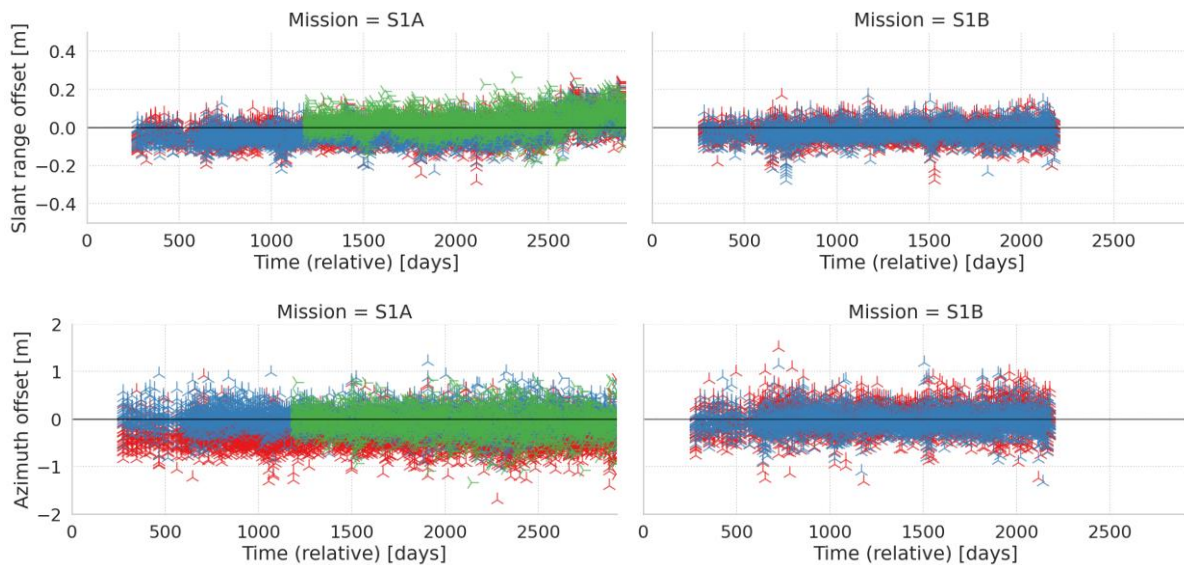


Figure 5-11: S-1A and S1-B IW SLC ALE time series for products over the *Surat Basin* site acquired between Oct 2016 and Dec 2023, with post-processing corrections.

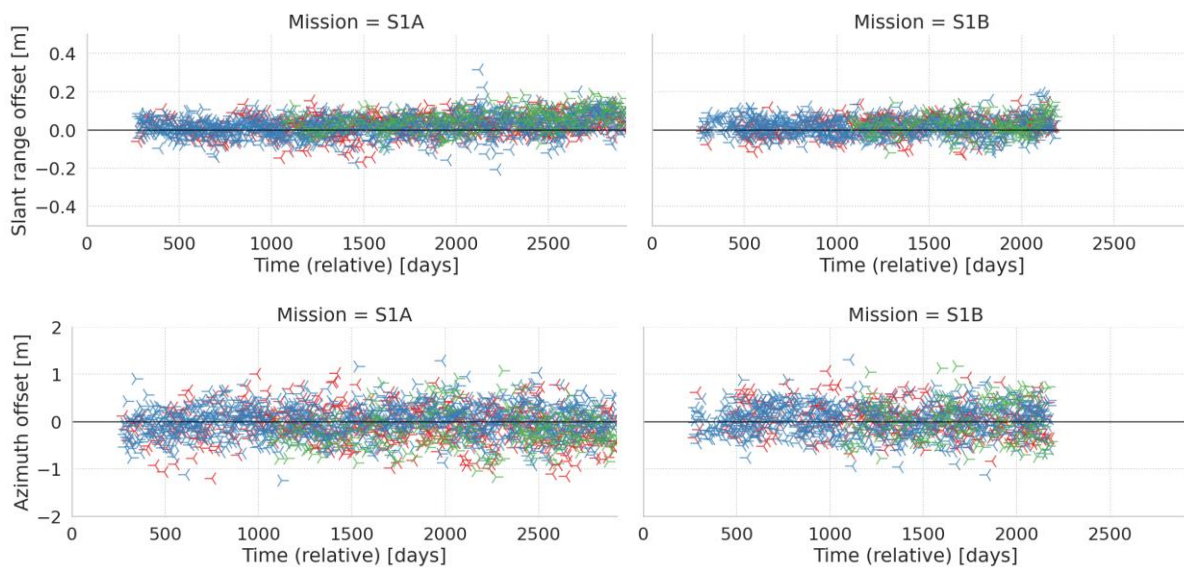


Figure 5-12: S-1A and S1-B IW SLC ALE time series for products over the *Geodetic Observatory* sites (Wetzell, Metsähovi, Yarragadee, Côte d’Azur) acquired between Oct 2016 and Dec 2023, with post-processing corrections.

For comparison, the times series and 2-D geolocation plots of 2023 were also generated without post-processing corrections, showing the “out of the box accuracy” of geolocation measurements. These results represent the geolocation accuracy of the S-1 products as delivered to the users, if no further correction or external orbit product are applied. Figure and Figure show the ALE time series and the ALE measurements without post-processing corrections over *Surat Basin* calibration site, respectively. The plots demonstrate that the overall bias and the spread in range and azimuth are on the order of one or more meters. With the post-processing corrections, the bias and the spread are instead on the order of the decimetres or less. Nevertheless, these results confirm a consistent level 1 IW product generation throughout 2023 for the *Surat Basin* test site and that the “out of the box accuracy” is within the 10m localization performance requirement [S1-RD-07].

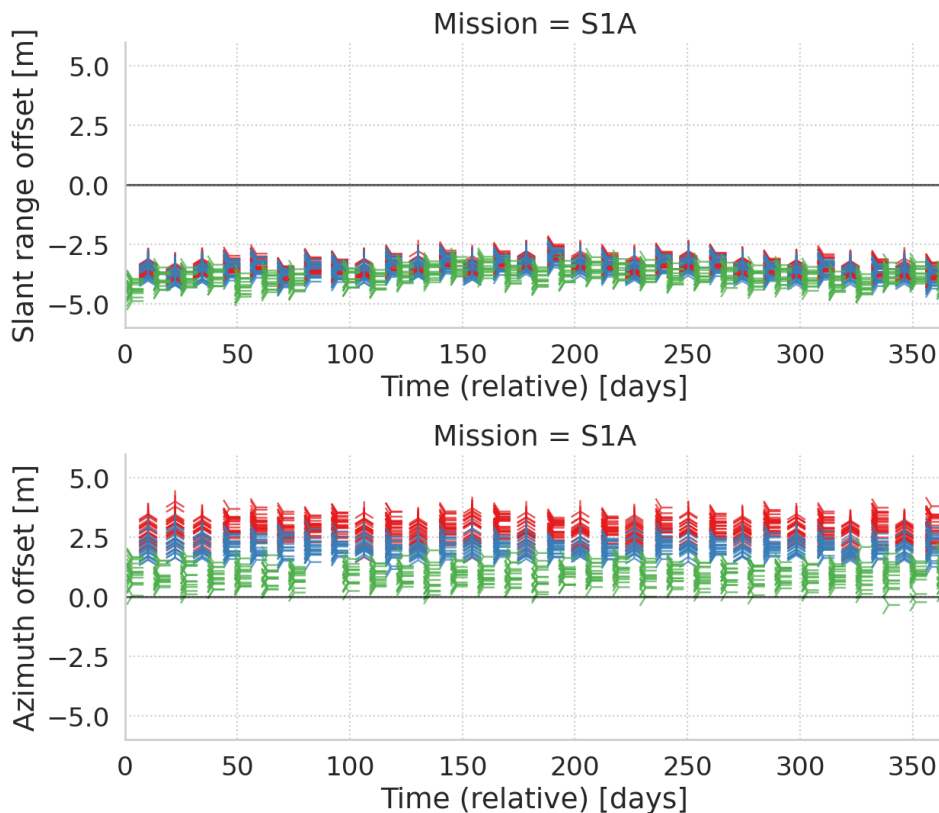


Figure 5-13: S-1A IW SLC ALE time series for products over the *Surat Basin* site acquired in 2023, without post-processing corrections.

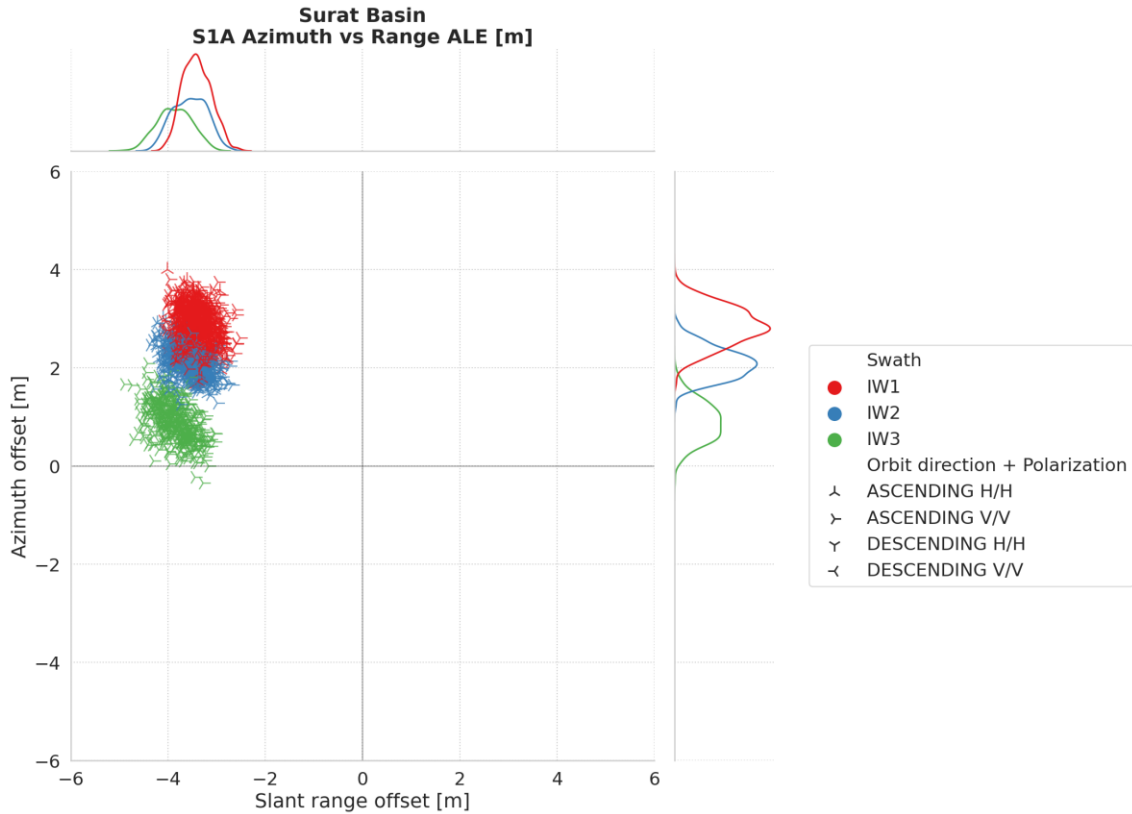


Figure 5-14: IW SLC product ALE estimates for S-1A for all 2023 acquisitions over the *Surat Basin* calibration site without the post-processing corrections.

| | Range ALE [m] | Azimuth ALE [m] |
|----------------------------|--------------------|-------------------|
| Sentinel-1A (108 products) | -3.565 ± 0.369 | 2.124 ± 0.857 |
| IW-1 | -3.407 ± 0.289 | 2.841 ± 0.392 |
| IW-2 | -3.552 ± 0.341 | 2.082 ± 0.312 |
| IW-3 | -3.863 ± 0.349 | 0.897 ± 0.402 |

Table 11: Summary of IW SLC product ALE estimates for S-1A for all 2023 acquisitions over the *Surat Basin* calibration site without the post-processing corrections.

5.2.2 Geometric Validation with ETAD Products

The ETAD product contains in one comprehensive package all the post-processing corrections as described in the previous chapter along with S-1 precise orbit solution [AD-09]. It is generated by the ground segment and distributed with a latency of 21 days after an acquisition for all SM and IW SLC level 1 products, as well as for EW SLC products at an experimental level. Initial production service started in April 2023 and products became publicly available for all data as of July 21st, 2023, via the Copernicus Data Space Ecosystem. For details on the ETAD correction methods, please refer to [AD-10].

Monitoring of ETAD product performance is performed at the calibration sites as part of S-1 geometric validation. The main calibration site of *Surat Basin* (Australia) [S1-RD-04] and its wide-spread distribution of targets allow for straight forward product monitoring when comparing the nominal results (chapter

5.2.1) with the results obtained from only applying the ETAD products. The processing steps are identical to nominal geometric validation except for the post-processing corrections, which are extracted at the known target location from the ETAD product of a given date.

The results comprise all disseminated ETAD products of the level 1 SLC IW data that have been acquired at Surat Basin calibration site, i.e., a data coverage between July and December 2023. The ALE time series and the 2-D geolocation plot are shown in Figure and Figure , respectively. The corresponding result statistics are summarized in Table 12.

The results including the ETAD corrections are in very close agreement with the nominal S-1A range and azimuth geometrical validation results of 2023. Again, we observe the residual range bias due to the ionospheric delays (see discussion in chapter 5.2.1), which has to be expected as ETAD products apply the same scaling factor of 0.9 to account for the top-side ionosphere [AD-10]. The variation in azimuth sub-swaths is a confirmed characteristic of the S-1A unit and is not addressed with current version of ETAD products. The spread in azimuth is equally observed with the nominal processing and is due to the coarse azimuth resolution of IW products, which limits attainable geolocation accuracy. Therefore, the ETAD performance as measured at Surat Basin calibration site is considered in agreement with the ETAD correction specification of 0.2 m range and 0.1 m azimuth (1σ , [AD-12]). Possible further improvements of the products will be studied in 2024 in order to address the limitations of ionospheric delay correction and to mitigate the sub-swath characteristics of S-1A.

| | Range ALE [m] | Azimuth ALE [m] |
|---------------------------|----------------------|-----------------------|
| Sentinel-1A (50 products) | 0.075 ± 0.059 | -0.144 ± 0.289 |
| IW-1 | 0.074 ± 0.063 | -0.288 ± 0.270 |
| IW-2 | 0.060 ± 0.052 | 0.014 ± 0.219 |
| IW-3 | 0.095 ± 0.053 | -0.094 ± 0.279 |

Table 12: Summary of IW SLC product ALE estimates for S-1A for July to December 2023 acquisitions over the *Surat Basin* calibration site with *ETAD* post-processing corrections.



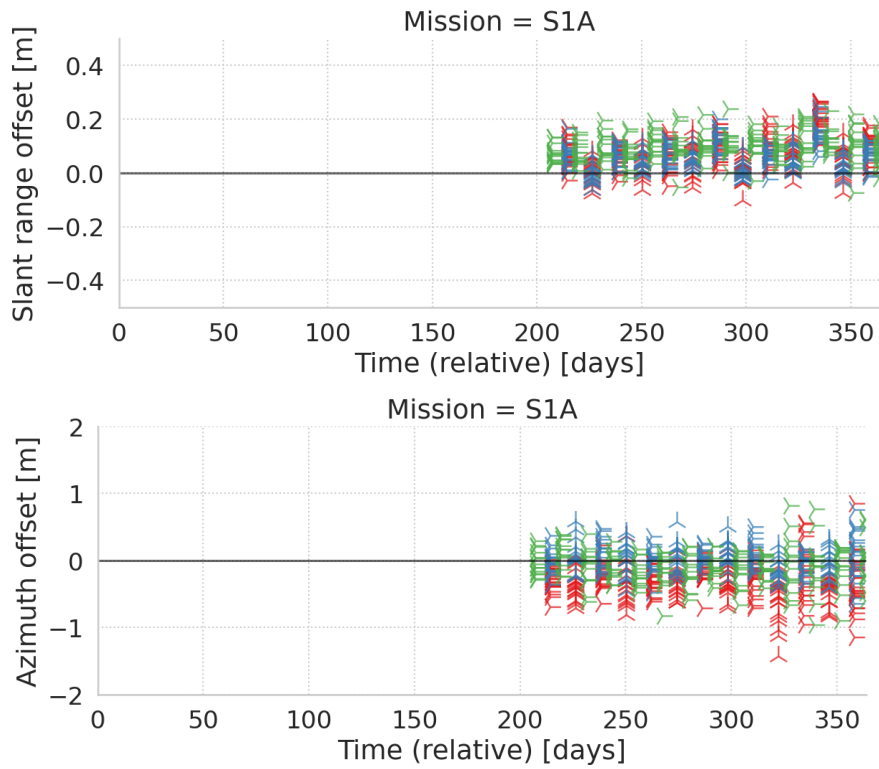


Figure 5-15: S-1A IW SLC ALE time series for products over the *Surat Basin* site acquired between July to December 2023, applying ETAD post-processing corrections.

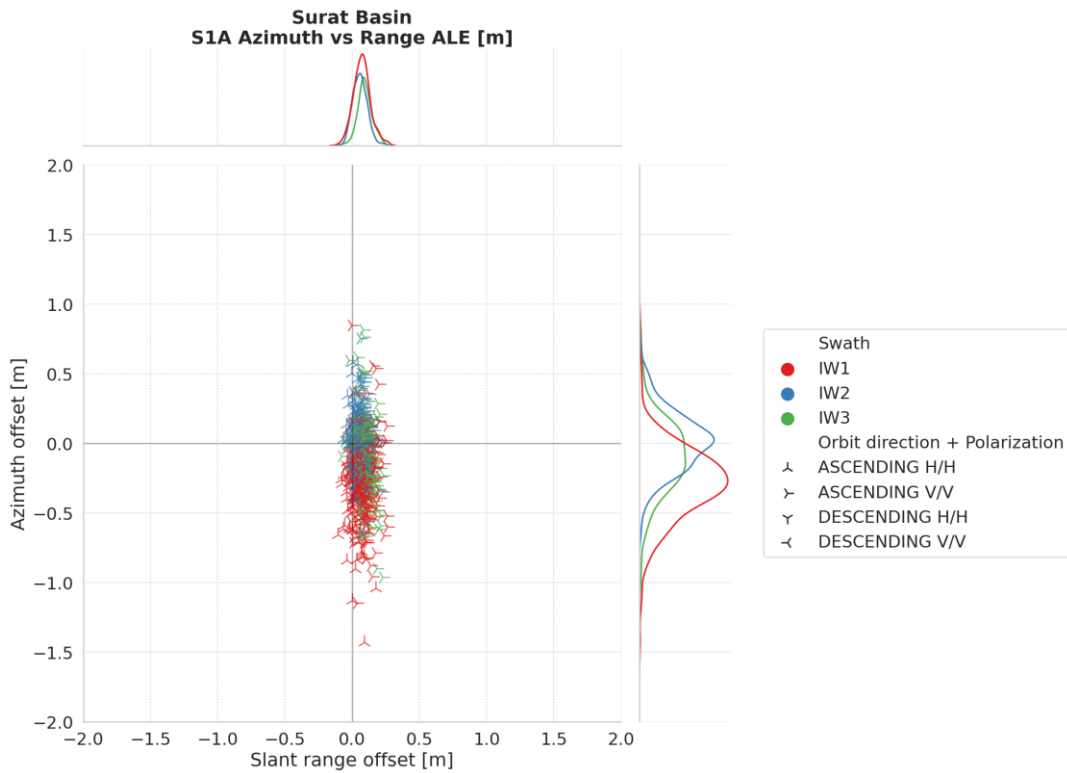


Figure 5-16: S-1A IW SLC ALE performance estimates for products over the *Surat Basin* site acquired between July to December 2023, applying ETAD post-processing corrections.

5.3 Polarimetric Calibration

5.3.1 Gain Imbalance

The DLR transponders [S1-RD-15] have also been used to derive the channel imbalance from the respective impulse responses. The gain imbalance is computed by the differences (in dB) between the calibration factor derived from the VV and the VH polarization images.

The gain imbalance is depicted in Figure 5-17 for the IW mode in DV polarization for S-1A covering the observation period 2023. The plot shows the mean values (red crosses) and standard deviations (red error bars) of the channel imbalance for each acquisition geometry, i.e., for measurements acquired with a certain elevation or look angle. For S-1A, a gain imbalance of 0.15 dB is determined on average with a standard deviation of 0.18 dB as listed in Table 13.

| Satellite/Mode | Gain Imbalance (dB) |
|-----------------|---------------------|
| S-1A IW (VV/VH) | 0.15 ± 0.18 |

Table 13: Gain Imbalance using the DLR transponders.

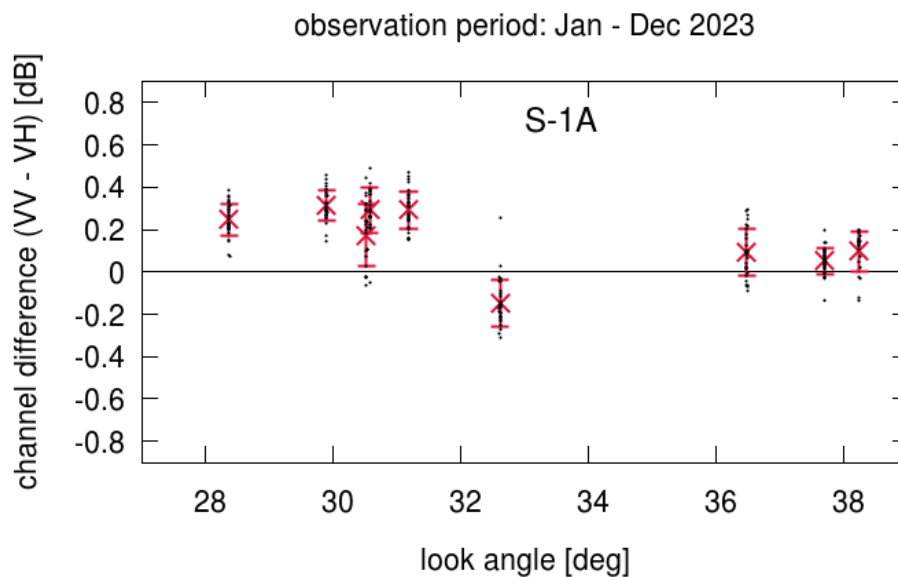


Figure 5-17: IW Gain Imbalance of S-1A using the DLR transponders.

5.3.2 Phase Imbalance

The channel imbalance in phase is determined similarly to the channel imbalance in amplitude as described in the previous section for the IW mode with DV polarizations acquired over the DLR transponders in 2023. The phase difference is computed by subtracting the VH polarization channel phase from the VV polarization channel phase. The remaining phase differences are very low and do not exceed 4 degrees. The mean values and standard deviations are listed in Table 14.

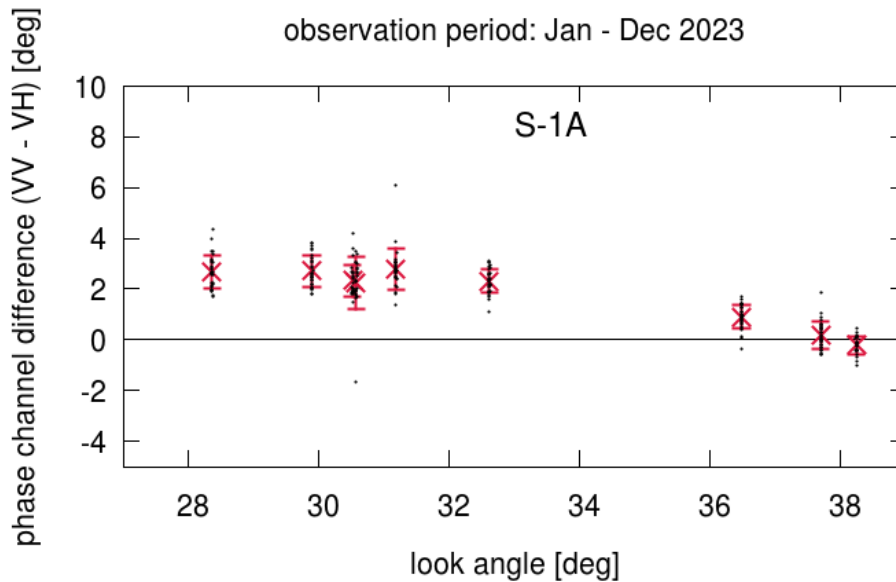


Figure 5-18: Phase Imbalance using the DLR transponders.

| Satellite/Mode | Phase Difference [deg] |
|----------------|------------------------|
| S-1A IW | 1.79 ± 1.25 |

Table 14: Phase Imbalance using the DLR transponders.

5.3.3 Coregistration

The DLR transponders [S1-RD-15] provide an impulse response in both polarisations of dual polarisation imagery which enables co-registration to be performed between the two polarisation images. Table 15 below shows that the average measured polarimetric co-registration derived from SLC products acquired during 2023 is very small (the IRF peak position is measured to a 1/8 of a pixel).

| Satellite / Mode | Range Co-registration Accuracy (m) | Azimuth Co-registration Accuracy (m) | Number of Measurements |
|------------------|------------------------------------|--------------------------------------|------------------------|
| S-1A IW | -0.01 ± 0.05 | 0.05 ± 0.25 | 243 |

Table 15: Polarimetric Calibration Measurements

5.3.4 Crosstalk

The trihedral corner reflectors of the DLR calibration site [S1-RD-15] with a leg length of 2.8 m enable to derive the crosstalk since they provide an impulse response only for co-polarisation (HH or VV) with sufficient energy. The derived crosstalk of S-1A is depicted in Figure 5-19 for the observation period in 2023. The mean crosstalk values with standard deviations for both instruments are listed in Table 16.

The derived crosstalk is very low and confirms the very good quality concerning the separation of the co- and cross polarization channels of the S-1A SAR instrument.

| Satellite | Crosstalk [dB] | Number of Measurements |
|-----------|----------------|------------------------|
| S-1A | -39.4 ± 4.9 | 255 |

Table 16: Cross-talk Measurements

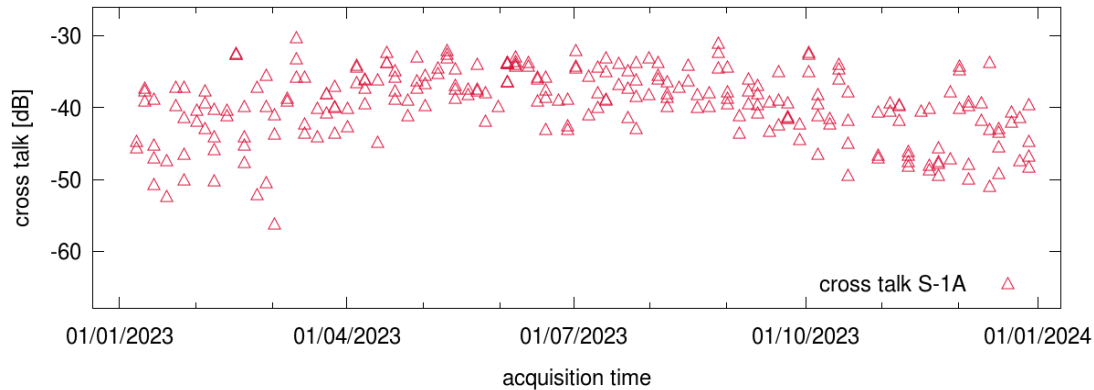


Figure 5-19: Crosstalk derived from DLR corner reflectors for S-1A.

5.4 Elevation Antenna Patterns

The validity of the Elevation Antenna Patterns is monitored through analysis of gamma profiles measured over Amazon Rain Forest [S1-RD-35].

There was no update to the S-1A elevation antenna patterns during 2023.

The characterisation of the elevation antenna pattern is provided in the AUX_CAL auxiliary data files. Refer to Appendix F - for the list of them and how to access them.

5.5 Azimuth Antenna Patterns

There was no update to the S-1A azimuth antenna patterns during 2023.

5.6 Noise Equivalent Radar Cross-section

S-1 imagery with low ocean backscatter can be used to estimate the Noise Equivalent Radar Cross-Section (NESZ). The S-1 L1 Annotation file contains a sequence of noise vectors that users can employ to compute the NESZ content of the L1 image [AD-01].

These annotated noise vectors of GRD products presented a shift in range, further described in [QD-90] that was solved after the deployment of IPF v3.5.1 since 23rd March 2022.

Additionally, for some specific acquisitions, the S-1 IPF contained a remaining software bug that resulted in the truncation of the annotated noise vectors. The following Figure 5-20 shows the effects of this anomaly. This issue was solved thanks to the deployment of S-1 IPF v3.6.1 on 2023-03-30.

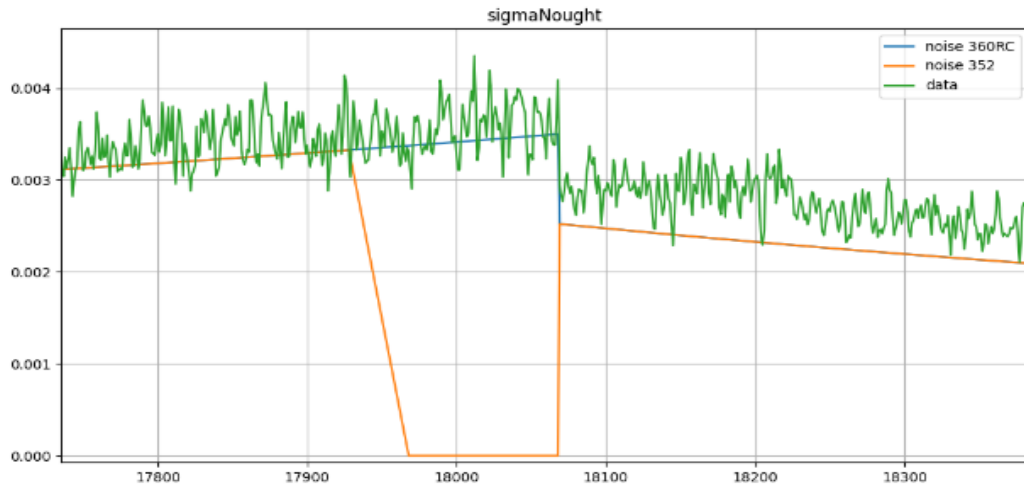


Figure 5-20: Annotated denoising vectors compare to measured NESZ. Green: low-backscatter image profile Orange: annotated noise vector with IPF 3.5.2. Blue: annotated noise vector with IPF 3.6.0

After the fix of the bugs mentioned above, a noise vectors recalibration activity was performed to improve the quality of the noise vectors in the SAFE products annotation. The activity focused first on the recalibration of S1A TopSAR IW and EW products. A set of bursts with low backscatter was identified through the *inBandOutBandPowerRatio* value annotated in the rfi folder of the SAFE products (introduced with IPF 3.4.0 in November 2021) [AD-01]. The variable represents the ratio between the energy within the chirp bandwidth and the energy outside the chirp bandwidth. A value close to 1 identifies a burst with very low (or no) back-scatter that can be used for the re-calibration of the noise vectors. Figure 5-21 shows an example of the range profile of a burst with ratio of 0.999. The burst range profile shape (in blue) matches well the noise vector shape (in yellow). The removal of the observed discrepancy between data and noise vector level is the objective of the re-calibration activity.

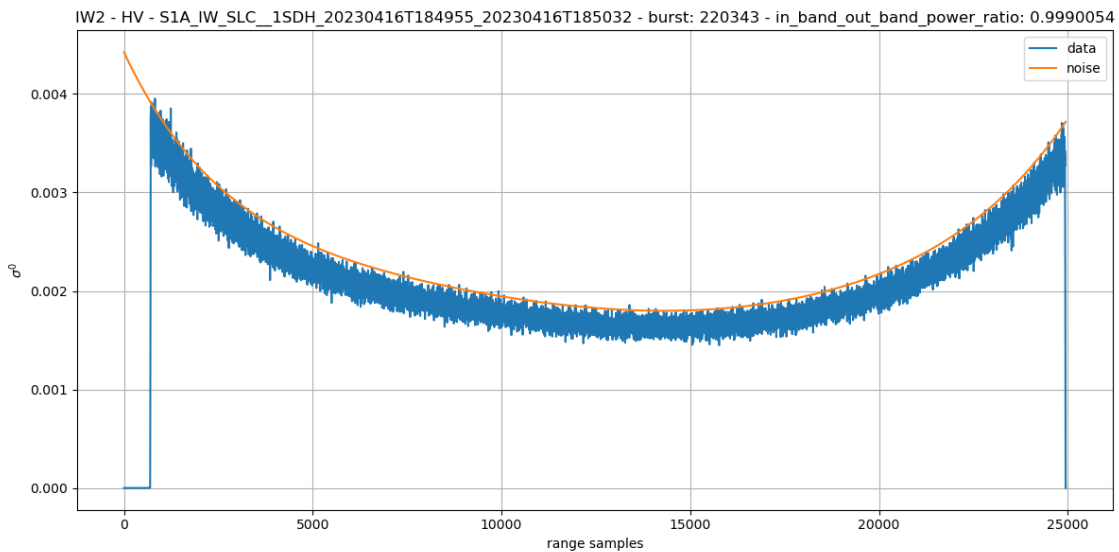


Figure 5-21: Range profile (blue) and corresponding noise vector (yellow) of a burst with very low backscatter level.

20 bursts per sub-swath and polarization (cross-pol only) have been selected to compute the delta noise calibration factor to get the best alignment between noise vectors and data. As an example, Figure 5-22 shows the result of the re-calibration activity for EW2 sub-swath in HV polarization. The image on the left represents the current difference between data and noise vectors. The image on the right represents the difference after applying the estimated correction factor (0.157 dB in this case). The distribution on the right is better centred around 0 dB.

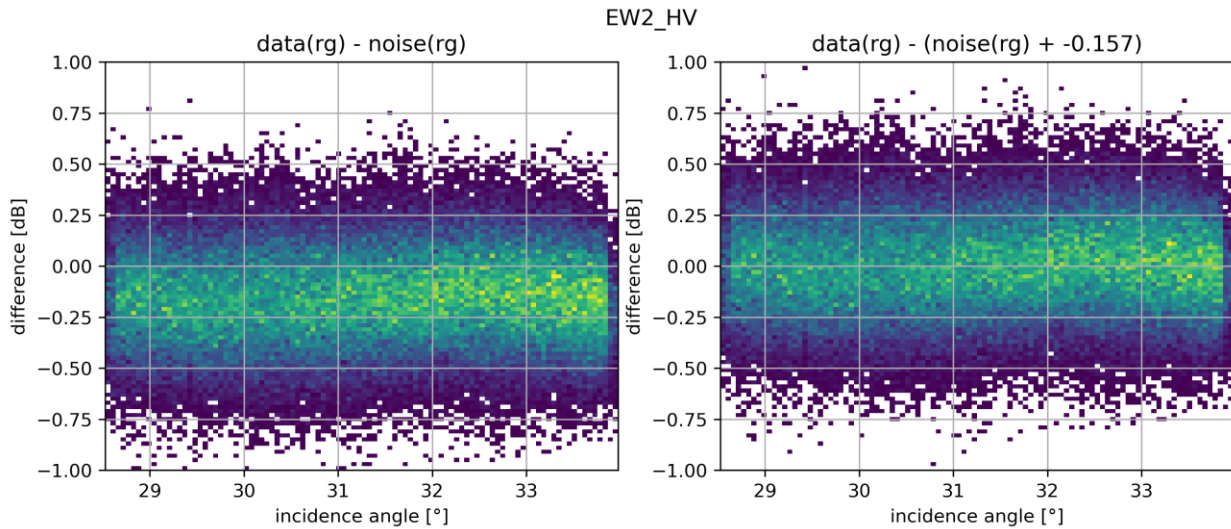


Figure 5-22: (Left) Distribution of the difference between data and noise vectors as a function of the incidence angle for EW2 HV beam. (Right) Same distribution after applying the estimated noise calibration correction factor.

The estimated noise calibration factors have been included in a new version of the S1A AUX-CAL file that was circulated in March 2024. In the next months a similar activity will be performed for WV data and for S1B TopSAR beams.

5.7 Interferometric Performances

The interferometric performances, and particularly the coherence level of an interferogram between two S-1 images, depend on several factors including:

- Stability of the imaged scene (temporal coherence)
- Thermal noise level of the considered acquisitions (see sections 4.3 and 5.6)
- Geometric decorrelation due to different acquisition geometry (orbit baseline)
- Volumetric decorrelation due to targets structure
- Synchronization of the acquisitions (for TOPSAR modes only)
- Stability of the sensor pointing to ensure Doppler spectrum overlap.

The S-1A performances related to geometric decorrelation and synchronisation of the acquisitions are reported in the following sections.

5.7.1 S-1 Orbit Baseline

Repeat pass interferometry requires that acquisitions at different times are performed with a similar orbit to ensure high coherence interferograms. The “distance” between the orbits of a pair of interferometric acquisition is called the interferometric baseline. The interferometric baseline is continuously monitored by the MPC, comparing S-1 State Vectors of current orbits (from AUX-RESORB files) with those of an arbitrary selected reference cycle in the past, namely the cycle number 60 (30 September - 12 October 2015) for S-1A.

Figure 5-23 shows the evolution during 2023 of the three interferometric baseline components (Parallel on top, Normal in the middle and Along-Track at the bottom). The hot colours are used for the maximum baseline value and the cold colours for the minimum baseline value measured for each orbit. The different colours represent the track number evolving for each cycle from 1 to 175.

The most critical baseline component for the interferometric coherence is the normal one, which must be significantly lower than the critical baseline to preserve interferometric coherence. For S-1A the critical baseline is about 5 km, depending on the considered swath) The measured normal baseline (mid plot) shows that normal baselines are below 10% of the critical one, i.e., the worst-case coherence loss due to the interferometric baseline is always well below 10%.

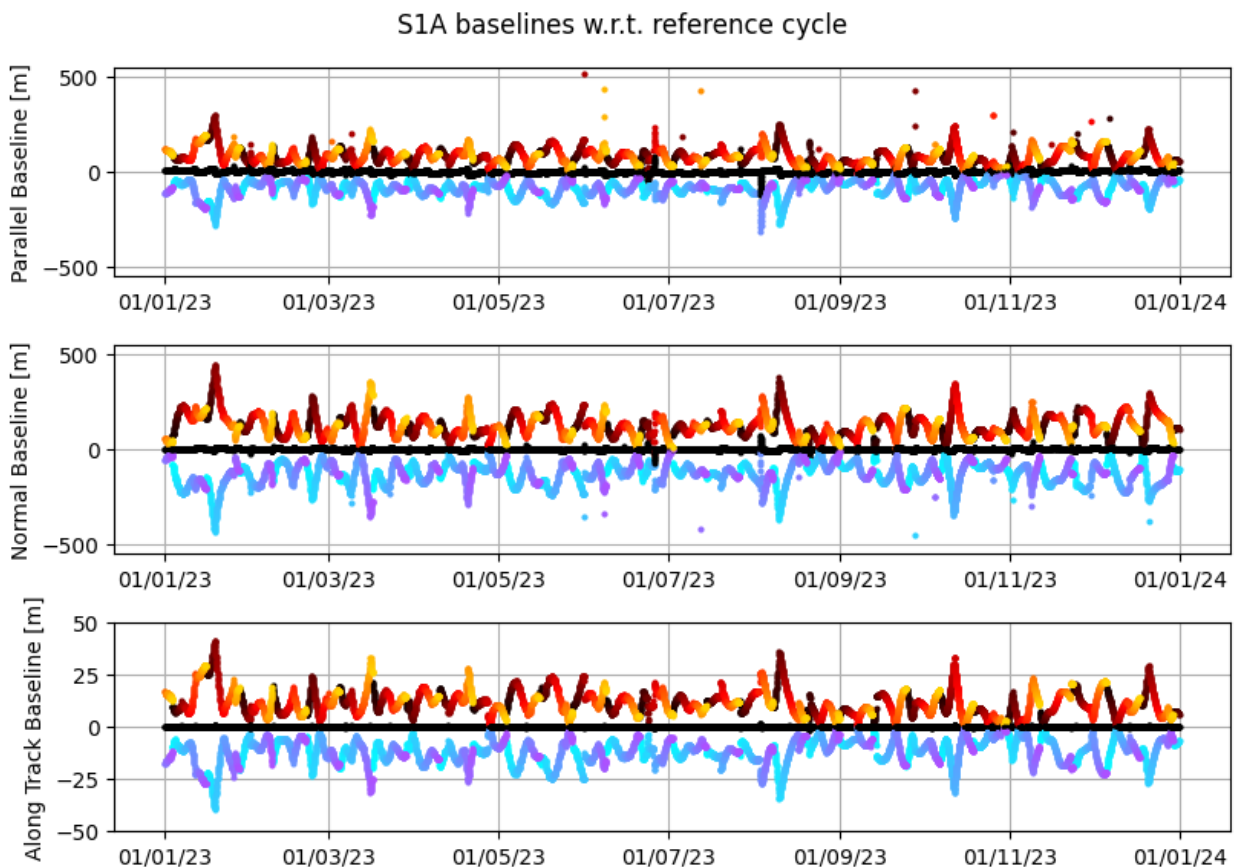


Figure 5-23: S-1A parallel (top), normal (mid) and along-track (bottom) interferometric baseline components during 2023, computed for the given cycle with respect to a fixed reference cycle. Warm colours are used for the maximum value and cold colours for the minimum value of each orbit. The colours represent the track number.

To complement the monitoring of the interferometric baseline computed with respect to a fixed reference cycle, a new monitoring has been implemented to evaluate the interferometric baseline of each cycle with respect to its previous one. The results are shown in Figure 5-24, expressed in the same

components and with the same colour schemes as the previous plot. Even this approach shows that the normal baseline has not exceeded the value of 500 m in 2023.

S1A baselines w.r.t. previous cycle

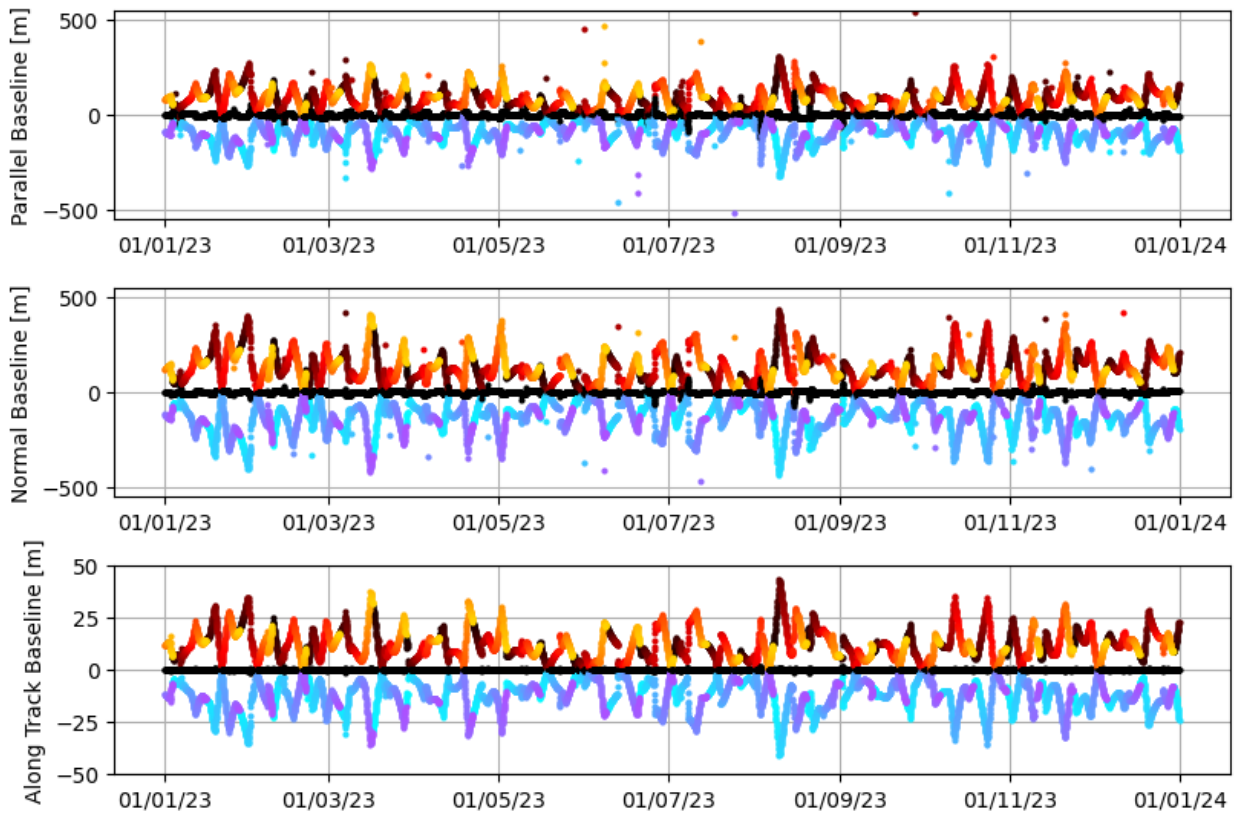


Figure 5-24 S-1A parallel (top), normal (mid) and along-track (bottom) interferometric baseline components during 2023, computed for the given cycle with respect to its previous one. Warm colours are used for the maximum value and cold colours for the minimum value of each orbit. The colours represent the track number.

Figure 5-25 and Figure 5-26 show the interferometric baselines, computed with the two monitoring approaches, from 2015 to 2023. Both approaches show that the max/min baseline components range has increased since the second half of 2022.

S1A baselines w.r.t. reference cycle

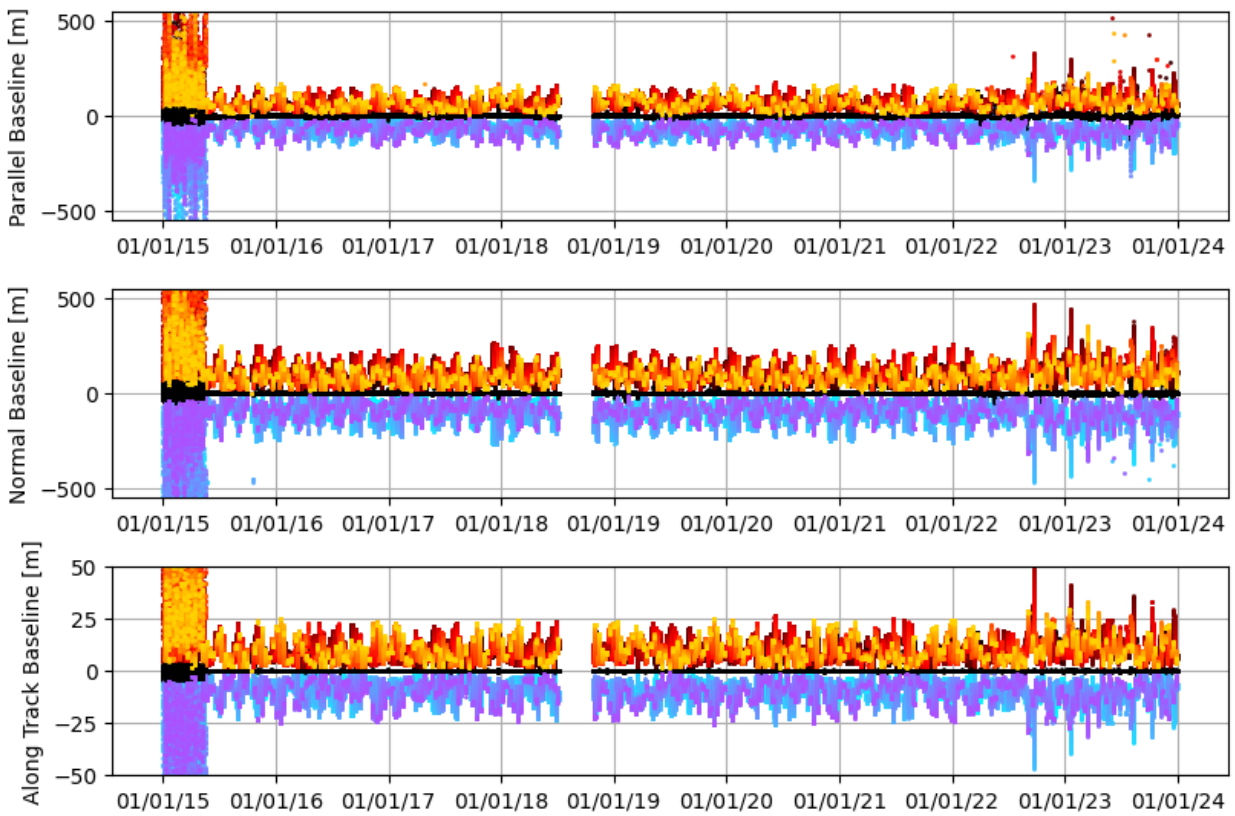


Figure 5-25 S-1A interferometric baseline components from 2015 to 2023, computed for the current cycle with respect to a reference cycle in 2015

S1A baselines w.r.t. previous cycle

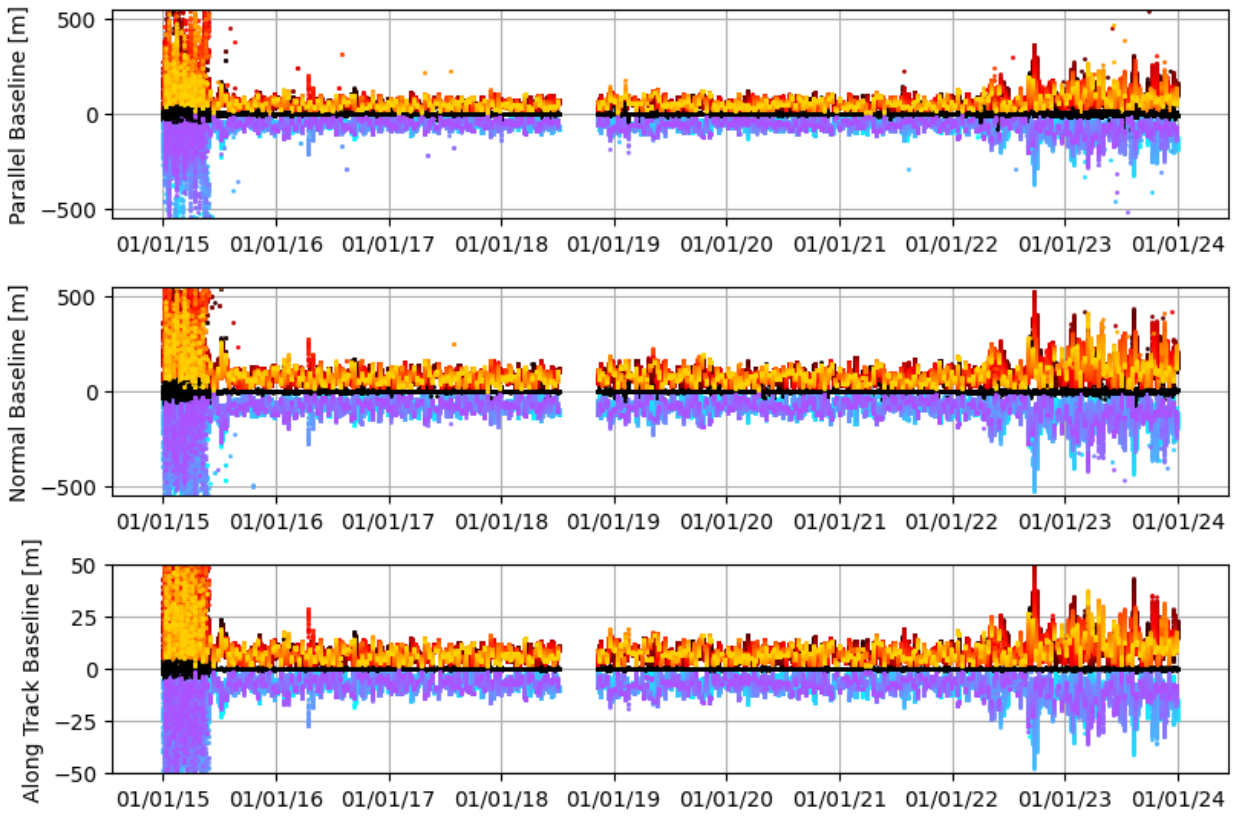


Figure 5-26 S-1A interferometric baseline components from 2015 to 2023, computed for the current cycle with respect to its previous cycle

5.7.2 S-1 Burst Synchronization

The burst synchronization between repeat pass interferometric acquisitions is relevant for the TOPSAR modes (IW and EW), to provide an indication of the quality of the interferometric phase that can be expected. The SAR acquisition start time is planned over a discrete set of points round orbit with precision down to milliseconds. The burst synchronization is systematically monitored by the MPC comparing the times of TopSAR acquisitions derived from current LOA products. The burst synchronization is always monitored by a relative comparison between two acquisitions. One way to implement this monitoring consists in evaluating the burst synchronization error of each acquisition with respect to the corresponding acquisition performed in a fixed reference cycle from the past. The results of this approach, denoted as “monitoring with respect to reference cycle”, performed considering as reference the cycle number 60 (30 September - 12 October 2015), are shown in Figure 5-27. The monitoring with respect to a reference cycle benefits from having a fixed cycle of comparison, but it strongly depends on the reference cycle. To complement this approach, another type of monitoring is performed in which each cycle is evaluated with respect to its previous one. The results of this approach for 2023 are shown in Figure 5-28. The results from the monitoring with respect to the previous cycle have a lower standard deviation at a fixed point in time, but they show a larger peak-to-peak variation, reaching a maximum variation of +/- 15 ms. This larger variation has been observed since the second half of 2022. The cause for the different results between the two methods is under investigation.

A requirement on the SAR instrument is to be capable of synchronizing bursts between interferometric pairs to better than 5 ms (3 sigma), see requirement SAR-046. The burst synchronisation is performed by the instrument against a theoretical orbit, while the monitoring is performed comparing two different real orbits: one as a reference (being either the previous one or a reference one) and another one, and none of them exactly matching the theoretical one. Then the comparison of two real orbits shall account for their respective mis alignment with the theoretical one. For this reason, we deem reasonable to use as corresponding requirement the value of $\sqrt{2} * 5$ ms, obtained from the combination of two independent pairs. With respect to this requirement, we compute the percentage of burst synchronization error measurements falling in between $\pm\sqrt{2} * 5$ ms. Then, in the monitoring with respect to the reference, the IW mode has a compliance of 83.7%, the EW mode has a compliance of 90.68%. In the monitoring with respect to previous cycle, the IW mode has a compliance of 90.68%, the EW mode a compliance of 93.01%.

A synchronization timing error between two bursts causes a mismatch in the Doppler bands under which targets are observed, which in turn causes a loss of coherence. It can be shown that the loss of coherence is approximately linearly proportional to the timing error, such that for S-1 an error of 5 ms, corresponding to a Doppler spectrum overlap reduction of about 10 Hz in the SLC products. This represents a coherence loss of about 3% for IW mode that has a processed bandwidth around 300 Hz. This estimate is obtained considering only the Doppler mis-match due to the burst de-synchronization; an additional error in pointing may either increase or decrease the Doppler error depending on the sign, thus increasing, or decreasing the coherence loss [S1-RD-36].

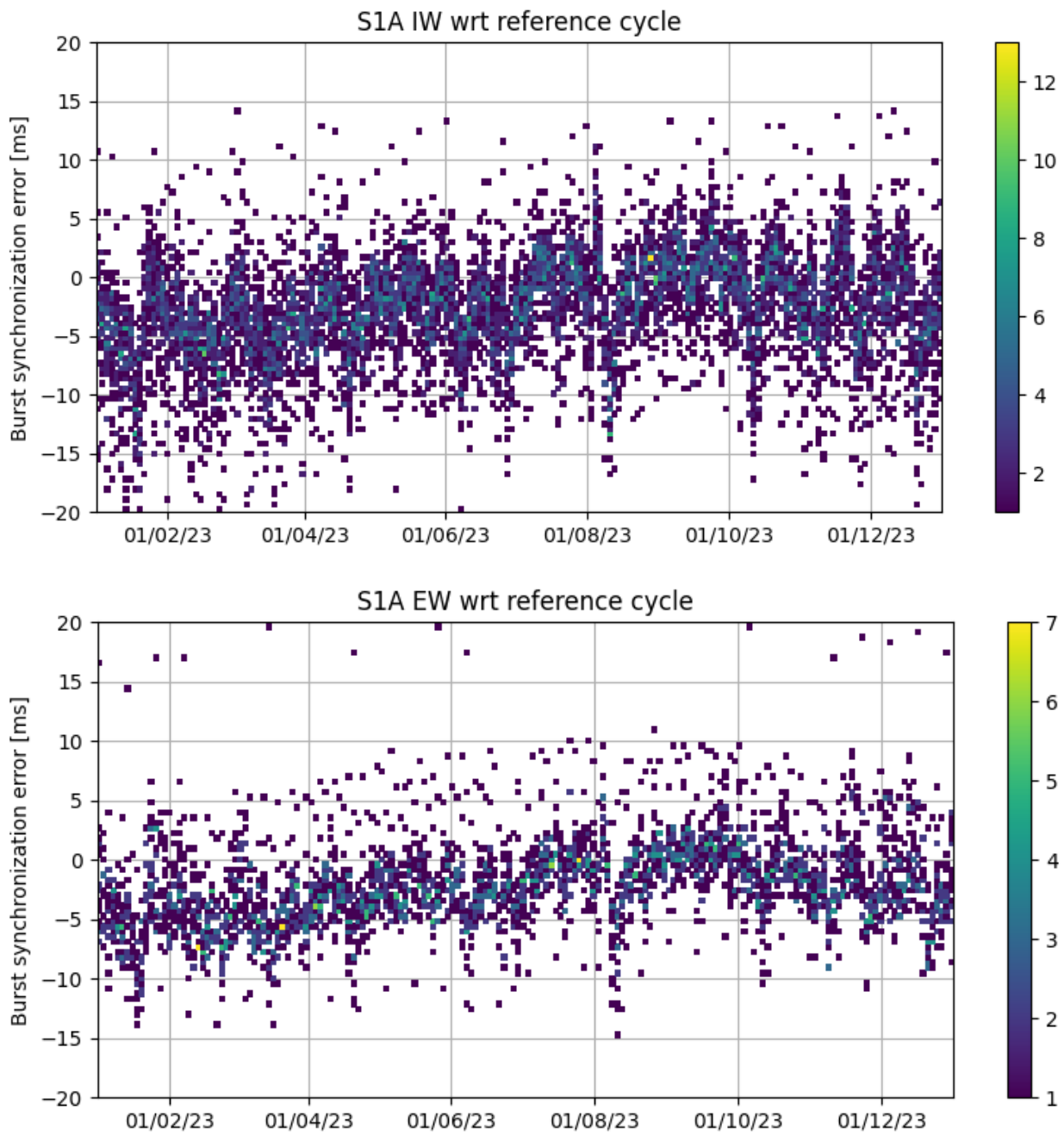


Figure 5-27: S-1A IW (top) and EW (bottom) burst synchronization error distribution during 2023, computed for each cycle with respect to a fixed reference cycle.

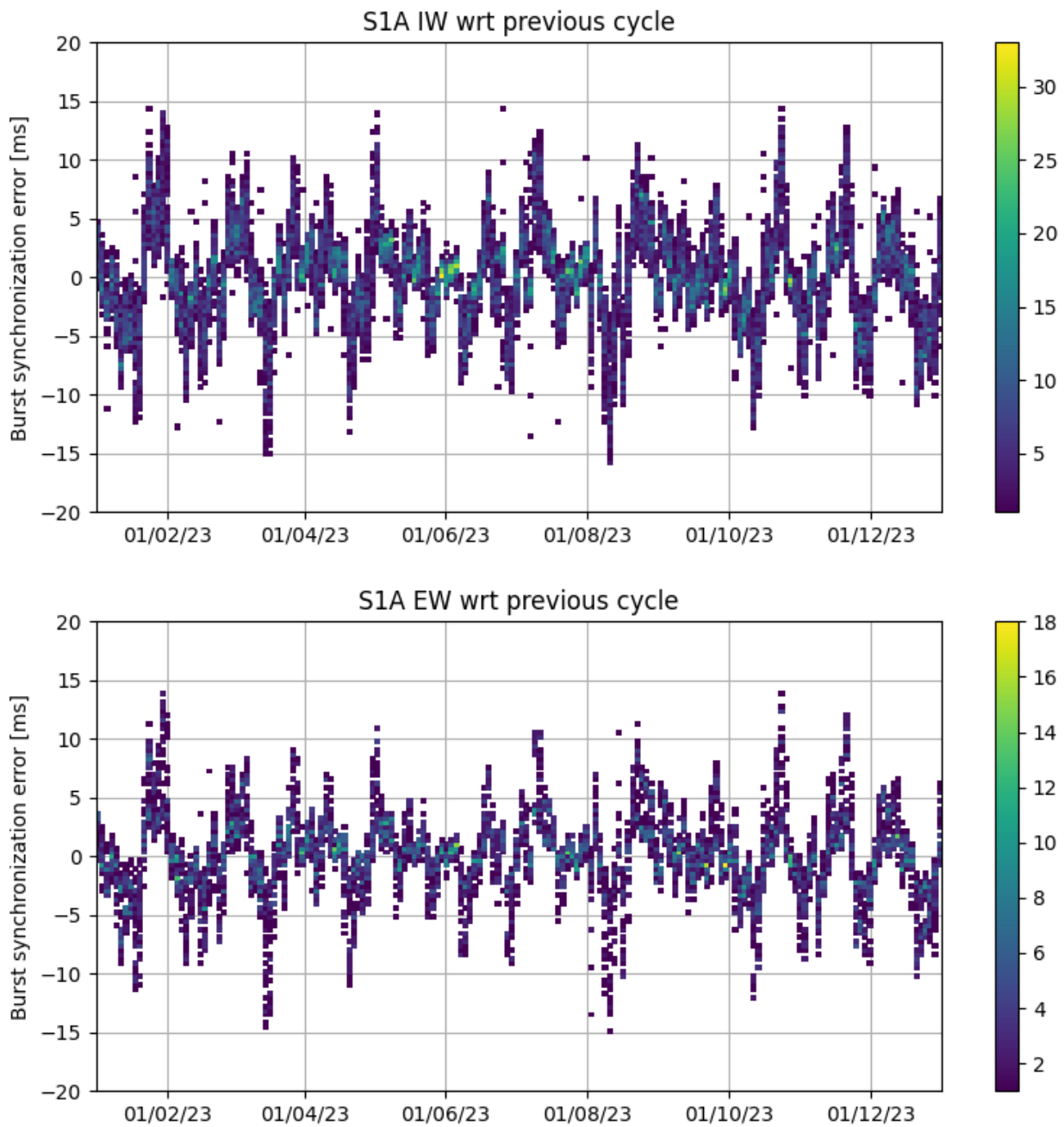


Figure 5-28 S-1A IW (top) and EW (bottom) burst synchronization error distribution during 2023, computed for each cycle with respect to its previous cycle.

Figure 5-29 to Figure 5-32 show the burst synchronization error trends, computed with the two monitoring approaches, for both IW and EW, from 2015 to 2023.

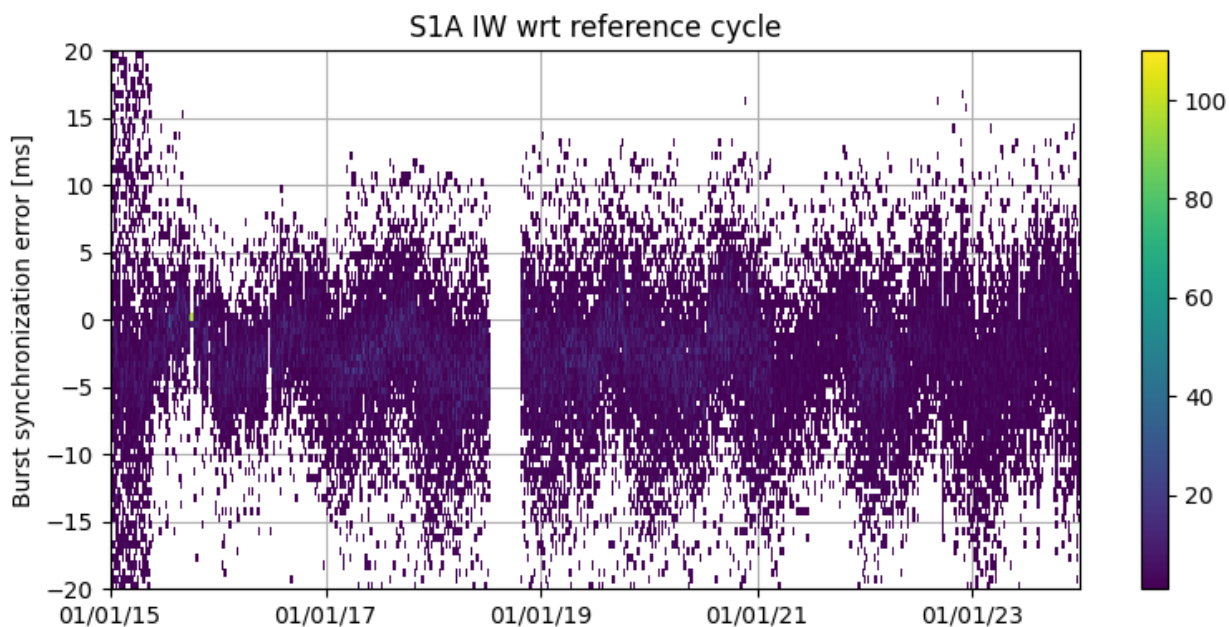


Figure 5-29 S-1A IW burst synchronization error distribution from 2015 to 2023, computed for each cycle with respect to a reference cycle

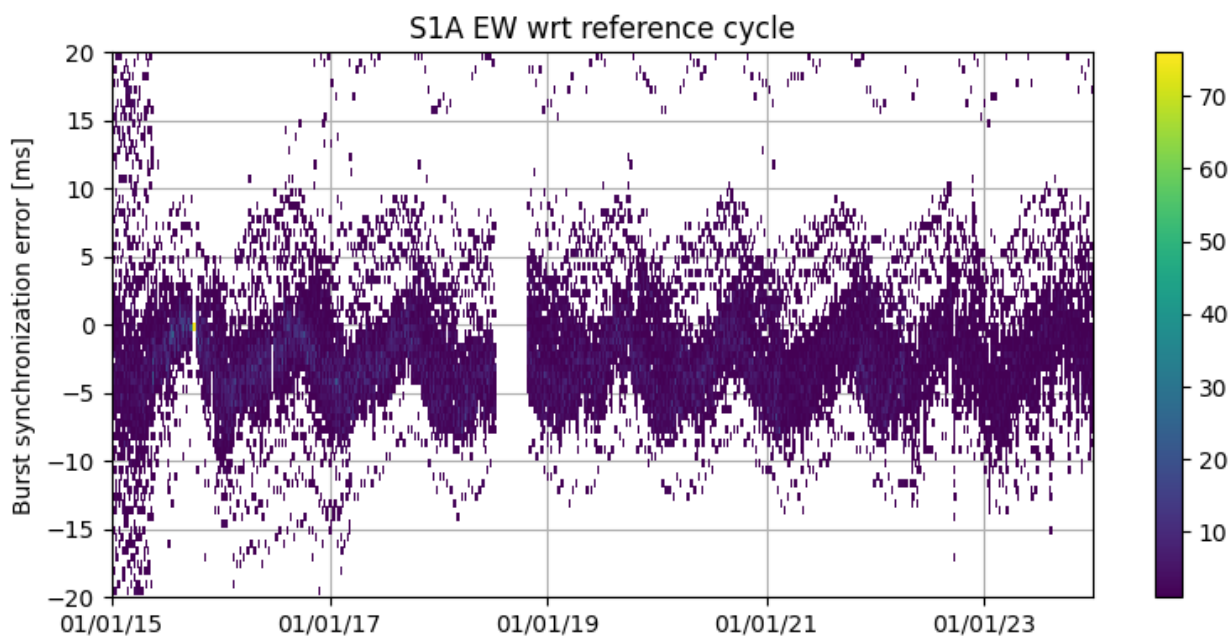


Figure 5-30 S-1A EW burst synchronization error distribution from 2015 to 2023, computed for each cycle with respect to a reference cycle

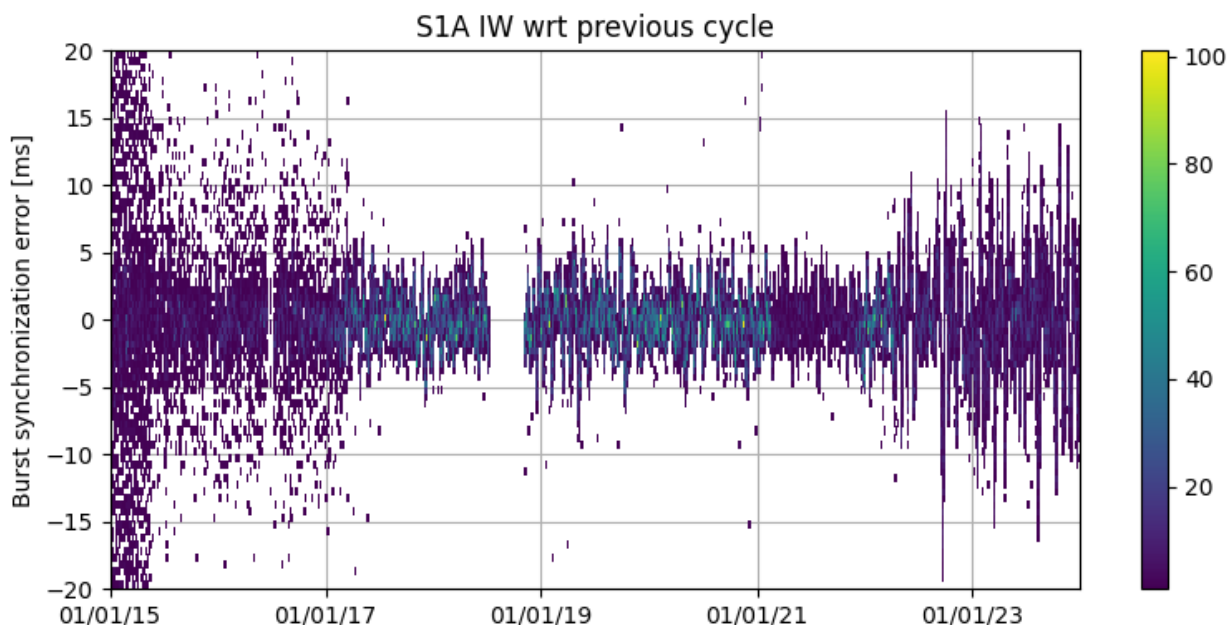


Figure 5-31 S-1A IW burst synchronization error distribution from 2015 to 2023, computed for each cycle with respect to its previous cycle

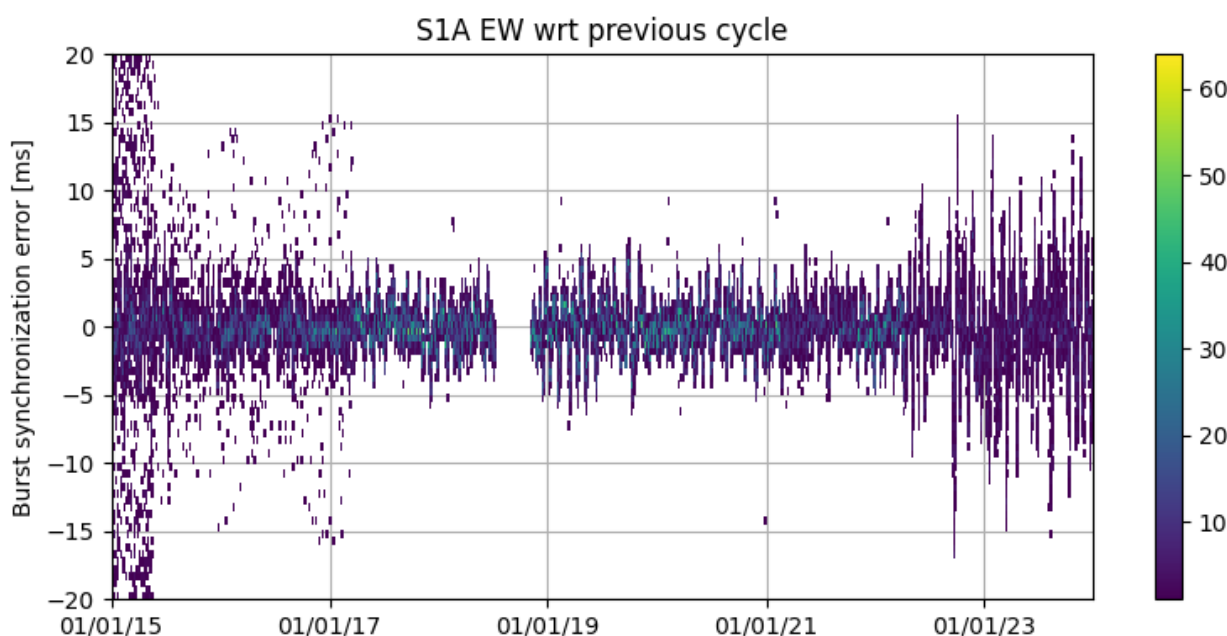


Figure 5-32 S-1A EW burst synchronization error distribution from 2015 to 2023, computed for each cycle with respect to its previous cycle

5.7.3 Instrument Pointing

The instrument pointing is continuously monitored exploiting the DC estimates from the data annotated in the L1A products. Figure 5-33 shows the Doppler Centroid evolution during 2023, and Figure 5-1 shows the same plot covering from mission start to 2023. DC jumps on the order of a few tens of Hz can be observed: this is a known issue, which can happen for S-1A when there is a change in the Star Trackers (STT) configuration. Figure 5-35 shows the DC evolution in 2023 correlated with the STT configuration at

each DC measurement. Sentinel-1A is provided with three STTs, and at any time it can be in a configuration where it uses one STT (CFG_STT_1, CFG_STT_2, CFG_STT3) or two STTs (CFG_STT_1_2, CFG_STT_1_3, CFG_STT_2_3). Inspection of the figure shows that switches from CFG_STT_1_2 to CFG_STT_1_3 and back have caused DC jumps up to 50 Hz, which are the largest observed since 2018. The two configurations have always suffered from positive and negative bias, respectively.

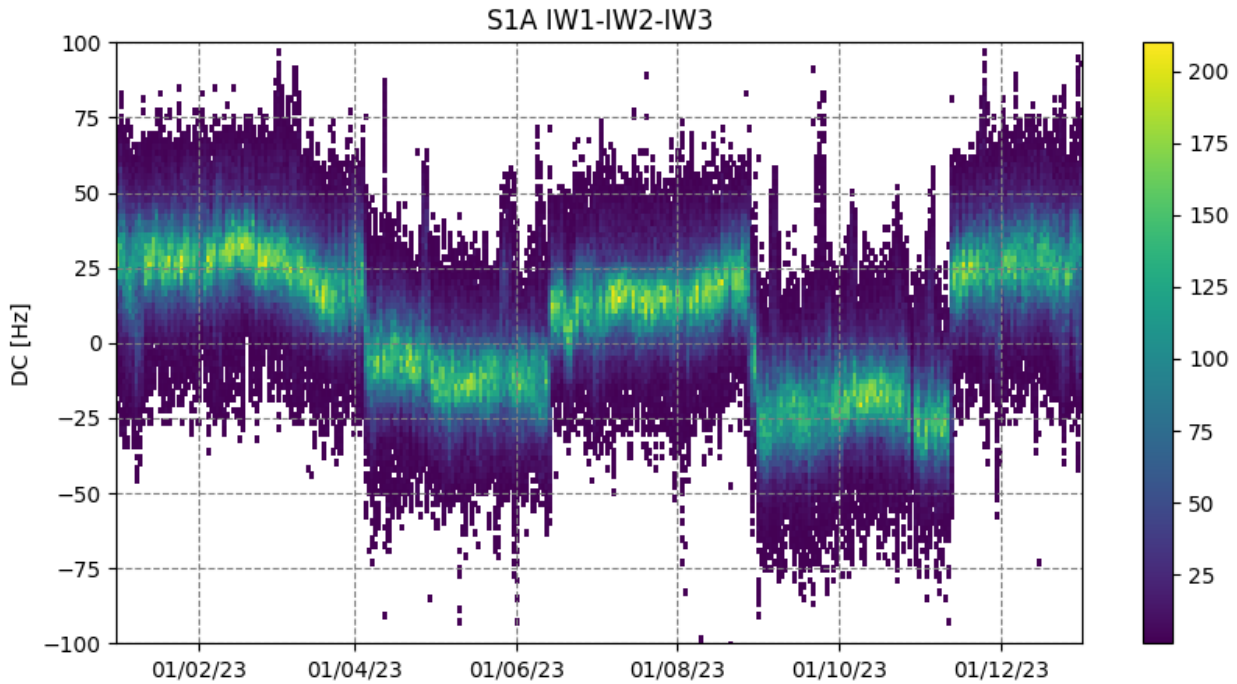


Figure 5-33: S-1A Doppler Centroid measured in 2023. Histogram bins are set to white if empty.

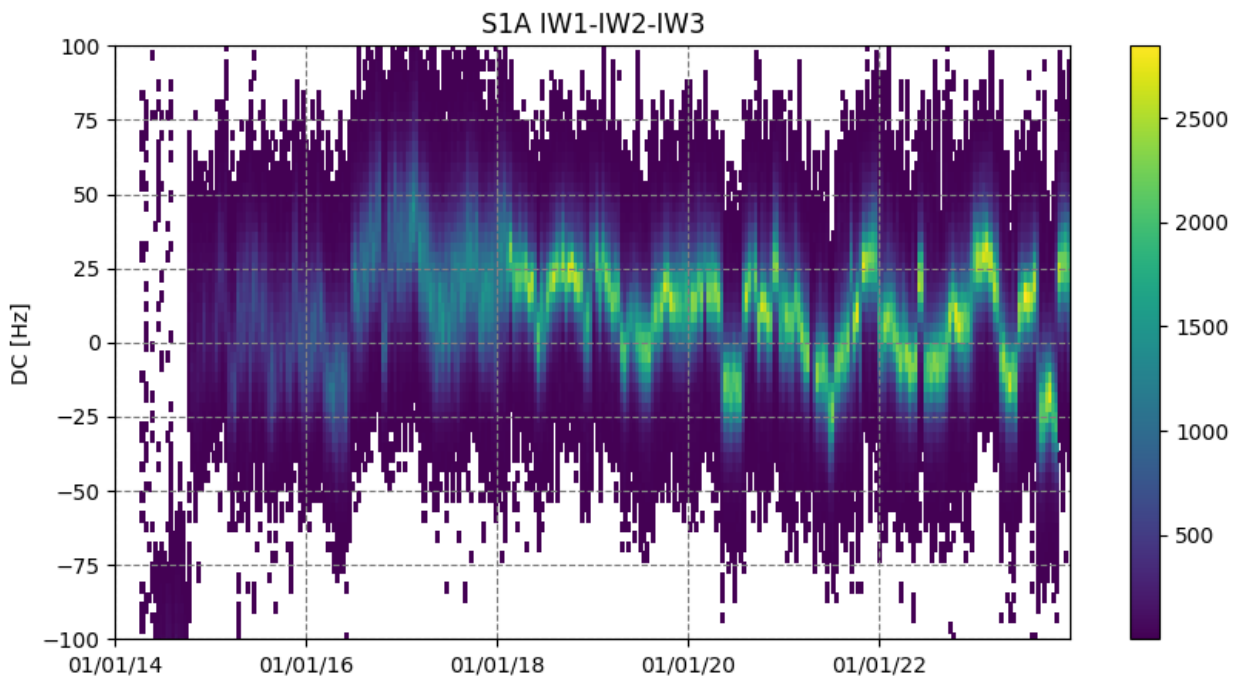


Figure 5-34 S-1A Doppler Centroid measured from mission start to 2023. Histogram bins are set to white if empty.

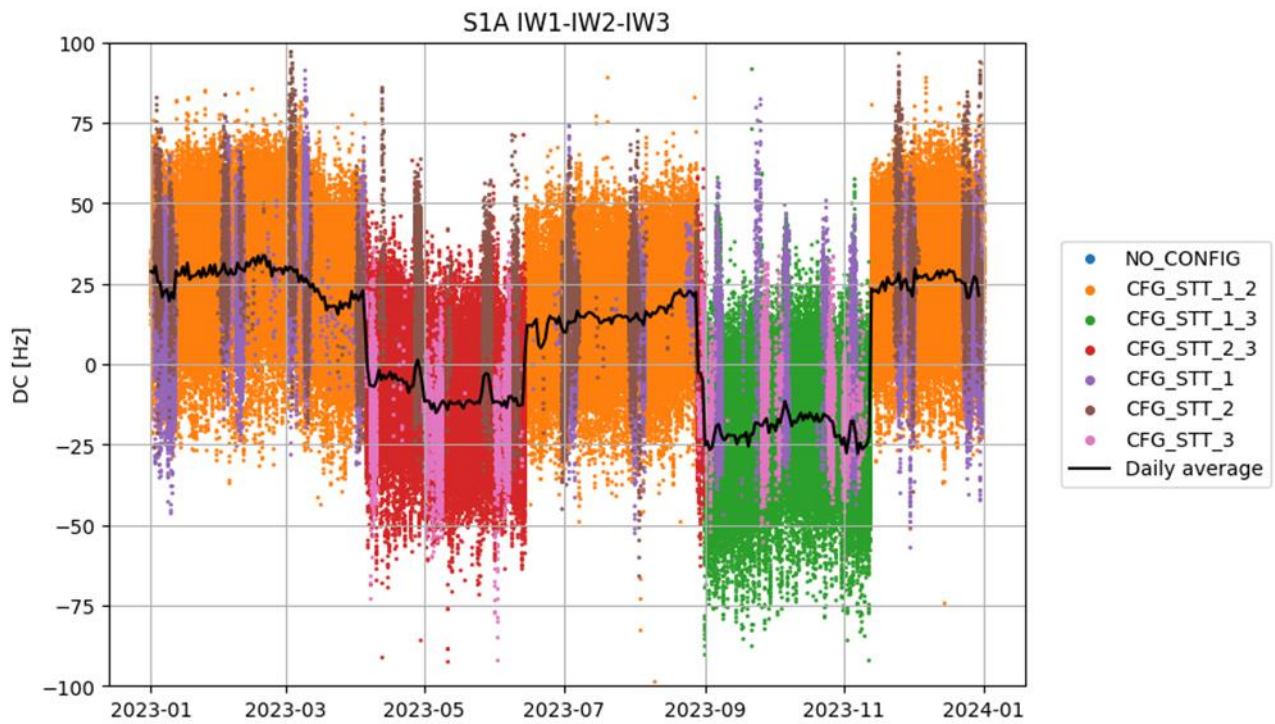


Figure 5-35 Doppler Centroid evolution in 2023, with legend labelling current Star Trackers configuration.

5.8 Radio Frequency Interferences

5.8.1 RFI annotations and RFI mitigation

On the 4 of November 2021, a new version of the SAR processor (IPF v3.4.0) was introduced. From this version the processor can perform an RFI mitigation based on various processing strategy.

The behaviour of the S-1 IPF for what concerns the RFI mitigation is based on three main successive steps:

- 1- A pre-screening of RFI evidence in noise measurements from specific pulses in the acquisition timeline. This pre-screening is performed (or not) depending on the configuration of the processor and the availability of the required noise measurements.
- 2- A detection of RFI from the measurement data. This detection step is configurable and can either be not applied at all, or only applied when RFI evidence are provided by the pre-screening step, or systematically applied.
- 3- A mitigation of RFI applied on the measurement data depending on the results of the previous steps.

The processing configuration applied since 2022 is such that:

- For TOPS modes (EW and IW), the pre-screening of RFI is performed and the results of this processing step is provided in a specific annotation file that can be used to collect evidence of potential RFI impacting the acquired data. Before the 23rd March 2022, no RFI detection (from data) and no mitigation is performed. Since this date, the detection (from data) and mitigation are performed.
- For SM and WV modes, no pre-screening is performed as the noise pulses are not available all along the data acquisition. No RFI detection (from data) and mitigation is performed.

The change of processing baseline concerning the RFI mitigation was applied through an update of AUX_PP1 auxiliary product (see section 0 and refer to Appendix F -for the list of ADF changes).

A specific technical note explaining how the Sentinel-1 SAR processor annotates the RFI detection and performs the RFI mitigation (when activated) is available on Sentinel Online web site: Sentinel-1 Using the RFI annotations, Issue 1.0, published on 11 February 2022. Refer to Appendix A -

5.8.2 Effectiveness of RFI mitigation

As expressed in previous section, the RFI mitigation in SAR processing is only applied since 23rd March 2022.

However, the overall pre-screening and mitigation process does not guarantee that 100% of the RFI are filtered out. The process was designed to reduce the number of RFI impacting the product quality but avoiding over filtering. Multiple elements can explain the observation of residual RFI even with the pre-screening/mitigation:

- The mitigation is only applied after a pre-screening. The pre-screening may fail to detect evidence of RFI if the noise echoes are not impacted.
- The mitigation may fail to filter out the RFI impact. Typical failure cases are inter alia RFI from a SAR signal with characteristics too close to the one of Sentinel-1, or corruption of the entire spectrum.

Figure 5-36 presents the locations of residual RFI observed for the month of May 2023 through visual inspection of the quicklooks of the corresponding nominal production. This corresponds to 185 IW products and 3 EW products over a production of 18552 EW and IW products in the same period, thus

corresponding to around 1% of the production. The list of quality disclaimers including the ones related to RFI mitigation is provided in appendix of this report.



Figure 5-36: Residual RFI for S1A and the month of May 2023.

The residual RFI from this map are spread all over the world on the area of actual image acquisitions. The products highlighted in this map are more frequently located in maritime and coastal areas. It may be due to the type of interfering radar sources on these specific areas, or due to the fact that they are easier to be spotted against the low background of sea clutter.

Over 2023, 2813 products have been identified with RFI residual and for most of them (2227 products, 80%) no RFI mitigation was activated at all, mostly since no evidence of RFI were spotted on the noise measurements. This is mostly caused by an absence of RFI signal in the noise measurements, in which case the data-based RFI detection and mitigation are not performed.

The percentage of products for which the SAR processor performs an RFI mitigation is monitored and is largely stable in time. However, it depends on the acquisition mode and polarization as expressed in following table.

| | VV | VH | HH | HV |
|-------------------------------------------------------------------------------------------------------------|--------------|--------------|----------------|-----------------|
| EW | 0 to 12% (*) | 0 to 14% (*) | 1 to 4% | 0.5 to 4.5% |
| IW | 18 to 21 % | 20 to 24% | 0 to 1.6 %(**) | 0 to 5.6 % (**) |
| (*) EW DV is rare, (**) IW DH are rare, then the percentage for those configurations are not representative | | | | |

Table 17: Percentage of products for which the RFI mitigation was activated for cycles 280 to 307 per mode and polarisation.

The percentage of IW/DV products for which the RFI mitigation is activated is between 18 and 23%.

The percentage of EW/DH products for which the RFI mitigation is activated is between 0.5 and 4.5%.

The other configurations of mode and polarisations are rarely used in the acquisition plan and the estimation of percentage of RFI mitigation in those configurations are not considered as reliable.

The larger percentage of RFI mitigation on IW/DV compared to EW/DH is believed to be due to acquisition over large populated areas for IW/DV products, while most of EW/DH products are acquired over the poles.

5.8.3 Regular reporting on RFI

Before the activation of the complete RFI mitigation process in the IPF (pre-screening, detection, and mitigation), the exhaustive list of impacted products was not reported.

Starting with the activation of this RFI mitigation on 23 March 2023, a more systematic monitoring and reporting of residual RFI is in place through the publication of quality disclaimers (refer to Appendix C - for the list of quality disclaimers published during 2022):

- A set of two Quality Disclaimers (one for S1A and one for S1B) was published for the period between the start of each mission on the 23rd of March 2023, reminding that RFI can be observed on the products, but not providing a list of products.
- Monthly Quality Disclaimers are then published with the list of residual RFI as detected from systematic quicklook inspection. Those monthly quality disclaimers contain some examples of major residual RFI.

Refer to Appendix C - on quality disclaimers and providing the link to their full list on the SAR-MPC web site. We provide below some examples of typical residual RFI observed either over sea or over land.

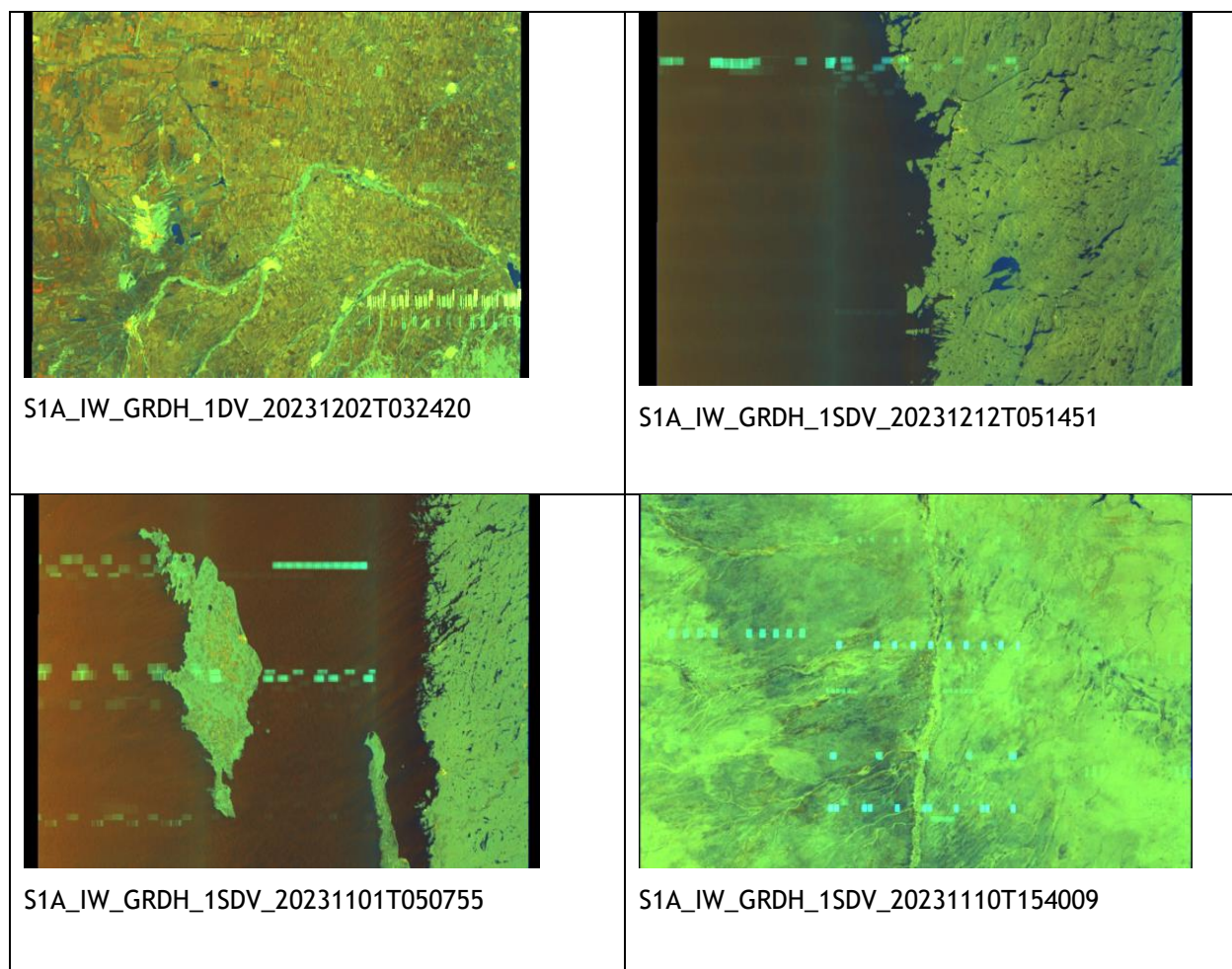


Figure 5-37: Examples of residual Radio Frequency Interference observed in 2023

5.8.4 Geographic distribution of RFI sources

The Sentinel-1 SAR processor performs a pre-screening of potential RFI on the rank echoes of the TOPS acquisition modes. The result of this pre-screening is annotated in the RFI annotations as described in section 5.8.1. Each result of pre-screening can be associated to a coarse geolocation allowing to map the coarse geolocation of the source of RFI. Such a result is provided in the two following figure separately for EW and IW modes and for ascending and descending tracks of cycle 309. The main identified sources are located near large settlements and borders.

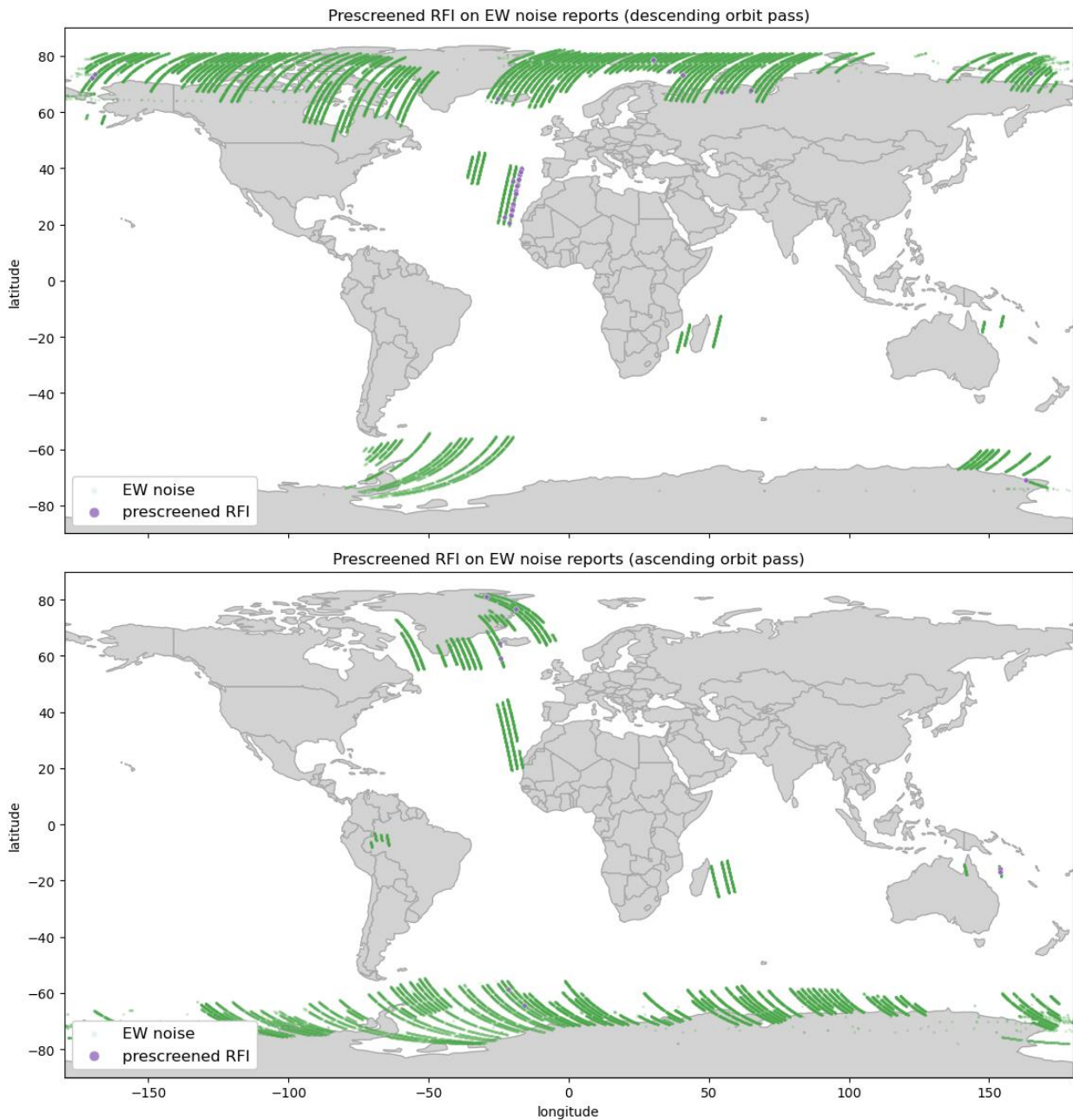


Figure 5-38: result of RFI pre-screening for EW products of cycle 309 (ascending and descending tracks)

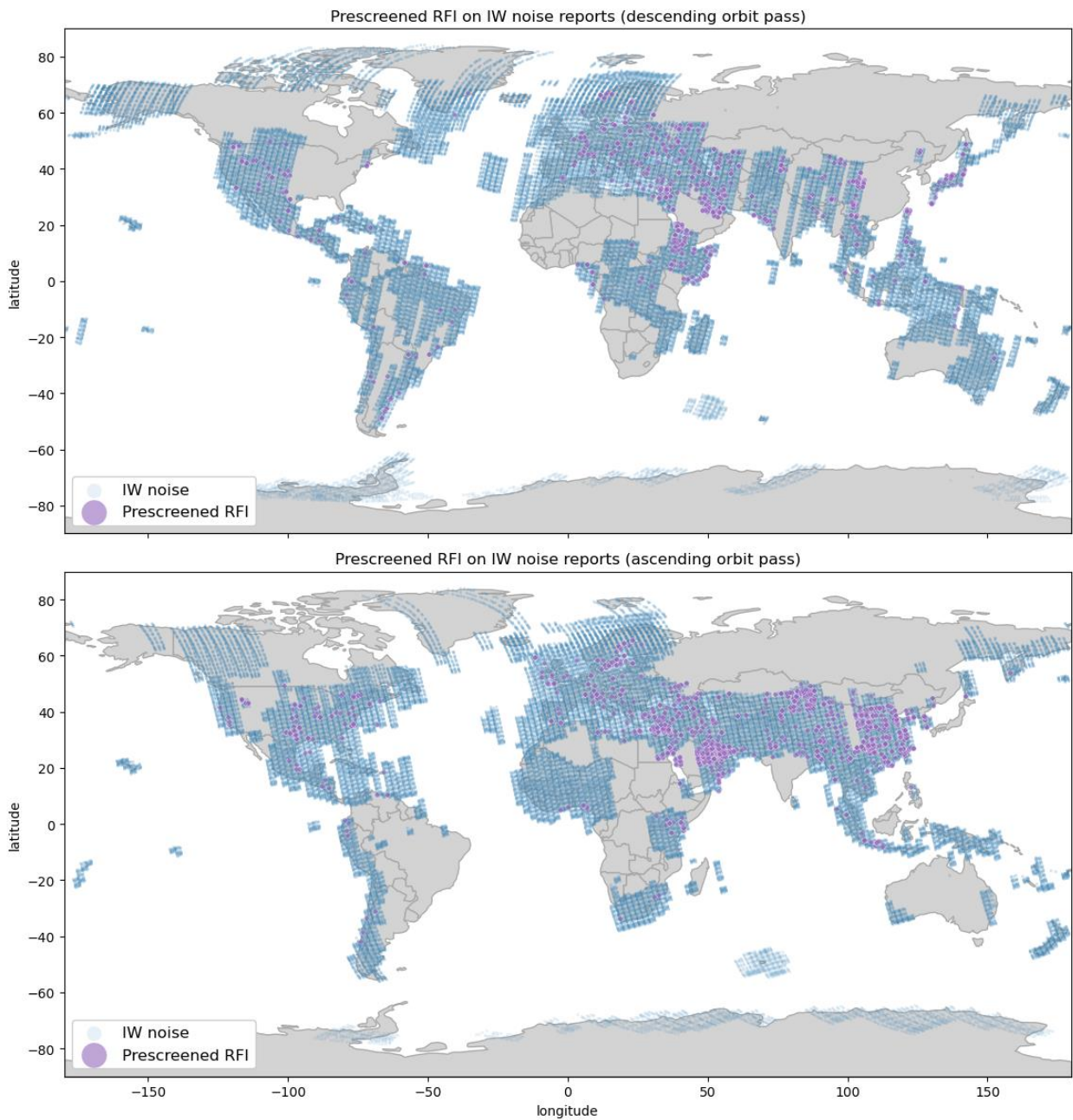


Figure 5-39: result of RFI pre-screening for IW products of cycle 309 (ascending and descending tracks)

The pre-screening of RFI is performed based on a threshold applied on the Max Fisher Z coefficient that can be considered as a kind of proxy of the RFI intensity. The following figure presents spatial distribution of this Max Fisher Z for EW and IW products for ascending and descending tracks.

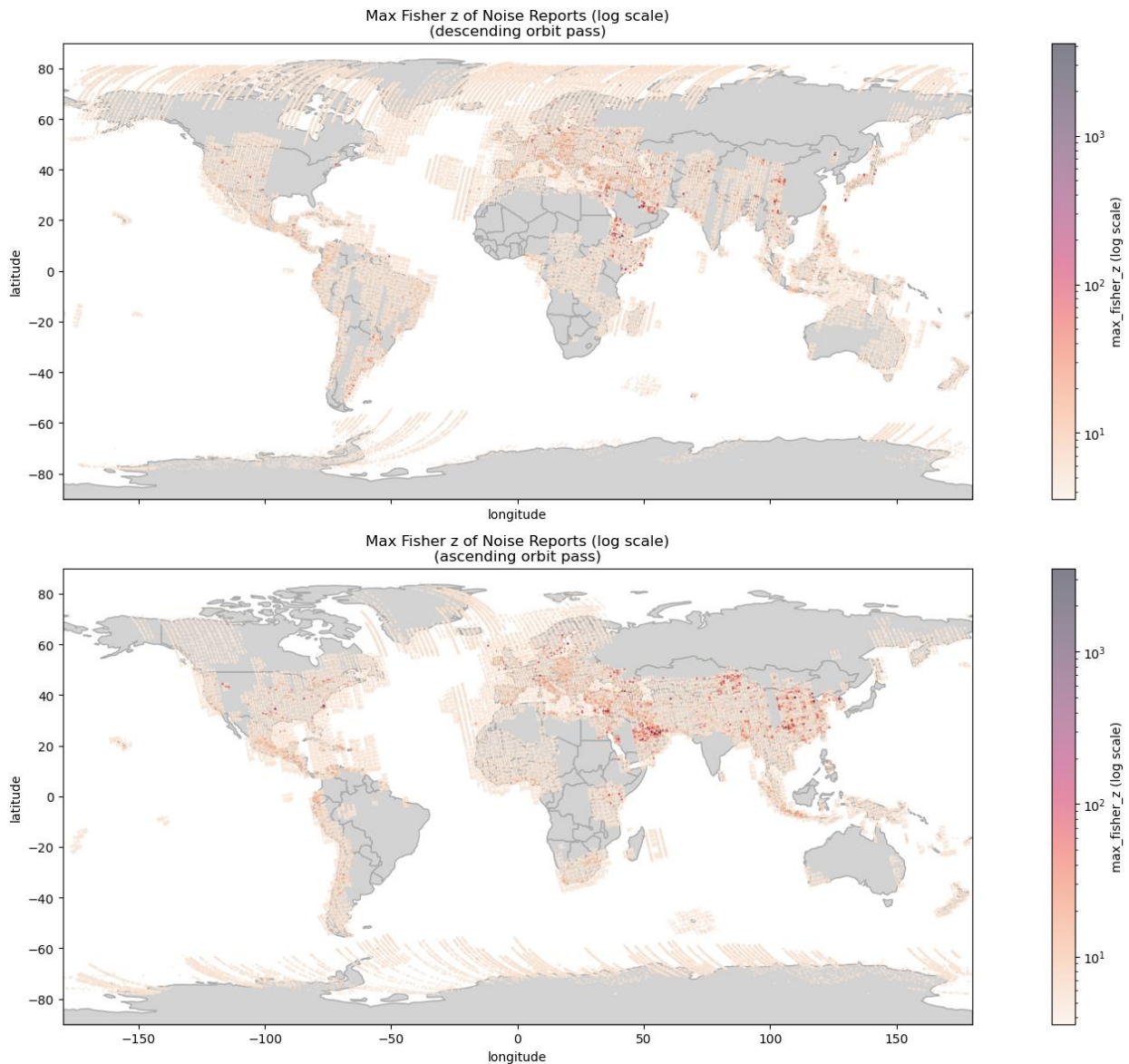


Figure 5-40: result of RFI characterisation through the Max Fisher Z coefficient for EW and IW products of cycle 309 (ascending and descending tracks)

5.8.5 Mutual Interferences with Radarsat-2

Radarsat-2 is a Canadian satellite operating a SAR in C Band. Mutual Radio Frequency interference between Radarsat-2 and S-1A can occur when the two spacecrafts are flying close on to the other and operating at the same time.

Due to slight differences in orbital period and inclinations, the locations of potential interferences are evolving with time. The orbital period difference is 120.91 sec, i.e., each orbit Sentinel-1 moves 120.91 sec ahead of Radarsat-2. The two satellites approach each other every 3.5 days (50 orbits for Sentinel-1 & 49 orbits for Radarsat-2) [S1-RD-23]

| | Sentinel-1 | Radarsat-2 |
|-----------------------|-----------------|-----------------|
| Orbit Type | Sun-Synchronous | Sun-Synchronous |
| Repeat Cycle (days) | 12 | 24 |
| Repeat Cycle (orbits) | 175 | 343 |
| Altitude | ~693 km | ~789 km |
| Orbital Period | 5924.57 s | 6045.481* |
| Orbital Inclination | 98.18° | 98.6° |
| MLST | ~18:00 hrs | ~18:00 hrs |

Table 18: Sentinel-1 and Radarsat-2 Orbit characteristics.

Location of potential RFI based on geometry

Figure 5-41 provides the potential location of IW images acquired during close fly-by of Sentinel-1A and Radarsat-2 during the year 2022. The colour code corresponds to different relative orbit numbers. The impacted relative orbit numbers are 20, 45, 70, 95, 120, 145 and 170. Those location are however only potential locations of RFI observations as Sentinel-1A is not acquiring constantly. Compared to the year 2022, the locations of potential RFI are slowly moving along the orbit.

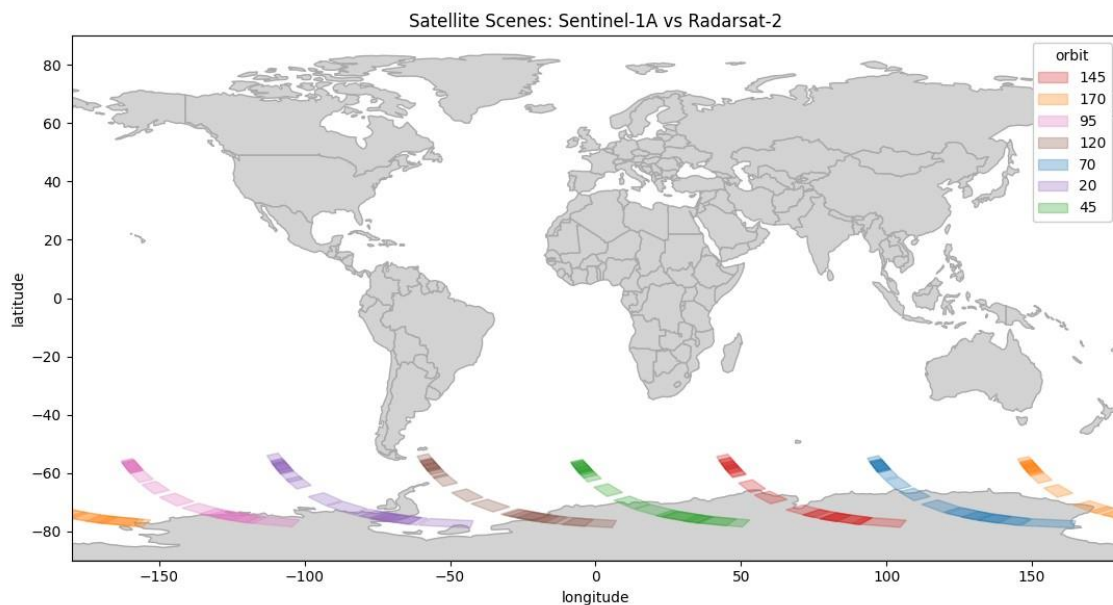


Figure 5-41: Potential locations of S-1A IW images at the time of close S1A vs RS-2 fly-bys in 2023.

Activation of RFI mitigation

Among those orbits, there are only S-1 acquisitions over some of the potential overpasses.

The following figure provides the status of RFI mitigation for products acquired within 30s of close fly by between Sentinel-1A and Radarsat-2.

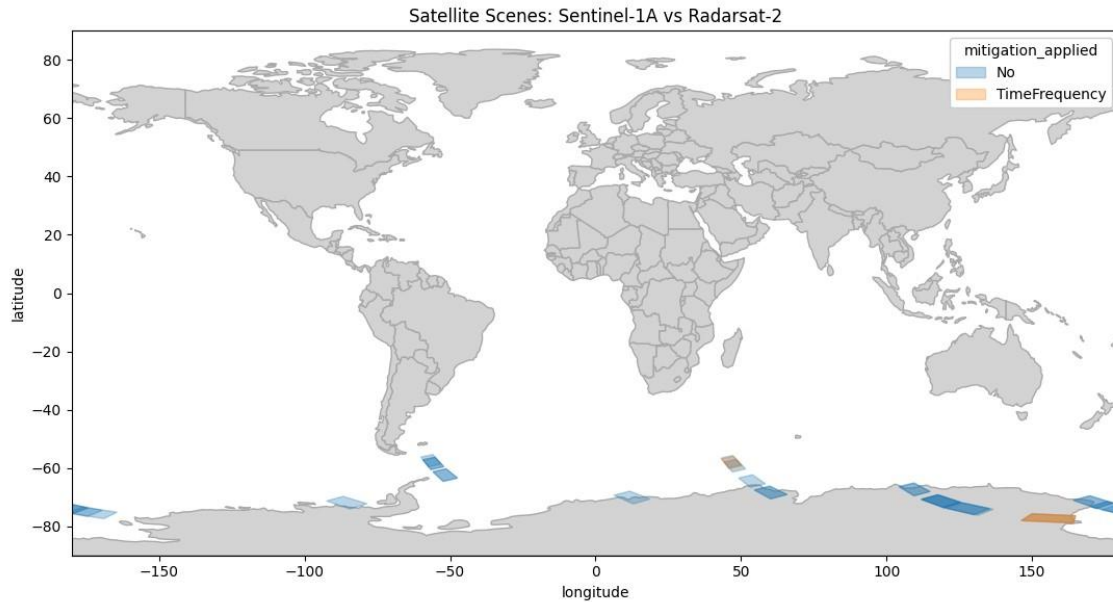


Figure 5-42: Location of S-1A products acquired close to S1A vs RS-2 fly-bys, and status of RFI mitigation in 2023.

Residual RFI

No residual RFI were spotted on the Sentinel-1A products acquired within 30s around the closest fly-by between the two satellites.

Summary

| | |
|------------------------------------------------------------------------|-------------|
| Sentinel-1 unit | Sentinel-1A |
| Other Satellite Name | Radarsat-2 |
| Other Satellite NORAD ID | 32382 |
| Period considered | 2023 |
| Fly-by events | 107 |
| Products acquired within 30s around fly-by | 31 |
| Products acquired within 30s around fly-by and with mitigation applied | 3 |
| Products with residual RFI | 0 |

Table 19: Summary of Sentinel-1A vs Radarsat-2 RFI mitigation in 2023

5.8.6 Mutual Interferences with Gaofen-3 constellation

Gaofen-3 is a Chinese constellation of satellites operating a SAR in C Band. Three spacecrafts are currently operated (Gaofen 3, Gaofen 3 02 and Gaofen 3 03). Their respective NORAD Id are 41727, 49492 and 52200 respectively.

Mutual Radio Frequency interference between Gaofen-3 and S-1A can occur when the two spacecrafts are flying close on to the other and operating at the same time.

Table 20 gives the orbital characteristics of S-1 and GAOFEN 3. GAOFEN 3 is in a higher orbit than S-1 and in a dusk-dawn orbit.

| | Sentinel-1 | GAOFEN 3 |
|---------------------------------------------------------------------------------------------------------------------------------------------------------------------------------------------|-----------------|-----------------|
| Orbit Type | Sun-Synchronous | Sun-Synchronous |
| Repeat Cycle (days) | 12 | 29 |
| Repeat Cycle (orbits) | 175 | 419* |
| Altitude | ~693 km | ~751 km |
| Orbital Period | 5924.57 s | 5980 s* |
| Orbital Inclination | 98.18° | 98.42° |
| MLST | ~18:00 hrs | ~18:00 hrs |
| * Deduced values. Those values are computed considering mean altitude, and orbit inclination as we did not find authoritative information on orbital period and repeat cycle of the mission | | |

Table 20: Sentinel-1 and GAOFEN 3 Orbit Characteristics.

Location of potential RFI based on geometry

The orbits of the Gaofen-03 satellites are such that only Gaofen-3-01 can be close to Sentinel-1A a certain specific date.

The respective repeat cycles of the two constellations in number of days is such that the close fly-bys are spaced irregularly. The following figure presents the locations of potential S1A acquisitions in IW mode that could be impacted by mutual RFI originating from Gaofen-3-01 satellite due to their proximity at a given time. The colour code considered for the figures corresponds to S-1A relative orbit number (the labels of relative orbit number are only provided for a subset of them).

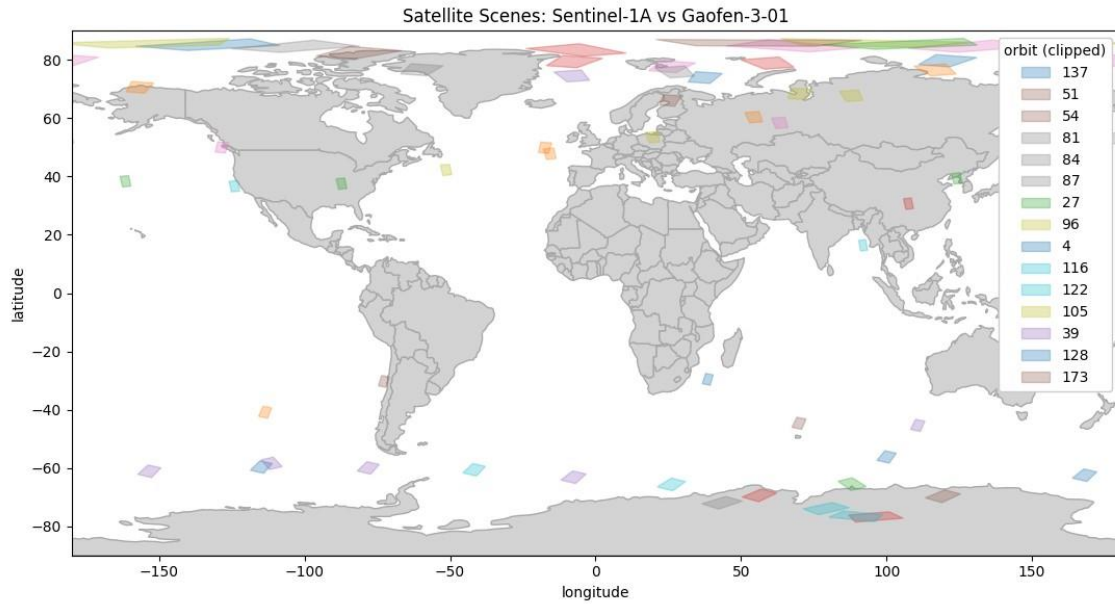


Figure 5-43: Potential locations of S-1A IW images at the time of close S1A vs GF-3-01 fly-bys in 2023.

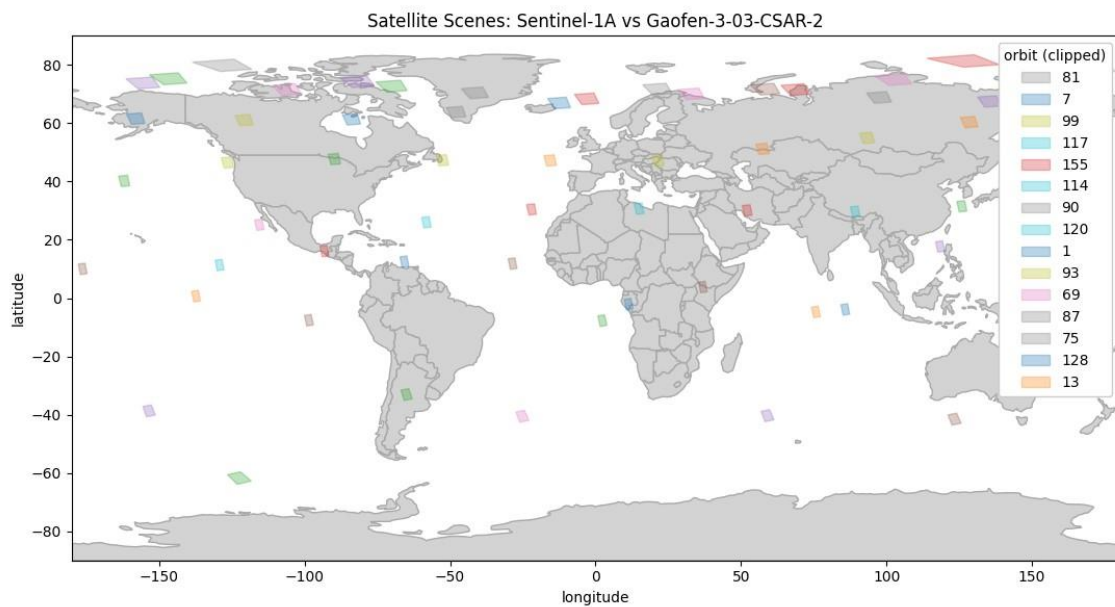


Figure 5-44: Potential locations of S-1A IW images at the time of close S1A vs GF-3-03 fly-bys in 2023.

Activation of RFI mitigation

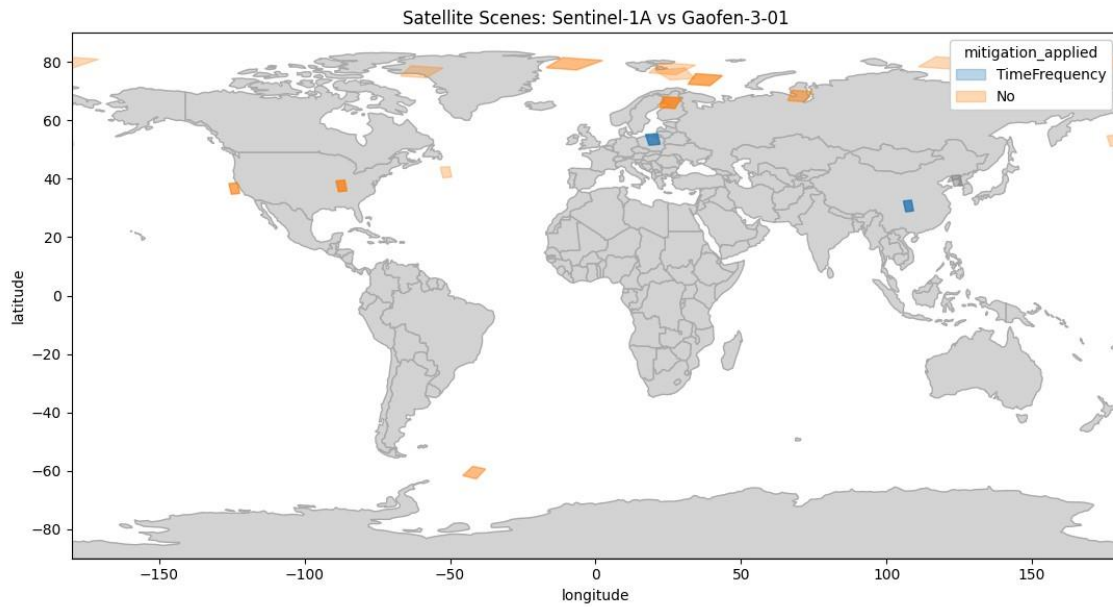


Figure 5-45: Location of S-1A products acquired close to S1A vs GF-3-01 fly-bys, and status of RFI mitigation in 2023.

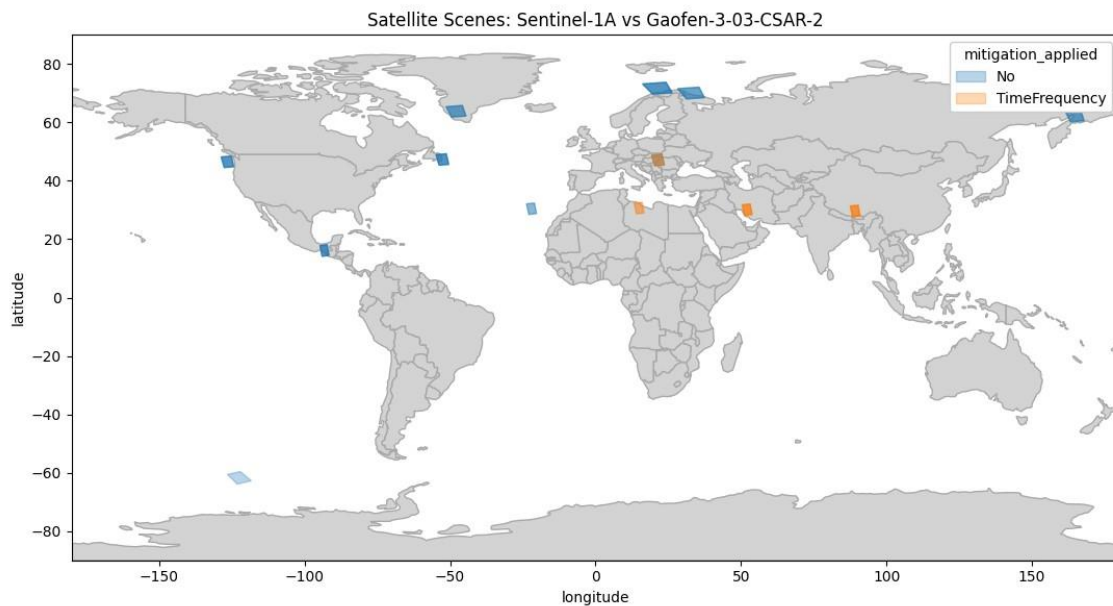


Figure 5-46: Location of S-1A products acquired close to S1A vs GF-3-03 fly-bys, and status of RFI mitigation in 2023.

Residual RFI

The inspection of the products acquired at those dates in 2023 allowed to detect residual RFI on products acquired close to fly-bys with the Gaofen-3 constellation. The list of products with residual RFI is provided in following figures. However, the shape and duration of the residual RFI makes it unlikely that their source is the Gaofen-3 constellation. It is more likely that the sources are ground emitters captured by coincidence at the time of the fly-bys.

This is an indication of good performances of the RFI mitigation strategy applied in the SAR processor as no long duration interference originating from Gaofen-3 is observed since activation of it. For examples of S1A / GF3 mutual RFI, you can refer to the Annual Performance Report of year 2022 [AD-07].

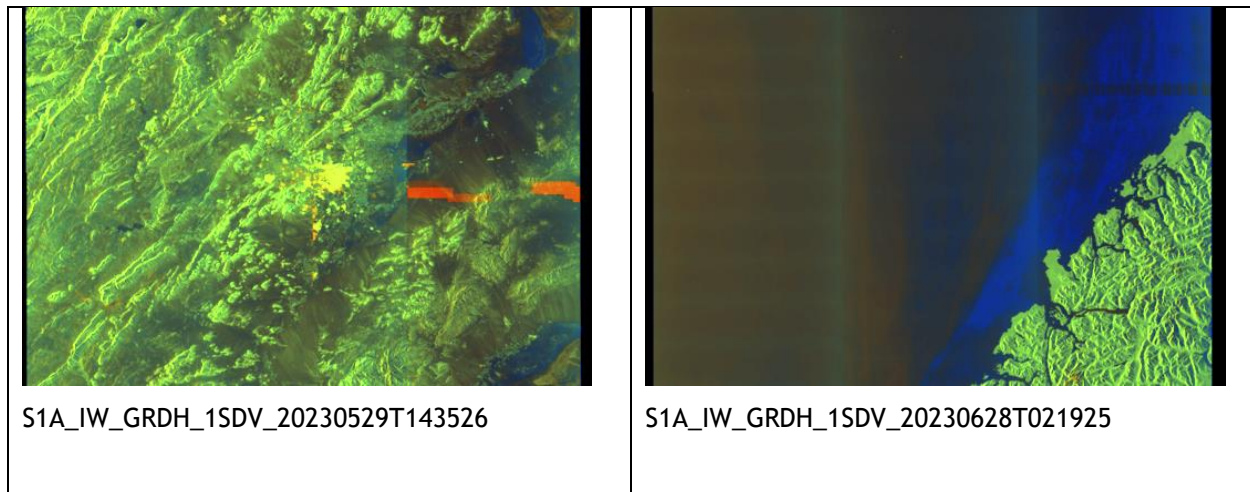


Figure 5-47: Residual RFI observed at time of fly-bys between S-1A and Gaofen-3-03 (most probably not due to Gaofen-3-03)

Summary

| | | | |
|------------------------------------------------------------------------|-------------|-------------|-------------|
| Sentinel-1 unit | Sentinel-1A | Sentinel-1A | Sentinel-1A |
| Other Satellite name | Gaofen-3-01 | Gaofen-3-02 | Gaofen-3-03 |
| Other Satellite NORAD ID | 41727 | 49492 | 52200 |
| Period considered | 2023 | 2023 | 2023 |
| Fly-by events | 64 | 0 | 62 |
| Products acquired within 30s around fly-by | 37 | 0 | 42 |
| Products acquired within 30s around fly-by and with mitigation applied | 9 | 0 | 12 |
| Products with residual RFI | 0 | 0 | 2 |

Table 21: Summary of Sentinel-1A vs Gaofen-03 mitigation in 2023

5.8.7 Mutual Interferences with the RCM constellation

The Radarsat Constellation Mission / RCM (NORAD ID 44322, 44323 and 44324) C-Band SAR satellites can interfere as well with Sentinel-1A. Table 22 gives the orbital characteristics of S-1 and RCM. RCM is in a lower orbit than S-1 and in a dusk-dawn orbit.

| | Sentinel-1 | RCM |
|-----------------------|-----------------|-----------------|
| Orbit Type | Sun-Synchronous | Sun-Synchronous |
| Repeat Cycle (days) | 12 | 12 |
| Repeat Cycle (orbits) | 175 | 179 |
| Altitude | ~693 km | ~592 km |
| Orbital Period | 5924.57 s | 5784 s |
| Orbital Inclination | 98.18° | 97.74° |
| MLST | -18:00 hrs | -18:00 hrs |

Table 22: Sentinel-1 and RCM 1/2/3 Orbit Characteristics

Location of potential RFI based on geometry

The locations of potential S-1 RCM interference are geographically localised in some specific area over the globe. Those potential RFI and mostly mitigated through the acquisition plan of Sentinel-1 (no acquisitions of S-1 were planned in some of those areas even before the launch of the RCM Constellation). The impact now is considered small and no changes in the acquisition plan of neither S1 nor RCM is currently in place with the specific goal of mitigating cross-sensor RFI. The situation is continuously monitored, and, if necessary, mitigation actions will be proposed and eventually coordinated with CSA.

Table 23 provides the list of area that can be potentially impacted by S1A vs RCM/1/2/3 mutual RFI. The figures below provide their geographic locations.

| Spacecrafts | Orbit number | Pass | Location |
|--------------|--------------|------------|------------------------------------------|
| S1A vs RCM-1 | 32 | Descending | Antarctica around 22:12:50 UTC |
| | 76 | Descending | Indonesia / Malaysia around 22:15:34 UTC |
| | 120 | Ascending | Canada around 22:13:37 UTC |
| | 163/164 | Ascending | Amazon around 22:15:06 UTC |
| S1A vs RCM-2 | 3 | Descending | Antarctica around 22:30:56 UTC |
| | 47 | Descending | Indonesia / Malaysia around 22:32:27 UTC |
| | 134/135 | Ascending | Amazon around 22:30:46 UTC |
| | 136 | Ascending | North Canada around 22:31:31 UTC |
| S1A vs RCM-3 | 18 | Ascending | North Canada around 22:22:36 UTC |
| | 61/62 | Ascending | Amazon around 22:41:49 UTC |
| | 105 | Descending | Antarctica around 22:21:49 UTC |
| | 149 | Descending | Indonesia / Malaysia around 22:24:08 UTC |

Table 23: Locations of potential S1A vs RCM 1/2/3 mutual RFI due based on geometry. The observation of RFI is not systematic (requiring that both spacecraft are operating at the same time and that the RFI mitigation in the processing is not sufficient).

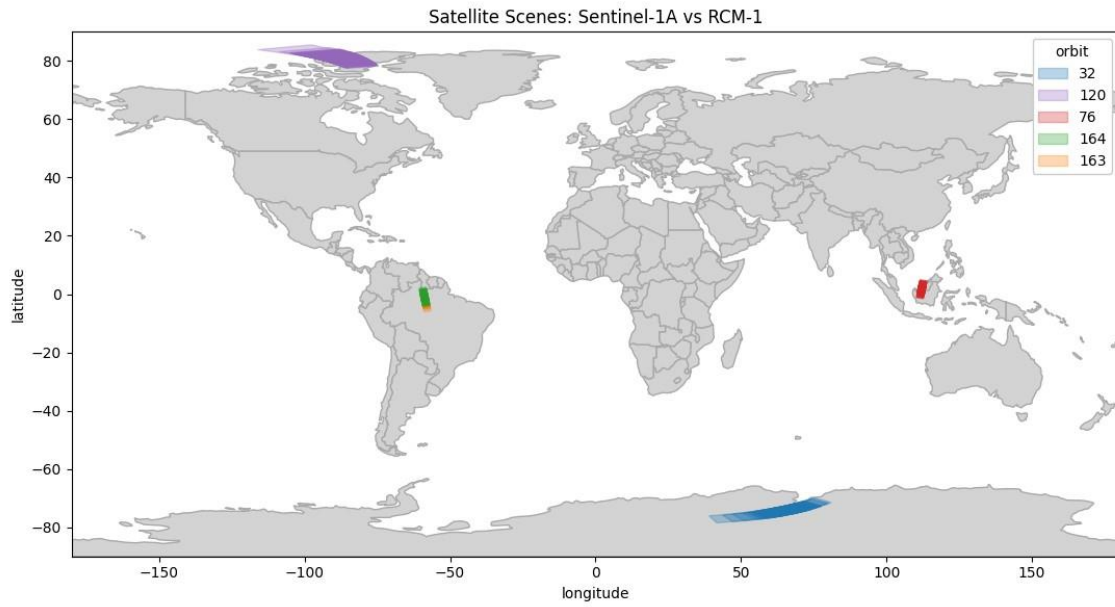


Figure 5-48: Locations of potential S1A vs RCM-1 RFI based on geometry (not associated to systematic acquisitions)

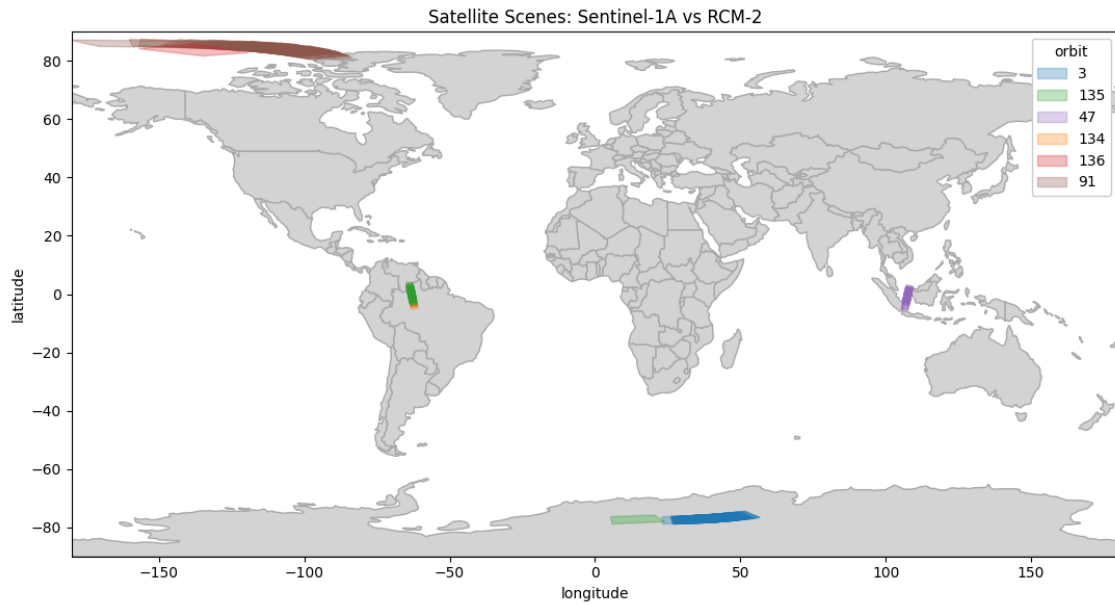


Figure 5-49: Locations of potential S1A vs RCM-2 RFI based on geometry (not associated to systematic acquisitions)

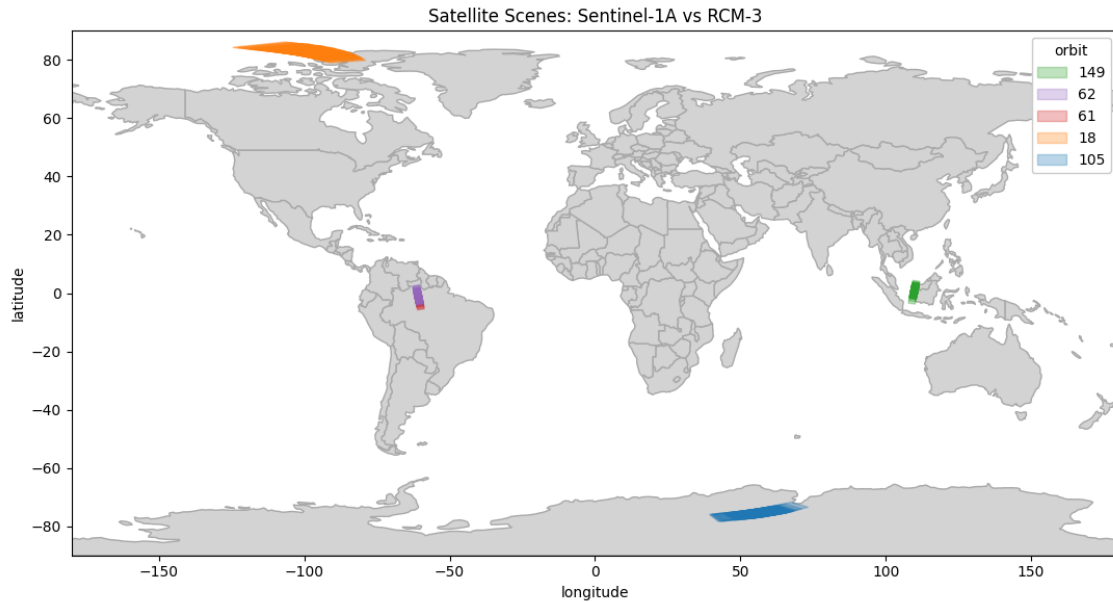


Figure 5-50: Locations of potential S1A vs RCM-3 RFI based on geometry (not associated to systematic acquisitions)

Activation of RFI mitigation

The following figures present the actual S-1A data acquired at RCM fly-bys and the status of the RFI mitigation. It must be noticed that the actual acquisitions of S-1A on fly-bys are only located in Indonesia and that the RFI mitigation is mostly activated, as expected.

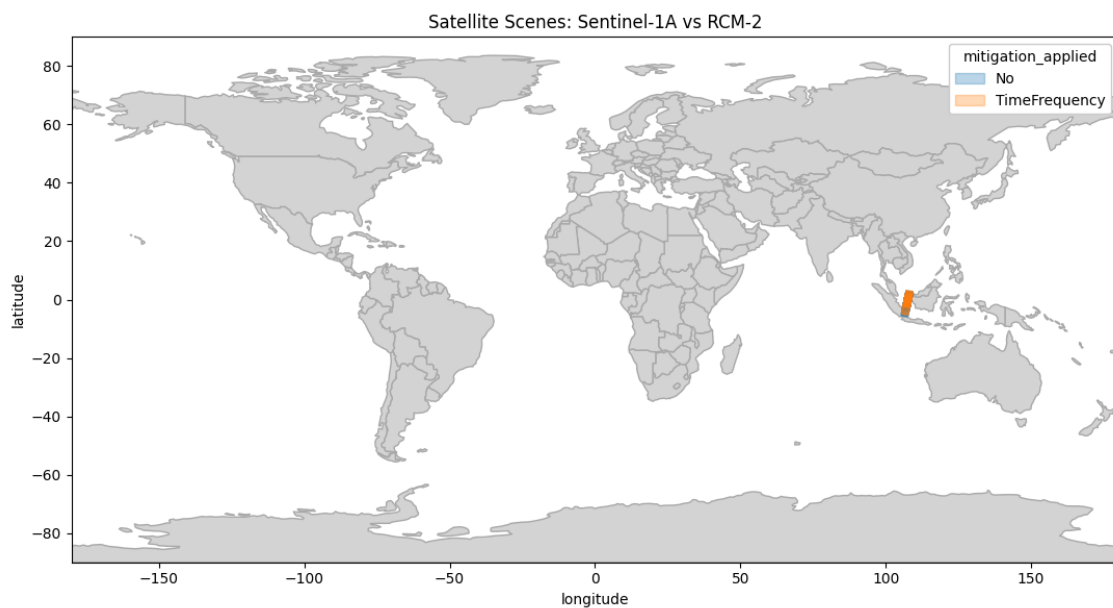


Figure 5-51: Location of S-1A products acquired close to S1A vs RCM-1 fly-bys, and status of RFI mitigation in 2023.

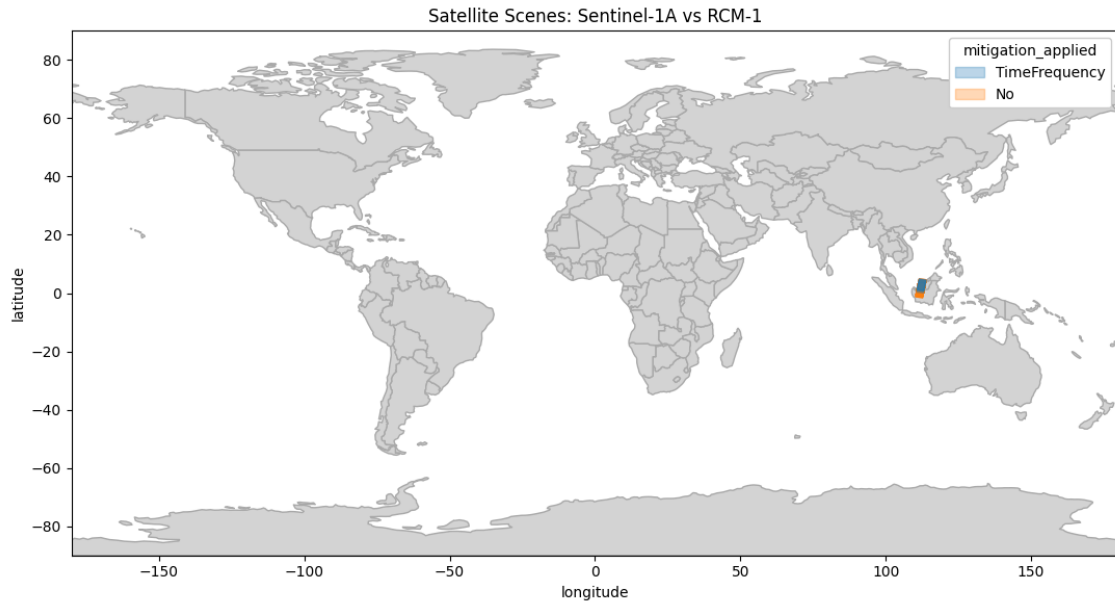


Figure 5-52: Location of S-1A products acquired close to S1A vs RCM-2 fly-bys, and status of RFI mitigation in 2023.

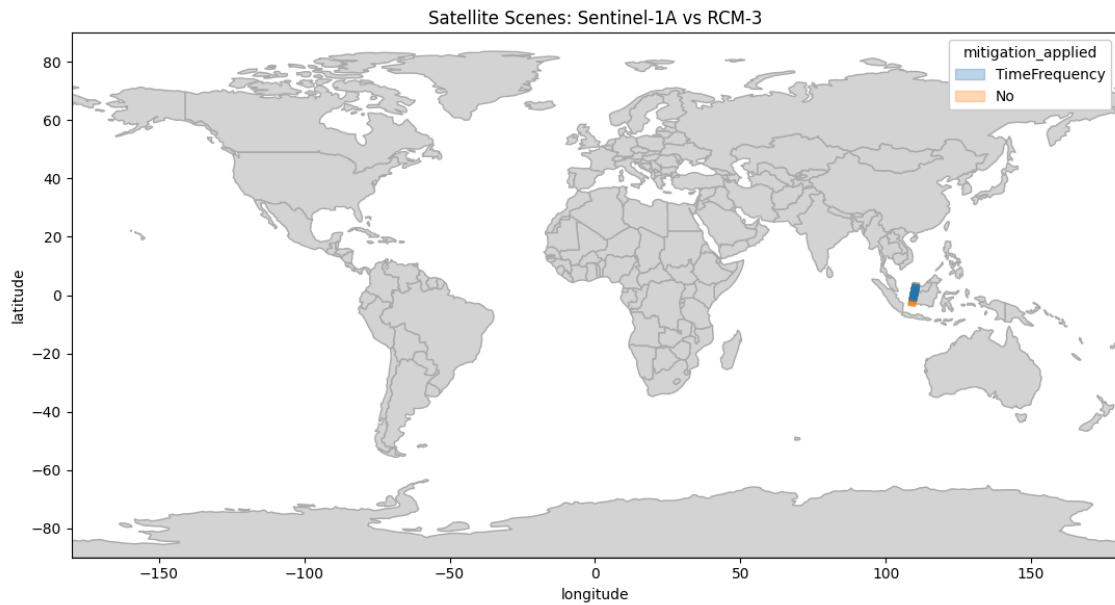
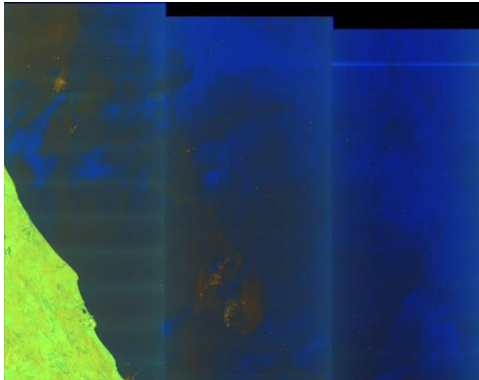


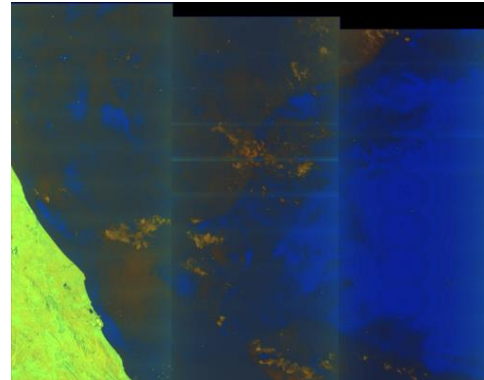
Figure 5-53: Location of S-1A products acquired close to S1A vs RCM-3 fly-bys, and status of RFI mitigation in 2023.

Observed residual RFI

The following figures are illustrating some residual RFI observed near S-1A and RCM fly-bys. No residual RFI were observed close to RCM-2 fly-bys.

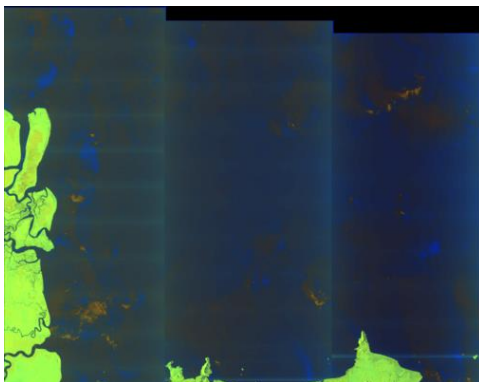


S1A_IW_GRDH_1SDV_20230824T221443

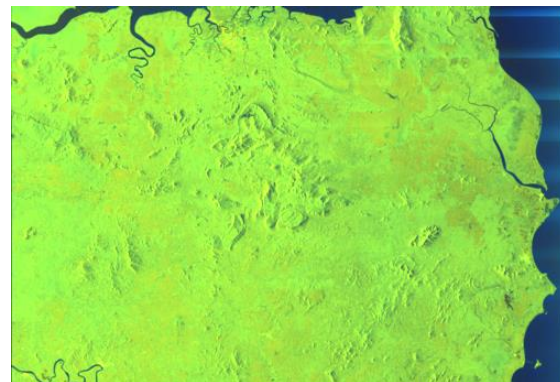


S1A_IW_GRDH_1SDV_20231210T221443

Figure 5-54: Examples of residual RFI observed close to S1A vs RCM-1 fly-bys in 2023



S1A_IW_GRDH_1SDV_20231203



S1A_IW_GRDH_1SDV_20231215T222354

Figure 5-55: Examples of residual RFI observed close to S1A vs RCM-3 fly-bys in 2023

Summary

| | | | |
|------------------------------------------------------------------------|-------------|-------------|-------------|
| Sentinel-1 unit | Sentinel-1A | Sentinel-1A | Sentinel-1A |
| Other Satellite Name | RCM-1 | RCM-2 | RCM-3 |
| Other Satellite NORAD ID | 44322 | 44323 | 44324 |
| Period considered | 2023 | 2023 | 2023 |
| Fly-by events | 121 | 123 | 122 |
| Products acquired within 30s around fly-by | 97 | 83 | 89 |
| Products acquired within 30s around fly-by and with mitigation applied | 5 | 19 | 15 |
| Products with residual RFI | 2 | 0 | 3 |

Table 24: Summary of Sentinel-1A vs RCM RFI mitigation in 2023

5.8.8 Mutual interferences with RISAT-1A (EOS4)

RISAT-1A (EOS4) is an Indian satellite operating a SAR in C Band. Mutual Radio Frequency interference between RISAT-1A and S-1A can occur when the two spacecrafts are flying close on to the other and operating at the same time.

Table 25 gives the orbital characteristics of S-1 and RISAT-1A.

| | Sentinel-1 | RISAT-1A (EOS4) |
|-----------------------|-----------------|-----------------|
| Orbit Type | Sun-Synchronous | Sun-Synchronous |
| Repeat Cycle (days) | 12 | 17 |
| Repeat Cycle (orbits) | 175 | 257 |
| Altitude | ~693 km | ~525 km |
| Orbital Period | 5924.57 s | 5715,17 s |
| Orbital Inclination | 98.18° | 97.5° |
| MLST | ~18:00 hrs | ~18:00 hrs |

Table 25: Sentinel-1 and RISAT-1A (EOS4) Orbit Characteristics

Location of potential RFI based on geometry

The following figure is presenting the location of potential S-1A scenes coverages that could be acquired at moments of close fly-bys between S-1A and EOS-4.

As there is no least common divisor between the orbit cycles of the two spacecraft, the locations of such potential images are spread globally and do not show a clear geographic pattern.



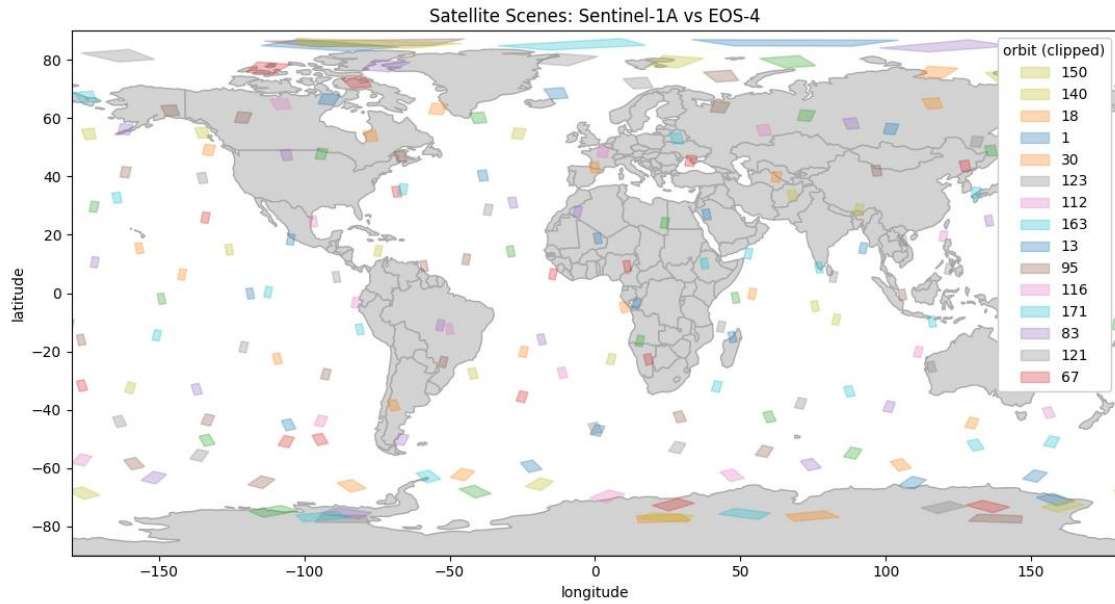


Figure 5-56: Locations of potential S1A vs EOS-4 RFI based on geometry (not associated to systematic acquisitions)

Activation of RFI mitigation

The following figure presents the status of S-1A acquisitions close to EOS-4 fly-bys and the activation of RFI mitigation.

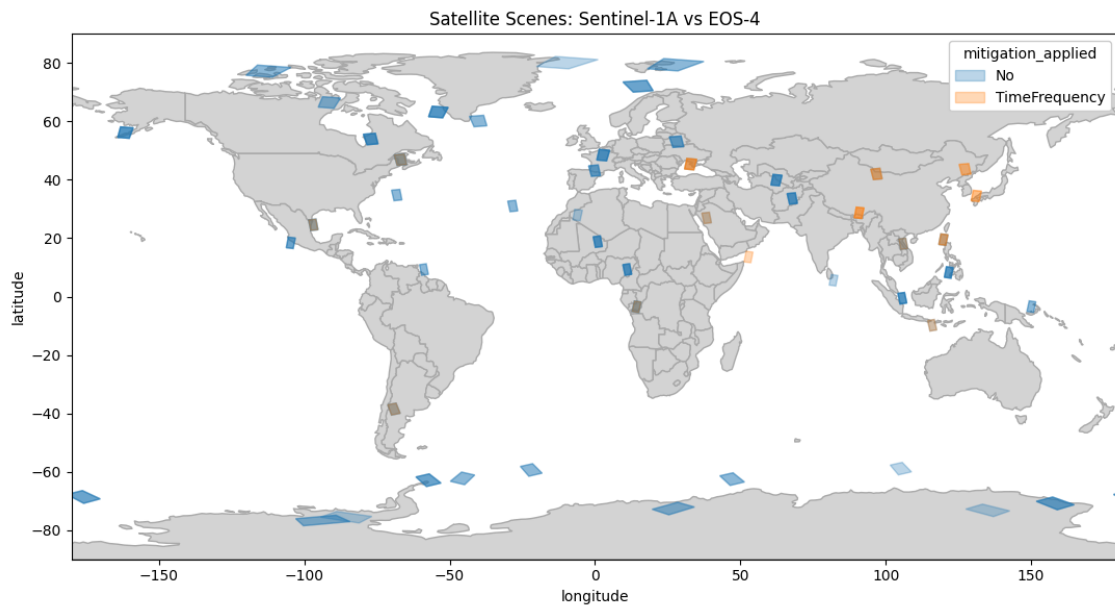
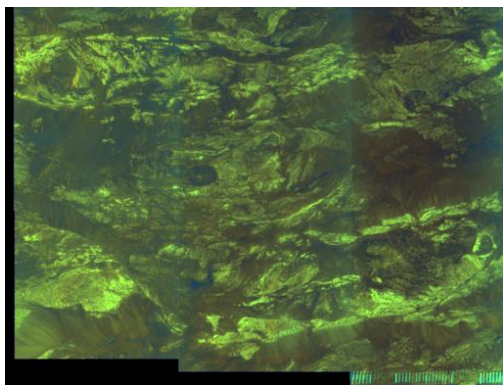
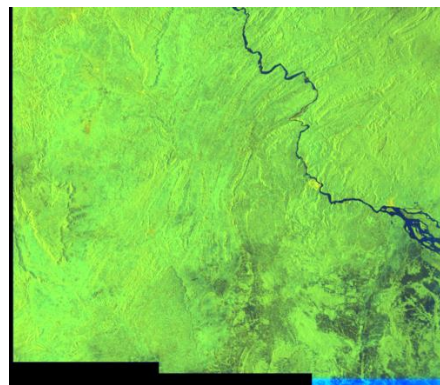


Figure 5-57: Location of S-1A products acquired close to S1A vs EOS-4 fly-bys, and status of RFI mitigation in 2023.

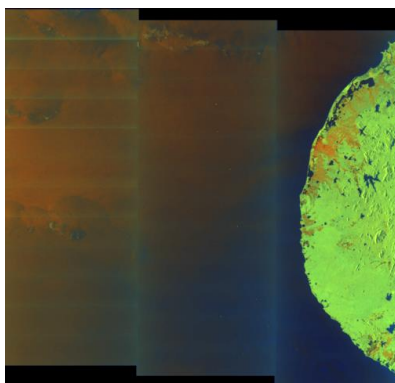
Observed residual RFI



S1A_IW_GRDH_1SDV_20230603T112855



S1A_IW_GRDH_1SDV_20231031T044418



S1A_IW_GRDH_1SDV_20231202T001723

The first two examples of residual RFI in this figure are not typical of long duration RFI originating from another spacecraft. They could be due to coincidental RFI from ground source captured by the Sentinel-1A sensor at the same time.

Figure 5-58: Examples of residual RFI observed close to S1A vs EOS-4 fly-bys in 2023

Summary

| | |
|------------------------------------------------------------------------|-------------|
| Sentinel-1 unit | Sentinel-1A |
| Other Satellite Name | EOS-4 |
| Other Satellite NORAD ID | 51656 |
| Period considered | 2023 |
| Fly-by events | 195 |
| Products acquired within 30s around fly-by | 139 |
| Products acquired within 30s around fly-by and with mitigation applied | 22 |
| Products with residual RFI | 3 |

Table 26: Summary of Sentinel-1A vs EOS-4 mitigation in 2023

5.8.9 Mutual Interferences with other sources

Other spaceborne emitters

The satellites of the Gaofen-12 constellation are known to be equipped with a SAR instrument emitting in C-Band ¹. However, the frequency band of the emission of this sensor is not known by the author of this report, and it is not confirmed that it is intersecting the reception band of Sentinel-1. Furthermore, studying the respective orbits of S-1A and Gaofen-12 constellation, no fly-bys were identified in 2023.

No other spaceborne emitters having a frequency band matching the one of Sentinel-1 were identified so far.

Other noticeable ground emitters

On previous Annual Performance reports [AD-07], a statement on RFI from unknown space sources was mentioned as long duration RFI were observed on some S-1A data-takes and no known spacecrafts equipped with C-Band transmitters were located near S-1A at the same time. No such RFI were observed since activation of the RFI mitigation, indicating either that the interfering emissions stopped or that the RFI mitigation is efficient enough.

Since then, it was confirmed that the S1 SAR processor performs an efficient mitigation of this RFI from “unknown” source. This was checked by performing test reprocessing of old impacted product with recent version of the processor (refer to Figure 5-59 for example of product without and with RFI mitigation activated). Furthermore, we collected some evidence on the source of this RFI as being related to the emissions of C-Band satellite tracking stations located in Hawaii, Texas and Ascension Island. The Figure 5-60 presents examples of long RFI patterns stopping when Sentinel-1 goes out of the intervisibility area between a tracking station in Houston, USA with a maximum elevation of 5 degrees.

¹ GF-12-04 is described as the 4th Gaofen C-Band SAR Satellite in https://space.oscar.wmo.int/satellites/view/gf_12_04

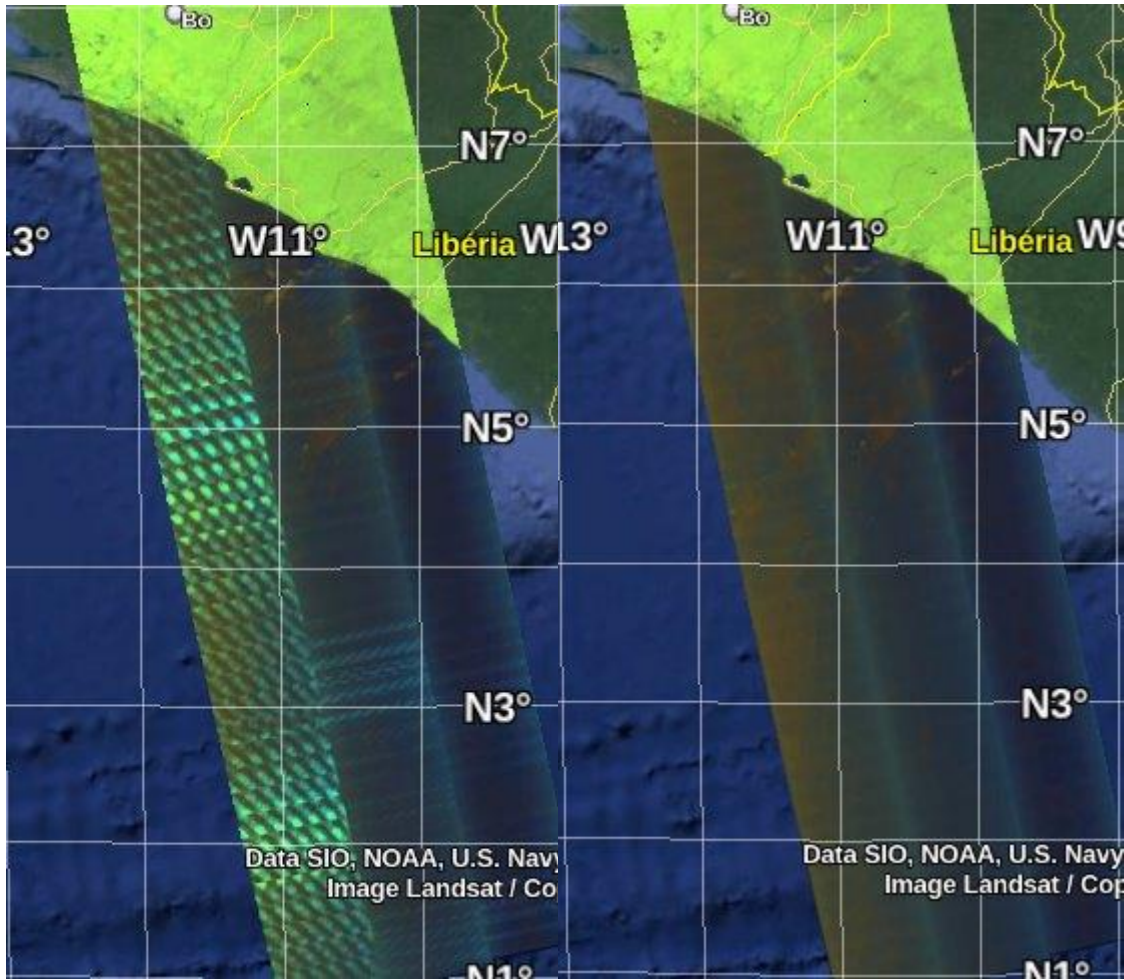


Figure 5-59: Example of RFI believed to be from a satellite tracking station. Left nominal processing, Right with RFI mitigation process activated (as for nominal production of Sentinel-1 data since 22nd March 2022). Sentinel-1A product acquired on 09/09/2021, orbit 39609, datatake 04AEA5

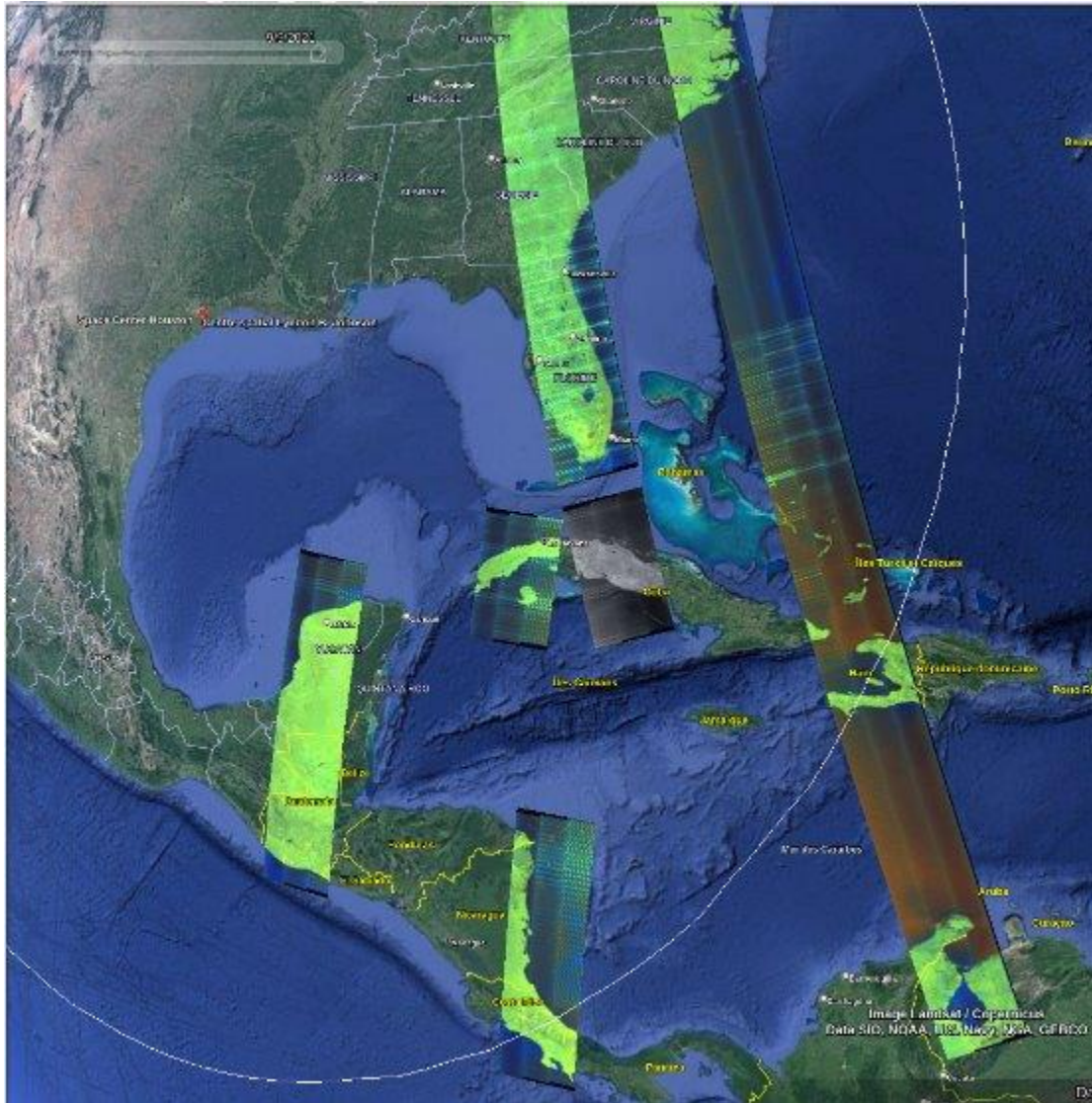


Figure 5-60: Example of long RFI patterns stopping close to the limit of intervisibility between Sentinel-1A and a tracking station in Houston, USA with an elevation of 5 degrees. All products being from Sentinel-1A unit acquired in 2016 and 2017

5.9 L1 Quality Disclaimers

S-1A Quality disclaimers issued on L1 products during 2023 are given in Appendix C -.



6. Level 2 Products

6.0 Wind Measurement

As in past years, the accuracy of the wind retrieval is assessed by comparing it with auxiliary wind source used as reference. In this scope, ESL performed systematic collocations between such reference data and core L2 OCN products [AD-07]. The used reference data in the reporting period included models from ECMWF (global) [S1-RD-33], Arome [[S1-RD-37], and Arpege (European)[S1-RD-38]

6.0.1 Image Mode (IW -EW)/ OWI

In 2023, the wind performance was mainly impacted by IPF and Auxiliary data updates (see section 3- Processing Updates)

Wind Speed

IPF update impacting the wind performances

The first IPF change from version 3.5.2 to 3.6.1 occurred on March 30th, 2023. The main changes were introduced in previous section of this document. As expected, this change did not affect significantly the wind performances, as is observed on Figure 6-1. Figure 6-1

Another update occurred from IPF 3.6.1 to IPF 3.6.2 on October 19th, 2023. As expected, this change did not affect significantly the wind performances, as is observed on Figure 6-1. Figure 6-1

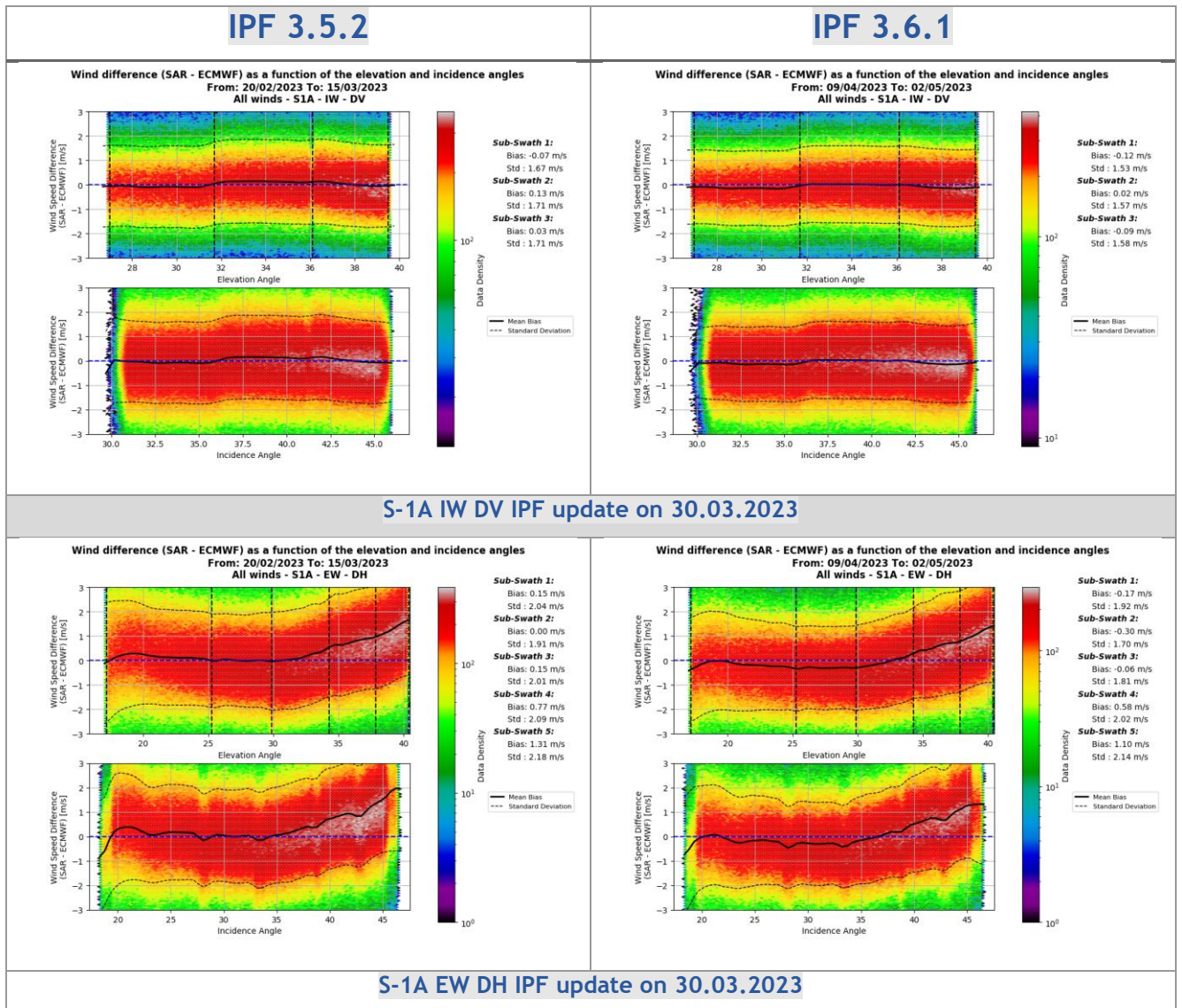


Figure 6-1: Effects of IPF update from 3.5.2 to 3.6.1 on the incidence and elevation angle dependent SAR wind speed bias with respect to ECMWF for the data sets concerned.

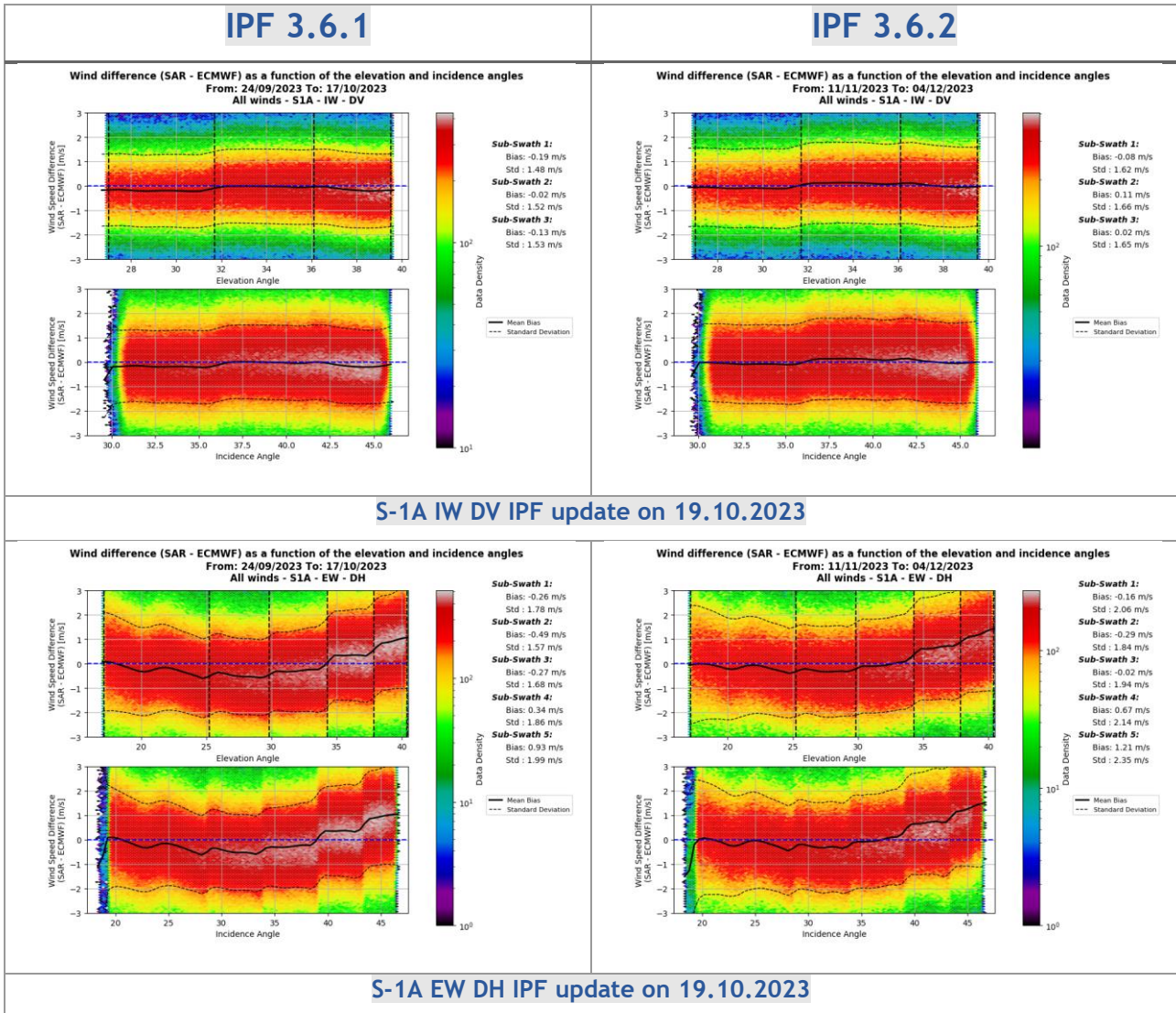


Figure 6-2: Effects of IPF update from 3.6.1 to 3.6.2 on SAR wind speed bias with respect to ECMWF as functions of the incidence and elevation angle.

Auxiliary data updates, impacting wind performances

In 2023, no auxiliary data update occurred that could have significantly impacted the wind performances.

Time series on the wind speed Performances

The Figure 6-3 shows the time series of S-1 Wind speed bias with respect to the ECMWF [S1-RD-33] and NCEP/GFS model [S1-RD-39], respectively. Figure 6-5 and Figure 6-6 represents the same comparison but for the wind speed standard deviation. For the moment, only DV polarization acquisitions are presented (for EW and IW). The mean bias is computed by averaging the difference between SAR wind speed and reference model wind speed on a bi-cycle period (two consecutive cycles), sub-swath by sub-swath. The associated standard deviation is also referred as Root Mean Square Error (RMSE). The IPF updates are in the upper part of all these plots. A significant RMSE increase is observed beginning of 2022, then shortly after, at the transition between IPF 003.51 and 003.52. Further studies in the course of year 2023 demonstrated that the first RMSE peak is compatible with a large scale ancillary wind

direction systematic bias offshore Norway during this period. Besides that, a seasonality similar to 2022 [AD-07] is observed.

Sub-swath bias statistic vs time for ECMWF collocation and polarization DV.

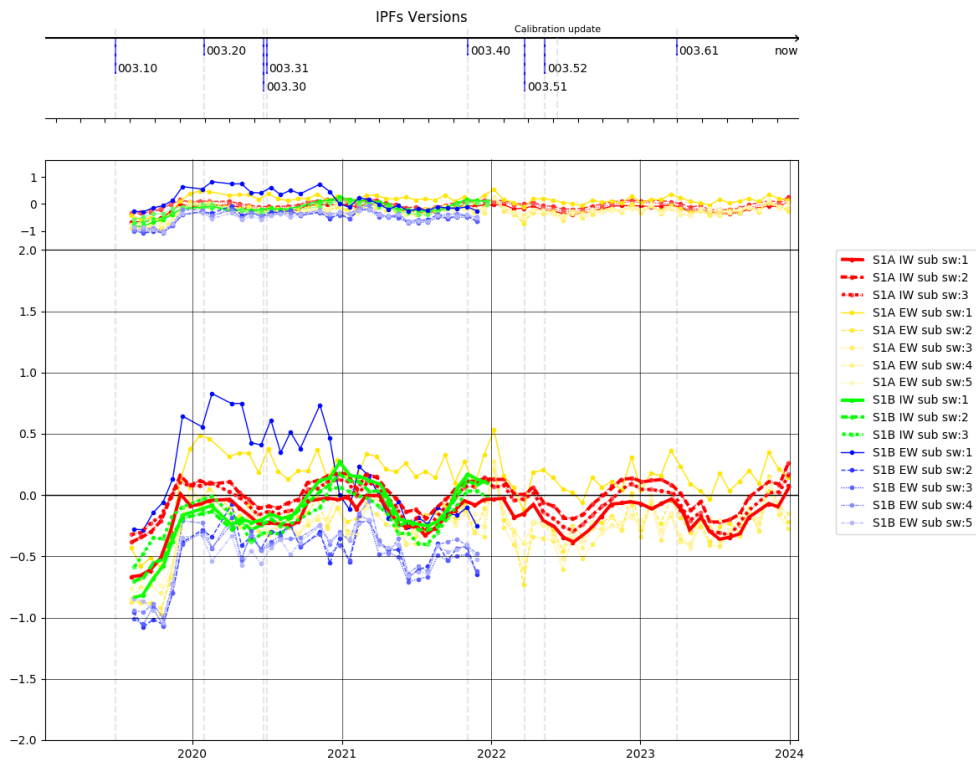


Figure 6-3: Mean SAR wind speed bias with respect to ECMWF model detailed by sub-swath along time for the DV polarization acquisitions. (Top: general trend, bottom: zoom on the trend curves)



Sub-swath bias statistic vs time for NCEP colocation and polarization DV.

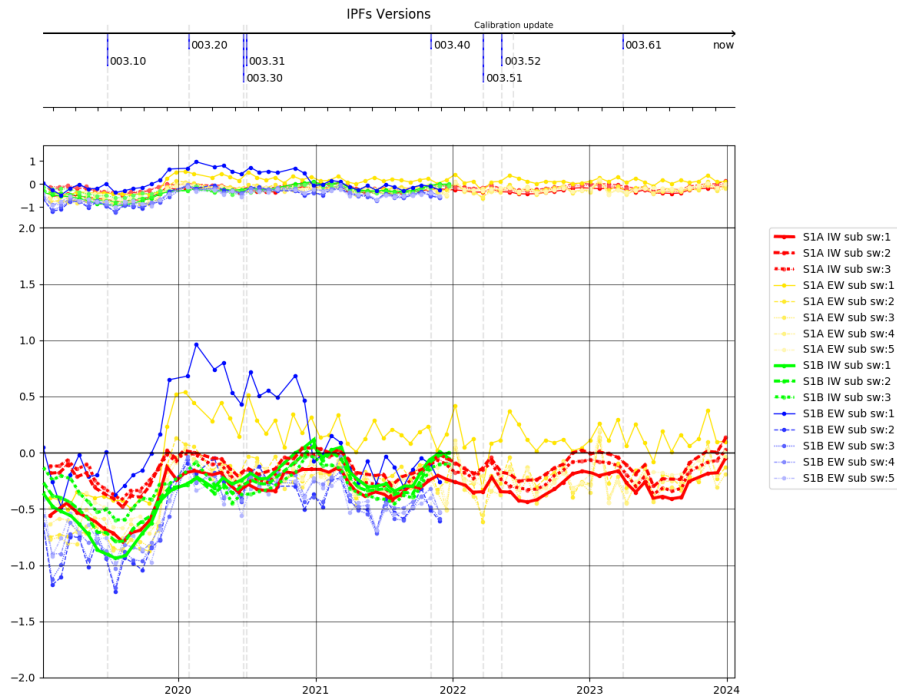


Figure 6-4: Mean SAR wind speed bias with respect to NCEP model detailed by sub-swath along time for the DV polarization acquisitions. (top: general trend, bottom: zoom on the trend curves)

Sub-swath std statistic vs time for ECMWF colocation and polarization DV.

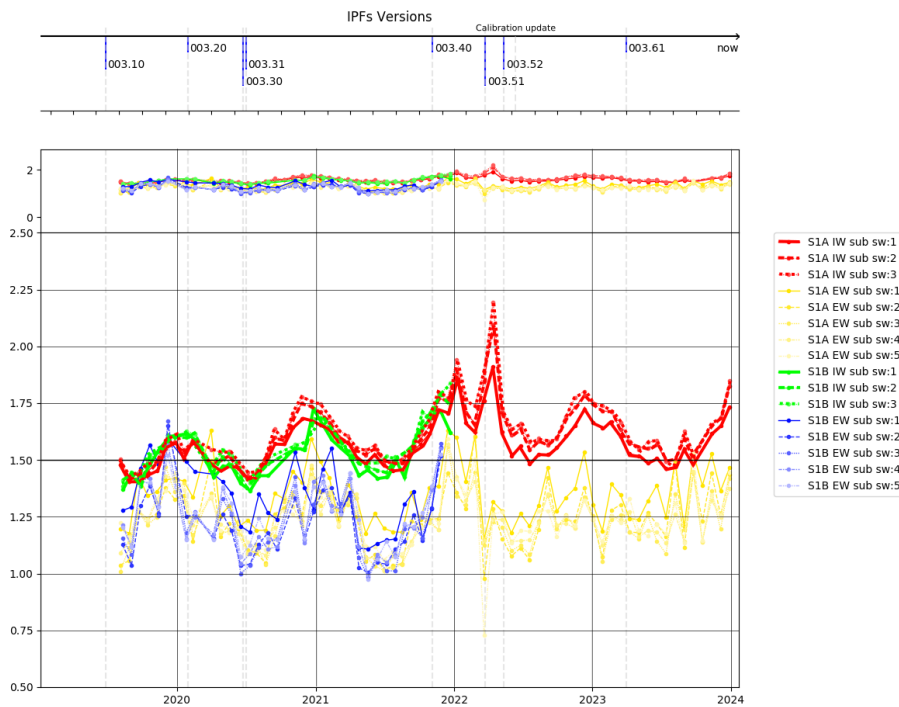


Figure 6-5: SAR wind speed standard deviation with respect to ECMWF model detailed by sub-swath along time for the DV polarization acquisitions. (Top: general trend, bottom: zoom on the trend curves)

Sub-swath std statistic vs time for NCEP colocation and polarization DV.

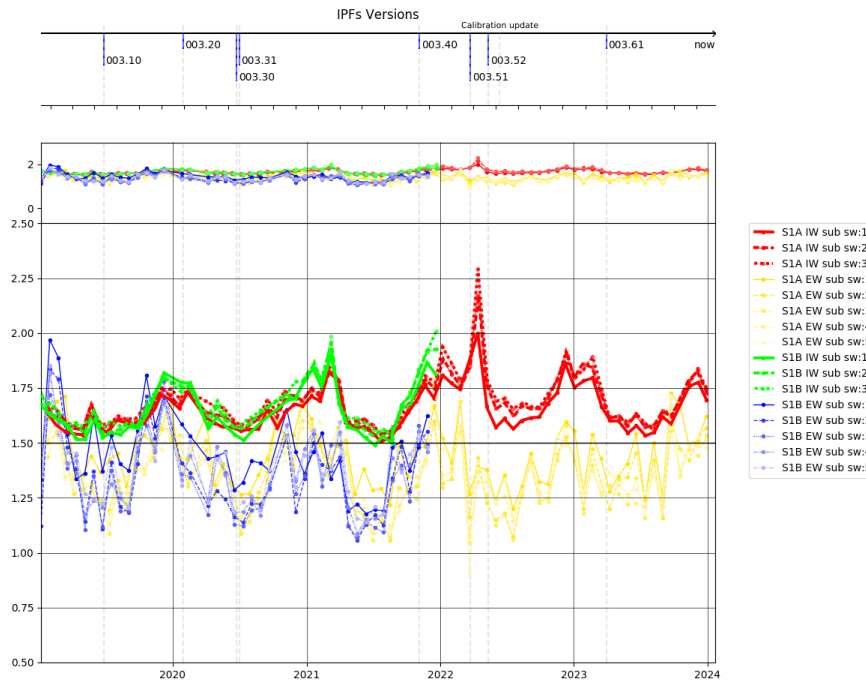


Figure 6-6: SAR wind speed standard deviation with respect to NCEP model detailed by sub-swath along time for the DV polarization acquisitions. (Top: general trend, bottom: zoom on the trend curves)

Wind direction

Ebuchi diagrams comparing between SAR and ECMWF wind direction are plotted in Figure 6-7. Both are in relatively good agreement. Performances are stable over the year.

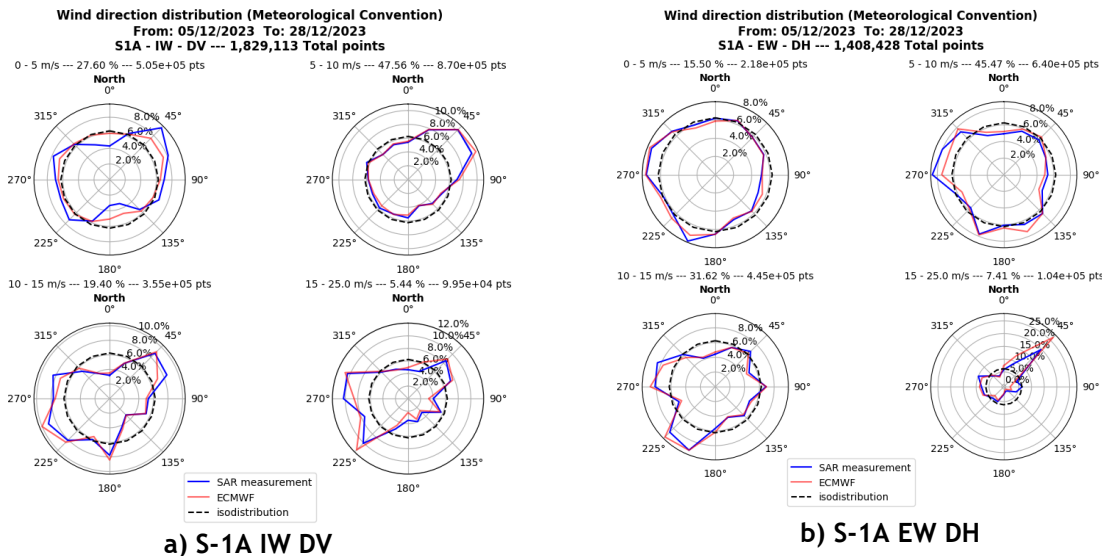


Figure 6-7: Ebuchi diagrams for S-1A SAR retrieved and ECMWF wind directions detailed by wind speed domain in December 2023.



6.0.2 Wave Mode / OWI

Since IPF 3.30, the OWI processing has been activated on Wave mode.

Wind Speed

The performances of the wind speed retrieval for wave modes are presented in Figure 6-8

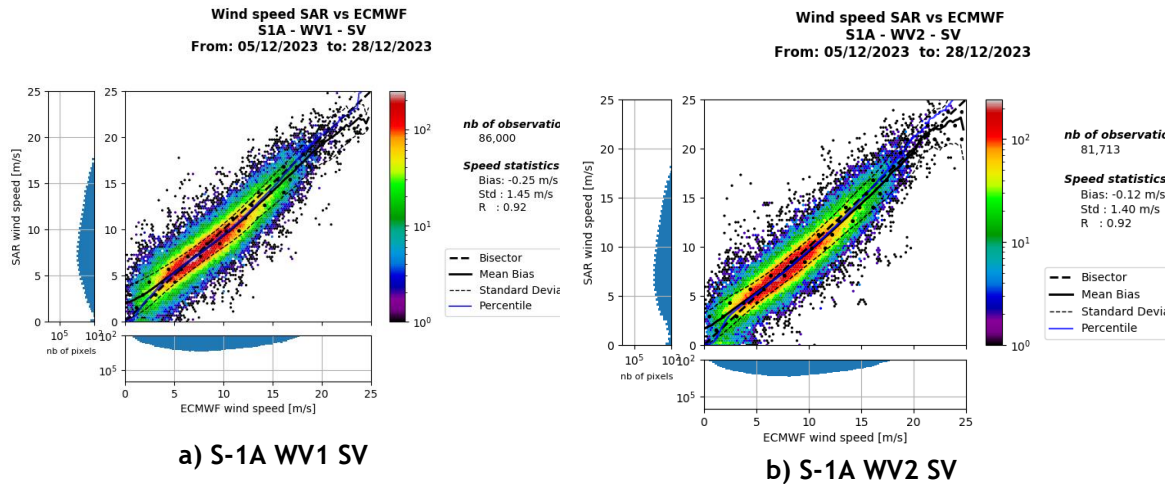


Figure 6-8: Scatter plots of SAR vs ECMWF wind speeds for Wave Modes in Dec. 2023, for S-1A.

Wind Direction

As for TOPS modes, the performances of wind direction retrieval are diagnosed on Figure 6-9. Performances are compliant with TOPS modes.

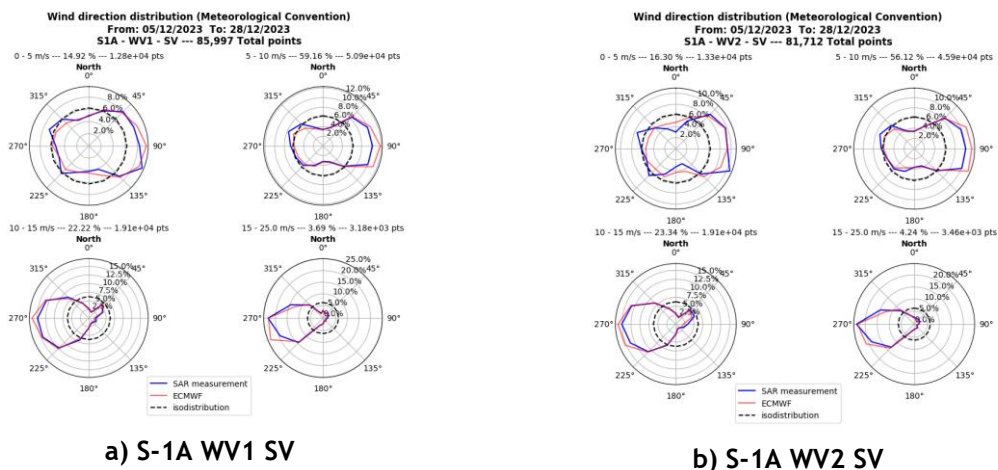


Figure 6-9: Ebuchi diagrams for S-1A SAR retrieved and ECMWF wind directions detailed by wind speed domain in December 2023.

6.0.3 Wave Mode / OSW

The WV acquisition mode onboard Sentinel-1 units is mostly dedicated to ocean applications. It is supposed to cover all open ocean surfaces except coastal areas dedicated to IW and sea ice (i.e. marginal ice zone) areas reserved for EW mode. The Figures below illustrate the coverage of the WV mode for year 2023. On the bottom figure showing the number of WV acquisition per 1°x1° bin, some large areas in Eastern South Pacific, Western Pacific and Southeast of Australia where the number of acquisitions during the year is close to zero. These gaps are not intended and discussion with Sentinel-1 mission planner are on-going.

SAR WV Sentinel-1 acquisitions Ocean surface wind speed and direction retrieved performances have been very stable during the past year, and they are both within the specifications.

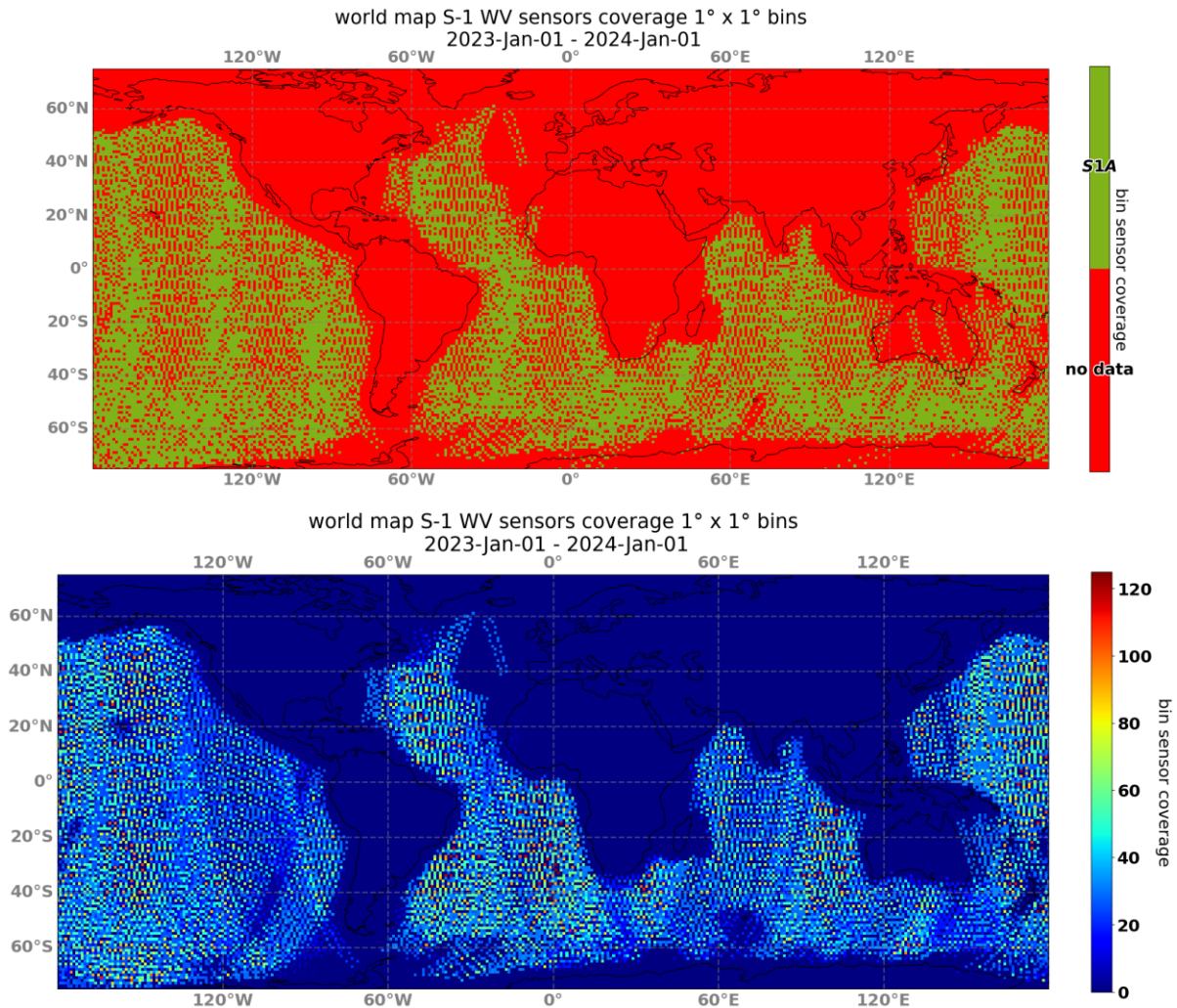


Figure 6-10: Coverage map of S-1 WV acquisition

Wind Speed

S-1 WV wind speed is validated with respect to ECMWF numerical model [S1-RD-33].

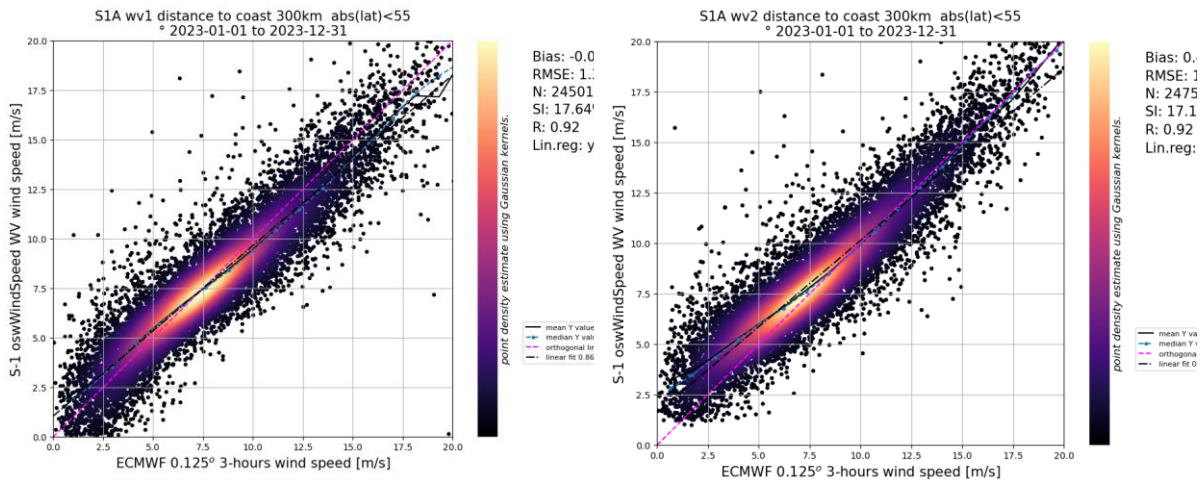


Figure 6-11: Scatter plot of *oswWindSpeed* as respect to ECMWF 0.125 (3h) left: S-1A WV1, right: S-1A WV2

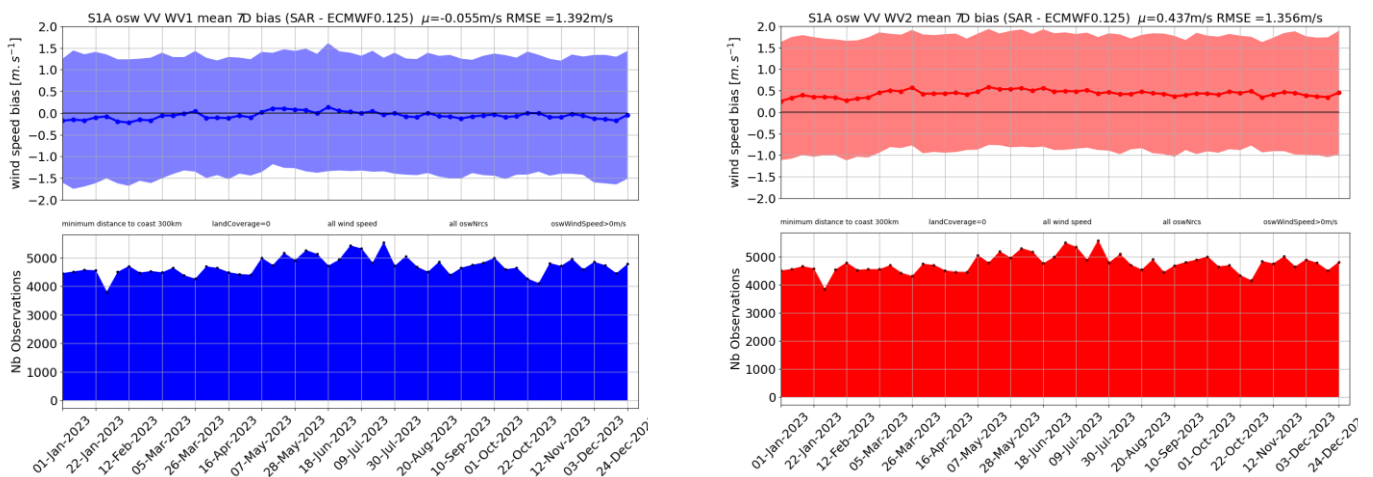


Figure 6-12: Difference in ocean surface wind speed between *oswWindSpeed* (S-1 WV OCN variable) and ECMWF numerical model (0.125° spatial resolution grid and 3-hours for time resolution). Bold line is the daily mean of the individual measurement differences and the background colour is the daily standard deviation.

Time evolution: There was no specific changes in 2023 regarding the *oswWindSpeed*:

- Since IPF v3.5.1 release, the *oswNrcsNeszCorr* variable is available (which is needed to do a direct GMF inversion with CMOD5n). But it is still *oswNrcs* (no noise correction) that is still used to estimate the *oswWindSpeed*. This should be fixed in IPF 003.80 release in2024.

Performances with respect to specifications: RMSE is within the 2 m/s specifications.

Discussion about the performances: The wind speed performances are directly linked to the geophysical calibration and the use of the Geophysical Model Function. Once the direct wind inversion will use denoised NRCS, it will improve the WV2 wind speed performances. This change is expected in 2024.

Wind Direction

The wind direction for *oswWindDirection* products is a copy of the forecast value given by ECMWF numerical model (data provided as AUX_WND input) available at the processing date. In the contrary to Sentinel-1 OWI wind inversion, there is no Bayesian inversion scheme for OSW module to combine SAR and ECMWF information to get the wind direction. The validation in this section is basically equivalent to a validation between the ECMWF forecast (which is present in the products in *oswWindDirection*: SAR wind direction) and ECMWF analysis.

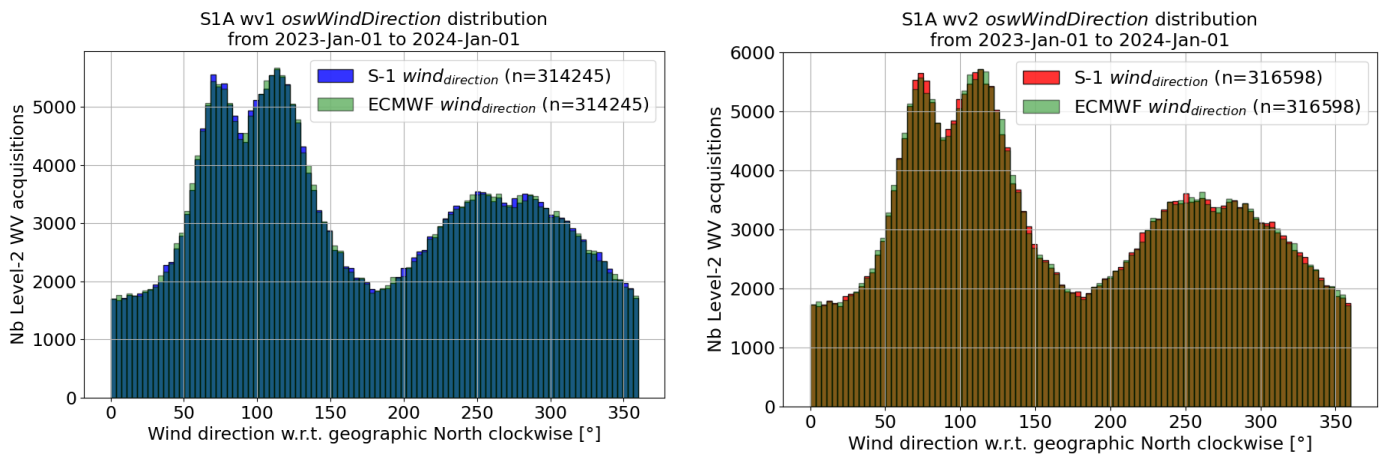


Figure 6-13: Distribution of the ocean surface wind direction, respectively *oswWindDirection* S-1 WV OCN variable and ECMWF numerical model (0.125° spatial resolution grid and 3-hours for time resolution).

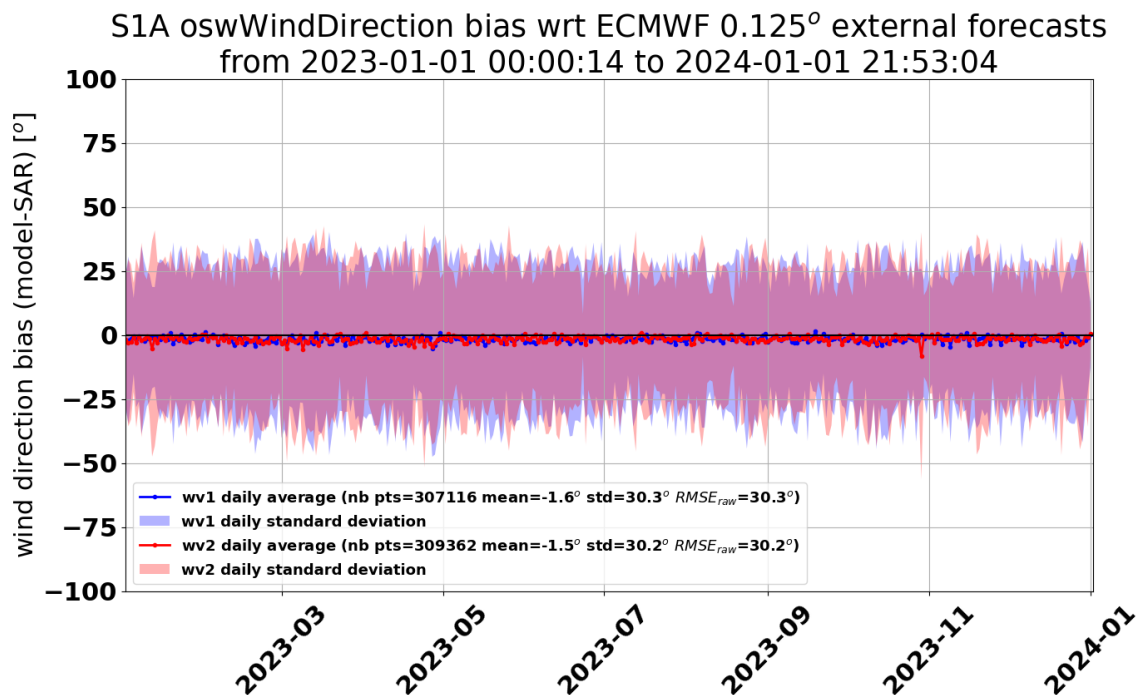


Figure 6-14 : ocean surface wind direction bias: *oswWindDirection* S-1 WV OCN variable compared to ECMWF numerical model (0.125° spatial resolution grid and 3-hours for time resolution) as function of Time.

The rationale behind this analysis is the need to validate both SAR derived parameters but also auxiliary information ingested in the processor and annotated in Level-2 products.

Time evolution: There is no significant trend regarding the wind direction performances with respect to time.

Inter comparison: similar results are obtained for WV1 and WV2.

Performances with respect to specifications: RMSE is within the 30° given by the specifications.

Discussion about the performances: The differences between the SAR wind direction (in fact forecast of ECMWF model) and ECMWF analysis are almost zero everywhere. The significant differences observed from time to time can be explained by specific meteorological situations such as low wind area of extreme events (cyclones) in which atmospheric front location in time and space show discrepancies between model forecast and analysis.

6.1 Swell Measurement

6.1.1 Wave Mode

Significant Wave Height without Partitioning

oswTotalHs performance

In June 2022, a variable *oswTotalHs* has been released in S-1 WV OCN products. This variable is an “altimetric like” significant wave height, using a Deep-Learning model result [AD-07]. The Inputs of the model are SAR polar image cross spectrum (real and imaginary) plus high-level features: incidence angle, longitude, latitude, NRCS, Normalized variance, time of day.

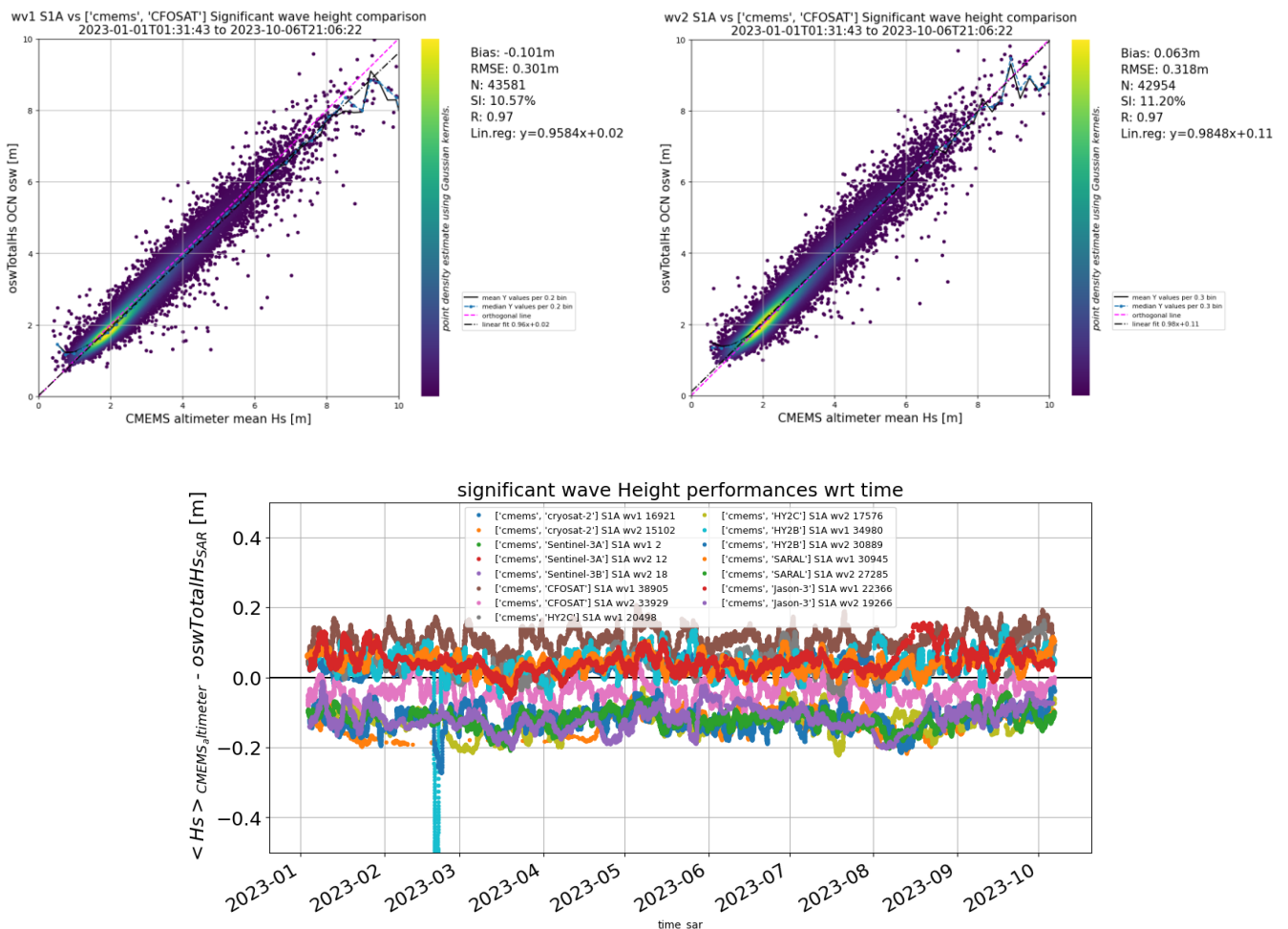


Figure 6-15 Top left: scatter plot of the *oswTotalHs* from L2 OCN WV1 products compared (and collocated) to CFOSAT nadir beam (product CMEMS WAV TAC L3). Top right: Same but with WV2. Bottom: SWH bias between S-1 WV1/2 versus different altimetric missions (j3: Jason-3, cfo: CFOSAT SWIM, al: SARAL-Altika, c2: Cryosat-2) from CMEMS WAV product.

Figure description: The methodology applied to produce the figures above is based on collocations SAR/Altimeters georeferenced in a 2° radius and ± 3 hours time window.



Time evolution: the visible fluctuation bias have different origins: the evolution of co-locations positions from cycle to cycle, the seasonal effect associated and the different sensor/calibration/inversion evolution of the currently flying satellites.

Inter comparison: WV2 SWH has a mean tendency to be overestimated compared to altimeter (e.g.: ~6 cm bias wrt CFOSAT) while WV1 is underestimated (~10 cm bias wrt CFOSAT). This is illustrated on the top left and top right graphs of Figure 6-15. The same tendency is as well observed while comparing vs other altimeters (Jason-3, SARAL-Altika, Cryosat-2) as illustrated in bottom graph of Figure 6-15.

Performances with respect to specifications: There is no specification on performances of “Total HS” in the Sentinel-1 mission product definition document [AD-13]. Nevertheless, the performances are aligned with RMSE<0.5 m and bias<0.1 m (using the same specification as for HS from partitions)

Discussion about the performances: Performances are described in papers cited in osw ATBD [AD-07], they reflect what was the best regression model at the time of publication, it may be possible to improve the accuracy and precision of SWH and its standard deviation by tuning other models, increasing the size of the training dataset (especially for acquisitions in strong sea st) or adding extra information helping the model.

Significant wave height derived from elevation wave spectrum performance

The S-1 WV OCN product also allows to compute a significant wave height from the SAR ocean spectrum (*oswPolSpec*). To validate the energy of the WV ocean wave spectrum, the concept of *effective significant wave height* is used against WW3 wave spectra. It consists in computing the wave parameters from WW3 on the spectral domain where the inversion is considered valid (below/inside the cut-off). On top of this mask applied on the spectral grid, a low frequency contamination mask is used to filter regions of the spectra SAR and also WW3. This contamination mask is provided in the WV OCN product since 26th June 2019 with IPF 3.1.0.

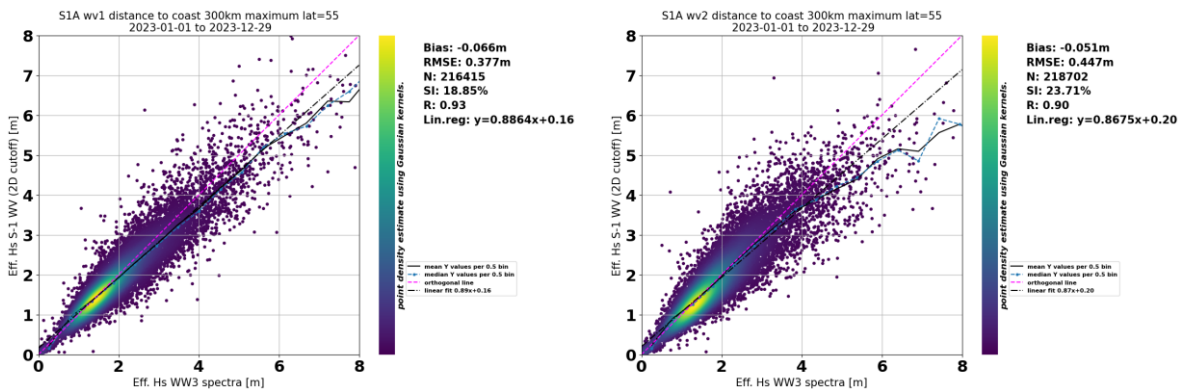


Figure 6-16: scatter plot of effective significant wave height computed on the whole spectra S-1 WV OCN and associated WW3 spectra. Top left: S-1A WV1, top right: S-1A WV2.

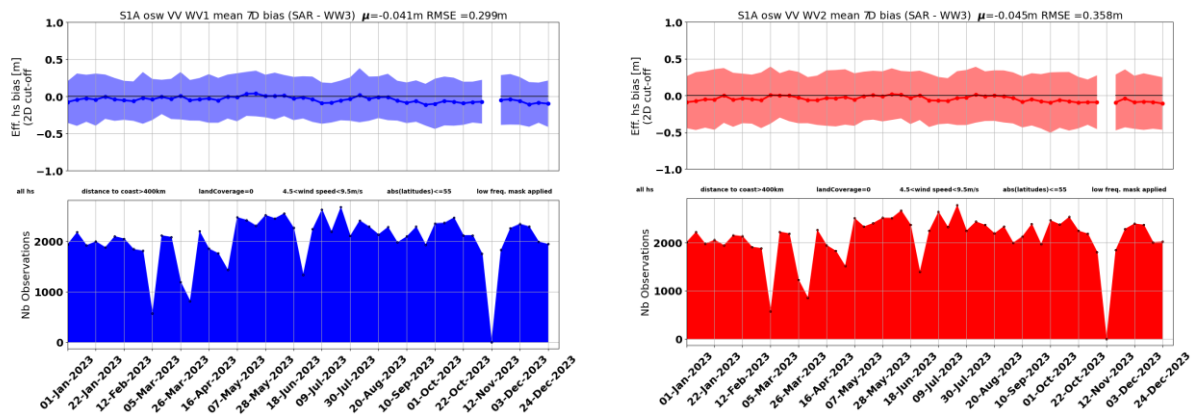


Figure 6-17: Daily difference of SAR effective azimuth + range 2D cut-off Hs and WW3 numerical model Hs (using same spectral cut-off domain). For each sensor, on the upper panel the bold line is the daily mean of the individual measurement differences, and the background colour is the daily standard deviation. On the lower panel the colour indicates the number of available matchups between WV (20 km by 20 km) S-1 acquisitions and WW3 spectra computed at the nearest 0.5° resolution grid point.

Time evolution: There is no significant trend regarding the effective Hs bias performances with respect to time.

Inter comparison The performances of WV1 and WV2 are very similar using this concept of effective Hs against WW3.

Performances with respect to specifications: The RMSE and the bias are within the specifications (0.5 m resp. 0.1 m) for S-1A and WV1/WV2 [AD-13].

Discussion about the performances: MTF (Model Transfer Function) used to retrieve wave parameters is suffering of underestimation of the energy for strong Hs, plus an anisotropic bias that underestimates the Hs along the range axis. With this MTF the OSW spectra tends to show splitting over range axis for near range travelling waves at moderate to high winds (> 7m/s). We assume that this is attributed to non-linear effects in the RAR MTF, currently not properly accounted for. In addition, a residual signal in the phase plane is systematically observed and now understood².

Two-dimensional ocean wave spectrum partitioning

The 2D ocean wave spectrum derived from the SAR is partitioned into different ocean wave systems. A spectra can be delineated in up to five swell systems, followed by the computation of integral parameters:

- swell significant wave height (oswHs),
- the pseudo-peak wave wavelength(oswWl),
- the pseudopeak wave direction (oswDirmet) for each partition

Swell partitions cross assignments between SAR and WW3 data

Each selected WW3 spectra is an hindcast at the closest (time-sp .SAR/WW3 cross-assignments at the partitioned swell level are based on spectral distance. The performance of each partition is assessed against WW3 numerical wave model with respect to the following three parameters: the significant wave height (oswHs), the wavelength (oswWl) and the wave direction (oswDirmet).

² impact of local incidence angle which has been neglected for in the computation of the cross spectrum between one look and another.



Since the IPF 003.51, March 2022, the quality of each partition is performed thanks to machine learning algorithm which aims to classify each swell partition as ‘very good’, ‘good’, ‘medium’, ‘low’ or ‘poor’ based on some SAR features [AD-07].

During year 2023, the OSW algorithm has remained stable and has not undergone any changes that have an impact on the wave inversion unit. Data over +/- 55° North are not considered for the validation.

oswQualityFlag distribution

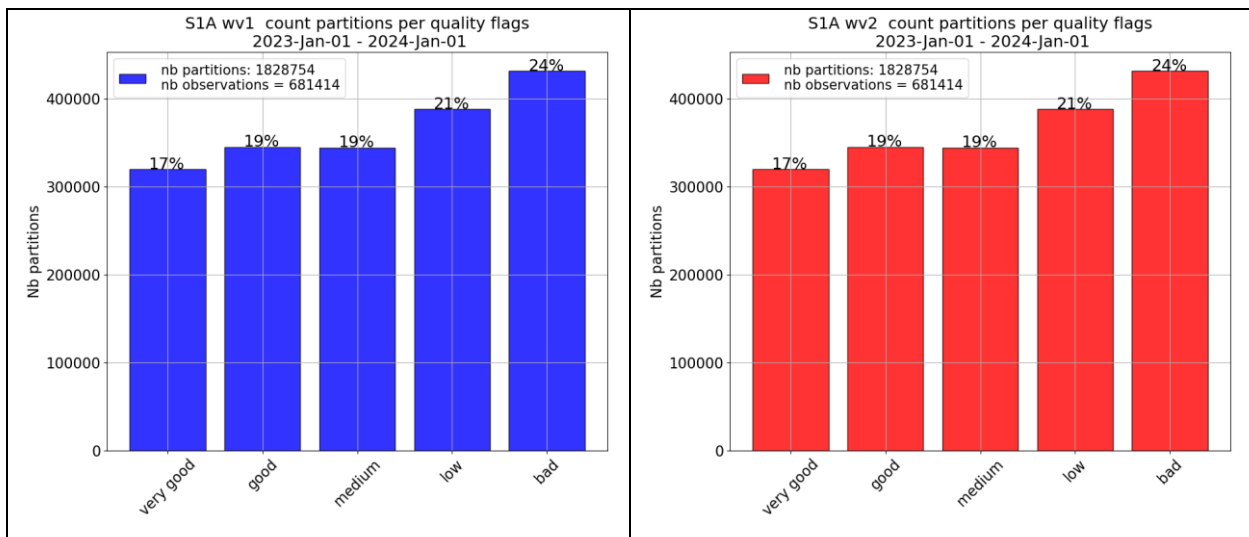


Figure 6-18 : Partition quality flag occurrence for both S1A-WV1 and S1A-WV2 for the year 2023.

As displayed in Figure 6-18 , we perform a balanced partitions representativity of between the different quality flag categories for both WV1 and WV2 :

The partitions labelled as “good” and “very good “have almost the same occurrence as the other categories and cover larger wind range of values and wave parameters such as effective Hs, compared to previous algorithm. As example, the “very good” data are extended to Hs > 7 m whereas the domain was limited to 6 m by in the previous classification version. This behaviour is well shown by the scatter plots in Figure 6-19

The following sections show the performance of the integral parameters at wave partition level with respect to WW3 partitions. The data are filtered to retain only those vignettes classified as pure ocean swell (POS). Performance is shown only for two extreme categories: "Very good" and "Poor".

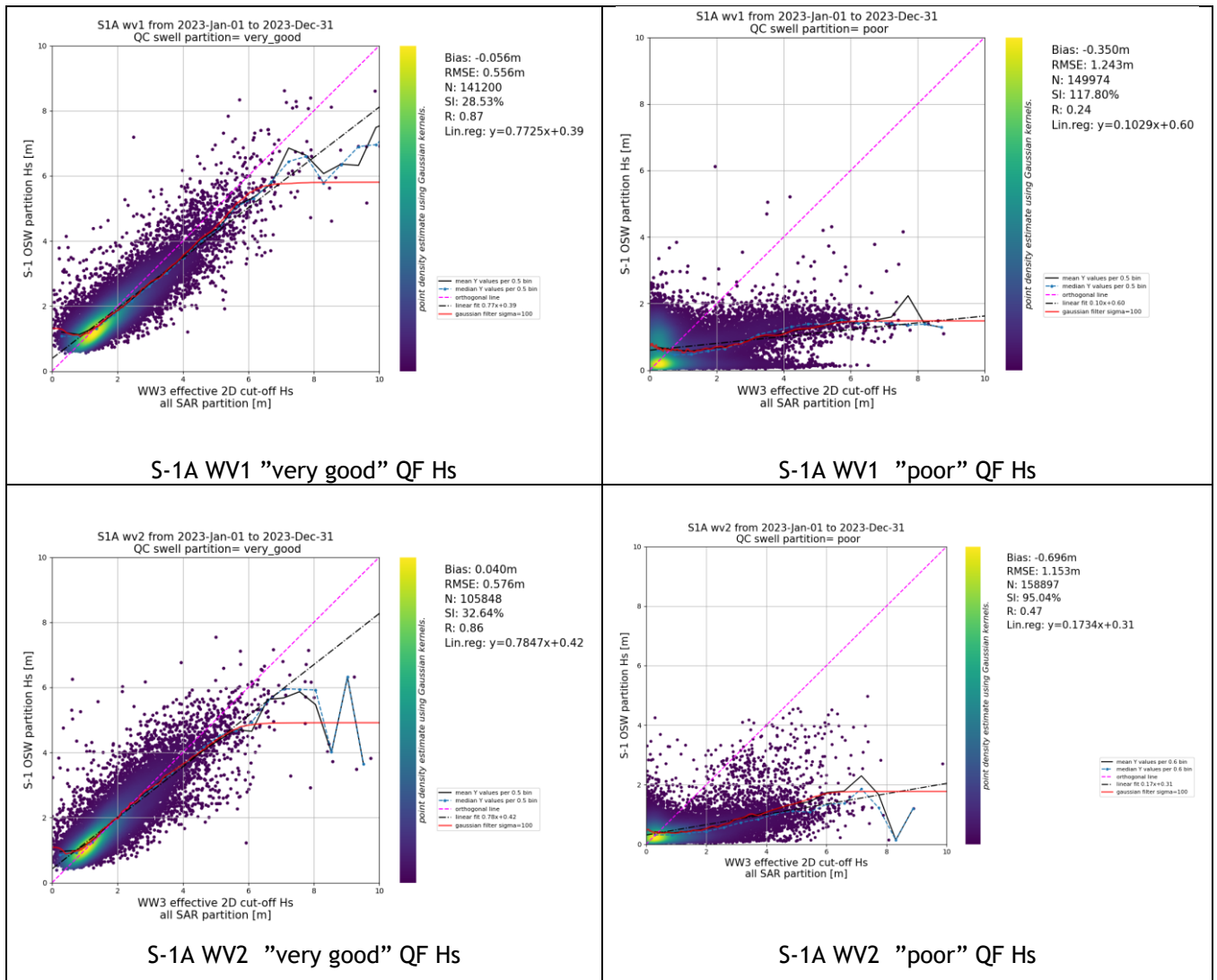


Figure 6-19: Partition effective Hs performance on partitions flagged with “very good” and “poor” class for both WV1 and WV2.

Partitions wavelengths performances with respect to WW3 numerical model



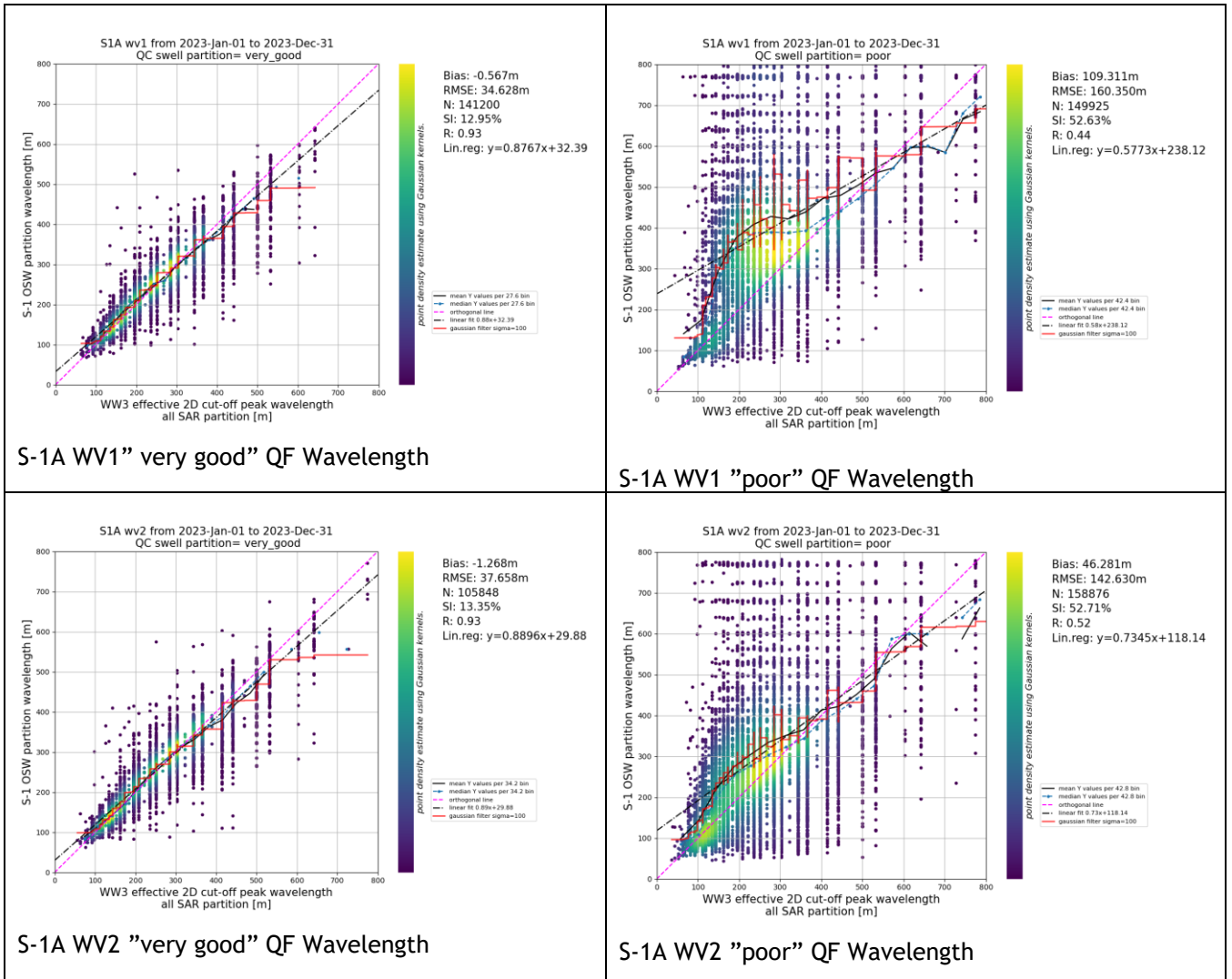


Figure 6-20 : Partitions wavelength performance on partitions flagged with “very good” and “poor” class for both WV1 and WV2.



Partitions wave directions performances with respect to WW3 numerical model

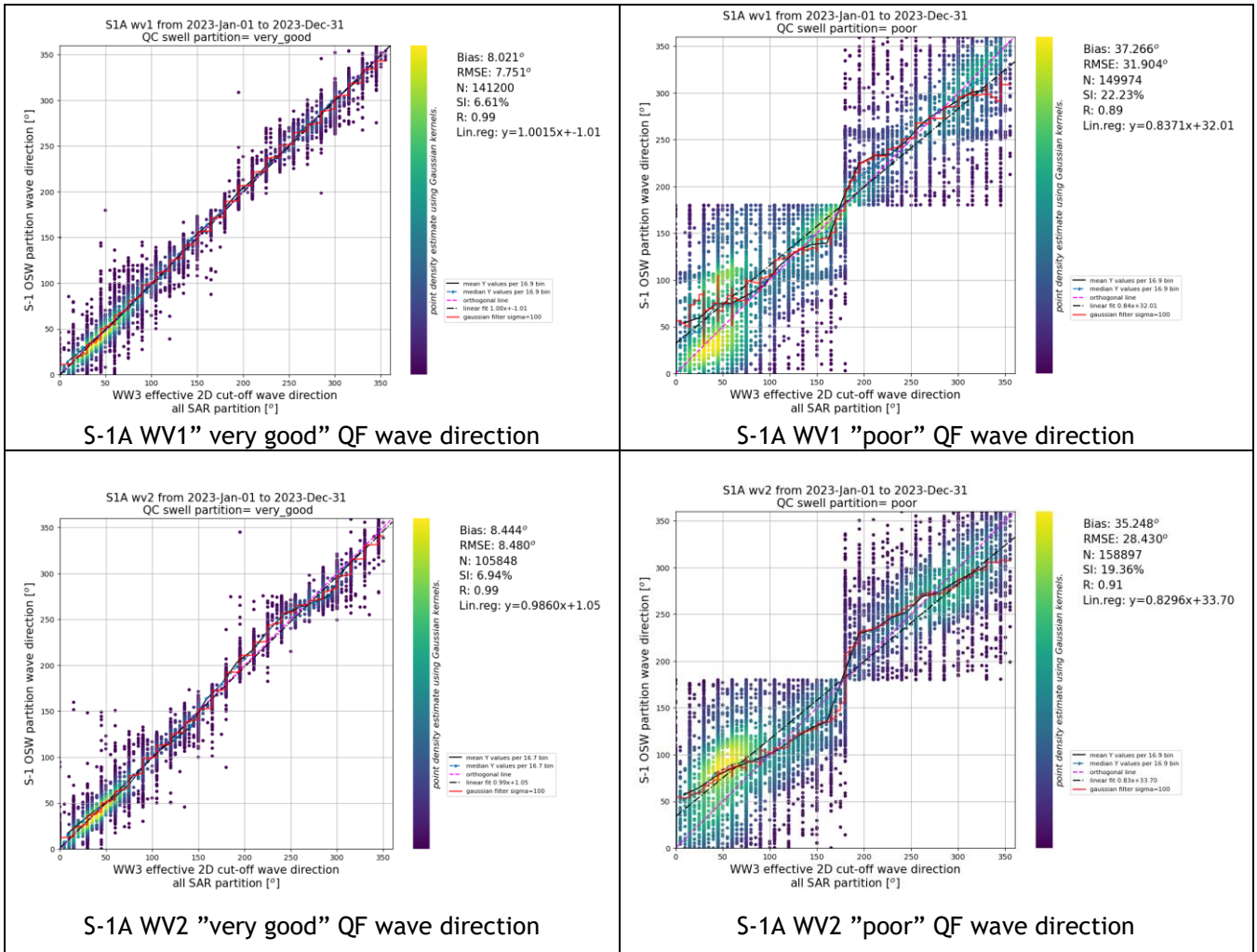


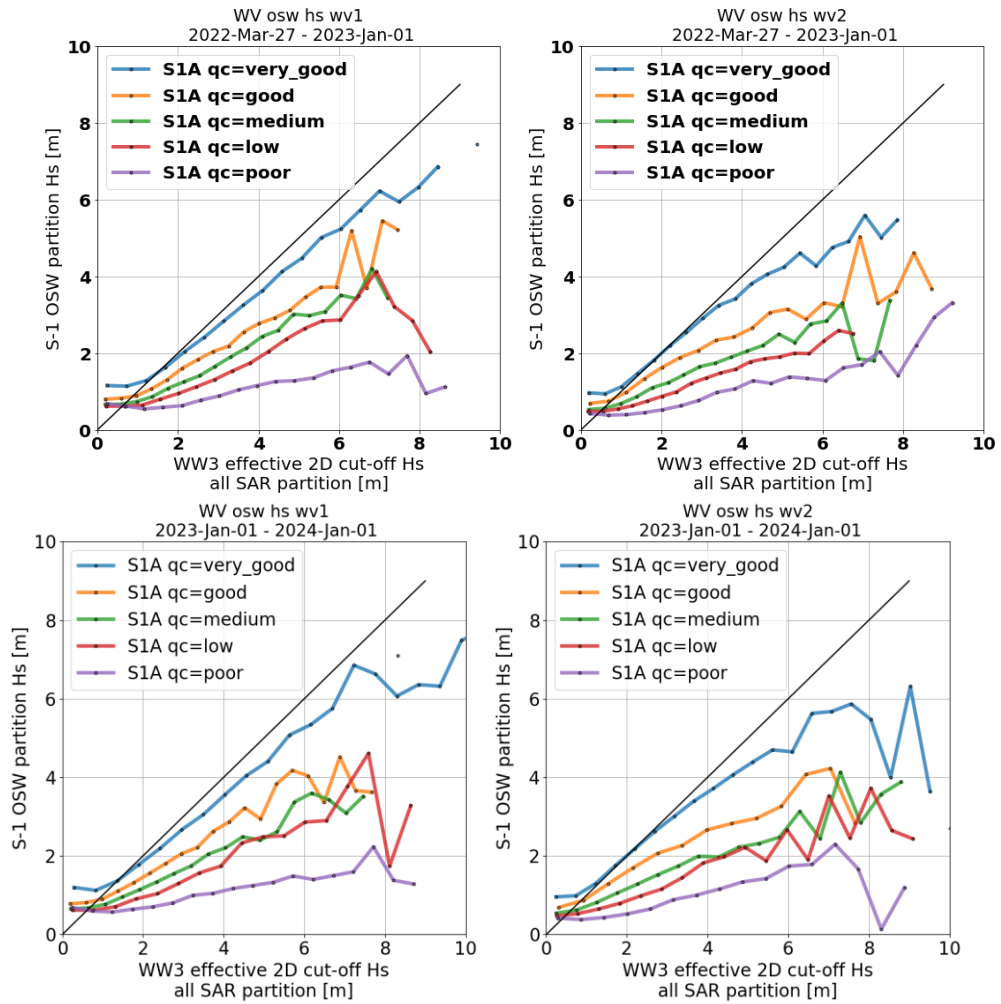
Figure 6-21 : Partitions wave directions performance on partitions flagged with “very good” and “poor” class for both WV1 and WV2

Performances comparison per partition quality flag value

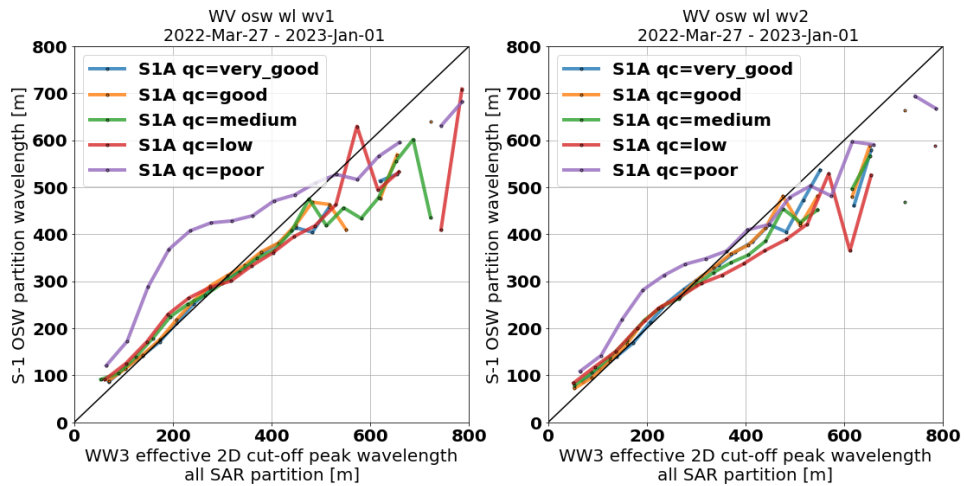
Considering all the partitions available for each SAR spectra (up to 5), this section illustrates the performances on significant wave height, wavelength and wave direction with respect to the peak parameter of the closest WW3 partition and separated by partition quality flag.

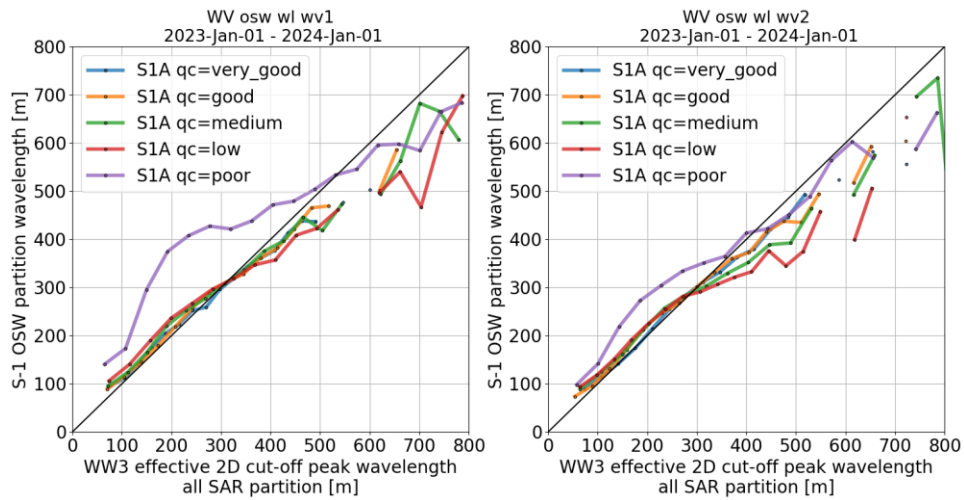


A)



B)





C)

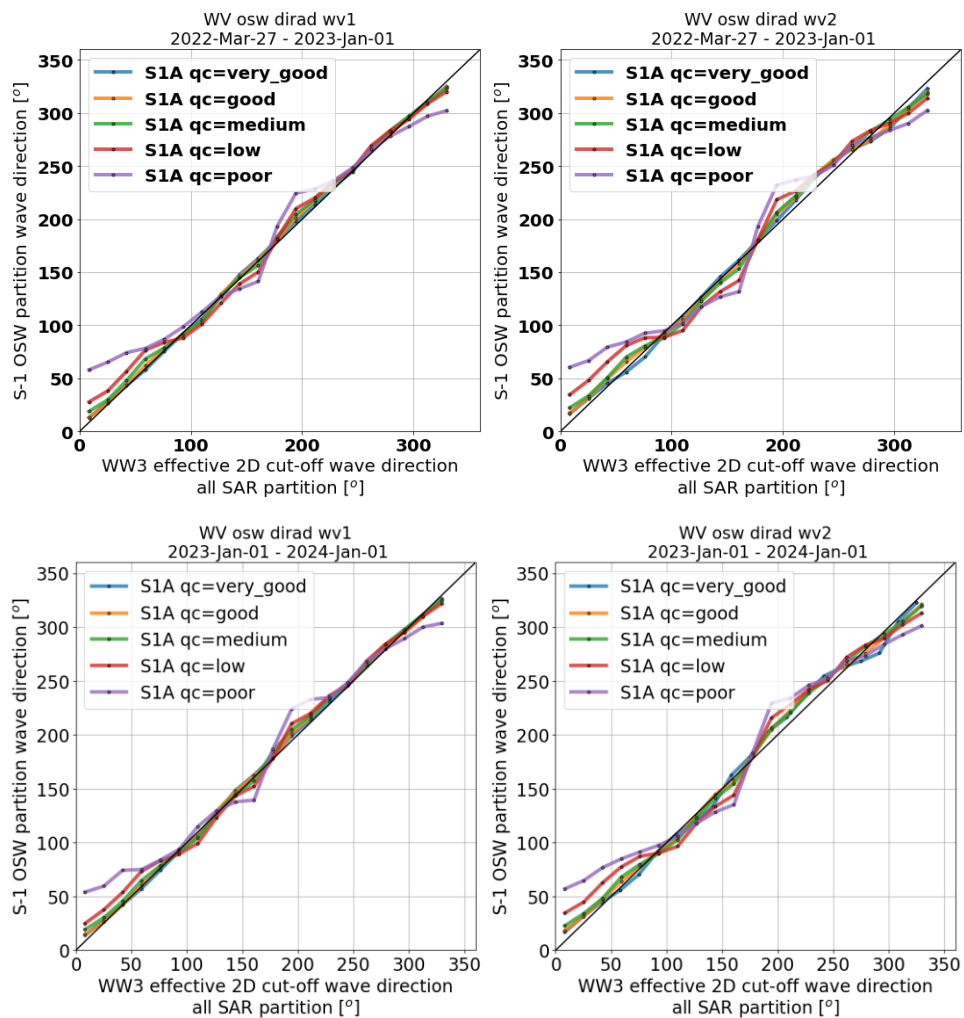


Figure 6-22: Figures of OSW wave partitions performances with respect to WW3 numerical model. The lines represent the mean bias for each wave partition quality flag. Minimum distance to coast is 100km. To avoid ice contamination: $-55^\circ < \text{latitude} < 55^\circ$. Left column is WV1 (24° incidence angle), right is WV2 (37° incidence angle). A): Significant wave height B): Peak wavelength, C): Peak wave direction.

The figures above depict the performances for acquisition from IPF 003.52 (starting 12th May 2022) 003.61 (starting 30th March 2023) and IPF 003.71 (starting 19th October 2023) . These 3 updates of the processor didn't change the wave parameters performances.

Time evolution: There is no significant trend regarding the performances of wave peak parameters bias with respect to time.

Inter comparison: Only S1A available.

Performances with respect to specifications: Only “very good” WV1 and “good” WV2 partitions are within Hs specifications (bias 0.1m RMSE 0.5m). For peak wavelength and peak direction, “very good” and “good” WV1 and WV2 are within the specs (bias 10 m RMSE 50 m resp. Bias 10° and RMSE 40°).

Discussion about the performances: The updated quality flag method is designed to make the “very good” and “good” partitions matching the wave parameters specifications. It is the case with the WV data acquired in 2023.

- The “very good” effective Hs for WV1 and WV2 is showing an overestimation at low Hs, this could be mitigated with a future ad hoc tuning of the MTF and the low frequency filter.
- The peak wavelength is underestimated by Sentinel-1 WV for wave with wavelength > 400 m, the revision of low frequency filter and/or the future application of Koch filters on the roughness image prior to the wave inversion could help to improve the high wavelength retrieval.
- Effective Hs from low quality partitions is impacted by the fact that in some cases the ambiguity removal cannot be done (due to the lack of contrast in the imaginary cross spectra) and then a wrong propagation swell direction is attributed to the swell system which is mis-associated to a WW3 swell system. Future works on the wave inversion and especially direction ambiguity removal will improve performances on both wavelength and wave direction parameters.
- The 180° error on the wave direction is observed in some WV acquisitions. This issue is now understood. It comes from the acquisition geometry change during the radar aperture, in particular local incidence angle change the backscatter between the beginning and the end of the look/burst and thus the cross spectra computed between the 2 looks in absence of compensation of this effect is interpreted as a change of phase for specific range of wavelength and specific range of significant wave height. A theoretical work to describe this effect is ongoing and a future strategy to mitigate the problem is under discussion.

The tables below are presenting the performances for effective significant wave height, peak wavelength and dominant wave direction, respectively Table 27, Table 28, Table 29. The tables are separated in 3 groups (mean bias, number of partitions, RMSE) of 2 columns (S-1A x WV1/WV2). The lines correspond to the value annotated in OCN osw WV products for the variable ‘oswQualityFlagPartition’.

| : | bias | | nb | | rmse | | |
|-------------|-----------|-----------|----------|----------|----------|----------|----------|
| | id2 | S1Aww1hs | S1Aww2hs | S1Aww1hs | S1Aww2hs | S1Aww1hs | S1Aww2hs |
| qcvals2 | | | | | | | |
| 0_very_good | -0.055640 | 0.040318 | 141200.0 | 105848.0 | 0.555945 | 0.576204 | |
| 1_good | -0.032697 | -0.103388 | 131213.0 | 137741.0 | 0.532686 | 0.602911 | |
| 2_medium | -0.137067 | -0.277268 | 105376.0 | 161827.0 | 0.625221 | 0.642987 | |
| 3_low | -0.246224 | -0.398047 | 97431.0 | 195591.0 | 0.776021 | 0.761362 | |
| 4_poor | -0.350229 | -0.695500 | 149974.0 | 158897.0 | 1.243230 | 1.152836 | |

Table 27: Effective significant wave height performances (w.r.t.) WW3 model in meter for S-1 WV swell partitions depending on the swell partition quality flag



The effective Hs mean bias are within a range of 0 cm to 69 cm.

Number of partitions per level of quality flag is quite homogeneous. Hs Bias and RMSE are showing performances in agreement with the level of quality flag, i.e. smaller Hs bias and found for “very good” annotated partitions compare to “poor” annotated partitions. This last comment is true for both WV1 and WV2.

| qcvals2 | bias | | nb | | rmse | |
|-------------|------------|-----------|----------|----------|------------|------------|
| | S1Awv1wl | S1Awv2wl | S1Awv1wl | S1Awv2wl | S1Awv1wl | S1Awv2wl |
| 0_very_good | -0.567076 | -1.268332 | 141200.0 | 105848.0 | 34.627522 | 37.657879 |
| 1_good | 4.585176 | 3.267809 | 131213.0 | 137741.0 | 41.841877 | 46.208324 |
| 2_medium | 7.204310 | 3.260080 | 105376.0 | 161827.0 | 55.704678 | 55.088459 |
| 3_low | 11.301971 | 3.171583 | 97431.0 | 195591.0 | 71.812164 | 70.501663 |
| 4_poor | 109.311295 | 46.280548 | 149925.0 | 158876.0 | 160.350037 | 142.630264 |

Table 28: Peak wavelength performances (w.r.t.) WW3 model in meter for S-1 WV swell partitions depending on the swell partition quality flag

The wavelength mean bias are within a range of -1 m to 109 m. As expected, “good” swell partitions have better bias and RMSE than “poor” ones. Also, the mean bias and RMSE on wavelength are better for WV2 compared to WV1, except for “very good” partitions.

| qcvals2 | bias | | nb | | rmse | |
|-------------|------------|------------|------------|------------|------------|------------|
| | S1Awv1wdir | S1Awv2wdir | S1Awv1wdir | S1Awv2wdir | S1Awv1wdir | S1Awv2wdir |
| 0_very_good | 8.021334 | 8.443707 | 141200.0 | 105848.0 | 7.750731 | 8.480235 |
| 1_good | 10.543201 | 11.635678 | 131213.0 | 137741.0 | 11.366212 | 12.649252 |
| 2_medium | 14.658611 | 15.283933 | 105376.0 | 161827.0 | 15.754833 | 15.336655 |
| 3_low | 20.563704 | 22.832258 | 97431.0 | 195591.0 | 21.030108 | 21.326263 |
| 4_poor | 37.265683 | 35.247893 | 149974.0 | 158897.0 | 31.904152 | 28.430404 |

Table 29: Dominant wave direction performances (w.r.t.) WW3 model in degree for S-1 WV swell partitions depending on the swell partition quality flag

The dominant wave direction mean bias are within a range of 8° to 37°. As expected RMSE are higher for “poor” Quality Flag partitions compared to “good” partitions. RMSE for “very good” partitions is about 8°. The fact that quality flag is “cutoff-dependent” explain the high difference between “very good” and “poor” partitions performances on the wave direction retrieval.

6.1.2 Other modes

The wave inversion is currently also activated on Strip-Map (SM) acquisitions but the limited number of acquisitions and the coastal areas where they are acquired make the monitoring of performances on annual basis not relevant enough to be discussed in this report. Activation of wave inversion on Interferometric Wide Swath (IW) and Extra Wide Swath (EW) is an on-going topic of investigation for the Expert Support Laboratories of the Mission Performances Centre.

6.2 Radial Velocity Measurement

In this section, a status on the Level 2 OCN RVL products is provided for Wave mode and TOPS modes. There are no particular events this year that impacted RVL products (leaving aside the calibration issues introduced in RVL section in the executive summary).

6.2.1 Wave Mode

The Sentinel-1 Level 2 Doppler centroid anomaly (DCA) and radial velocity (RVL) measurements are currently coloured by the Doppler frequency derived from AOCS. The attitude Doppler centroid (DC) frequency computed from the downlinked quaternions is around zero, and do not reflect the actual attitude DC frequency. This prevents the current version of the Level 2 processor to provide calibrated DCA and RVL estimates. The analysis of restituted attitude data and Gyro data shows DC variations of around 10Hz long the orbit. The use of these data sources is currently not part of the Level 2 processor. However, promising results are achieved off-line using the calibrated Gyro information provided by ESTEC [S1-RD-13], and a post-processing approach has been implemented and validated as part of the "Copernicus Sentinel-1 RVL Assessment" project.

The S-1A WV OCN RVL show nominal performance. The typical behaviour of the nominal daily mean WV OCN RVL Doppler (rvlDcObs) for January and December months are shown in the plots of Figure 625. However, jumps (of around 20 Hz) in Doppler are sometimes observed, which are attributed to change in star-tracker configuration. For the same two months we show in Figure 626 the scatterplot between radial velocity and the ECMWF range wind speed.

The main contributions to the non-geophysical Doppler are from satellite attitude and from antenna electronic miss-pointing. The latter is impacted significantly by the temperature compensation applied to the antenna. A model approach based on the temperature compensation information and the antenna model is undertaken to predict these DC jumps along the orbit.

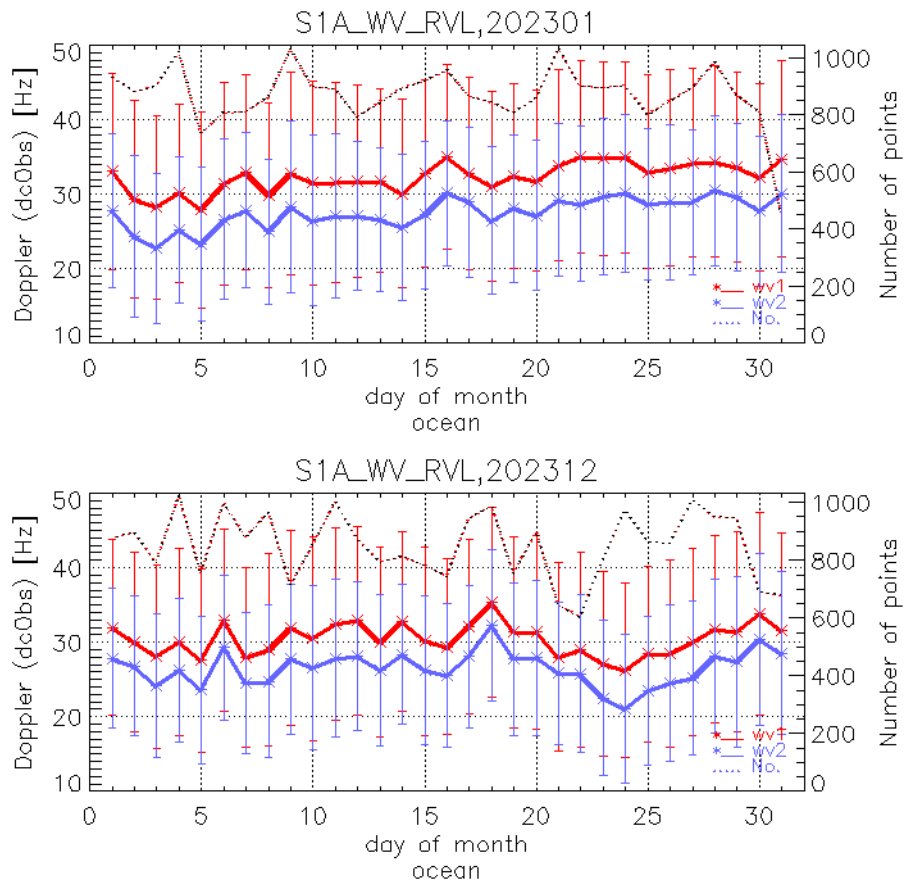


Figure 6-23: Daily mean S-1A WV OCN Doppler frequency (rvlDcObs) for January 2023 (upper) and December 2023 (lower).

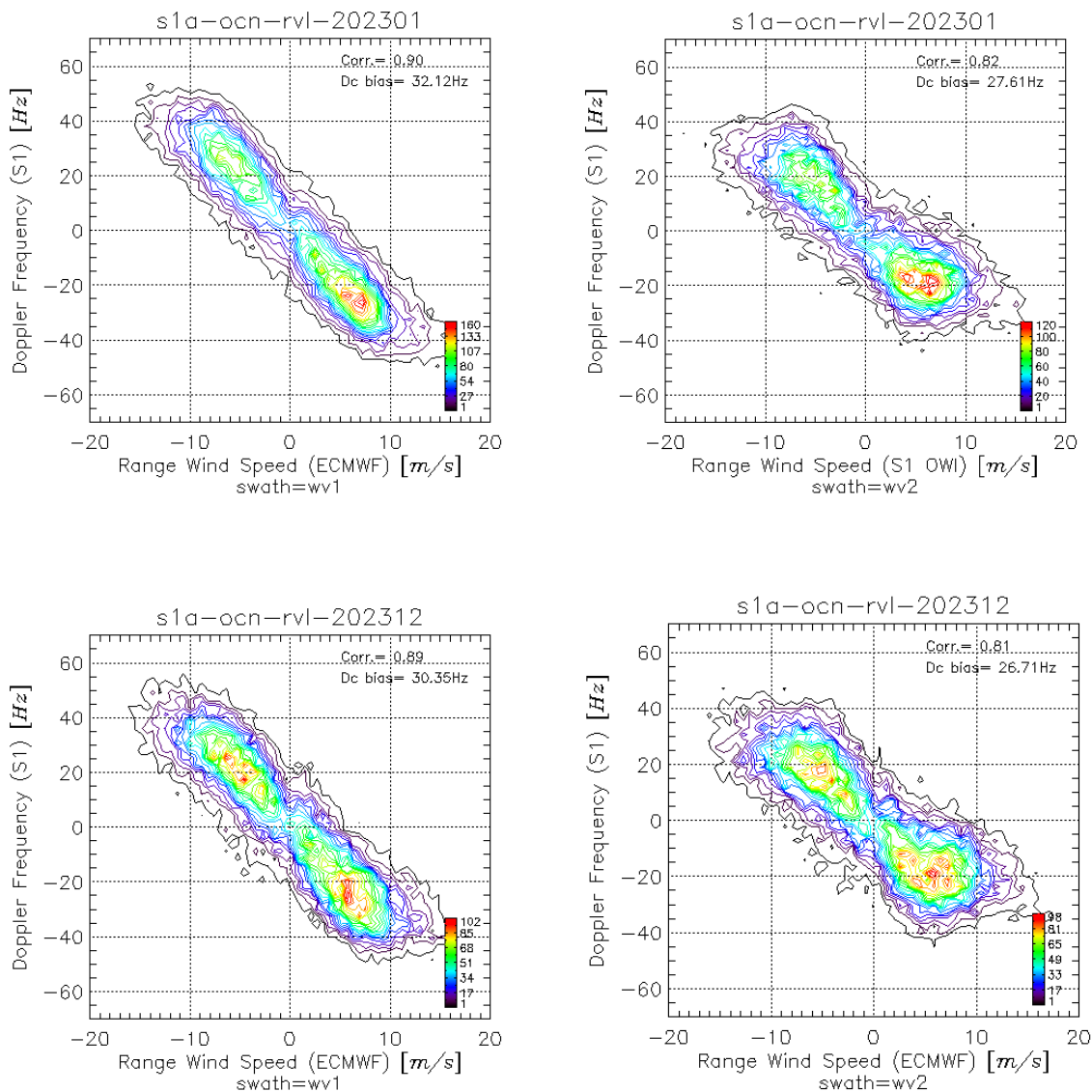


Figure 6-24: Scatterplot of of S-1A WV1 OCN RVL Doppler frequency (rvIDcObs) versus ECMWF range wind speed acquired over global ocean areas. Upper: January 2023, Lower: December 2023, Left: Swath WV1, Right: Swath WV2

Time evolution: stable performance except for short periods related to change of star-tracker configuration.

Inter comparison: close performances between WV1 and WV2 Doppler.

Performances with respect to specifications: not applicable since absolute calibration of the DC is not feasible at present.

Discussion about the performances: the main problems are: a) the fast attitude variations along orbit not predictable from the downlinked quaternions, b) the temperature compensation applied to the antenna not easily predictable. For WV mode the temperature compensations occur between WV data takes and between WV imagettes inside a data take.

6.2.2 TOPS Mode

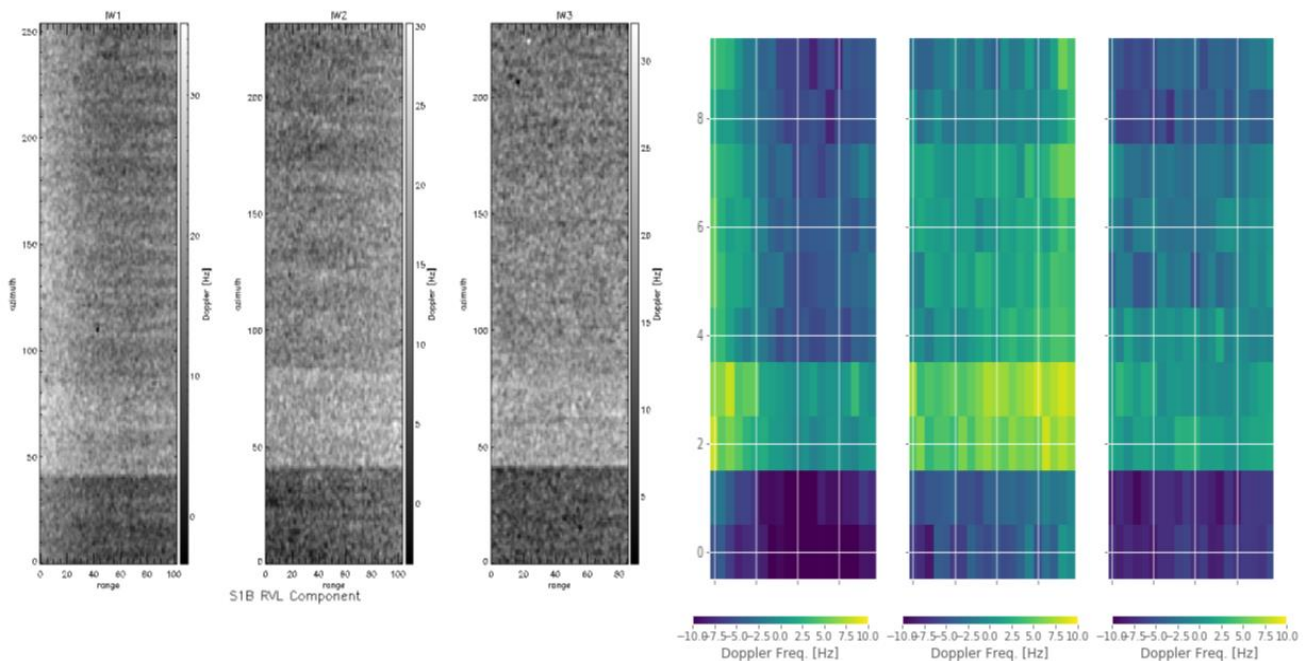
Time evolution: No specific degradation or improvements

Inter comparison: Not applicable.

Performances with respect to specifications: not applicable since absolute calibration of the DC is not feasible at present.

Discussion about the performances: the main problems are: a) the fast attitude variations along orbit not predictable from the downlinked quaternions, b) the temperature compensation applied to the antenna not easily predictable. For TOPS mode the temperature compensations occur within data takes.

The DC jumps (>10Hz) observed previously in the Sentinel-1 DC measurement are still present. These sudden jumps in DC (>10Hz) from one burst to another persist over all swaths Figure 6-25. These jumps are observed consistently in both Level 2 DC and raw data DC. Investigations show that the jumps come from temperature compensation which subsequently alters the antenna characteristics. There is at present no means to predict when and where this occurs. A data driven approach is under consideration, as well as a model approach based on the temperature compensation information and the antenna model.



S1B_IW_RAW__OSDV_20180730T215018_20180730T215050_012046_0162DF_6858.SAFE

Figure 6-25: Example of S-1B IW DC showing jumps in both Level 2 OCN Dc (left) and Level 0 IPF Dc (right).

Another kind of DC jump was observed from one burst to another. These jumps come from the L0 to SL2 IPF processing which may alter the Doppler spectrum of SL2 products depending on L0 DC estimates. The SL2 products are then used as input for the L2 Doppler estimation. The modification of L0 to SL2 processing is under consideration. Unlike temperature compensation jumps, these jumps do not necessarily occur over all swaths as shown by Figure 6-26.

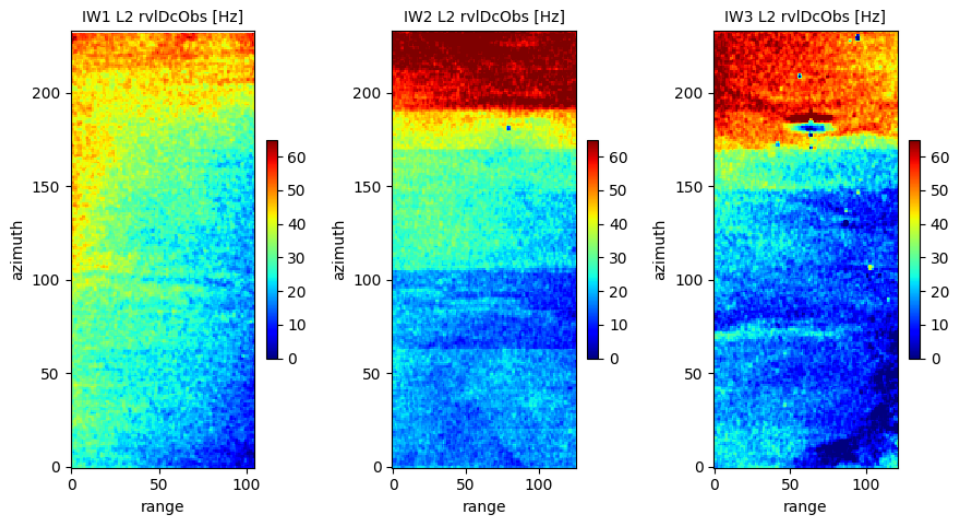


Figure 6-26: Another example of IW DC jumps
 (S1A_IW_OCN__2SDV_20191023T171202_20191023T171227_029589_035E66_FF1F.SAFE)

6.3 L2 Quality Disclaimers

S-1A Quality disclaimers issued on L2 products during 2022 are given in Appendix C -.

Appendix A - S-1A & S-1B Technical Reports

Beyond this report, the following S-1A & S-1B Technical Reports can be of interest for the Sentinel-1 product users. Otherwise explicitly stated, this documentation is available on:

Sentinel Online Library

<https://sentinels.copernicus.eu/web/sentinel/user-guides/sentinel-1-sar/document-library>

Sentinel-1 Level 0 Product Format Specification

This document, starting from SAFE documentation aims to provide the Level 0 format specifications for Sentinel-1 mission.

Sentinel-1 Level 0 Data Decoding Package

The purpose of this note is to gather in one place all the documentation necessary to decode Sentinel-1 Level-0 products. In addition to the documentation, it provides a sample of Level-0 product with the associated RAW decoded data to support the users.

Sentinel-1 Product Specification

This document provides the format specification of Sentinel-1 Level 1 and Level 2 products.

The format specification can change from one version of the SAR processor to another. In that case, the production specification is made available in advance to the end -users.

Sentinel-1 IPF Auxiliary Product Specification

This document describes the auxiliary data required by the Sentinel-1 Instrument Processing Facility (IPF) to perform L1 and L2 processing. It defines the content and format of auxiliary data files and provides references for the governing documentation. The corresponding parameters corresponds inter alia to the parameters considered by the SAR processor. As a complement, the full set of IPF ADF (for AUX_INS, AUX_CAL, AUX_PP1, AUX_PP2, AUX_SCS) is available here: <https://sar-mpc.eu/>

Sentinel-1 Level 1 Detailed Algorithm Definition

This document describes the processing algorithms employed by the Sentinel-1 Image Processing Facility (IPF) for the generation of Sentinel-1 Level 1 products. The algorithms apply to the processing of Sentinel-1 acquisition modes: Stripmap, Interferometric Wide-swath, Extra-wide-swath and Wave.

Sentinel-1 Burst ID Map

Sentinel-1 performs systematic acquisition of bursts in both IW and EW modes. The bursts overlap almost perfectly between different passes and are always located at the same place. With the deployment of the SAR processor S1-IPF 3.4, a new element has been added to the products annotations: the Burst ID, which should help the end user to identify a burst area of interest and facilitate searches. Now, we publish complementary auxiliary products, the Burst ID maps allowing to index the bursts. The burst ID Map is available here: <https://sar-mpc.eu/test-data-sets/>

Sentinel-1 Level 2 Ocean Processor Main Algorithm Definition

The Level 2 Ocean Processor (OCN) is in charge to generate the Level 2 products constituted of three components related to Ocean Wind Field (OWI), Ocean Swell (OSW), and Ocean Radial Velocity (RVL). Each of those three components have a dedicated ATBD document (see below). However, they share few algorithms that are described in this Main ATBD.

Sentinel-1 Ocean Wind Fields (OWI) Algorithm Definition

The objective of this document is to define and describe the algorithm implemented in the S-1 L2 IPF and the processing steps for the generation of the Ocean Wind Field (OWI) component of the Sentinel-1 Level 2 Ocean (OCN) product.

Sentinel-1 Ocean Swell Wave Spectra (OSW) Algorithm Definition

This document describes and defines the prototype software for the generation of the Sentinel-1 Ocean Swell Spectra (OSW) component of the OCN product. The main objective of the document is to provide a clear definition and description of the algorithm and processing system that are consistent with the S-1 L2 processor.

Guide to Sentinel-1 Geocoding

This document describes methodologies to geocode S-1 images that present themselves in a single 2-D raster radar geometry (slant or ground range). It has been written for ESA to provide a reference for users wishing to know the details of Range-Doppler geocoding, and potentially also developers working on software to geocode S-1 SAR products.

Sentinel-1 long duration mutual interference

This technical note describes the long duration mutual interference that has occurred between Sentinel-1 and the Canadian RADARSAT-2 satellite, the Chinese Gaofen 3 satellite and an unknown satellite which operate at the same frequency as Sentinel-1. The mutual interferences are observed on specific locations and times of the orbits and only when both instruments are transmitting simultaneously.

Masking "No-value" pixels on GRD products generated by the Sentinel-1 ESA IPF

This technical note describes an approach for masking the "no-pixel" values for GRD products generated by the Sentinel-1 ESA IPF.

Release Note of S-1 IPF for End Users of Sentinel-1 products

This document was initially published on Sentinel online but was unpublished as deprecated. It initially contained the list of main changes of processing baseline (version of processor and auxiliary configuration). The same information can now be found on the Sentinel-1 QC Web Server here: <https://sar-mpc.eu/ipf/>

Thermal denoising of products generated by the Sentinel-1 IPF

This technical note describes the approach for removing the thermal noise contribution (aka product denoising step).

Sentinel-1 RadarSat-2 mutual interference

This technical note describes the mutual interference that can occur between Sentinel-1 and the Canadian Radarsat-2 satellite which operates at the same frequency as Sentinel-1. The mutual interferences are observed on specific locations and times of the orbits and only when both instruments are transmitting simultaneously.

This document provides description of (1) the respective orbits of Sentinel-1 and Radarsat-2 is described in Section 2, and (2) examples of the mutual interference given in Section 3. A list of mutual interferences found at the Mission Performance Centre (MPC) Coordination Centre are given in Appendices of the document.

Definition of the TOPS SLC deramping function for products generated by the Sentinel-1 IPF

This document defines the procedure for performing the deramping of Sentinel-1 TOPS IWS and EWS of Level-1 SLC products generated by the Sentinel-1 IPF.

Report on the debris impact on S-1A solar panel on 23rd August 2016

The present technical note discusses the debris collision that occurred on 23rd August 2016 whereby the Sentinel-1A solar panel was struck by a small mm sized particle. The implications for products are given in the report.

Sentinel-1A Antenna Failure - Anomaly Characterization Report

This technical note discusses the impact of the Sentinel-1A tile 11 issue that occurred during June 2016.

Sentinel-1 IPF: Impact of the Elevation Antenna Pattern Phase Compensation on the Interferometric Phase Preservation

The Elevation Antenna Patterns (EAPs) used by the S-1 Instrument Processing Facility (IPF) are derived from the S-1 Antenna Model (AM) which is able to predict with great accuracy the gain and phase patterns.

The EAP correction by the S-1 IPF was at launch only considering the gain, similarly to what was done for ASAR. As an outcome of the S-1A Commissioning Phase, it has been decided to upgrade the S-1 IPF to also compensate for the EAP phase, in order to correct for the induced phase difference between the polarimetric channels.

This correction was introduced in March 2015 with the IPF V243. Performing interferograms between products generated with the IPF V243 and the former version V236 leads to interferometric phase variation in range.

This technical note explains the nature of the phase offset and provides recommendation towards its correction.

Sentinel-1 Radiometric Calibration of Products

This document defines the procedure to radiometrically calibrate Sentinel-1 Level 1 products generated by the Sentinel-1 IPF.

Sentinel-1: Using the RFI Annotations

The purpose of this document is to guide the Sentinel-1 product users on how to use the Radio Frequency Annotations (RFI) introduced by the IPF (SAR processor) v3.4.0.

The document explains the different set of annotations that may be available depending on the processor versions and their actual configuration.

It complements the Sentinel-1 product specification (describing the product format) and the Sentinel-1 Detailed algorithm definition (describing the RFI mitigation process).

S-1A & S-1B Annual Performance Reports

Those documents provide information on the S-1 L1 and L2 product performance on a yearly period. These reports replace the N-Cyclic Reports covering the same period.

S-1A N-Cyclic Reports

Those documents provide information on the S-1 L1 performance on a 4-cycle period, for the current year. These reports are replaced by the Annual performance report covering the same period at the end of the year.

Appendix B - S-1A Instrument Unavailability

The S-1A instrument was unavailable during 2023:

| Start Date/Time | End Date/Time | MPC Reference | Summary |
|------------------|------------------|---------------|--------------------------------------------------------|
| 02/02/2023 03:00 | 02/02/2023 12:41 | SOB-4336 | Sentinel-1A Unavailability on 02/02/2023 |
| 29/03/2023 09:09 | 29/03/2023 15:47 | SOB-4337 | Sentinel-1A Unavailability on 29/03/2023 |
| 26/10/2023 12:23 | 26/10/2023 18:13 | SOB-4553 | Sentinel-1A Unavailability on 26/10/2023 |
| 28/10/2023 16:46 | 29/10/2023 14:27 | SOB-4554 | Sentinel-1A Unavailability on 28/10/2023 and 29/10/202 |

Appendix C - S-1A & S-1B Quality Disclaimers

The complete set of Quality Disclaimers since the beginning of the mission can be found on the SAR-MPC Web site [HERE](#)

The following S-1A & S-1B quality disclaimers were issued or updated during 2023 and/or refer to products acquired/generated in 2023:

| Num | Sensor | Description | Start Validity Date | End Validity Date |
|---------------------|--------|------------------------------------------------------------------------------------------------------------|---------------------|---------------------|
| #26 | S1A | S-1A products processed with invalid Restituted Orbit Files (AUX_RESORB) between 2017-09-06 and 2017-09-07 | 2017-09-06 18:57:47 | 2017-09-07 08:07:45 |
| #27 | S1B | S-1B products processed with invalid Restituted Orbit Files (AUX_RESORB) between 2017-09-06 and 2017-09-07 | 2017-09-06 18:07:43 | 2017-09-07 07:17:41 |
| #28 | S1A | S-1A L2 OCN products provide reverse OSW wind direction respect to the specification | 2015-11-24 12:03:51 | 2018-03-13 02:30:17 |
| #29 | S1B | S-1B L2 OCN products provide reverse OSW wind direction respect to the specification | 2016-09-26 00:00:00 | 2018-03-13 03:21:48 |
| #42 | S1A | Test of the new S-1A antenna configuration, aiming improvement of WV2 performances | 2019-02-28 09:42:51 | 2019-03-11 09:12:44 |
| #45 | S1B | Test of the new S-1B antenna configuration, aiming improvement of WV2 performances | 2019-05-14 09:15:57 | 2019-05-28 08:32:37 |
| #77 | S1A | Invalid Burst ID for some S-1A products | 2021-11-02 23:07:50 | 2030-01-01 00:00:00 |
| #78 | S1B | Invalid Burst ID for some S-1B products | 2021-11-02 23:42:03 | 2030-01-01 00:00:00 |
| #79 | S1A | Invalid annotation of acquisition anXTime for some S1-A RAW products | 2014-09-30 15:17:26 | 2030-01-01 00:00:00 |
| #80 | S1B | Invalid annotation of acquisition anXTime for some S1-B RAW products | 2016-10-13 15:36:00 | 2030-01-01 00:00:00 |
| #81 | S1A | S-1A OCN products with invalid xsd files | 2022-03-23 07:50:46 | 2022-05-12 08:15:27 |

| | | | | |
|----------------------|-----|-------------------------------------------------------------------------------------------------------------------------|---------------------|---------------------|
| #86 | S1A | Sentinel-1A swell inversion (OCN/OSW processing) performed using invalid a priori wind speed and direction | 2022-04-08 00:00:00 | 2022-05-12 08:25:01 |
| #87 | S1A | Auxiliary product information not properly projected on the SAR image, leading to major degradation of OCN measurements | 2022-03-23 07:50:46 | 2022-05-12 08:25:01 |
| #89 | S1B | The Sentinel-1B StripMap OCN products are not operationally qualified | 2016-09-29 22:26:06 | 2030-01-01 00:00:00 |
| #109 | S1A | Products with residual RFI degradation acquired in December 2022 | 2022-12-01 00:00:00 | 2023-01-01 00:00:00 |
| #110 | S1A | Products with residual RFI degradation acquired in January 2023 | 2023-01-01 00:00:00 | 2023-02-01 00:00:00 |
| #111 | S1A | S-1A products generated without POD orbit files | 2023-02-01 05:25:50 | 2023-02-01 22:39:24 |
| #112 | S1A | Products with residual RFI degradation acquired in February 2023 | 2023-02-01 00:00:00 | 2023-03-01 00:00:00 |
| #113 | S1A | Products with residual RFI degradation acquired in March 2023 | 2023-03-01 00:00:00 | 2023-04-01 00:00:00 |
| #114 | S1A | Products with residual RFI degradation acquired in April 2023 | 2023-04-01 00:00:00 | 2023-05-01 00:00:00 |
| #115 | S1A | Invalid burst ID annotations (S1A IW/EW SLC in cycles 245 to 258) | 2021-11-05 17:10:59 | 2022-04-10 18:51:34 |
| #117 | S1A | S1A TOPS SLC Range Denoising Vector range annotation | 2014-09-30 15:17:26 | 2023-10-19 07:51:35 |
| #118 | S1B | S1B TOPS SLC Range Denoising Vector range annotation | 2016-08-20 00:00:00 | 2021-12-23 06:53:58 |
| #119 | S1A | S-1A WV SLC annotated noise vectors were improperly calibrated with IPF 2.9x | 2018-03-13 00:34:07 | 2019-06-25 22:58:06 |
| #120 | S1B | S-1B WV SLC annotated noise vectors were improperly calibrated with IPF 2.9x | 2018-03-13 03:34:38 | 2019-06-25 20:55:36 |

| | | | | |
|----------------------|-----|----------------------------------------------------------------|---------------------|---------------------|
| #121 | S1A | Invalid burst ID annotations (S1A IW/EW SLC in cycle 259) | 2022-04-15 10:56:21 | 2022-04-27 06:20:22 |
| #122 | S1A | Invalid burst ID annotations (S1A IW/EW SLC in cycle 260) | 2022-04-27 18:59:41 | 2022-05-08 07:05:09 |
| #123 | S1A | Invalid burst ID annotations (S1A IW/EW SLC in cycle 261) | 2022-05-09 18:59:42 | 2022-05-20 14:29:26 |
| #124 | S1A | Invalid burst ID annotations (S1A IW/EW SLC in cycle 262) | 2022-05-21 18:59:43 | 2022-05-29 06:32:40 |
| #125 | S1A | Invalid burst ID annotations (S1A IW/EW SLC in cycle 263) | 2022-06-02 18:59:44 | 2022-06-09 18:51:37 |
| #126 | S1A | Invalid burst ID annotations (S1A IW/EW SLC in cycle 264) | 2022-06-14 18:59:45 | 2022-06-25 12:00:01 |
| #127 | S1B | Invalid burst ID annotations (S1B IW SLC in cycles 175 to 179) | 2021-11-04 09:50:37 | 2021-12-22 18:59:00 |
| #128 | S1A | Invalid burst ID annotations (S1A IW/EW SLC in cycle 265) | 2022-06-26 18:59:46 | 2022-07-06 15:54:48 |
| #129 | S1A | Invalid burst ID annotations (S1A IW/EW SLC in cycle 266) | 2022-07-08 18:59:46 | 2022-07-17 07:12:49 |
| #130 | S1A | Invalid burst ID annotations (S1A IW/EW SLC in cycle 267) | 2022-07-20 18:59:47 | 2022-07-30 11:16:51 |
| #131 | S1A | Invalid burst ID annotations (S1A IW/EW SLC in cycle 268) | 2022-08-01 18:59:48 | 2022-08-08 18:51:41 |
| #132 | S1A | Invalid burst ID annotations (S1A IW/EW SLC in cycle 269) | 2022-08-13 10:56:29 | 2022-08-20 18:51:42 |
| #133 | S1A | Invalid burst ID annotations (S1A IW/EW SLC in cycle 270) | 2022-08-25 18:59:49 | 2022-09-04 19:08:22 |
| #134 | S1A | Invalid burst ID annotations (S1A IW/EW SLC in cycle 271) | 2022-09-10 10:25:51 | 2022-09-11 07:45:35 |
| #135 | S1A | Invalid burst ID annotations (S1A IW/EW SLC in cycle 272) | 2022-09-18 10:56:30 | 2022-09-25 07:42:53 |
| #136 | S1A | Invalid burst ID annotations (S1A IW/EW SLC in cycle 273) | 2022-10-07 10:48:19 | 2022-10-09 07:12:53 |

| | | | | |
|----------------------|-----|-----------------------------------------------------------|---------------------|---------------------|
| #137 | S1A | Invalid burst ID annotations (S1A IW/EW SLC in cycle 274) | 2022-10-14 10:41:14 | 2022-10-23 14:30:24 |
| #138 | S1A | Invalid burst ID annotations (S1A IW/EW SLC in cycle 275) | 2022-10-24 01:36:52 | 2022-11-04 15:05:13 |
| #139 | S1A | Invalid burst ID annotations (S1A IW/EW SLC in cycle 276) | 2022-11-04 19:48:21 | 2022-11-13 10:08:51 |
| #140 | S1A | Invalid burst ID annotations (S1A IW/EW SLC in cycle 277) | 2022-11-18 06:39:57 | 2022-11-20 06:24:31 |
| #141 | S1A | Invalid burst ID annotations (S1A IW/EW SLC in cycle 278) | 2022-12-02 06:23:27 | 2022-12-04 07:59:03 |
| #142 | S1A | Invalid burst ID annotations (S1A IW/EW SLC in cycle 279) | 2022-12-16 07:45:33 | 2022-12-18 09:17:55 |
| #143 | S1A | Invalid burst ID annotations (S1A IW/EW SLC in cycle 280) | 2022-12-23 10:56:28 | 2022-12-25 07:21:02 |
| #144 | S1A | Invalid burst ID annotations (S1A IW/EW SLC in cycle 281) | 2023-01-06 10:41:11 | 2023-01-15 08:40:20 |
| #145 | S1A | Invalid burst ID annotations (S1A IW/EW SLC in cycle 282) | 2023-01-20 03:55:12 | 2023-01-27 12:00:02 |
| #146 | S1A | Invalid burst ID annotations (S1A IW/EW SLC in cycle 283) | 2023-01-28 01:36:49 | 2023-02-04 07:29:15 |
| #147 | S1A | Invalid burst ID annotations (S1A IW/EW SLC in cycle 284) | 2023-02-09 22:18:18 | 2023-02-19 09:53:00 |
| #148 | S1A | Invalid burst ID annotations (S1A IW/EW SLC in cycle 285) | 2023-02-23 10:41:09 | 2023-03-04 15:05:10 |
| #149 | S1A | Invalid burst ID annotations (S1A IW/EW SLC in cycle 286) | 2023-03-04 19:48:18 | 2023-03-16 11:54:01 |
| #150 | S1A | Invalid burst ID annotations (S1A IW/EW SLC in cycle 287) | 2023-03-16 19:48:17 | 2023-03-26 08:58:00 |
| #151 | S1A | Invalid burst ID annotations (S1A IW/EW SLC in cycle 288) | 2023-03-30 11:35:13 | 2023-04-09 10:21:28 |
| #152 | S1A | Invalid burst ID annotations (S1A IW/EW SLC in cycle 289) | 2023-04-14 07:04:38 | 2023-04-21 15:05:10 |

| | | | | |
|----------------------|-----|------------------------------------------------------------------------------------------------------------------|---------------------|---------------------|
| #153 | S1A | Invalid burst ID annotations (S1A IW/EW SLC in cycle 290) | 2023-04-21 19:48:18 | 2023-04-23 06:40:57 |
| #154 | S1A | Products with residual RFI degradation acquired in May 2023 | 2023-05-01 00:00:00 | 2023-06-01 00:00:00 |
| #155 | S1A | Products with residual RFI degradation acquired in June 2023 | 2023-06-01 00:00:00 | 2023-07-01 00:00:00 |
| #156 | S1A | Invalid burst ID annotations (S1A IW/EW SLC in cycle 291) | 2023-05-04 12:33:54 | 2023-05-14 07:58:59 |
| #157 | S1A | Invalid burst ID annotations (S1A IW/EW SLC in cycle 292) | 2023-05-20 05:25:51 | 2023-05-27 15:05:12 |
| #158 | S1A | Invalid burst ID annotations (S1A IW/EW SLC in cycle 293) | 2023-05-27 19:48:20 | 2023-06-04 07:29:17 |
| #159 | S1A | Products processed using degraded orbit files due to solar activity | 2023-01-15 02:30:48 | 2023-07-22 07:42:56 |
| #160 | S1A | Invalid burst ID annotations (S1A IW/EW SLC in cycle 294) | 2023-06-09 01:36:51 | 2023-06-18 07:12:52 |
| #161 | S1A | Products with residual RFI degradation acquired in July 2023 | 2023-07-01 00:00:00 | 2023-08-01 00:00:00 |
| #162 | S1A | Products with residual RFI degradation acquired in August 2023 | 2023-08-01 00:00:00 | 2023-09-01 00:00:00 |
| #163 | S1A | Invalid burst ID annotations (S1A IW/EW SLC in cycle 295) | 2023-06-22 21:18:55 | 2023-07-02 08:40:23 |
| #164 | S1A | Invalid burst ID annotations (S1A IW/EW SLC in cycle 296) | 2023-07-08 07:44:54 | 2023-07-14 14:29:32 |
| #165 | S1A | Invalid burst ID annotations (S1A IW/EW SLC in cycle 297) | 2023-07-14 19:48:23 | 2023-07-23 10:08:53 |
| #166 | S1A | Invalid burst ID annotations (S1A IW/EW SLC in cycle 298) | 2023-07-28 21:18:58 | 2023-08-07 05:18:45 |
| #167 | S1A | Products processed using degraded orbit files due to solar activity (26 July 2023 to 03 September 2023 included) | 2023-07-26 10:15:54 | 2023-09-03 13:12:46 |
| #168 | S1A | Invalid burst ID annotations (S1A IW/EW SLC in cycle 299) | 2023-08-08 05:58:53 | 2023-08-19 14:30:24 |

| | | | | |
|----------------------|-----|---------------------------------------------------------------------------------------------------------------------|---------------------|---------------------|
| #169 | S1A | Invalid burst ID annotations (S1A IW/EW SLC in cycle 300) | 2023-08-20 01:36:56 | 2023-08-27 07:29:22 |
| #170 | S1A | Invalid burst ID annotations (S1A IW/EW SLC in cycle 301) | 2023-09-01 10:56:35 | 2023-09-10 08:58:08 |
| #171 | S1A | Invalid burst ID annotations (S1A IW/EW SLC in cycle 302) | 2023-09-14 21:19:00 | 2023-09-24 08:40:28 |
| #172 | S1A | Products with residual RFI degradation acquired in September 2023 | 2023-09-01 00:00:00 | 2023-10-01 00:00:00 |
| #173 | S1A | Degraded radiometric calibration due to acquisition close to a manoeuvre | 2023-09-20 22:00:48 | 2023-09-20 22:01:18 |
| #174 | S1A | S-1A Products generated without POD orbit files | 2023-10-04 04:46:41 | 2023-10-04 07:29:28 |
| #175 | S1A | Invalid burst ID annotations (S1A IW/EW SLC in cycle 303) | 2023-09-29 05:25:16 | 2023-10-06 15:05:19 |
| #176 | S1A | Products processed using degraded orbit files due to solar activity (12 September 2023 to 09 October 2023 included) | 2023-09-12 05:17:43 | 2023-10-09 18:46:09 |
| #177 | S1A | Invalid burst ID annotations (S1A IW/EW SLC in cycle 304) | 2023-10-06 19:48:27 | 2023-10-15 06:32:51 |
| #178 | S1B | S1B Products acquired during its In Orbit Commissioning Phase are not operationally qualified | 2016-08-20 00:00:00 | 2016-09-27 00:00:00 |
| #179 | S1A | Products with residual RFI degradation acquired in October 2023 | 2023-10-01 00:00:00 | 2023-11-01 00:00:00 |
| #180 | S1A | Invalid burst ID annotations (S1A IW SLC in cycle 305) | 2023-10-19 23:37:55 | 2023-10-30 16:22:17 |
| #181 | S1A | Invalid burst ID annotations (S1A IW SLC in cycle 306) | 2023-10-31 23:37:55 | 2023-11-11 16:22:16 |
| #182 | S1A | Invalid denoising vector due to contamination by RFI | 2023-01-31 15:55:17 | 2023-01-31 16:09:35 |
| #183 | S1A | Invalid burst ID annotations (S1A IW SLC in cycle 307) | 2023-11-12 23:37:55 | 2023-11-23 16:22:16 |

| | | | | |
|----------------------|-----|-----------------------------------------------------------------------------------------------------------------------------------|--------------------------------------------|---------------------|
| #184 | S1A | Products with residual RFI degradation acquired in November 2023 Products with residual RFI degradation acquired in November 2023 | 2023-11-01 00:00:00 2023-11-01 00:00:00 | 2023-12-01 00:00:00 |
| #185 | S1A | Invalid burst ID annotations (S1A IW SLC in cycle 308) | 2023-11-24 23:37:54 | 2023-12-05 16:22:16 |
| #186 | S1A | Invalid burst ID annotations (S1A IW SLC in cycle 309) | 2023-12-06 23:37:54 | 2023-12-17 16:22:15 |



Appendix D - S-1A Orbit Cycles

The table below gives the S-1A cycle number with start and stop acquisition dates during 2023.

The start of a cycle is at approximately 18:00 UT on the dates below.

| Cycle | Start Date | End Date |
|-------|------------|------------|
| 280 | 22/12/2022 | 03/01/2023 |
| 281 | 03/01/2023 | 15/01/2023 |
| 282 | 15/01/2023 | 27/01/2023 |
| 283 | 27/01/2023 | 08/02/2023 |
| 284 | 08/02/2023 | 20/02/2023 |
| 285 | 20/02/2023 | 04/03/2023 |
| 286 | 04/03/2023 | 16/03/2023 |
| 287 | 16/03/2023 | 28/03/2023 |
| 288 | 28/03/2023 | 09/04/2023 |
| 289 | 09/04/2023 | 21/04/2023 |
| 290 | 21/04/2023 | 03/05/2023 |
| 291 | 03/05/2023 | 15/05/2023 |
| 292 | 15/05/2023 | 27/05/2023 |
| 293 | 27/05/2023 | 08/06/2023 |
| 294 | 08/06/2023 | 20/06/2023 |
| 295 | 20/06/2023 | 02/07/2023 |
| 296 | 02/07/2023 | 14/07/2023 |
| 297 | 14/07/2023 | 26/07/2023 |
| 298 | 26/07/2023 | 07/08/2023 |
| 299 | 07/08/2023 | 19/08/2023 |
| 300 | 19/08/2023 | 31/08/2023 |
| 301 | 31/08/2023 | 12/09/2023 |
| 302 | 12/09/2023 | 24/09/2023 |
| 303 | 24/09/2023 | 06/10/2023 |
| 304 | 06/10/2023 | 18/10/2023 |
| 305 | 18/10/2023 | 30/10/2023 |
| 306 | 30/10/2023 | 11/11/2023 |
| 307 | 11/11/2023 | 23/11/2023 |

| | | |
|-----|------------|------------|
| 308 | 23/11/2023 | 05/12/2023 |
| 309 | 05/12/2023 | 17/12/2023 |
| 310 | 17/12/2023 | 29/12/2023 |
| 311 | 29/12/2023 | 10/01/2024 |



Appendix E - S-1A Transmit Receive Module Failures

There were no S-1A antenna Transmit/Receive Modules (TRMs) failures during 2023.

Appendix F - S-1A & S-1B Auxiliary Data Files

The complete set of S-1A and S-1B Auxiliary Data files since the beginning of the mission can be found on the SAR-MPC Web site [HERE](#).
Alternatively, those data files can be queried using REST API documented [HERE](#)

The following S-1A Auxiliary Data Files (ADFs) were updated during 2023:

S-1A Instrument ADF (AUX_INS)

| ADF | Update Reason |
|-----|---------------|
| | |

S-1A Calibration ADF (AUX_CAL)

| ADF | Update Reason |
|-----|---------------|
| | |

S-1A L1 Processor Parameters ADF (AUX_PP1)

| ADF | Update Reason |
|-----|---------------|
| | |

S-1A L2 Processor Parameters ADF (AUX_PP2)

| ADF | Update Reason |
|-----|---------------|
| | |

S-1A Simulated Cross Spectra ADF (AUX_SCS)

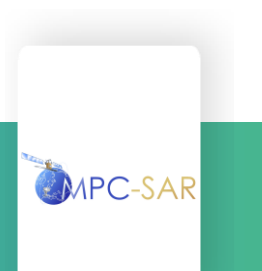
| ADF | Update Reason |
|-----|---------------|
| | |

S-1A Instrument Timing Calibration (AUX_ITC)

| ADF | Update Reason |
|---------------------------------------------------------------|-------------------------------------------------------------------------------------------------------------------------------------------------------------------------------------------------------------------------------------------------------------------------------------------------------------------------------------------------------------------------------------------------------------------------------------------------|
| S1A_AUX_ITC_V20160627T000000_G20230330T093840 | First version of the operational S-1A AUX ITC prepared by SAR-MPC for SETAP-IPF. This calibration product provides Sentinel-1A specific azimuth and range reference timing correction values and the beam and polarization dependent time offset values for the generation of S-1 ETAD products. According to the timing offset calibration status as of August 2022, the offset values are set to zero. The AUX ITC is specified in [AD-11] |
| S1A_AUX_ITC_V20160627T000000_G20230406T084701 | Operational S-1A AUX ITC prepared by SAR-MPC for SETAP-IPF. This calibration product provides updated Sentinel-1A specific range and azimuth reference timing correction values for the generation of S-1 ETAD products: <ul style="list-style-type: none"> - The value <rangeCalibration> changed from 1.1281e-09 to 7.4103e-10 s - The value <azimuthCalibration> changed from 1.2873e-05 to 6.3522e-06 s |

S-1A SETAP Configuration File (AUX_SCF)

| ADF | Update Reason |
|--------------------------------------------------------------|----------------------------------------------------------------------------------------------------------------------------------------------------------------------------------------------------------------------------------------------------------------------------------------------------------------------------------------------------------------------|
| S1_AUX_SCF_V20140406T133000_G20221003T130002 | First version of the AUX SCF prepared by SAR-MPC for the SETAP-IPF. The product is applicable to all S-1 sensors (S-1A, S-1B, ...) The product provides the default configuration for the computation of correction layers of nominal S-1 ETAD products. This version of AUX SCF is applicable to SETAP-IPF version 2.0 and later, see specification [AD-11]. |



The following S-1B Auxiliary Data Files (ADFs) were updated during 2023:

S-1B Instrument ADF (AUX_INS)

| ADF | Update Reason |
|-----|---------------|
| | |

S-1B Calibration ADF (AUX_CAL)

| ADF | Update Reason |
|-----|---------------|
| | |

S-1B L1 Processor Parameters ADF (AUX_PP1)

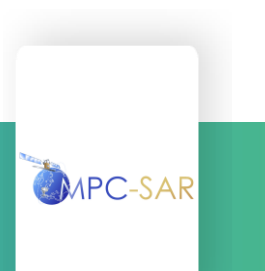
| ADF | Update Reason |
|-----|---------------|
| | |

S-1B L2 Processor Parameters ADF (AUX_PP2)

| ADF | Update Reason |
|-----|---------------|
| | |

S-1B Simulated Cross Spectra ADF (AUX_SCS)

| ADF | Update Reason |
|-----|---------------|
| | |

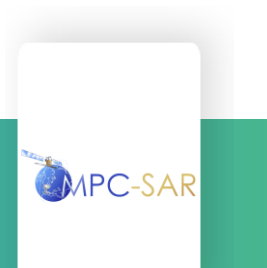


S-1B Instrument Timing Calibration (AUX_ITC)

| ADF | Update Reason |
|---------------------------------------------------------------|----------------------------------------------------------------------------------------------------------------------------------------------------------------------------------------------------------------------------------------------------------------------------------------------------------------------------------------------------------------------------------------------------------------------------------------------------|
| S1B AUX ITC V20160422T000000 G20230330T094000 | First version of the operational S-1B AUX ITC prepared by SAR-MPC for SETAP-IPF. This calibration product provides Sentinel-1B specific azimuth and range reference timing correction values and the beam and polarization dependent time offset values for the generation of S-1 ETAD products. According to the timing offset calibration status as of August 2022, the offset values are set to zero. The AUX ITC is specified in [AD-11]. |
| S1B AUX ITC V20160422T000000 G20230406T084600 | Operational S-1B AUX ITC prepared by SAR-MPC for SETAP-IPF. This calibration product provides updated Sentinel-1B specific range and azimuth reference timing correction values for the generation of S-1 ETAD products: <ul style="list-style-type: none"> - The value <rangeCalibration> changed from 6.4566e-11 to -1.2855e-10 s - The value <azimuthCalibration> changed from -4.9701e-05 to -3.5523e-05 s |

S-1B SETAP Configuration File (AUX_SCF)

| ADF | Update Reason |
|-----|---------------|
| | |





END OF DOCUMENT

